

AN ABSTRACT OF A THESIS

**MODELING, STABILITY ANALYSIS AND CONTROL OF A
DIRECT AC/AC MATRIX CONVERTER BASED SYSTEMS**

Melaku Mihret

Master of Science in Electrical and Computer Engineering

The AC-AC matrix converters are pulse-width modulated using either a carrier-based pulse width modulation (PWM) or space vector modulation techniques. Both modulation techniques are analyzed for a three phase-to-three phase matrix converter. It is desirable to be able to synthesize the three-phase voltages with minimum harmonics and the highest voltage gain possible.

A new methodology for designing an input filter for the matrix converter is proposed. This approach is based on the Fourier series of the switching signals and harmonic balance technique. The parameters of the filter are determined based on a specified maximum allowable source current and input capacitor voltage ripple as well as the overall system stability.

A complete dynamic modeling and a new approach of steady state analysis for an AC/AC matrix converter fed induction motor drive are set forth. The dynamic responses as well as the steady state performance characteristics of the system are studied under various load conditions while the voltage source operates under a unity power factor. Similar modeling is also done for a matrix converter feeding a passive RL load.

A new generalized model for stability analysis based on small signal modeling is proposed for a matrix converter fed induction motor drive system under a constant Volt/Hertz operation. Different factors which affect the matrix converter stability are analyzed.

A high performance vector control for a matrix converter fed induction motor with input power factor control is set forth in this work. Detailed controller designs are presented after studying the internal and zero dynamics of the overall drive system. The robustness of the proposed control scheme is verified through computer simulation.

Finally, the actual firing pulses for the bidirectional switches of the matrix converter are generated using LabVIEW/FPGA on a national instrument NIcRIO chassis. A computer simulation has been done based on these actual pulses obtained from the FPGA terminals.

**MODELING, STABILITY ANALYSIS AND CONTROL OF A
DIRECT AC/AC MATRIX CONVERTER BASED SYSTEMS**

A Thesis

Presented to

The Faculty of the Graduate School

Tennessee Technological University

By

Melaku Mihret

In Partial Fulfillment

Of the Requirements of the Degree

MASTER OF SCIENCE

Electrical Engineering

December 2011

CERTIFICATE OF APPROVAL OF THESIS

**MODELING, STABILITY ANALYSIS AND CONTROL OF A
DIRECT AC/AC MATRIX CONVERTER BASED SYSTEMS**

By

Melaku Mihret

Graduate Advisory Committee:

Joseph Ojo, Chairperson

Date

Ghadir Radman

Date

Ahmed Kamal

Date

Approved for the Faculty:

Francis Otuonye
Associate Vice President
for Research and Graduate Studies

Date

DEDICATION

This work is dedicated to my parents

ACKNOWLEDGEMENTS

I would like my deepest gratitude to the chair person of my advisory committee, Dr. Joseph Ojo for his expertise guidance, generous support and encouragement during the course of the research. I would also like to express my sincere thanks to Dr. Ghadir Radman and Dr. Ahmed Kamal for their effort in reviewing and evaluating my work.

I am grateful to the office of Center for Energy Systems Research (CESR) for the financial support provided during my graduate study. I would also like to thank ECE department for creating nice atmosphere and kind treatment with special thanks goes to Mr. Robert Peterson and Mr Conard Murray for their invaluable support.

I owe my deepest gratitude to Meharegzi Abrham for his time in all the technical discussions throughout my thesis. And I would also thank him and his wife Elizabeth for their care and support. I would like to thank Sosthenes, Hossein, Kennedy, Jeff, Mehari and Will. I am so grateful to my roommates Bijaya, Amrit and Puran for their technical support and making my stay so cherished.

It is my great pleasure to thank my friends Abebe, Ahmed, Wende and Abel for their friendship and moral support. I extend my sincere thanks to Dr. Solomon Bekele for his advice.

My heartfelt appreciation goes toward my families for their unconditional love and encouragement in all my endeavors.

Lastly, I offer my regards and blessings to all of those who supported me in any respect during the completion of the work.

TABLE OF CONTENTS

	Page
LIST OF TABLES.....	xi
LIST OF FIGURES.....	xii
CHAPTER 1	1
INTRODUCTION	1
1.1 Introduction.....	1
1.2 Overview of Static AC/AC Power Frequency Conversion.....	1
1.2.1 Indirect Power Frequency Converter	2
1.2.2 Direct AC/AC Converter	4
1.3 Objectives of the Thesis.....	6
1.4 Thesis Outline	7
CHAPTER 2	10
LITERATURE REVIEW	10
2.1 Modulation Strategies	10
2.2 Input Filter Design	12
2.3 Stability Analysis of a Matrix Converter System	14
2.4 Control of Matrix Converter Drive System	15
CHAPTER 3	19

	Page
MODULATION TECHNIQUES	19
3.1 Introduction.....	19
3.2 Carrier Based Modulation.....	19
3.2.1 Switching Signal Generations.....	24
3.3 Space Vector Modulation.....	26
3.3.1 Direct Space Vector modulation.....	26
3.3.2 Indirect Space Vector modulation	45
3.3.3 Common Mode Voltage Expression Based on Duty Cycle Space Vector Modulation.....	60
3.4 Simulation Results and Discussion	75
3.5 Conclusion	83
CHAPTER 4	85
INPUT FILTER DESIGN	85
4.1 Introduction.....	85
4.2 Fourier Series Analysis of Switching Signals of a Matrix Converter.....	86
4.3 Input Filter Parameters Specification.....	97
4.3.1 Harmonic Balance Technique.....	99
4.3.2 Stability Analysis for Matrix converter feeding an RL load.....	106

	Page
4.4 Simulation Results and Discussion	111
4.5 Conclusion	118
CHAPTER 5	119
DYNAMIC AND STEADY STATE MODELLING OF MATRIX CONVERTER SYSTEMS	119
5.1 Introduction	119
5.2 Matrix Converter Feeding an RL Load.....	120
5.2.1 Dynamic Modelling	120
5.2.2 Dynamic Simulation Results and Discussion	127
5.2.3 Generalized Steady State Analysis	131
5.2.4 Steady State Simulation Results and Discussions	136
5.3 Modelling of Matrix Converter Fed Induction Machine	139
5.3.1 Dynamic Modelling	139
5.3.2 Dynamic Simulation Results and Discussion	141
5.3.3 Generalized Steady State Analysis	144
5.3.4 Steady State Simulation Results and Discussions	147
5.4 Conclusion	150
CHAPTER 6	151

	Page
6.1 Introduction.....	151
6.2 Modeling of the Drive System.....	152
6.3 Small Signal Analysis	157
6.4 Simulation Results and Discussions	162
6.5 Steady State Operating Conditions	168
6.6 Simulation Result for Volt/Hz Control	170
6.7 Conclusion	174
CHAPTER 7	175
VECTOR CONTROL OF MATRIX CONVERTER FED INDUCTION MACHINE ..	175
7.1 Introduction.....	175
7.2 Field Oriented Control for Matrix Converter Fed Induction Motor with Unity Input Power Factor Control	176
7.2.1 Indirect Field Oriented Control.....	176
7.2.2 Unity Input Power Factor Control	181
7.2.3 Input-Output Feedback Linearization	183
7.2.4 Stator Flux Estimation	202
7.3 Simulation Results and Discussions	208
7.4 Conclusion	222

	Page
CHAPTER 8	223
SWITCHING SIGNALS GENERATION IN NI-cRIO CHASIS.....	223
8.1 Introduction.....	223
8.2 Switching signal generation using direct digital synthesis	224
8.2.1 Accumulator.....	225
8.2.2 Lookup Table	226
8.3 Conclusion	232
CHAPTER 9	233
CONCLUSSION AND FUTURE SUGGESTION	233
9.1 Summary of the Thesis	233
9.2 List of Contributions	236
9.3 Future Work.....	237
REFERENCES	241
APPENDIX A.....	253
APPENDIX B.....	270
APPENDIX C.....	293
APPENDIX D.....	298
APPENDIX E.....	305

	Page
APPENDIX F	319
VITA.....	330

LIST OF TABLES

	Page
Table 3.1 Possible output voltage space vectors	28
Table 3.2 Possible input current space vectors	34
Table 3.3 Possible switching configuration of a matrix converter	39
Table 3.4 The Selected switching configurations for the possible sector combinations ...	41
Table 3.5: Truth table for rectifier stage	47
Table 3.6 Truth table of inverter	52
Table 3.7 Modes for voltage and current sectors.....	58
Table 3.8 Switching configuration for the combined matrix.....	58
Table 3.9 Modes result in zero voltage and current vectors	58
Table 3.10 Sequence of switching devices	59
Table 3.11 Neutral voltage in output voltage Sector I and input current sector II	60
Table 4.1 System parameters	110
Table 5.1 System Parameters.....	150
Table 6.1 System parameters used in the stability study	171
Table 7.1 Control system parameters	201

LIST OF FIGURES

	Page
Figure 1.1 Diode rectifier-PWM VSI converter	3
Figure 1.2 PWM rectifier-PWM VSI converter	3
Figure 1.3 Direct three phase-to-three phase matrix converter	5
Figure 3.1 A schematics of a simplified matrix converter.....	21
Figure 3.2: Illustration of voltage ratio of a) 50%, (b) 75% and (c) 86.7%	24
Figure 3.3 Generation of switching pulses for phase ‘a’	25
Figure 3.4 Output voltage space vectors.....	40
Figure 3.5 Input current space vector	40
Figure 3.6 Output voltage vector synthesis	41
Figure 3.7 Input current vector synthesis	43
Figure 3.8 Equivalent circuit for indirect matrix converter	46
Figure 3.10 Rectifier current space vector.....	48
Figure 3.9 Diagram for synthesis of the reference current	50
Figure 3.11 Inverter voltage space vector.....	53
Figure 3.12 Diagram for synthesis of the reference voltage.....	53
Figure 3.13 Modulation signals for output phase ‘a’ voltage.....	77
Figure 3.14 FFT for the modulation signal M_{aA}	77
Figure 3.15 Carrier based pulse width modulation.....	78
Figure 3.16 Intermediate signals used to generate switching signals.....	78

	Page
Figure 3.17 Switching signals for output phase ‘a’ voltage	79
Figure 3.18 Modulation signals for output phase ‘b’ voltage.....	79
Figure 3.19 Switching signals for output phase ‘b’ voltage	80
Figure 3.20 Modulation signals for output phase ‘c’ voltage.....	80
Figure 3.21 Switching signals for output phase ‘c’ voltage	81
Figure 3.22 Input three phase voltages	81
Figure 3.23 synthesized output three phase voltages.....	82
Figure 3.24 Phase ‘a’ input capacitor voltage and input matrix converter current with unity input power factor.....	83
Figure 4.1 Schematics of input filter circuit	98
Figure 4.2 A matrix converter feeding an RL load.....	100
Figure 4.3 Dominant harmonics components of the input current	101
Figure 4.4 Stability limit of a matrix converter with RL load	112
Figure 4.5 Dominant Eigen Values for various damping resistance	112
Figure 4.6 Phase ‘a’ source voltage and current.....	113
Figure 4.7 Phase ‘a’ input capacitor voltage and current of the MC	113
Figure 4.8 Phase ‘a’ output voltage and current	114
Figure 4.9 Input current and source current.....	114
Figure 4.10 FFT of input current of the MC.....	115
Figure 4.11 FFT of the source current	115
Figure 4.12 FFT of the input capacitor voltage	116
Figure 4.13 Stability limit for a load current of 5A.....	117

	Page
Figure 4.14 Bode plot of the designed input filter	117
Figure 5.1 Schematic diagram of AC/AC matrix converter feeding an RL load	121
Figure 5.2 Switching pulses for phase 'a' output voltage	127
Figure 5.4 MC output three phase voltages	128
Figure 5.5 Input three phase capacitor voltages	129
Figure 5.6 Filtered three phase capacitor voltages	129
Figure 5.7 MC three phase input current	130
Figure 5.8 Three phase source currents	130
Figure 5.9 Output active and reactive power for possible output power factor operations	136
Figure 5.10 Input active and reactive powers	137
Figure 5.11 Magnitude of input capacitor voltage.....	137
Figure 5.12 Magnitude of source current.....	138
Figure 5.13 Converter output to input voltage ratio	138
Figure 5.14 Schematic diagram of the AC/AC matrix converter fed induction motor ...	140
Figure 5.15 Starting transient and dynamic response of (a) rotor speed and (b) electromagnetic torque.....	142
Figure 5.16 MC output (a) line-to-line voltage (b) phase voltage	142
Figure 5.17 (a) Input capacitor phase voltage (b) filtered capacitor voltage.....	143
Figure 5.18 (a) MC input phase current (b) source phase current	143
Figure 5.19 Steady state torque-slip characteristics of an induction machine	148
Figure 5.20 Magnitude of capacitor voltage and (b) magnitude of source current	148

	Page
Figure 5.21 (a) Active power and (b) reactive power drawn from the source.....	149
Figure 6.1 Schematic diagram of the AC/AC matrix converter fed induction motor	153
Figure 6.2 Stability limit of matrix converter gain against filter time constant	164
Figure 6.3 Matrix converter stability limit for varying Filter time constant.....	164
Figure 6.4 Stability limit of the matrix converter for varying damping resistance	165
Figure 6.5 The impact of Stator and rotor resistance on the stability of the system	165
Figure 6.6 The impact of power factor on the stability of the system	166
Figure 6.7 (a) Rotor speed and (b) electromagnetic torque	167
Figure 6.8 Output line to line voltage and (b) input capacitor phase voltage.....	167
Figure 6.9 MC input phase current and (b) source phase current.....	168
Figure 6.10 Induction motor Electromagnetic torque.....	172
Figure 6.11 Magnitude of source current.....	172
Figure 6.12 Converter voltage transfer ratio against rotor speed.	173
Figure 6.13 Ratio of reactive power to the apparent power at the input of the converter	173
Figure 7.1 Schematic diagram of the matrix converter fed induction motor without damping resistor.....	177
Figure 7.2 Control input and output of the system	185
Figure 7.3 Linearization diagram for rotor flux controllers.....	192
Figure 7.4 Block diagram for the rotor speed controller	193
Figure 7.5 Inner stator current controller block diagram.....	196
Figure 7.6 Block diagram for the input current controllers	198

	Page
Figure 7.7 Block diagram for the input current controllers	200
Figure 7.8 Block diagram of the stator flux estimation using LPF.....	204
Figure 7.9 Block diagram of the proposed control scheme	207
Figure 7.10 Simulink model of the proposed control scheme	209
Figure 7.11 Speed command, actual speed and electromagnetic torque	210
Figure 7.12 Estimated and reference rotor flux linkages.....	211
Figure 7.13 Actual and reference stator currents	211
Figure 7.14 Source currents commands and actual values	212
Figure 7.15 Inner capacitor voltage controller's reference and actual values	212
Figure 7.16 Matrix converter output and input capacitor voltage	213
Figure 7.17 Phase 'a' source current and reactive power drawn from the source	213
Figure 7.18 Speed command, actual speed and electromagnetic torque	214
Figure 7.19 Estimated and reference rotor flux linkages.....	215
Figure 7.20 Source currents commands and actual values	216
Figure 7.21 Actual and reference stator currents	216
Figure 7.22 Inner capacitor voltage controller's reference and actual values	217
Figure 7.23 Phase 'a' source current and reactive power drawn from the source	217
Figure 7.24 Speed command, actual speed and electromagnetic torque	218
Figure 7.25 Estimated and actual rotor flux linkages	219
Figure 7.26 Source currents commands and measured values	219
Figure 7.27 Actual and reference stator currents	220
Figure 7.28 Inner capacitor voltage controller's reference and actual values	220

	Page
Figure 7.29 Matrix converter output and input capacitor voltage	221
Figure 7.30 Phase ‘a’ source current and reactive power drawn from the source	221
Figure 8.1 Controller used to generate the switching signals	224
Figure 8.2 FPGA direct digital syntheses	227
Figure 8.3 Ch1-SaA, Ch2-SbA and Ch3-ScA	228
Figure 8.4 Switching signals for phase ‘a’ output voltage	229
Figure 8.5 Switching signals for phase ‘b’ output voltage	229
Figure 8.6 Switching signals for phase ‘c’ output voltage	230
Figure 8.7 Three phase voltages at the input terminal of MC	231
Figure 8.8: Three phase output voltage of MC	231
Figure 9.1 Block diagram for the experimental set up	238
Figure 9.2 Laboratory prototype 3x3 matrix converter	239
Figure 9.3 Current sensor-FPGA interface board	239
Figure 9.4 Compact cRio-FPGA interfacing board	240
Figure F.1 (a) Single phase inverter leg, (b) carrier signal	327
Figure F.2 Theoretical results based on derived expressions	327
Figure F.3 FFT results-a simulation time of 1/400 times the switching frequency.....	328
Figure F.4 Symmetrical regular sampling.	328
Figure F.5 Asymmetrical regular sampling.	329
Figure F.6 FFT results for natural sampling	330
Figure F.7 FFT results for symmetrical regular sampling	330
Figure F.8 FFT results for asymmetrical regular sampling	331

Figure F.9 Output voltage spectrum with modulation signal containing two non-integer harmonics a and b with $f_o = 50$, $\frac{f_c}{f_o} = 62.5$, $a = 4.5$ and $b = 7.7$	323
Figure F.11 The harmonic spectrum of the voltage under modulation signal given below	325
Figure F.12 Effect of the phase angle of the harmonics on the modulation signals in the linear modulation region.	326
Figure F.13 Effect of phase angle of harmonics in the modulation signal when the carrier frequency ratio is Integer	328

CHAPTER 1

INTRODUCTION

1.1 Introduction

This chapter gives a brief overview on the static AC/AC power frequency conversion structures and introduces the matrix converter (MC), which is the topic of this thesis. This thesis focuses on the modulation schemes, input filter design, modelling and stability analysis of a direct AC/AC three phase to three phase matrix converter feeding a passive load as well as an induction motor. It also presents vector control of a matrix converter fed induction motor. The objectives of this work are clearly described. And finally, the organization of the thesis is presented.

1.2 Overview of Static AC/AC Power Frequency Conversion

The first study of direct AC/AC frequency converters was presented in 1976 by Gyugyi and Pelly [1]. In a general sense, an AC/AC power frequency conversion is the processes of transforming AC power of one frequency to AC power of another frequency. In addition to the capability of providing continuous control of the output frequency relative to the input frequency the power frequency converter provide a continuous control of the amplitude of the output voltage. These converters have inherent bidirectional power flow capability.

The major application of this converter is in variable-speed AC motor drive. Here the converter generates output voltage with continuously variable frequency and amplitude from a fixed frequency and amplitude input AC voltage source for the purpose of controlling the speed of an AC machine. The second application is providing a closely regulated fixed-frequency output from input source of varying frequency. The third major application is as reactive power compensator for an AC system. Here the power frequency converter is used essentially as a continuously variable reactance providing controllable reactive power for the AC system.

Static power frequency converters can be divided in to two main categories. The first type is a two stage power converter with an intermediate DC link called indirect AC/DC/AC power frequency converter. The second type is called a direct AC/AC power frequency converter. This latter type is a one stage power converter which consists basically of an array of semiconductor switches connected directly between the input and output terminals.

1.2.1 Indirect Power Frequency Converter

The most traditional topology for AC/AC power converter is a diode rectifier based pulse width modulated voltage source inverter (PWM-VSI) which is shown in Figure 1.1. This consists of two power stages and an intermediate energy storage element. In the first stage the AC power is converted to uncontrolled DC power by the means of a diode rectifier circuit. The converted DC power is then stored in DC link capacitor.

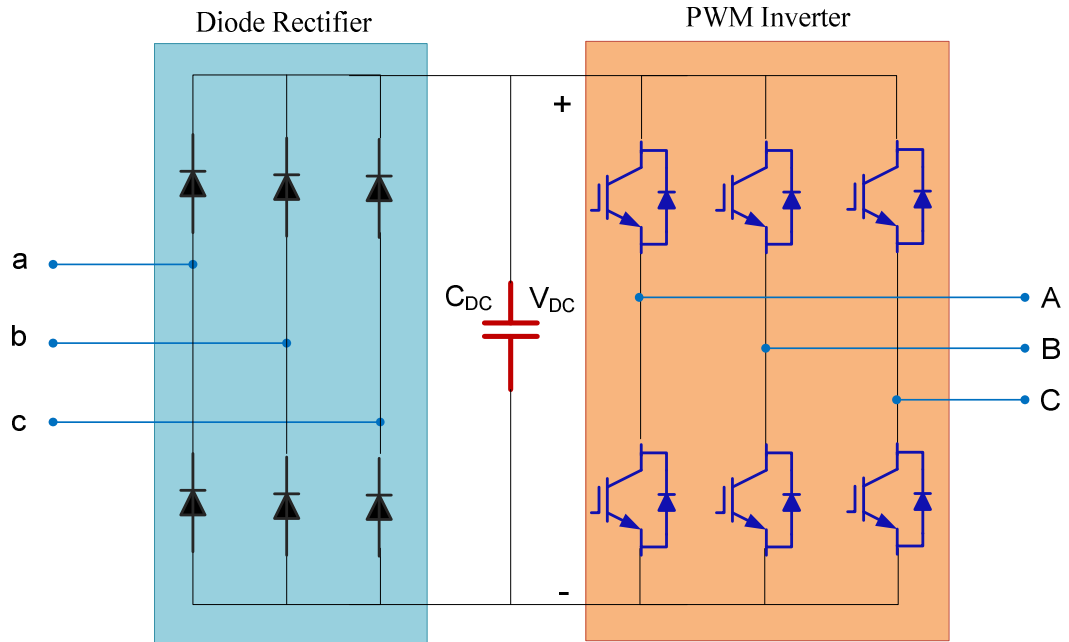


Figure 1.1 Diode rectifier-PWM VSI converter

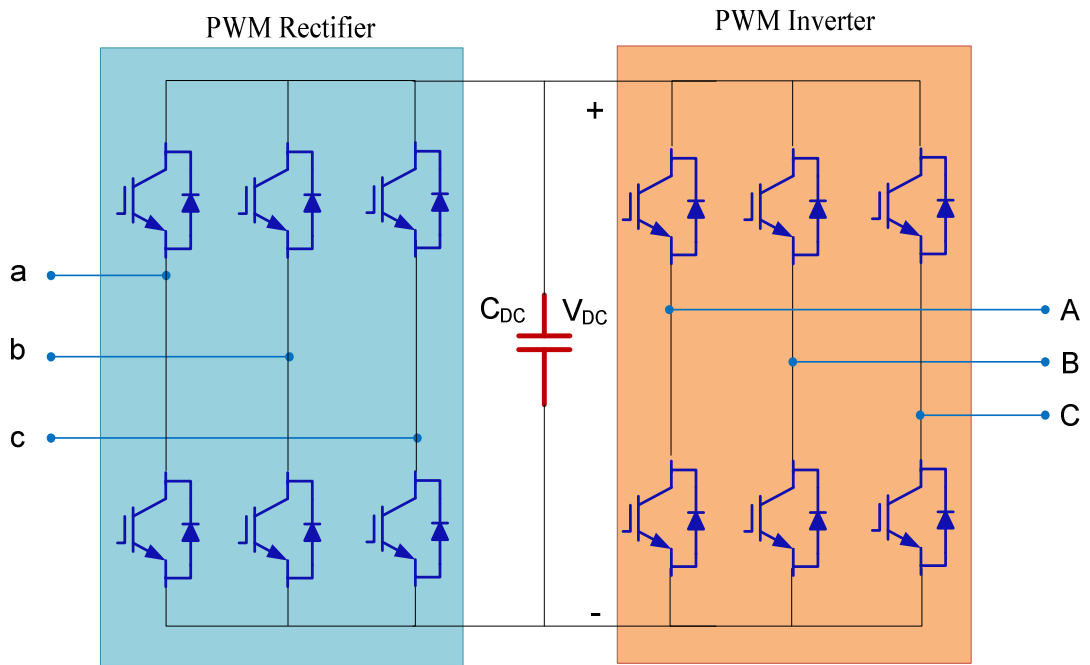


Figure 1.2 PWM rectifier-PWM VSI converter

In the second stage a high frequency switching operated PWM-VSI generates AC signals with arbitrary amplitude and frequency.

Although this type of AC/AC converter is very cost-effective and reliable, it has lots of drawbacks. Due to the uncontrolled operations of diode rectifiers, the current drawn by the rectifier contains a large amount of unwanted harmonics with poor power factor. The other topology for AC/AC power converter replaces the diode bridge with PWM rectifier resulting in a back-to-back converter as shown in Figure 1.2. This converter overcomes the input harmonic problem of the former topology.

1.2.2 Direct AC/AC Converter

The direct AC/AC converter provides a direct connection between the input and output terminals without an intermediate energy storage element through an array of semiconductor switches. A direct converter can be identified as three distinct topological approaches. The first and simplest topology can be used to change the amplitude of an AC waveform. It is known as an ac controller and functions by simply chopping symmetric notches out of the input waveform. The second can be utilized if the output frequency is much lower than the input source frequency. This topology is called a cyclo-converter, and it approximates the desired output waveform by synthesizing it from pieces of the input waveform. The last is the matrix converter and it is most versatile without any limits on the output frequency and amplitude. It replaces the multiple conversion stages and the intermediate energy storage element by a single power conversion stage, and uses a matrix of semiconductor bidirectional switches,

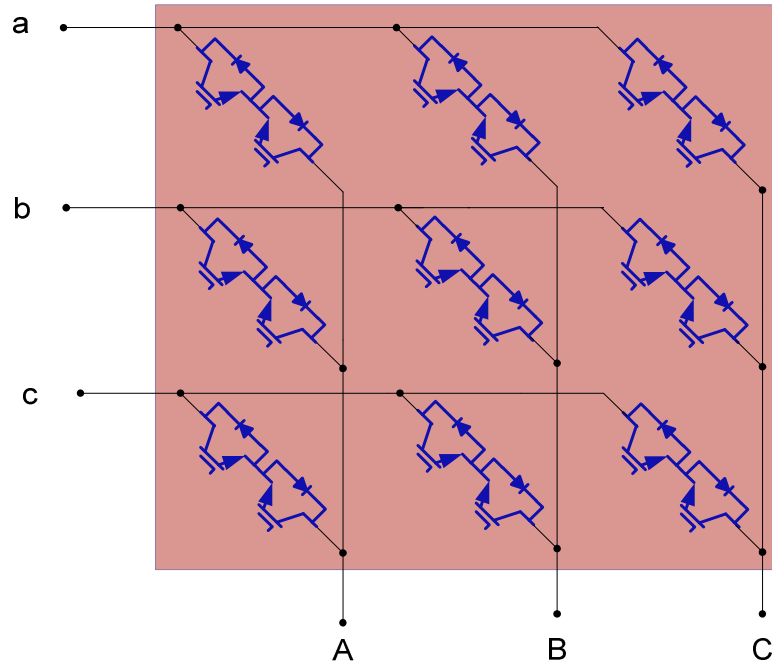


Figure 1.3 Direct three phase-to-three phase matrix converter

There are many advantages presented by the matrix converter compared to the indirect power frequency converters. The main features of matrix converter are the following [1-20].

- Unlike naturally commutated cyclo-converters, the output frequency of a MC can be controlled in wide ranges which can be higher or lower than the input frequency.
- MC does not have the large energy storage element which results in a compact power circuit. This makes MC attractive for applications demanding compact size.
- For the matrix converter, input power factor can be controlled for any output load. Hence, unity power factor control can be easily realized
- It has inherent bidirectional power flow capability

- MC has a sinusoidal input current and output voltage.
- It has found utility in high temperature, high vibration and low volume/weight applications such as aerospace

However, it has the following disadvantages

- Although the absence of the DC link capacitor makes the converter compact, it decreases the maximum amplitude of the output voltage to be 86.67% of the input voltage amplitude.
- Relatively large number of semiconductor switches and driver circuits are required compared to AC/DC/AC converter. The MC requires 18 IGBTs (Insulated Gate Bipolar Transistor) and 18 fast recovery diodes where as the indirect converter only require 12 IGBTs and 12 fast recovery diodes. Therefore, this increases the cost of the converter and affects the overall system reliability.

1.3 Objectives of the Thesis

The major objectives of the thesis are as follows

- To adapt space vector modulation, both direct and indirect space vector modulations, and carrier based pulse width modulation techniques on a three phase-to-three phase matrix converter.
- To design an input filter based on the Fourier series analysis of the switching signals.

- To examine the transient and steady state response of a matrix converter feeding a passive load as well as induction motor along with the interaction between the interaction between the input and outputs through this converter.
- To derive a generalized steady state performance analysis which can be used for unity as well as non-unity input power factor operations.
- To examine the different factors which affect the stability of a matrix converter fed induction motor drives.
- To develop a control scheme which consists of vector control for a MC fed induction motor and input unity power factor regulation.

1.4 Thesis Outline

This thesis is categorized in nine chapters. Chapter 1 presents the overview of an AC/AC power frequency converter. The different topologies of indirect AC/AC converters along with the operational principles and features are introduced. The drawbacks and limitations of these topologies are also included. The matrix converter topology and operations are presented. Detailed comparisons between the indirect and direct AC/AC converters are also included. This chapter also gives clear research objectives of the thesis followed by the organization of the thesis. Then, reviews of previous work for the matrix converter are addressed in chapter 2.

In chapter 3, both space vector and carrier based pulse width modulation techniques for the most known three phase-to-three phase matrix converter are derived and presented in detail. The space vector modulation techniques are analyzed into two categories, direct and indirect space vector approaches. The generation of the actual switching pulses from the modulation signals are demonstrated.

Design of an input filter for a matrix converter system are presented in chapter 4 along with complete step by step derivation for Fourier representation of switching signals of the MC. The methods used in this thesis are based on the maximum allowable source current and input capacitor voltage ripple as well as the stability of the overall system.

Chapter 5 presents the complete dynamic modelling of MC fed induction motor and a MC connected to a linear RL load. Simulations are done in both cases to examine the transient and steady state response of the overall system. Generalized steady state formulations are also presented considering both cases which helps to analyze the system operating in both unity and non-unity input power factor operations. This chapter also includes the computer simulation results of dynamic and steady state performance characteristics and it also provides comparisons between these two results.

In chapter 6, a new generalized model for stability analysis for a MC fed induction motor based on small signal modeling is proposed. This approach considers the analysis when the drive system operates at unity as well as non-unity input power factor at the source side. With the help of this model, different factors which affect the matrix converter stability are analyzed including stator and rotor resistance variation due to motor heating and the impact of non-zero reactive power at the source side. Computer

simulations are carried out to verify theoretical analysis on stability as well as on the steady state performance characteristics.

A high performance vector control of matrix converter fed induction motor is presented in chapter 7. In this chapter, an indirect rotor field oriented control (FOC) is developed along with unity power factor control in the source side. The chapter also includes a thorough controller designs and non-linear feedback linearization techniques as the overall system is nonlinear. A proposed control scheme is verified using computer simulation. Results are also included which verify the controllers' robustness.

Chapter 8 gives a brief overview on the progress in the experimental results is presented. The actual nine switching signals are generated with an NI instruments compact RIO in a LabVIEW FPGA environment. The validity of these signals is proved using a computer simulation.

Finally, the concluding remarks and summary of the work is presented in chapter 9. Moreover, the contributions of this research work and future suggestions are included in this chapter.

CHAPTER 2

LITERATURE REVIEW

A survey of literature reviews related to this thesis is presented in this chapter. The chapter consists of four sections. In the section 2.1, the different modulation strategies for matrix converter are reviewed. Section 2.2 discusses a survey of input filter design techniques developed for this converter. The works done related to the stability of a matrix converter system are presented in section 2.3. Finally in section 2.4, existing control methods for the matrix converter are described.

2.1 Modulation Strategies

It is very important to study the modulation strategies of a matrix converter because the actual firing pulses of the nine bidirectional switches are generated through these appropriate modulation signals [75,81]. Modulation methods of matrix converter are complex and are generally classified in two different groups, the carrier-based (duty-cycle) modulation and the space-vector modulation (SVM). A first solution has been proposed in [2] obtained by using the duty-cycle approach. This strategy allows the control of the output voltages magnitude and frequency and input power factor. The maximum voltage transfer ratio of this modulation scheme is limited to 0.5. A solution which improves maximum voltage transfer ratio to 0.866 has been presented in [3] by including a third harmonics of the input and output voltage waveforms into the

modulation signals. As demonstrated in [4], the inclusion of only input third harmonics improves the maximum ratio to 0.75 and further inclusion of output third harmonic lead to the maximum possible voltage ratio. It is necessary to note that this value is a theoretical maximum voltage transfer ratio of a three phase-to-three phase matrix converter under balanced input and output voltages under unity power factor at the input of the matrix converter. This output voltage-to-input voltage transfer ratio is greatly decreased when the converter operates at non-unity power factor. However, the improvement in the range of operation of a matrix converter under non-unity power factor is presented in [67]. These duty cycle approaches in matrix converter are further investigated for voltage source and current source converters [5].

The second type of modulation technique is Space Vector Modulation (SVM) which can be further categorized into direct and indirect SVM. The indirect SVM approach, which is first implemented in [6], introduces an imaginary dc link which fictitiously divides the matrix converter into a rectifier and an inverter stages. A generalized PWM technique based on indirect SVM is implemented in [27] which permits independent control of the input current and output voltage and the detailed techniques of implementation is presented in [28]. However, the direct SVM compresses the modulation process since it does not need imaginary dc link. Besides, direct SVM gives the maximum possible voltage transfer ratio with the addition of the third-harmonic components which is first implemented in [7]. A general and complete solution to the problem of the modulation strategy of three phase-to-three phase matrix converters is presented in [26]. In [29], performance evaluations of these modulation schemes along with a loss reduced space vector approach are presented.

Recently, a new modulation strategy that improves the control range of the matrix converter is presented in [21]. This strategy can be used to improve the performance of the matrix converter to compensate the reactive power of the input filter capacitor whenever is needed, or just to increase the voltage margin of an electric drive.

A space vector modulation strategy for matrix converter has been modified for abnormal input-voltage conditions, in terms of unbalance, non-sinusoid, and surge. As presented in [83], this modified modulation strategy can eliminate the influence of the abnormal input voltages on output side without an additional control circuit, and three-phase sinusoidal symmetrical voltages or currents can be obtained under normal and abnormal input-voltage conditions.

In [84], a general form of the modulation functions for matrix converters is derived using geometric transformation approach. This paper considers a matrix converter as generalized three-level inverters to apply the double-carrier-based dipolar modulation technique of the three-level inverter to the matrix converter.

2.2 Input Filter Design

The input filter in matrix convert is needed to mitigate undesired harmonic components from injecting into the AC main line [48-56]. These undesired harmonics are generated due to the high frequency switching of the matrix converter. On the other hand, this filter smoothen the input current and input capacitor voltage ripples to meet the electro-magnet interference (EMI) requirements [51]. A single stage LC filter is the most

commonly used filter topology since it is simple, low cost and reduced size as compared to multi-stage and integrated filter topologies. However, the multi-stage topology provides a better harmonic attenuation at the switching frequency [54]. The input filter has to be designed to meet the following requirements [48-52]:

- The cut-off frequency of the filter should be lower than the switching frequency and higher than the fundamental frequency of the input AC source.
- The input power factor should be kept maximum for a given minimum output power.
- The lowest volume and/or weight of capacitor and chokes is used.
- The voltage drop in the inductor should be minimum.
- The filter parameters should disturb the overall system stability.

The procedure to specify the value of the filter capacitor and inductor is presented in detail in [50-51]. The existence of the filter circuit dominantly induces capacitive reactive power in the line resulting in lower input power factor. This effect becomes more significant at low power operation [51]. Therefore, the maximum value of the capacitor is first determined based on the minimum power factor requirement at a given minimum output power operation. The value of the minimum power factor is specified to be 0.8 in [50-51] and 0.85 in [52] at 10% rated power operation, although there is no standard value for it. Once the capacitor value is known, the filter inductor is determined based on the chosen characteristic frequency. In [79], the study of different switching strategies has been compared in terms of the rms value of the line current ripple and the result can be used for input filter design.

This approach gives only the maximum value of capacitor. The lower the capacitance, the higher the input power factor. However, lower capacitance leads to higher ripple input voltage and current. Similar to the maximum capacitance specification, it is necessary to determine the minimum required capacitor value corresponding to the maximum ripple voltage or current.

Recently, an integrated analytical approach towards filter design for a three phase matrix converter is reported in [85]. This design method addresses both general filter design aspects like attenuation, regulation and also MC-specific issues like the damping resistors at the input filter.

2.3 Stability Analysis of a Matrix Converter System

It is reported that the input filter can be one of the elements which possibly leads to instability operation in MC system [11]; for this reason several works related to stability issues are addressed using small signal and large signal modeling [7-12]. In [8], it has been shown that filtering the input capacitor voltage has an impact on the stability of the converter. In addition, independent filtering of the angle and the magnitude of this input voltage has significantly improved the stability as presented in [10]. The stability of the MC is also influenced by the grid impedance, filter inductances and capacitance and filter time constants as intensively discussed in [10].

One of the contributions of this thesis is the presentation of a new approach of stability analysis which does not make any assumptions on the phase angle of the input capacitor voltage and reference output voltage. In the small signal analysis presented in

[39-44], the phase angle of the capacitor voltage and reference output voltage are arbitrarily chosen to be zero which masks the effect of these angles on the stability of the system. In addition, arbitrarily choosing the phase angle of the capacitor voltage makes it impossible to operate at unity power factor at the source side. Therefore, it is essential to investigate the effect of this angle on the stability of the system. This thesis also presents a generalized steady state and small signal modeling which can be used for both zero and non-zero reactive power at the source side. As the matrix converter may be used for reactive power compensation, with the help of this model, the impact of non-zero reactive power on the overall system stability is also presented. Since stator and rotor resistances may vary up to 100% and 50%, respectively because of rotor heating [74], this work also includes the influence of these stator and rotor resistances variation on the system stability. Although [39] reported that adding a damping resistance across the input filter inductor increases the power limit of the stable operation, this thesis in particular clearly shows the effect of this variation in detail.

2.4 Control of Matrix Converter Drive System

Variable ac drives have been used in the past to perform relatively undemanding roles [77]. Vector control technique incorporating high performance processors and DSPs have made possible the application of induction motor and synchronous motor drives for high performance applications where traditionally only dc drives were applied. Induction motor drives fed by MC have been developed for the last decades [47]. The matrix converter drive can theoretically offer better advantages over the traditional voltage

source inverter based drives. The main advantages that are often cited are the compactness, the bidirectional power flow capability and the higher current quality [67].

A new and relatively simple sensorless control for induction motor drives fed by matrix converter using the imaginary power flowing to the motor and the constant air gap flux is proposed in [47]. This scheme was independent of the parameters and employs a non linear compensation strategy to improve the performance of the speed control in the low speed region. In [81], an improvement on the performance of the direct torque control for matrix converter driven interior permanent magnet synchronous machine drive was studied in detail. This is realized through the modified hysteresis direct torque control in [80] and the associated problems with this control are also investigated.

Induction machines are widely used in the industrial drive system due to its various advantages over other machines as regards to price, size, robustness, etc [62-64, 77]. They are very suitable for constant speed applications; however, the controller algorithms become more complex when used for variable speed drive [63]. Due to the great advancement of power electronics and digital signal processing, they also offer a high performance as well as independent control on torque and flux linkages, which is similar to that of the DC machine. There are various control schemes available for induction machine drives like scalar control, direct torque control, vector control and adaptive control [77].

The scalar control is a simple and robust type of control which only considers the magnitude variation of the machine variables and ignores the coupling effect that exists in the machine [63]. The commonly used scalar control is Volt/Hertz control. In this scheme the ratio of the applied voltage and frequency must be constant to maintain a

constant air gap flux. Generally, such control schemes are only implemented for low performance application.

The vector control is a widely used control approach for high performance induction machine applications [77]. Unlike scalar control, both amplitude and phase of the AC excitation are the control variables. Vector control of the voltages and currents results in the control of the spatial orientation of the electromagnetic fields in the machine, leads to field orientation. Field orientation control (FOC), consists of controlling the stator current represented by a vector. The control is based on projections which transform a three phase time and speed dependent system into a two co-ordinate time invariant system. This projection leads to a structure similar to that of a dc machine control. However, this requires information about magnitude and position of rotor flux vector. A vector control can be further categorized into a direct and indirect FOC, depending on the how the rotor flux position is determined. If the rotor flux is directly evaluated, the control is called a direct FOC. In indirect FOC, the stator currents are used to calculate the instantaneous slip frequency which later be integrated and added to the measured rotor position to give a better estimation of flux vector position. The indirect FOC can be further classified into rotor flux, stator flux and air gap flux oriented control. In rotor flux oriented control, the rotor flux vector is aligned in d-axis of synchronously rotating reference frame. Therefore, the q axis rotor flux is zero.

In this thesis, the indirect rotor field oriented control for matrix converter fed induction machine with unity input power factor control is presented to realize the high performance control of the drive.

Recently, the most common control and modulation strategies are briefly reviewed in [75]. The paper used the theoretical complexity, quality of load current, dynamic response and sampling frequency as a measure of performance of different control strategies. These control strategies include direct torque control (DTC), predictive current and torque control. As reported in [75], predictive control is the best alternatives due to its simplicity and flexibility to include additional aspects in the control. However, the author finally concluded that it is not possible to establish which method is the best. In [14], the model based predictive control (MPC) targeted to obtain low-distortion input currents, controlled power factor and high performance drive even when the source contains disturbances. Basically it applied to establish a method to control the current of an induction machine. Besides it allows the control of the input current and reactive power to the system.

Simulation plays a relevant role in the analysis and design of modern power systems and power electronics converters. A unique method of matrix converter simulation technique called Switching State Matrix Averaging (SSMA) is presented in [82]. This technique drastically speeds up the simulation and provides a possibility of simulating even more complex systems which would not be possible within a reasonable time frame in a conventional computer.

CHAPTER 3

MODULATION TECHNIQUES

3.1 Introduction

This chapter presents the two modulation strategies used for the direct matrix converter. Complete derivation of the modulation signals for the carrier based modulation is given in section 3.2. Both direct and indirect space vector approaches are also presented in this chapter. The improvement in the voltage transfer ration of a matrix converter using a third harmonic injection is illustrated. A methodology for generation of the actual firing pulses of the bidirectional switches is demonstrated. Computer simulation has also be done to verify the theoretical modulation technique and results demonstrate the generation of the switching signals which synthesize the balanced set of output three phase voltages.

3.2 Carrier Based Modulation

A typical three phase-to-three phase matrix converter consisting of nine bidirectional switches is shown in Figure 1.1. The switching function of the bi-directional switch connecting the input phase i to output phase j is denoted by S_{ij} . The relevant existence switching function S_{ij} ($i = ap, bp, cp$, and $j = as, bs, cs$) defines the states of the bi-directional switches.

When the switch is turned ON the switching function $S_{ij} = 1$, and when turned OFF, the switching function $S_{ij} = 0$. There are two requirements must be fulfilled at any time during switching [59, 79]. The input voltages of the MC should not be short circuited; therefore, all three switches connected to an output phase voltage must not be turned ON at the same time. The second requirement is that there should be always a path for the output current; in other word, the output line must be connected all the time to a single input line.

$$\begin{aligned}
S_{aA} + S_{bA} + S_{cA} &= 1 \\
S_{aB} + S_{bB} + S_{cB} &= 1 \\
S_{aC} + S_{bC} + S_{cC} &= 1
\end{aligned} \tag{3.1}$$

The mapping of the input phase voltages and output phase voltages of the converter are given as:

$$\begin{aligned}
V_{as} + V_{pn} &= V_{ap} S_{aA} + V_{bp} S_{bA} + V_{cp} S_{cA} \\
V_{bs} + V_{pn} &= V_{ap} S_{aB} + V_{bp} S_{bB} + V_{cp} S_{cB} \\
V_{cs} + V_{pn} &= V_{ap} S_{aC} + V_{bp} S_{bC} + V_{cp} S_{cC}
\end{aligned} \tag{3.2}$$

Given the converter three phase input voltages, V_{ap} , V_{bp} and V_{cp} the expressions for the switching functions S_{ij} are to be determined with the specification of the desired three phase output voltages, V_{as} , V_{bs} and V_{cs} . And the V_{pn} is a zero sequence voltage between the neutral point of input capacitor voltage, p , and output voltage's neutral point, n . Equations (3.1) and (3.2) can be written in matrix form as given below.

For two vectors X and Y related by a non-square matrix A as given in (1.4), X can be expressed in terms of Y by inverting the fat matrix [60] by minimizing the sum of the squares of all the elements of X.

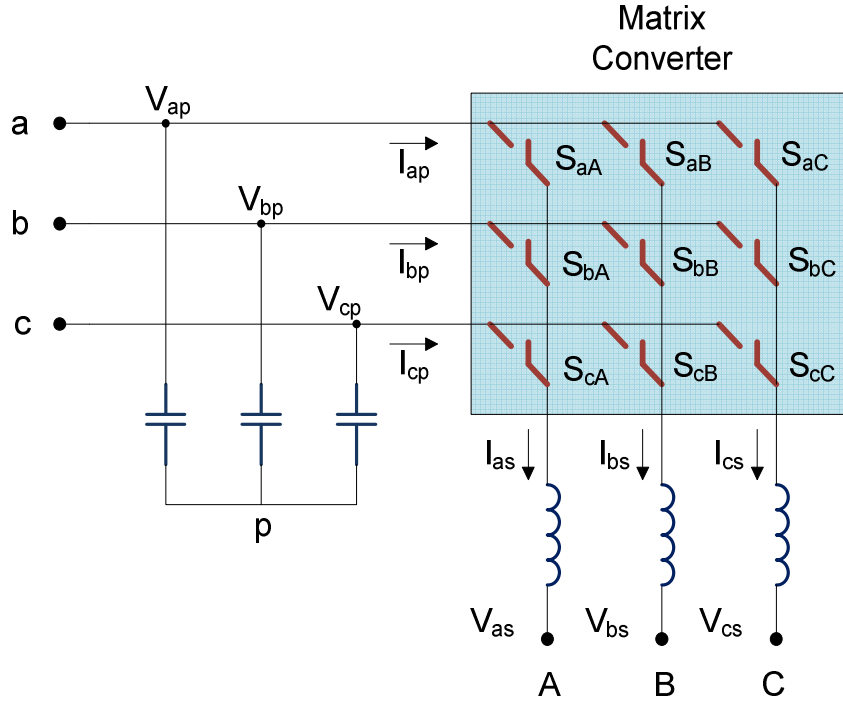


Figure 3.1 A schematics of a simplified matrix converter

The inverse of the underdetermined equation can be calculated as follows.

$$AX = Y \tag{3.4}$$

$$X = A^T (AA^T)^{-1} Y \tag{3.5}$$

$$\underbrace{\begin{bmatrix} V_{ap} & V_{bp} & V_{cp} & 0 & 0 & 0 & 0 & 0 & 0 \\ 0 & 0 & 0 & V_{ap} & V_{bp} & V_{cp} & 0 & 0 & 0 \\ 0 & 0 & 0 & 0 & 0 & 0 & V_{ap} & V_{bp} & V_{cp} \\ 1 & 1 & 1 & 0 & 0 & 0 & 0 & 0 & 0 \\ 0 & 0 & 0 & 1 & 1 & 1 & 0 & 0 & 0 \\ 0 & 0 & 0 & 0 & 0 & 0 & 1 & 1 & 1 \end{bmatrix}}_A \underbrace{\begin{bmatrix} S_{aA} \\ S_{bA} \\ S_{cA} \\ S_{aB} \\ S_{bB} \\ S_{cB} \\ S_{aC} \\ S_{bC} \\ S_{cC} \end{bmatrix}}_X = \underbrace{\begin{bmatrix} V_{as} + V_{pn} \\ V_{bs} + V_{pn} \\ V_{cs} + V_{pn} \\ 1 \\ 1 \\ 1 \end{bmatrix}}_Y \tag{3.3}$$

The average switching functions are determined as shown in (3.6). It is necessary to note that V_{no} is the average of V_{pn} . This expression is general and applied for both balanced and unbalanced input voltage.

$$\langle S_{ij} \rangle = k_1 (V_{js} + V_{no}) (3V_{ip} - (V_{ap} + V_{bp} + V_{cp})) - k_1 (V_{ap} + V_{bp} + V_{cp}) V_{ip} + k_2 \quad (3.6)$$

where the k_1 and k_2 are defined in (3.7)

$$k_1 = \frac{1}{2(V_{ap}^2 + V_{bp}^2 + V_{cp}^2 - V_{ap}V_{bp} - V_{bp}V_{cp} - V_{cp}V_{ap})} \quad (3.7)$$

$$k_2 = \frac{V_{ap}^2 + V_{bp}^2 + V_{cp}^2}{2(V_{ap}^2 + V_{bp}^2 + V_{cp}^2 - V_{ap}V_{bp} - V_{bp}V_{cp} - V_{cp}V_{ap})}$$

For balanced three phase input voltages and using trigonometric relations, the averaged switching signals expressions are simplified as given in (3.8).

Therefore, the modulation signal which is the approximation of the switching signals is determined.

$$\begin{bmatrix} V_{ap} \\ V_{bp} \\ V_{cp} \end{bmatrix} = V_p \begin{bmatrix} \cos(\omega_p t) \\ \cos(\omega_p t - \frac{2\pi}{3}) \\ \cos(\omega_p t + \frac{2\pi}{3}) \end{bmatrix} \quad (3.8)$$

where V_p and ω_p is the peak of input phase voltage and input angular frequency, respectively.

$$k_1 = \frac{2}{9V_p^2} \text{ and } k_2 = \frac{1}{3} \quad (3.9)$$

$$\langle S_{ij} \rangle = M_{ij} = \frac{1}{3} + \frac{2V_{ip}}{3V_p^2} (V_{js} + V_{no}) \quad (3.10)$$

These expressions of modulation signal are the same as the expression given in [8]. These give a more convenient for practical implementation. In (10), in the absence of the neutral voltage, the output to input voltage ratio (q) is 50% which has a little drawback in real applications. The voltage transfer ratio can be improved to 75% by adding a neutral voltage, third harmonic of the input voltage, on the desired output voltage [4].

$$V_{no} = \frac{V_p}{4} \cos(3\omega_p t) \quad (3.11)$$

This voltage ratio can further be improved to 86.7%, maximum voltage gain possible for three phase-to-three phase matrix converter, by injecting an additional third harmonic of the output voltage which results in an expression neutral voltage expression given in (3.12). V_s

and ω_s is the magnitude of output phase voltage and output angular frequency, respectively.

$$V_{no} = \frac{V_p}{4} \cos(3\omega_p t) - \frac{V_s}{6} \cos(3\omega_s t) \quad (3.12)$$

Figure 1.2 demonstrates the effect of adding a neutral voltage improves the voltage transfer ratio considering input balanced three phase voltage with amplitude of 1pu. The envelope is determined using the instantaneous maximum and minimum input voltages. If the output voltage is out of this envelope is known as over modulated. Without neutral voltage, the output voltage cannot exceed 0.5 pu in the linear modulation region. With the addition of a third harmonic of an input voltage, as seen in Figure 1.2b the output voltage can be increased up to 0.75 pu and still inside the envelope. Figure 1.2c shows the practical maximum voltage transfer limit of 0.87 using the neutral voltage expression given in (3.12).

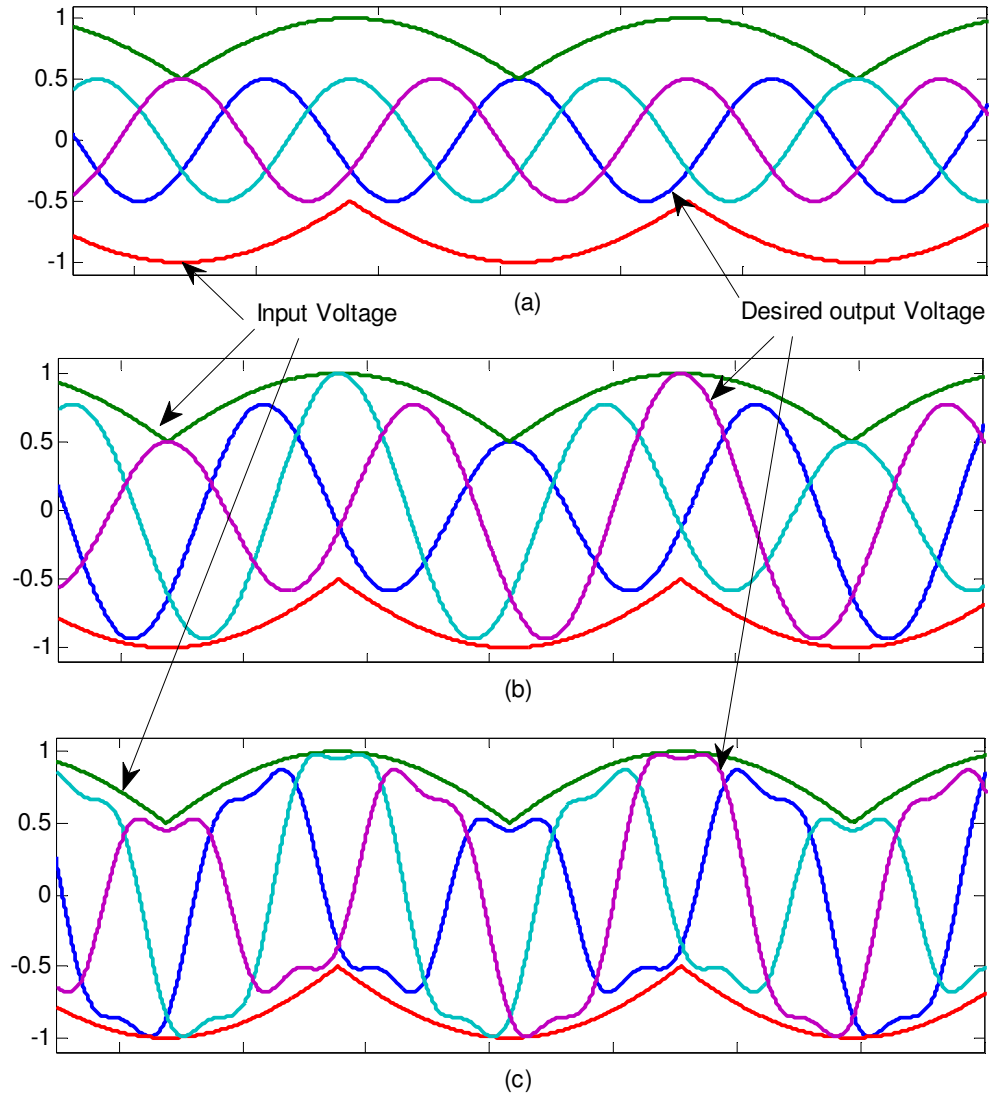


Figure 3.2: Illustration of voltage ratio of a) 50%, (b) 75% and (c) 86.7%

3.2.1 Switching Signal Generations

The actual switching pulses are generated by using the modulation signals obtained using (3.10) with a high frequency triangular carrier signal.

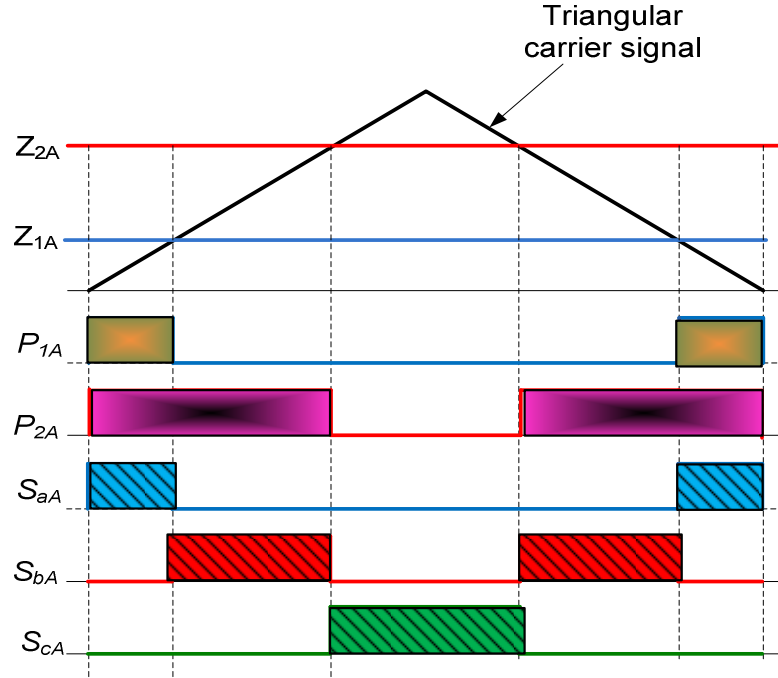


Figure 3.3 Generation of switching pulses for phase 'a'

Generating the three switching signals for a phase 'j' output voltage involves two intermediate signals. Z_{1j} , Z_{2j} and Z_{3j} are the signals compared with the triangular carrier and calculated from the modulation signals using (3.13).

$$\begin{aligned}
 Z_{1j} &= M_{aj} \\
 Z_{2j} &= M_{aj} + M_{bj} \\
 Z_{3j} &= M_{aj} + M_{bj} + M_{cj} = 1
 \end{aligned}
 \tag{3.13}$$

After comparing the above signals with the triangular waveform, three intermediate pulses P_{1j} , P_{2j} and P_{3j} are generated. The sum of the three modulation signals which produce an output phase 'j' voltage is 1 the pulse P_{3j} is always ON.

$$\begin{aligned}
P_{1j} &= \begin{cases} 1; \text{if } Z_{1j} > \text{Triag} \\ 0; \text{if } Z_{1j} < \text{Triag} \end{cases} \\
P_{2j} &= \begin{cases} 1; \text{if } Z_{2j} > \text{Triag} \\ 0; \text{if } Z_{2j} < \text{Triag} \end{cases} \\
P_{3j} &= 1
\end{aligned} \tag{3.14}$$

Finally, the actual switching signals are determined from (3.15) where $\overline{P_{1A}}$ a complement of is P_{1A} .

$$\begin{aligned}
S_{aj} &= P_{1j} \\
S_{bj} &= \overline{P_{1j}} P_{2j} \\
S_{cj} &= \overline{P_{1j}} \overline{P_{2j}}
\end{aligned} \tag{3.15}$$

Figure 1.3 shows the switching functions S_{aA} , S_{bA} and S_{cA} generated using the algorithm explained above. These pulses are used to construct output phase ‘a’ voltage and using the similar approaches the other six switching signals are found for phase ‘b’ and phase ‘c’ output voltages.

3.3 Space Vector Modulation

3.3.1 Direct Space Vector modulation

The second type of modulation technique is called space vector modulation and it has the following advantages over the carrier based modulation [12]:

- maximum voltage transfer ratio without utilizing the third harmonic component injection method
- accommodate any input power factor independent of the output power factor
- reduce the effective switching frequency in each cycle, and thus the switching losses
- minimize the input current and output voltage harmonics

The space vector modulation technique is based on instantaneous output voltage and input current vectors representation. There are 27 possible switching configuration states. However, only 21 can be usefully employed in space vector algorithm. As seen in Table 3.1, these switching states are classified into three categories:

Group I: All output terminals are connected to a particular input phases. For example: mode AAA: all output terminals connected to input phase a voltage. These results in a zero space vectors, hence, they are also called zero switching states.

Group II: Each output terminal is connected to a different input terminal. For example, mode BAC- phase 'a' output connected to phase 'b' input voltage, phase 'b' output with phase 'a' input and phase 'c' output with phase 'c' input. As observed in Table 1.1, these space vectors have constant amplitudes and rotate at the input frequency. Therefore, these modes cannot be used to synthesize the reference vectors.

Group III: this group consists of 18 switching configurations and the two output terminals are connected to one input terminal, and the third output terminal is connected to one of the other input terminals. The space vectors have time varying amplitude which depends up on the instantaneous input line-to-line voltages or output currents.

Table 3.1 Possible output voltage space vectors

	Mode	S_{ap}	S_{bp}	S_{cp}	V_{as}	V_{bs}	V_{cs}	V_{qs}	V_{ds}	V_s	α_s
Group I	AAA	0	0	0	V_{ap}	V_{ap}	V_{ap}	0	0	0	-
	BBB	1	1	1	V_{bp}	V_{bp}	V_{bp}	0	0	0	-
	CCC	2	2	2	V_{cp}	V_{cp}	V_{cp}	0	0	0	-
Group II	ABC	0	1	2	V_{ap}	V_{bp}	V_{cp}	V_{ap}	$-1/\sqrt{3}V_{bcp}$	V_p	$\omega_p t$
	ACB	0	2	1	V_{bp}	V_{cp}	V_{bp}	V_{ap}	$1/\sqrt{3}V_{bcp}$	V_p	$-\omega_p t$
	BAC	1	0	2	V_{bp}	V_{ap}	V_{cp}	V_{bp}	$1/\sqrt{3}V_{cap}$	V_p	$-\omega_p t + 2\pi/3$
	BCA	1	2	0	V_{bp}	V_{cp}	V_{ap}	V_{bp}	$-1/\sqrt{3}V_{cap}$	V_p	$\omega_p t - 2\pi/3$
	CAB	2	0	1	V_{cp}	V_{ap}	V_{bp}	V_{cp}	$-1/\sqrt{3}V_{abp}$	V_p	$-\omega_p t - 2\pi/3$
	CBA	2	1	0	V_{cp}	V_{bp}	V_{ap}	V_{cp}	$1/\sqrt{3}V_{abp}$	V_p	$\omega_p t + 2\pi/3$
Group III	AAB	0	0	1	V_{ap}	V_{ap}	V_{bp}	$1/3V_{abp}$	$-1/\sqrt{3}V_{abp}$	$2/3V_{abp}$	$\pi/3$
	AAC	0	0	2	V_{ap}	V_{ap}	V_{cp}	$-1/3V_{cap}$	$1/\sqrt{3}V_{cap}$	$2/3V_{cap}$	$-2\pi/3$
	ABA	0	1	0	V_{ap}	V_{bp}	V_{ap}	$1/3V_{abp}$	$1/\sqrt{3}V_{abp}$	$2/3V_{abp}$	$-\pi/3$
	ABB	0	1	1	V_{ap}	V_{bp}	V_{bp}	$2/3V_{abp}$	0	$2/3V_{abp}$	0
	ACA	0	2	0	V_{bp}	V_{cp}	V_{ap}	$-1/3V_{cap}$	$-1/\sqrt{3}V_{cap}$	$2/3V_{cap}$	$2\pi/3$
	ACC	0	2	2	V_{bp}	V_{cp}	V_{cp}	$-2/3V_{cap}$	0	$2/3V_{cap}$	π
	BAA	1	0	0	V_{bp}	V_{ap}	V_{ap}	$-2/3V_{abp}$	0	$2/3V_{abp}$	π
	BAB	1	0	1	V_{bp}	V_{ap}	V_{bp}	$-1/3V_{abp}$	$-1/\sqrt{3}V_{abp}$	$2/3V_{abp}$	$2\pi/3$
	BBA	1	1	0	V_{bp}	V_{bp}	V_{ap}	$-1/3V_{abp}$	$1/\sqrt{3}V_{abp}$	$2/3V_{abp}$	$-2\pi/3$
	BBC	1	1	2	V_{bp}	V_{bp}	V_{cp}	$1/3V_{bcp}$	$-1/\sqrt{3}V_{bcp}$	$2/3V_{bcp}$	$\pi/3$
	BCB	1	2	1	V_{bp}	V_{cp}	V_{bp}	$1/3V_{bcp}$	$1/\sqrt{3}V_{bcp}$	$2/3V_{bcp}$	$-\pi/3$
	BCC	1	2	2	V_{bp}	V_{cp}	V_{cp}	$2/3V_{bcp}$	0	$2/3V_{bcp}$	0
	CAA	2	0	0	V_{cp}	V_{ap}	V_{ap}	$2/3V_{cap}$	0	$2/3V_{cap}$	0
	CAC	2	0	2	V_{cp}	V_{ap}	V_{cp}	$1/3V_{cap}$	$1/\sqrt{3}V_{cap}$	$2/3V_{cap}$	$-\pi/3$
	CBB	2	1	1	V_{cp}	V_{bp}	V_{bp}	$-2/3V_{bcp}$		$2/3V_{bcp}$	π
	CBC	2	1	2	V_{cp}	V_{bp}	V_{cp}	$-1/3V_{bcp}$	$-1/\sqrt{3}V_{bcp}$	$2/3V_{bcp}$	$2\pi/3$
	CCA	2	2	0	V_{cp}	V_{cp}	V_{ap}	$1/3V_{cap}$	$-1/\sqrt{3}V_{cap}$	$2/3V_{cap}$	$\pi/3$
	CCB	2	2	1	V_{cp}	V_{cp}	V_{bp}	$-1/3V_{bcp}$	$1/\sqrt{3}V_{bcp}$	$2/3V_{bcp}$	$-2\pi/3$

The directions of these vectors are stationary and occupy six positions equally spaced by 60° in qd reference frame. To determine the space vector switching strategy, consider a balanced sinusoidal input and desired output three phase voltages.

$$\begin{bmatrix} V_{ap} \\ V_{bp} \\ V_{cp} \end{bmatrix} = V_p \begin{bmatrix} \cos(\omega_p t) \\ \cos(\omega_p t - \frac{2\pi}{3}) \\ \cos(\omega_p t + \frac{2\pi}{3}) \end{bmatrix} \quad (1.16)$$

$$\begin{bmatrix} V_{as} \\ V_{bs} \\ V_{cs} \end{bmatrix} = V_s \begin{bmatrix} \cos(\omega_s t) \\ \cos(\omega_s t - \frac{2\pi}{3}) \\ \cos(\omega_s t + \frac{2\pi}{3}) \end{bmatrix} \quad (3.17)$$

The output voltage space vector \overline{V}_s , can be resolved into two q- and d-axes. V_{qs} and V_{ds} are the *q*-axis and *d*-axis components of the output voltage space vector which can be found using stationary *qd* transformation.

$$\overline{V}_s = V_{qs} + jV_{ds} \quad \begin{bmatrix} V_{qs} \\ V_{ds} \end{bmatrix} = \frac{3}{2} \begin{bmatrix} 1 & -\frac{1}{2} & -\frac{1}{2} \\ 0 & -\frac{\sqrt{3}}{2} & \frac{\sqrt{3}}{2} \end{bmatrix} \begin{bmatrix} V_{as} \\ V_{bs} \\ V_{cs} \end{bmatrix}$$

The transformation used is a stationary reference frame. The two axes voltages are used to determine the magnitude and angle of the output space vector.

$$\begin{aligned} V_{qs} &= \frac{1}{3}(2V_{as} - V_{bs} - V_{cs}) \\ V_{ds} &= \frac{1}{\sqrt{3}}(V_{cs} - V_{bs}) \end{aligned} \quad (3.18)$$

The magnitude and the angle, α_s of the output voltage space vector are calculated for each possible switching state using the expression (3.19).

$$\begin{aligned} V_s &= \sqrt{V_{qs}^2 + V_{ds}^2} \\ \alpha_s &= -\tan^{-1}\left(\frac{V_{ds}}{V_{qs}}\right) \end{aligned} \quad (3.19)$$

(3.18) and (3.19) are used to determine the space vector for the output and input current space vectors for the 27 modes.

In Table 3.1, the switching functions S_{ap} , S_{bp} and S_{cp} determine how the phase ‘a’, ‘b’ and ‘c’ output terminals are mapped with the input terminals, respectively. For example, when the output phase a voltage is connected to input phase a voltage $S_{ap} = 0$, if it is connected to phase ‘b’, $S_{ap} = 1$ and $S_{ap} = 2$ when it is connected to phase c input voltage.

Output Voltage Space Vectors. The output voltage space vectors associated to each switching state are given in Table 3.1. These space vectors are exemplified considering three cases, one from each group.

- Mode AAA

In this mode all the output voltage terminals are connected to input phase ‘a’ voltage. Hence, $S_{ap} = S_{bp} = S_{cp} = 0$ and $V_{as} = V_{bs} = V_{cs} = V_{ap}$. The q -axis and d -axis components of the output voltage space vector are determined as

$$V_{qs} = \frac{2}{3} \left(V_{as} - \frac{1}{2} V_{bs} - \frac{1}{2} V_{cs} \right) = \frac{2}{3} \left(V_{ap} - \frac{1}{2} V_{ap} - \frac{1}{2} V_{ap} \right) = 0$$

$$V_{ds} = \frac{1}{\sqrt{3}} (V_{cs} - V_{bs}) = \frac{1}{\sqrt{3}} (V_{ap} - V_{ap}) = 0$$

Then the magnitude and angle of the output voltage space vector becomes zero. All modes in group I do not produce any output voltage and they are a zero switching states.

$$V_p = \sqrt{V_{qs}^2 + V_{ds}^2} = 0$$

$$\alpha_s = \tan^{-1} \left(\frac{-V_{ds}}{V_{qs}} \right) = 0$$

- Mode ABC

This mode belongs to group II where each output terminal is connected to different input voltages. In this particular mode, phase ‘a’ output voltage is connected to phase ‘a’ input voltage, phase ‘b’ with phase ‘b’ and phase ‘c’ with phase ‘c’. Hence the switching functions $S_{ap} = 0$, $S_{bp} = 1$ and $S_{cp} = 2$ and the output voltages $V_{as} = V_{ap}$, $V_{bs} = V_{bp}$ and $V_{cs} = V_{cp}$. The q -axis and d -axis output voltage space vector are computed as.

$$V_{qs} = \frac{2}{3} \left(V_{as} - \frac{1}{2} V_{bs} - \frac{1}{2} V_{cs} \right) = \frac{2}{3} \left(V_{ap} - \frac{1}{2} V_{bp} - \frac{1}{2} V_{cp} \right) = V_{ap}$$

$$V_{ds} = \frac{1}{\sqrt{3}} (V_{cs} - V_{bs}) = \frac{1}{\sqrt{3}} (V_{cp} - V_{bp}) = -\frac{1}{\sqrt{3}} V_{bcp}$$

The possible input line-to-line voltage, V_{ab} , V_{bc} and V_{ca} are given as

$$V_{ab} = \sqrt{3} V_p \sin(\omega_p t + \frac{2\pi}{3})$$

$$V_{bc} = \sqrt{3} V_p \sin(\omega_p t)$$

$$V_{ca} = \sqrt{3} V_p \sin(\omega_p t - \frac{2\pi}{3})$$

The magnitude of all space vectors in this mode is constant and equal to the magnitude of the input voltage. Unlike other modes, modes in this group II do not have fixed directions. This direction rotates with the same frequency as that of the input voltage.

$$V_s = \sqrt{V_{qs}^2 + V_{ds}^2} = \sqrt{V_{ap}^2 + \frac{1}{3} V_{bcp}^2} = V_p$$

$$\alpha_s = \tan^{-1} \left(\frac{-V_{ds}}{V_{qs}} \right) = \tan^{-1} \left(\frac{\frac{1}{\sqrt{3}} \sqrt{3} V_p \sin(\omega_p t)}{V_p \cos(\omega_p t)} \right) = \omega_p t$$

- Mode AAB

This mode is from the active switching groups where two of the output terminals, phase ‘a’ and ‘b’ are both connected to phase ‘c’ input terminal. $S_{ap} = S_{bp} = 0$ and $S_{cp} = 1$ the output voltage are related with the input voltages as $V_{as} = V_{bs} = V_{ap}$ and $V_{cs} = V_{bp}$

The q -axis and d -axis output voltage space vector are determined as

$$V_{qs} = \frac{2}{3} \left(V_{as} - \frac{1}{2} V_{bs} - \frac{1}{2} V_{cs} \right) = \frac{2}{3} \left(V_{ap} - \frac{1}{2} V_{ap} - \frac{1}{2} V_{bp} \right) = \frac{1}{3} V_{abp}$$

$$V_{ds} = \frac{1}{\sqrt{3}} (V_{cs} - V_{bs}) = \frac{1}{\sqrt{3}} (V_{bp} - V_{ap}) = -\frac{1}{\sqrt{3}} V_{abp}$$

Note that the magnitude of the space vector is time-varying with the line-to-line voltage V_{ab} . And the direction of this vector is fixed to 60° . All vectors in this group have fixed direction and time varying amplitude which takes the instantaneous value of the input line to line voltage.

$$V_p = \sqrt{V_{qs}^2 + V_{ds}^2} = \sqrt{\left(\frac{1}{3} V_{ab}\right)^2 + \left(-\frac{1}{\sqrt{3}} V_{ab}\right)^2} = \frac{2}{3} V_{abp}$$

$$\alpha_s = \tan^{-1} \left(\frac{-V_{ds}}{V_{qs}} \right) = \tan^{-1} \left(\frac{\frac{1}{\sqrt{3}} V_{abp}}{\frac{1}{3} V_{abp}} \right) = \tan^{-1}(\sqrt{3}) = \frac{\pi}{3}$$

The complete derivation of the output voltage space vector for the 27 modes is given in

Appendix I.

Input current space vectors. The input current space vectors are determined based on the output three phase currents and output power factor. Table 3.2 shows input current space vectors for the possible 27 switching modes.

Consider a balanced three phase output current given in (3.20) with an output power factor of φ_s . Where I_s is the peak output phase current and ω_s is the angular frequency of the output current which is the same as the output voltage frequency.

$$\begin{bmatrix} I_{as} \\ I_{bs} \\ I_{cs} \end{bmatrix} = I_s \begin{bmatrix} \cos(\omega_s t - \varphi_s) \\ \cos(\omega_s t - \frac{2\pi}{3} - \varphi_s) \\ \cos(\omega_s t + \frac{2\pi}{3} - \varphi_s) \end{bmatrix} \quad (3.20)$$

The magnitude and the angle, β_p of the input current space vector are also computed using the stationary qd -transformation followed by expression (3.21).

$$\begin{aligned} I_p &= \sqrt{I_{qp}^2 + I_{dp}^2} \\ \beta_p &= \tan^{-1} \left(\frac{-I_{dp}}{I_{qp}} \right) \end{aligned} \quad (3.21)$$

The calculation of input current space vector is exemplified using three modes, each mode from different groups.

Table 3.2 Possible input current space vectors

	Mode	S_{ap}	S_{bp}	S_{cp}	I_{ap}	I_{bp}	I_{cp}	I_{qp}	I_{dp}	I_p	β_p
Group I	AAA	0	0	0	0	0	0	0	0	0	-
	BBB	1	1	1	0	0	0	0	0	0	-
	CCC	2	2	2	0	0	0	0	0	0	-
Group II	ABC	0	1	2	I_{ap}	I_{bp}	I_{cp}	I_{ap}	$1/\sqrt{3}(I_{cs}-I_{bs})$	I_s	$\omega_s t - \varphi_s$
	ACB	0	2	1	I_{ap}	I_{cp}	I_{bp}	I_{ap}	$1/\sqrt{3}(I_{cs}-I_{bs})$	I_s	$-\omega_s t + \varphi_s$
	BAC	1	0	2	I_{bp}	I_{ap}	I_{cp}	I_{bp}	$1/\sqrt{3}(I_{cs}-I_{as})$	I_s	$-\omega_s t + \varphi_s - 2\pi/3$
	BCA	1	2	0	I_{bp}	I_{cp}	I_{ap}	I_{bp}	$1/\sqrt{3}(I_{cs}-I_{as})$	I_s	$\omega_s t - \varphi_s + 2\pi/3$
	CAB	2	0	1	I_{cp}	I_{ap}	I_{bp}	I_{cp}	$1/\sqrt{3}(I_{bs}-I_{as})$	I_s	$-\omega_s t + \varphi_s - 2\pi/3$
	CBA	2	1	0	I_{cp}	I_{bp}	I_{ap}	I_{cp}	$-1/\sqrt{3}(I_{bs}-I_{as})$	I_s	$\omega_s t - \varphi_s + 2\pi/3$
Group III	AAB	0	0	1	$-I_{cp}$	I_{cp}	0	$-I_{cp}$	$-1/\sqrt{3}I_{cs}$	$2/\sqrt{3}I_{cs}$	$5\pi/6$
	AAC	0	0	2	$-I_{cp}$	0	I_{cp}	$-I_{cp}$	$1/\sqrt{3}I_{cs}$	$2/\sqrt{3}I_{cs}$	$7\pi/6$
	ABA	0	1	0	$-I_{bp}$	I_{bp}	0	$-I_{bp}$	$-1/\sqrt{3}I_{bs}$	$2/\sqrt{3}I_{bs}$	$5\pi/6$
	ABB	0	1	1	I_{ap}	$-I_{ap}$	0	I_{ap}	$1/\sqrt{3}I_{as}$	$2/\sqrt{3}I_{as}$	$-\pi/6$
	ACA	0	2	0	$-I_{bp}$	0	I_{bp}	$-I_{bp}$	$1/\sqrt{3}I_{bs}$	$2/\sqrt{3}I_{bs}$	$7\pi/6$
	ACC	0	2	2	I_{ap}	0	$-I_{ap}$	I_{ap}	$-1/\sqrt{3}I_{as}$	$2/\sqrt{3}I_{as}$	$\pi/6$
	BAA	1	0	0	$-I_{ap}$	I_{ap}	0	$-I_{ap}$	$-1/\sqrt{3}I_{as}$	$2/\sqrt{3}I_{as}$	$5\pi/6$
	BAB	1	0	1	I_{bp}	$-I_{bp}$	0	I_{bp}	$1/\sqrt{3}I_{bs}$	$2/\sqrt{3}I_{bs}$	$-\pi/6$
	BBA	1	1	0	I_{cp}	$-I_{cp}$	0	I_{cp}	$1/\sqrt{3}I_{cs}$	$2/\sqrt{3}I_{cs}$	$-\pi/6$
	BBC	1	1	2	0	$-I_{cp}$	I_{cp}	0	$1/\sqrt{3}I_{cs}$	$2/\sqrt{3}I_{cs}$	$-\pi/2$
	BCB	1	2	1	0	$-I_{bp}$	I_{bp}	0	$1/\sqrt{3}I_{bs}$	$2/\sqrt{3}I_{bs}$	$-\pi/2$
	BCC	1	2	2	0	I_{ap}	$-I_{ap}$	0	$-1/\sqrt{3}I_{as}$	$2/\sqrt{3}I_{as}$	$\pi/2$
	CAA	2	0	0	$-I_{ap}$	0	I_{ap}	$-I_{ap}$	$1/\sqrt{3}I_{as}$	$2/\sqrt{3}I_{as}$	$7\pi/6$
	CAC	2	0	2	I_{bp}	0	$-I_{bp}$	I_{bp}	$-1/\sqrt{3}I_{bs}$	$2/\sqrt{3}I_{bs}$	$\pi/6$
	CBB	2	1	1	0	$-I_{ap}$	I_{ap}	0	$-1/\sqrt{3}I_{as}$	$2/\sqrt{3}I_{as}$	$-\pi/2$
	CBC	2	1	2	0	I_{bp}	$-I_{bp}$	0	$-1/\sqrt{3}I_{bs}$	$2/\sqrt{3}I_{bs}$	$\pi/2$
	CCA	2	2	0	I_{cp}	0	$-I_{cp}$	I_{cp}	$-1/\sqrt{3}I_{cs}$	$2/\sqrt{3}I_{cs}$	$\pi/6$
	CCB	2	2	1	0	I_{cp}	$-I_{cp}$	0	$-1/\sqrt{3}I_{cs}$	$2/\sqrt{3}I_{cs}$	$\pi/2$

- Mode AAA

Since the output terminals are connected to input phase 'a' voltage. Hence, $S_{ap} = S_{bp} = S_{cp} = 0$ and there is no path for the input currents, $I_{ap} = I_{bp} = I_{cp} = 0$. The q -axis and d -axis input current space vector are determined as

$$I_{qp} = \frac{2}{3} \left(I_{ap} - \frac{1}{2} I_{bp} - \frac{1}{2} I_{cp} \right) = \frac{2}{3} (I_{as} + I_{bs} + I_{cs}) = 0$$

$$I_{dp} = \frac{1}{\sqrt{3}} (I_{cp} - I_{bp}) = 0$$

Similar to the output voltage space vectors, in this zero switching mode the magnitude and direction of the input current space vector are both zero.

$$I_p = \sqrt{I_{qp}^2 + I_{dp}^2} = \frac{2}{3} (I_{as} + I_{bs} + I_{cs}) = 0$$

$$\beta_p = \tan^{-1} \left(\frac{-I_{dp}}{I_{qp}} \right) = 0$$

- Mode ABC

When $S_{ap} = 0$, $S_{bp} = 1$ and $S_{cp} = 2$ implies $I_{ap} = I_{as}$, $I_{bp} = I_{bs}$ and $I_{cp} = I_{cs}$. The q -axis and d -axis input current space vector are determined as

$$I_{qp} = \frac{2}{3} \left(I_{ap} - \frac{1}{2} I_{bp} - \frac{1}{2} I_{cp} \right) = \frac{2}{3} \left(I_{as} - \frac{1}{2} (I_{bs} + I_{cs}) \right) = I_{as}$$

$$I_{dp} = \frac{1}{\sqrt{3}} (I_{cp} - I_{bp}) = \frac{1}{\sqrt{3}} (I_{cs} - I_{bs})$$

The input line-to-line currents can be defined as

$$I_{abp} = \sqrt{3} I_p \sin \left(\omega_s t - \varphi_s + \frac{2\pi}{3} \right)$$

$$I_{bcp} = \sqrt{3}I_p \sin(\omega_s t - \varphi_s)$$

$$I_{cap} = \sqrt{3}I_p \sin(\omega_s t - \varphi_s - \frac{2\pi}{3})$$

The magnitude of all input current space vectors in this mode is also constant and equal to the magnitude of the input voltage. Besides, modes in this group do not have fixed directions. The direction of the input current rotates with the output current frequency; therefore, they are not being used in space vector modulation.

$$I_p = \sqrt{I_{qp}^2 + I_{dp}^2} = \sqrt{I_{as}^2 + \frac{1}{3}(I_{cs} - I_{bs})^2}$$

$$\beta_p = \tan^{-1}\left(\frac{-I_{dp}}{I_{qp}}\right) = \tan^{-1}\left(\frac{-\frac{1}{\sqrt{3}}(I_{cs} - I_{bs})}{I_{as}}\right) = \omega_s t - \varphi_s$$

- Mode AAB

When $S_{ap} = S_{bp} = 0$ and $S_{cp} = 1$ implies $I_{ap} = -I_{cs}$, $I_{bp} = I_{cs}$ and $I_{cp} = 0$. The q -axis and d -axis input current space vector are determined as below.

$$I_{qp} = \frac{2}{3}\left(I_{ap} - \frac{1}{2}I_{bp} - \frac{1}{2}I_{cp}\right) = \frac{2}{3}\left(-I_{cs} - \frac{1}{2}I_{cs}\right) = -I_{cs}$$

$$I_{dp} = \frac{1}{\sqrt{3}}(I_{cp} - I_{bp}) = -\frac{1}{\sqrt{3}}I_{cs}$$

The magnitude of the input current space vectors in this mode has time-varying amplitude depending on the instantaneous output phase 'c' current. And the direction of this vector is also fixed 150° . All vectors in this group have fixed direction and time-varying amplitude which takes the instantaneous output currents.

$$I_p = \sqrt{I_{qp}^2 + I_{dp}^2} = \sqrt{I_{cs}^2 + \frac{1}{3}I_{cs}^2} = \frac{2}{\sqrt{3}}I_{cs}$$

$$\beta_p = \tan^{-1}\left(\frac{-I_{dp}}{I_{qp}}\right) = \tan^{-1}\left[\frac{\frac{1}{\sqrt{3}}I_{cs}}{-I_{cs}}\right] = \frac{5\pi}{6}$$

The complete derivation of the input current space vector for the possible 27 modes is given in Appendix II.

Based on Table 3.1 and Table 3.2, the actual space vectors implemented in the direct space vector modulation techniques are only 21. In other words, only group I and II are used in the modulation. It can be also seen that the 18 non-zero space vector are displaced with equal 60° with each other. Three of these vectors lie on the same direction but they have different magnitudes. For example modes ACA, BAB and BAB produce an output voltage vectors which all lie at 120° in space and similarly, CCB, BCC and CBC comprise an input current space vector lying on 90° in space. Moreover, there are always two space vectors having same magnitude with opposite directions. For example, Modes AAB and BBA produces pairs of voltage space vector with equal magnitude and placed on -120° and 60° , respectively. And they also result in a pair of input current space vectors of equal magnitude placed on 150° and -30° , respectively. As a result these modes are denoted as -7 and +7 switching states, respectively.

The output voltage vector and input current space vectors generated by the active switching modes, group II, and are shown in Figure 3.4 and 3.5. Switching states +1, +2 and +3 have a direction of zero and -1, -2 and -3 switching states lie on 180° as seen in Figure 3.4. Similarly, Figure 3.5 -60° , 90° and -120° corresponds to the positive switching states and negative switching states lie on the opposite direction.

The algorithm for space vector modulation basically involves two procedures: the selections of appropriate switching states and determine the duty cycle of the selected switching states. To construct desired output voltage and input current simultaneously, the states are chosen such that they are adjacent to the both output voltage and input current vectors and they involve the lowest switching transition as possible.

Consider both the desired output voltage and input current lie on sector 1, the vector V_s can be synthesized using two adjacent vectors V_s' and V_s'' as seen in Figure 3.6 corresponds to the upper and the lower adjacent vectors, respectively. V_s' can be synthesized using six possible switching configurations (± 7 , ± 8 , ± 9) and only four of them (± 7 , ± 9) simultaneously allow the modulation of input current direction. Similarly, there are also six possible configuration to construct V_s'' (± 1 , ± 2 , ± 3) in which (± 1 , ± 3) is selected since it can also be used to synthesize the input current vector. The four switching states which gives the lowest switching is found to be (+9, -7, -3, +1).

This technique of determining the switching states used for any possible combination of output voltage and input current is given in Appendix IV and summarized in Table 3.4.

Table 3.3 Possible switching configuration of a matrix converter

Switching state	Mode	V_s	α_s	I_p	β_p
0_a	AAA	0	-	0	-
0_b	BBB	0	-	0	-
0_c	CCC	0	-	0	-
-7	AAB	$2/3V_{abp}$	$\pi/3$	$2/\sqrt{3}I_{cs}$	$5\pi/6$
+9	AAC	$2/3V_{cap}$	$-2\pi/3$	$2/\sqrt{3}I_{cs}$	$7\pi/6$
-4	ABA	$2/3V_{abp}$	$-\pi/3$	$2/\sqrt{3}I_{bs}$	$5\pi/6$
+1	ABB	$2/3V_{abp}$	0	$2/\sqrt{3}I_{as}$	$-\pi/6$
+6	ACA	$2/3V_{cap}$	$2\pi/3$	$2/\sqrt{3}I_{bs}$	$7\pi/6$
-3	ACC	$2/3V_{cap}$	π	$2/\sqrt{3}I_{as}$	$\pi/6$
-1	BAA	$2/3V_{abp}$	π	$2/\sqrt{3}I_{as}$	$5\pi/6$
+4	BAB	$2/3V_{abp}$	$2\pi/3$	$2/\sqrt{3}I_{bs}$	$-\pi/6$
+7	BBA	$2/3V_{abp}$	$-2\pi/3$	$2/\sqrt{3}I_{cs}$	$-\pi/6$
-8	BBC	$2/3V_{bcp}$	$\pi/3$	$2/\sqrt{3}I_{cs}$	$-\pi/2$
-5	BCB	$2/3V_{bcp}$	$-\pi/3$	$2/\sqrt{3}I_{bs}$	$-\pi/2$
+2	BCC	$2/3V_{bcp}$	0	$2/\sqrt{3}I_{as}$	$\pi/2$
+3	CAA	$2/3V_{cap}$	0	$2/\sqrt{3}I_{as}$	$7\pi/6$
-6	CAC	$2/3V_{cap}$	$-\pi/3$	$2/\sqrt{3}I_{bs}$	$\pi/6$
-2	CBB	$2/3V_{bcp}$	π	$2/\sqrt{3}I_{as}$	$-\pi/2$
+5	CBC	$2/3V_{bcp}$	$2\pi/3$	$2/\sqrt{3}I_{bs}$	$\pi/2$
-9	CCA	$2/3V_{cap}$	$\pi/3$	$2/\sqrt{3}I_{cs}$	$\pi/6$
+8	CCB	$2/3V_{bcp}$	$-2\pi/3$	$2/\sqrt{3}I_{cs}$	$\pi/2$

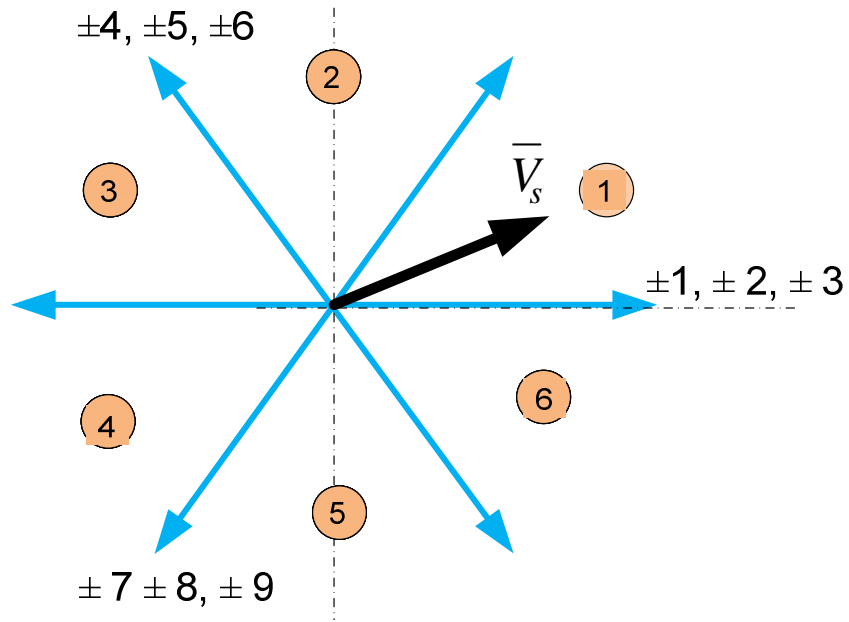


Figure 3.4 Output voltage space vectors

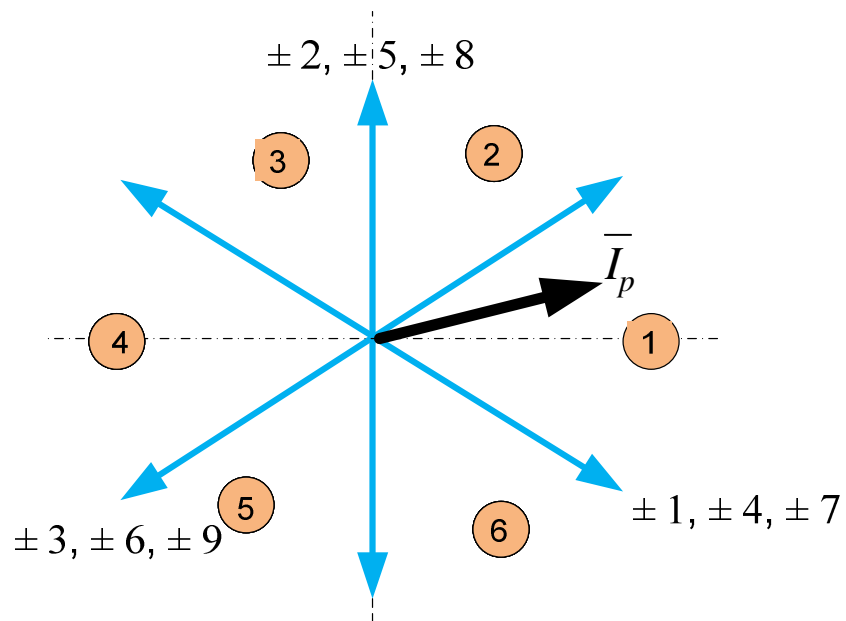


Figure 3.5 Input current space vector

Table 3.4 The Selected switching configurations for the possible sector combinations

		Sector of output voltage vector																							
		1				2				3				4				5				6			
In put Current Vector Sector	1	+9	-7	-3	+1	-6	+4	+9	-7	+3	-1	-6	+4	-9	+7	+3	-1	+6	-4	-9	+7	-3	+1	+6	-4
	2	-8	+9	+2	-3	+5	-6	-8	+9	-2	+3	+5	-6	+8	-9	-2	+3	-5	+6	+8	-9	+2	-3	-5	+6
	3	+7	-8	-1	+2	-4	+5	+7	-8	+1	-2	-4	+5	-7	+8	+1	-2	+4	-5	-7	+8	-1	+2	+4	-5
	4	-9	+7	+3	-1	+6	-4	-9	+7	-3	+1	+6	-4	+9	-7	-3	+1	-6	+4	-9	+7	+3	-1	-6	+4
	5	+8	-9	-2	+3	-5	+6	+8	-9	+2	-3	-5	+6	-8	+9	+2	-3	+5	-6	-8	+9	-2	+3	+5	-6
	6	-7	+8	+1	-2	+4	-5	-7	+8	-1	+2	+4	-5	+7	-8	-1	+2	-4	+5	-7	+8	+1	-2	-4	+5
Times		t_1	t_2	t_3	t_4	t_1	t_2	t_3	t_4	t_1	t_2	t_3	t_4	t_1	t_2	t_3	t_4	t_1	t_2	t_3	t_4	t_1	t_2	t_3	t_4

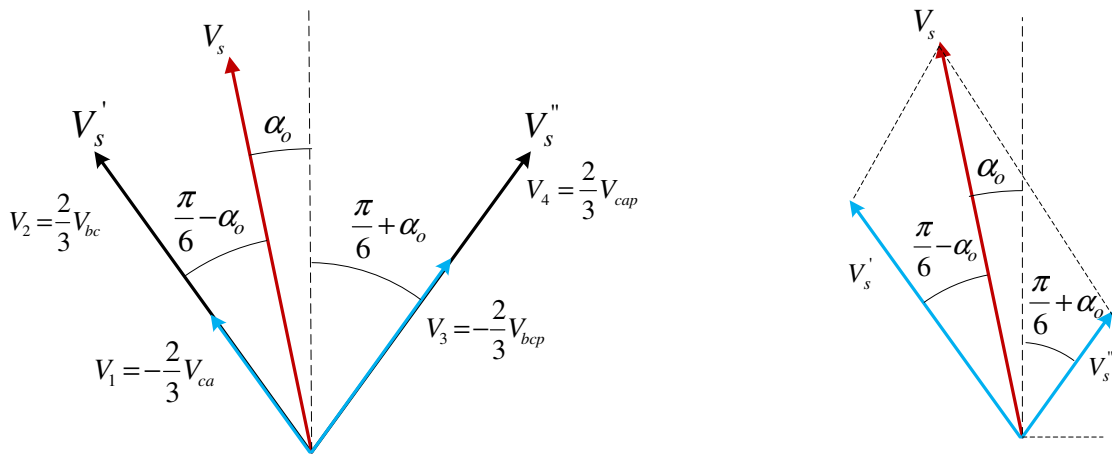


Figure 3.6 Output voltage vector synthesis

Once these four states are determined, a zero switching states are applied to complete the switching period which provides maximum output to input voltage transfer ratio. The expressions for the normalized times (duty cycles) can be done by considering the synthesis of output desired voltage and input current phase angle. Consider the input current angle lie on sector 5 and the desired output voltage on sector 3. The selected switching configuration is -5 +6 +8 -9 based on Table 3.4.

In switching state -5, the output voltage and input current space vectors V_l and I_l are found in Table 3.3 as

$$V_1 = \frac{2}{3}V_{bcp} \angle -\frac{\pi}{3} = -\frac{2}{3}V_{bcp} \angle \frac{2\pi}{3}$$

$$I_1 = \frac{2}{\sqrt{3}}I_{bs} \angle -\frac{\pi}{2}$$

And the voltage and current space vectors in mode +6, V_2 and I_2 are

$$V_2 = \frac{2}{3}V_{cap} \angle \frac{2\pi}{3}$$

$$I_2 = \frac{2}{\sqrt{3}}I_{bs} \angle \frac{4\pi}{3}$$

V_3 and I_3 corresponding with output voltage and input current vectors in switching state +8 are

$$V_3 = \frac{2}{3}V_{bcp} \angle \frac{4\pi}{3} = -\frac{2}{3}V_{bcp} \angle \frac{\pi}{3}$$

$$I_3 = \frac{2}{\sqrt{3}}I_{cs} \angle -\frac{\pi}{2}$$

The fourth output voltage and input current vectors V_4 and I_4 at switching mode -9 are

$$V_4 = \frac{2}{3}V_{cap} \angle \frac{\pi}{3}$$

$$I_4 = \frac{2}{\sqrt{3}}I_{cs} \angle \frac{4\pi}{3}$$

Since each adjacent vectors are synthesized from two voltage vectors having the same directions.

$$V_s' = V_1 + V_2$$

$$V_s'' = V_3 + V_4 \tag{3.22}$$

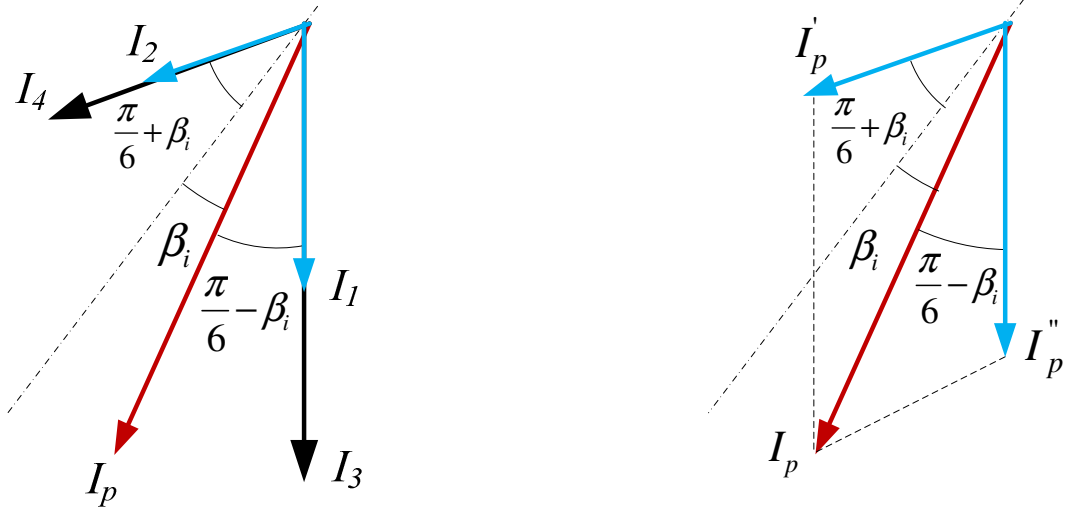


Figure 3.7 Input current vector synthesis

Define the two local angles which are measured from the bisection line of the sectors; α_o the angle of desired voltage measured from the bisection line of the voltage sectors and β_i the angle of input current measured from the bisection line of the current sectors. Applying sine rule on Figure 3.6 result in one of the relation between duty ratios t_1 and t_2 in terms of the output and input voltages.

$$\frac{V_s'}{\sin(\frac{\pi}{6} + \alpha_o)} = \frac{V_s}{\sin(\frac{2\pi}{3})}$$

$$-\frac{2}{3}V_{ca}t_1 + \frac{2}{3}V_{bc}t_2 = \frac{2}{\sqrt{3}}V_s \sin(\frac{\pi}{6} + \alpha_o) \quad (3.23)$$

Using the same sine law on the input current vector shown in Figure 3.7, another relationship between the duty cycles t_1 and t_2 is obtained as given in 3.24. It is very interesting to note that the output current magnitude does not show up the equation.

Therefore, it can be concluded that the duty cycles for each switching configurations does not depend on the magnitude of the output current rather it depends on the desired output voltage, input voltage, input current angle and output voltage angle.

$$\frac{\frac{2}{\sqrt{3}} I_{bs} t_1}{\sin(\frac{\pi}{6} + \beta_i)} = \frac{\frac{2}{\sqrt{3}} I_{bs} t_2}{\sin(\frac{\pi}{6} - \beta_i)}$$

$$t_2 = \frac{\sin(\frac{\pi}{6} - \beta_i)}{\sin(\frac{\pi}{6} + \beta_i)} t_1 \quad (3.24)$$

Solving (3.23) and (3.24) simultaneously gives the expression of t_1 as follows

$$t_1 = \frac{\frac{2}{\sqrt{3}} V_s \sin(\frac{\pi}{6} + \alpha_o) \sin(\frac{\pi}{6} + \beta_i)}{-\frac{2}{3} V_{ca} \sin(\frac{\pi}{6} + \beta_i) + \frac{2}{3} V_{bc} \sin(\frac{\pi}{6} - \beta_i)}$$

Simplifying the denominator, and define the output voltage transfer ratio $q = V_s/V_p$

$$t_1 = \frac{2q \sin(\frac{\pi}{6} + \alpha_o) \sin(\frac{\pi}{6} + \beta_i)}{\sqrt{3} \cos(\phi)}$$

Where Φ denotes the input power factor angle and using a trigonometric property, the sine term can be replaced by the cosine and the final expression for t_1 can be given as

$$t_1 = \frac{2q \cos(\alpha_o - \frac{\pi}{3}) \cos(\beta_i - \frac{\pi}{3})}{\sqrt{3} \cos(\phi)} \quad (3.25)$$

Substituting back the expression (3.25) into (3.24), the duty cycle t_2 is

$$t_2 = \frac{2q \cos(\alpha_o - \frac{\pi}{3}) \cos(\beta_i + \frac{\pi}{3})}{\sqrt{3} \cos(\phi)} \quad (3.26)$$

Similarly, using the other adjacent voltage vector, the normalized time t_3 and t_4 can easily be computed. t_5 is the duty cycles for the zero switching state and the expressions of these times are given as

$$t_3 = \frac{2q \cos(\alpha_o + \frac{\pi}{3}) \cos(\beta_i - \frac{\pi}{3})}{\sqrt{3} \cos(\phi)} \quad (3.27)$$

$$t_4 = \frac{2q \cos(\alpha_o + \frac{\pi}{3}) \cos(\beta_i + \frac{\pi}{3})}{\sqrt{3} \cos(\phi)} \quad (3.28)$$

$$t_5 = 1 - t_1 - t_2 - t_3 - t_4 \quad (3.29)$$

3.3.2 Indirect Space Vector modulation

3.3.2.1 Space Vector for Rectifier Stage. This modulation technique applies the well developed PWM strategies of converters to a matrix converter modulation algorithm. The objective is still the same as the direct space vector; synthesize the output voltages vectors from the input voltages and the input current vector from the output currents. However, the output voltage and input current are controlled independently in indirect space vector modulation [6].

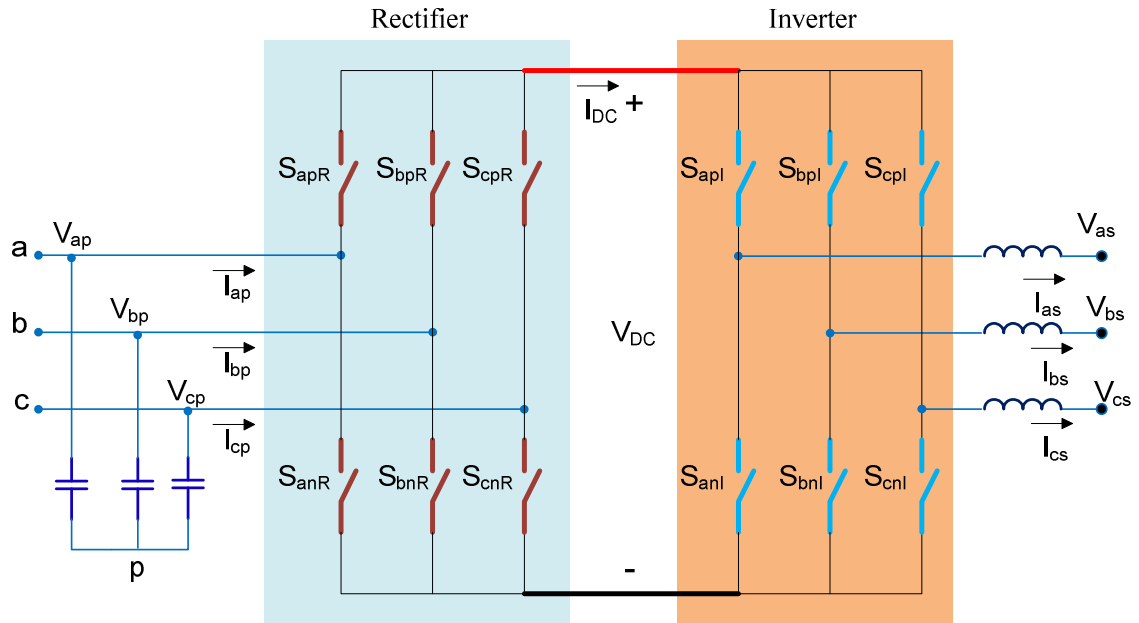


Figure 3.8 Equivalent circuit for indirect matrix converter

The advantage of this modulation scheme is that it is easier to implement the well established PWM converters modulation to the matrix converter. Besides, it is potentially possible to directly implement PWM inverter based controller such as vector control for induction machine, to the matrix converter [6].

As the matrix converter can equivalently represent as inverter and rectifier stages spitted by a fiction dc link. As seen in Figure 3.8, both the rectifier and inverter power stages consist of 6 switches.

The input current can be expressed as the virtual dc link current and the rectifier stage switching states. Similarly, the virtual DC link voltage is mapped with the input three phase voltages as given in (3.31).

Table 3.5: Truth table for rectifier stage

Mode	Vector	On Devices		I_{ap}	I_{bp}	I_{cp}	I_{qp}	I_{dp}	I_p	β_p	V_{DC}
1.	I_6	S_{apR}	S_{bnR}	I_{DC}	$-I_{DC}$	0	I_{DC}	$1/\sqrt{3}I_{DC}$	$2/\sqrt{3}I_{DC}$	$-\pi/6$	V_{abp}
2.	I_1	S_{apR}	S_{cnR}	I_{DC}	0	$-I_{DC}$	I_{DC}	$-1/\sqrt{3}I_{DC}$	$2/\sqrt{3}I_{DC}$	$\pi/6$	$-V_{cap}$
3.	I_3	S_{bpR}	S_{anR}	$-I_{DC}$	I_{DC}	0	$-I_{DC}$	$-1/\sqrt{3}I_{DC}$	$2/\sqrt{3}I_{DC}$	$5\pi/6$	$-V_{abp}$
4.	I_2	S_{bpR}	S_{cnR}	0	I_{DC}	$-I_{DC}$	0	$-1/\sqrt{3}I_{DC}$	$2/\sqrt{3}I_{DC}$	$\pi/2$	V_{bcp}
5.	I_4	S_{cpR}	S_{anR}	$-I_{DC}$	0	I_{DC}	$-I_{DC}$	$1/\sqrt{3}I_{DC}$	$2/\sqrt{3}I_{DC}$	$-5\pi/6$	V_{cap}
6.	I_5	S_{cpR}	S_{bnR}	0	$-I_{DC}$	I_{DC}	0	$1/\sqrt{3}I_{DC}$	$2/\sqrt{3}I_{DC}$	$-\pi/2$	$-V_{bcp}$
7.	0_{I1}	S_{apR}	S_{anR}	0	0	0	-	-	-	-	-
8.	0_{I2}	S_{bpR}	S_{bnR}	0	0	0	-	-	-	-	-
9.	0_{I3}	S_{cpR}	S_{cnR}	0	0	0	-	-	-	-	-

$$\begin{bmatrix} I_{ap} \\ I_{bp} \\ I_{cp} \end{bmatrix} = \begin{bmatrix} S_{apR} & S_{anR} \\ S_{bpR} & S_{bnR} \\ S_{cpR} & S_{cnR} \end{bmatrix} \begin{bmatrix} I_{DC+} \\ I_{DC-} \end{bmatrix} \quad (3.30)$$

$$\begin{bmatrix} V_{DC+} \\ V_{DC-} \end{bmatrix} = \begin{bmatrix} S_{apR} & S_{bpR} & S_{cpR} \\ S_{anR} & S_{bnR} & S_{cnR} \end{bmatrix} \begin{bmatrix} V_{ap} \\ V_{bp} \\ V_{cp} \end{bmatrix} \quad (3.31)$$

To comply with Kirchhoff's voltage and current laws on the rectifier stage, only one switch from the three top switches (S_{apR} , S_{bpR} and S_{cpR}) and one from the bottom switches (S_{anR} , S_{bnR} and S_{cnR}) can be turned ON simultaneously. The possible nine switching combinations in which three of them gives zero input current and the other six gives non-zero input current as shown in Table 3.5.

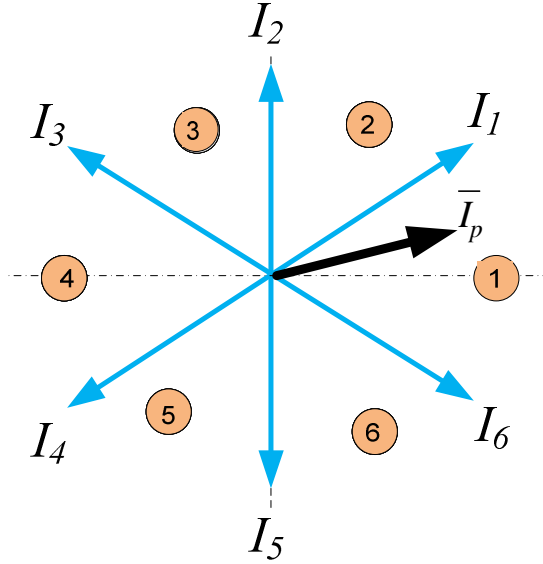


Figure 3.10 Rectifier current space vector

The input currents space vectors can be determined using a stationary *qdo* transformation. The complete derivation of the input current space vectors shown in Table 3.5 is given in Appendix III

$$\begin{bmatrix} I_{qp} \\ I_{dp} \\ I_{op} \end{bmatrix} = \frac{2}{3} \begin{bmatrix} 1 & -\frac{1}{2} & -\frac{1}{2} \\ 0 & \frac{\sqrt{3}}{2} & \frac{\sqrt{3}}{2} \\ \frac{1}{2} & \frac{1}{2} & \frac{1}{2} \end{bmatrix} \begin{bmatrix} I_{ap} \\ I_{bp} \\ I_{cp} \end{bmatrix} \quad (3.32)$$

Using (3.32), the q- and d- axis components of the input current space vector is given as

$$\begin{aligned} I_{qp} &= \frac{2}{3} (2I_{ap} - I_{bp} - I_{cp}) \\ I_{dp} &= \frac{1}{\sqrt{3}} (I_{cp} - I_{bp}) \end{aligned} \quad (3.33)$$

The magnitude and the angle of the input current space vectors can be determined from

(3.34)

$$\begin{aligned} I_{qdp} &= \sqrt{I_{qp}^2 + I_{dp}^2} \\ \theta_{qdp} &= -\tan^{-1}\left(\frac{I_{dp}}{I_{qp}}\right) \end{aligned} \quad (3.34)$$

Consider the following sector to synthesize the desired input current using the two adjacent vectors as seen in Figure 3.9. θ_V is the angle of desired current measured from the lower adjust voltage vector and θ_I is the angle of desired current measured from the lower adjust current.

In Figure 3.9, the reference current can be expressed as the sum of the products of the duty cycles with the respective current space vector.

$$I_{ref} = t_a I_a + t_b I_b \quad (3.35)$$

From the sine law,

$$\frac{t_a I_a}{\sin\left(\frac{\pi}{3} - \theta_I\right)} = \frac{I_{ref}}{\sin\left(\frac{2\pi}{3}\right)} \quad (3.36)$$

The duty cycle t_a can be expressed as (3.37) using (3.36) and substituting the value of I_a from Table 3.5.

$$t_a = q_I \sin\left(\frac{\pi}{3} - \theta_I\right) \quad (3.37)$$

Where the current modulation index q_I as follows

$$q_I = \frac{I_{ref}}{I_{DC}}$$

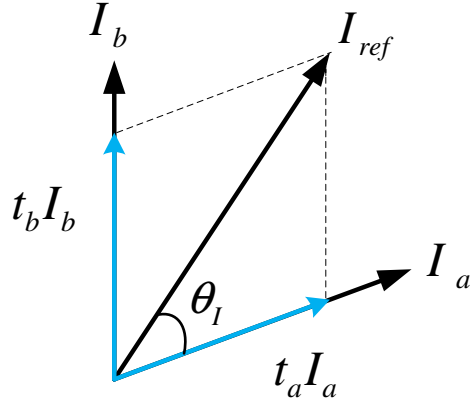


Figure 3.9 Diagram for synthesis of the reference current

Similarly, applying sine laws to get a relation for duty cycle t_b ,

$$\frac{t_b I_b}{\sin(\theta_I)} = \frac{I_{ref}}{\sin(\frac{2\pi}{3})} \quad (3.38)$$

And substituting the value of I_b from the Table 3.5

$$t_b I_b = \frac{2}{\sqrt{3}} I_{ref} \sin(\theta_I)$$

$$t_b = q_I \sin(\theta_I) \quad (3.38)$$

The rest time will be allocated for the three zero vectors such that,

$$t_{0I} = 1 - t_a - t_b \quad (3.39)$$

3.3.2.2 Space Vector for Inverter Stage. The output three phase voltages can be written in terms of the virtual dc voltage and the switching functions. Using the switching state of the inverter stages, the output voltages are related with the virtual dc voltage as follows.

Table 3.6 gives the complete truth table for this stage.

$$\begin{bmatrix} V_{as} \\ V_{bs} \\ V_{cs} \end{bmatrix} = \begin{bmatrix} S_{apR} & S_{anR} \\ S_{bpR} & S_{bnR} \\ S_{cpR} & S_{cnR} \end{bmatrix} \begin{bmatrix} V_{DC+} \\ V_{DC+} \end{bmatrix} \quad (3.40)$$

And the mapping between the input virtual dc link current and the output current can be done using the same switching state transfer matrix.

$$\begin{bmatrix} I_{DC+} \\ I_{DC+} \end{bmatrix} = \begin{bmatrix} S_{apR} & S_{bpR} & S_{cpR} \\ S_{anR} & S_{bnR} & S_{cnR} \end{bmatrix} \begin{bmatrix} I_{as} \\ I_{bs} \\ I_{cs} \end{bmatrix} \quad (3.41)$$

To make the analysis more convenient the output voltages can be expressed by using only the top devices as given in (3.42).

$$\begin{aligned} V_{as} &= \frac{V_{DC}}{3} (2S_{apI} - S_{bpI} - S_{cpI}) \\ V_{bs} &= \frac{V_{DC}}{3} (-S_{apI} + 2S_{bpI} - S_{cpI}) \\ V_{cs} &= \frac{V_{DC}}{3} (-S_{apI} - S_{bpI} + 2S_{cpI}) \end{aligned} \quad (3.42)$$

Using stationary reference frame transformation, the q-axis and d-axis output voltage vectors are expressed as:

$$\begin{aligned} V_{qs} &= \frac{V_{DC}}{3} (2S_{apI} - S_{bpI} - S_{cpI}) \\ V_{ds} &= \frac{1}{\sqrt{3}} (V_{cs} - V_{bs}) \end{aligned} \quad (3.43)$$

The expressions for the magnitude and angle of the voltage space vector for the inverter stage are given as:

Table 3.6 Truth table of inverter

Mode	Vector	S _{apl}	S _{bpl}	S _{cpl}	V _{as}	V _{bs}	V _{cs}	V _{qs}	V _{ds}	V _s	α _s	I _{DC}
1.	0 _{V1}	0	0	0	0	0	0	-	-	-	-	-
2.	V ₄	0	0	1	-1/3V _{DC}	-1/3V _{DC}	2/3V _{DC}	-1/3V _{DC}	1/√3V _{DC}	2/3V _{DC}	-2π/3	I _{cs}
3.	V ₂	0	1	0	-1/3V _{DC}	2/3V _{DC}	-1/3V _{DC}	-1/3V _{DC}	-1/√3V _{DC}	2/3V _{DC}	2π/3	I _{bs}
4.	V ₃	0	1	1	-2/3V _{DC}	1/3V _{DC}	1/3V _{DC}	-2/3V _{DC}	0	2/3V _{DC}	π	-I _{as}
5.	V ₆	1	0	0	2/3V _{DC}	-1/3V _{DC}	-1/3V _{DC}	2/3V _{DC}	0	2/3V _{DC}	0	I _{as}
6.	V ₅	1	0	1	1/3V _{DC}	-2/3V _{DC}	1/3V _{DC}	1/3V _{DC}	1/√3V _{DC}	2/3V _{DC}	-π/3	I _{bs}
7.	V ₁	1	1	0	1/3V _{DC}	1/3V _{DC}	-2/3V _{DC}	1/3V _{DC}	-1/√3V _{DC}	2/3V _{DC}	π/3	I _{cs}
8.	0 _{V2}	1	1	1	0	0	0	-	-	-	-	-

$$V_s = \sqrt{V_{qs}^2 + V_{ds}^2}$$

$$\alpha_s = \tan^{-1} \left(\frac{-V_{ds}}{V_{qs}} \right) \quad (3.44)$$

As shown in Figure 3.12, the desired output voltage is synthesized using the same space vector modulation used in voltage source converter. θ_v is the angle of desired voltage measured from the lower adjacent voltage vector and

Since the reference output voltage are produced using the adjacent two vectors, it can be expressed as the sum of the duty cycles multiplied by the respective voltage vector.

$$V_{ref} = t_c V_c + t_d V_d \quad (3.45)$$

Using sine law,

$$\frac{t_c V_c}{\sin(\frac{\pi}{3} - \theta_v)} = \frac{V_{ref}}{\sin(\frac{2\pi}{3})}$$

$$t_c = \frac{2}{\sqrt{3}} \frac{V_{ref}}{V_c} \sin\left(\frac{\pi}{3} - \theta_v\right)$$

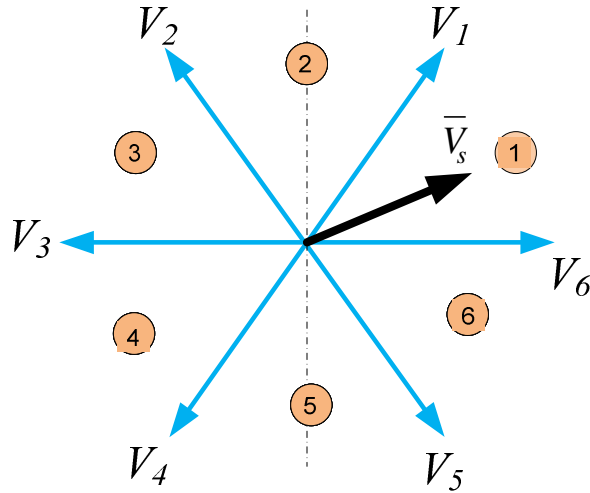


Figure 3.11 Inverter voltage space vector

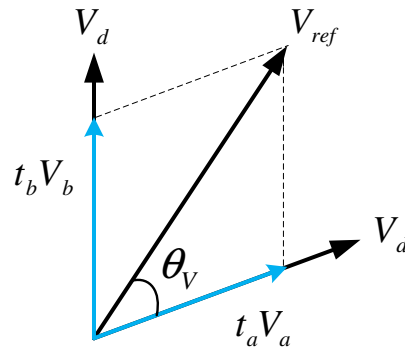


Figure 3.12 Diagram for synthesis of the reference voltage

Substituting the value of V_c

$$t_c = \frac{2}{\sqrt{3}} \frac{V_{ref}}{V_c} \sin\left(\frac{\pi}{3} - \theta_v\right) = \frac{2}{\sqrt{3}} \frac{V_{ref}}{\frac{2}{3} V_{DC}} \sin\left(\frac{\pi}{3} - \theta_v\right) = \sqrt{3} \frac{V_{ref}}{V_{DC}} \sin\left(\frac{\pi}{3} - \theta_v\right)$$

Define a voltage modulation index q_v as $q_v = \frac{V_{ref}}{V_{DC}}$

$$V_c = \frac{2}{3}V_{DC}$$

The duty cycle t_c can be expressed as

$$t_c = \sqrt{3}q_v \sin\left(\frac{\pi}{3} - \theta_v\right) \quad (3.46)$$

Similarly,

$$\frac{t_d V_d}{\sin(\theta_v)} = \frac{I_{ref}}{\sin\left(\frac{2\pi}{3}\right)}$$

And the duty cycle to the other adjacent voltage is given in (3.47)

$$t_d = \sqrt{3}q_v \sin(\theta_v) \quad (3.47)$$

The rest time is allocated for the two zero vectors

$$t_{0V} = 1 - t_c - t_d \quad (3.48)$$

3.3.2.3 Indirect Space Vector for Matrix Converter. Using two space vectors derived in the previous sections, the matrix converter output voltage space vectors can be obtained using the inverter stage space vectors. And the input current space vector of the matrix converter is synthesized employed using the rectifier power stage space vectors.

The four normalized times for the entire matrix converter is computed using the product of the duty cycles of rectifier and inverter stages.

$$\begin{aligned}
t_1 &= t_b t_d = \sqrt{3} q_v q_I \sin(\theta_v) \sin(\theta_I) \\
t_2 &= t_a t_d = \sqrt{3} q_v q_I \sin(\theta_v) \sin\left(\frac{\pi}{3} - \theta_I\right) \\
t_3 &= t_b t_c = \sqrt{3} q_v q_I \sin\left(\frac{\pi}{3} - \theta_v\right) \sin(\theta_I) \\
t_4 &= t_a t_c = \sqrt{3} q_v q_I \sin\left(\frac{\pi}{3} - \theta_v\right) \sin\left(\frac{\pi}{3} - \theta_I\right)
\end{aligned} \tag{3.49}$$

Applying power balance equations in the rectifier stage

$$P_{outCSR} = P_{inCSR} \tag{3.50}$$

The output power of the rectifier is

$$P_{outCSR} = V_{DC} I_{DC} \tag{3.51}$$

And the input three phase power is given (3.52)

$$P_{inCSR} = \frac{3}{2} V_p I_p \cos(\phi) \tag{3.52}$$

Where ϕ is the input power factor angle and V_p is peak of the input voltage

$$V_{DC} I_{DC} = \frac{3}{2} V_p I_{ref} \cos(\phi) \tag{3.53}$$

The product $q_v q_I$ can be evaluated as:

$$q_v q_I = \frac{V_{ref} I_{ref}}{V_{dc} I_{DC}} = \frac{V_{ref} I_{ref}}{V_{dc} I_{DC}} \tag{3.54}$$

Using (3.53) and (3.54)

$$q_v q_I = \frac{V_{ref} I_{ref}}{\frac{3}{2} V_p I_{ref} \cos(\phi)} = \frac{2}{3} \frac{V_{ref}}{V_p \cos(\phi)} \tag{3.55}$$

Define q as the ratio of the output voltage to the input voltage, $q = \frac{V_{ref}}{V_p}$

(3.55) can be expressed in terms of the voltage ratio as follows

$$q_I q_I = \frac{2}{3} \frac{q}{\cos(\phi)} \quad (3.56)$$

Substituting (3.56) into (3.49),

$$t_1 = \sqrt{3} q_V q_I \sin(\theta_V) \sin(\theta_I) = \sqrt{3} \left(\frac{2}{3} \frac{q}{\cos(\phi)} \right) \sin(\theta_V) \sin(\theta_I) = \frac{2q \sin(\theta_V) \sin(\theta_I)}{\sqrt{3} \cos(\phi)}$$

The expressions for the first active duty cycles are given in (3.57).

$$\begin{aligned} t_1 &= \frac{2q \sin(\theta_V) \sin(\theta_I)}{\sqrt{3} \cos(\phi)} \\ t_2 &= \frac{2q \sin(\theta_V) \sin(\frac{\pi}{3} - \theta_I)}{\sqrt{3} \cos(\phi)} \\ t_3 &= \frac{2q \sin(\frac{\pi}{3} - \theta_V) \sin(\theta_I)}{\sqrt{3} \cos(\phi)} \\ t_4 &= \frac{2q \sin(\frac{\pi}{3} - \theta_V) \sin(\frac{\pi}{3} - \theta_I)}{\sqrt{3} \cos(\phi)} \end{aligned} \quad (3.57)$$

And the normalized time for the zero vectors is,

$$t_5 = 1 - t_1 - t_2 - t_3 - t_4 \quad (3.58)$$

To compare the results of the direct and indirect space vector modulation techniques, define two angles α_o and β_i . α_o is the angle of desired voltage measured from the bisection line of the voltage sectors, β_i is the angle of input current measured from the bisection line of the current sectors. And it is stated that θ_v is the angle of desired voltage measured from the lower adjust voltage vector and θ_I is the angle of desired current measured from the lower adjust voltage vector. It is possible to relate the two sets of angles as follows.

$$\begin{aligned}\theta_v &= \alpha_o + \frac{\pi}{6} \\ \theta_i &= \beta_i + \frac{\pi}{6}\end{aligned}\tag{3.59}$$

Therefore, the expressions for the duty cycles in terms of the local angles is given in (3.60)

$$\begin{aligned}t_1 &= \frac{2\sigma \cos(\alpha_o - \frac{\pi}{3}) \cos(\beta_i - \frac{\pi}{3})}{\sqrt{3} \cos(\phi)} \\ t_2 &= \frac{2\sigma \cos(\alpha_o - \frac{\pi}{3}) \cos(\beta_i + \frac{\pi}{3})}{\sqrt{3} \cos(\phi)} \\ t_3 &= \frac{2\sigma \cos(\alpha_o + \frac{\pi}{3}) \cos(\beta_i - \frac{\pi}{3})}{\sqrt{3} \cos(\phi)} \\ t_4 &= \frac{2\sigma \cos(\alpha_o + \frac{\pi}{3}) \cos(\beta_i + \frac{\pi}{3})}{\sqrt{3} \cos(\phi)}\end{aligned}\tag{3.60}$$

$$t_5 = 1 - t_1 - t_2 - t_3 - t_4\tag{3.61}$$

Comparing the results given above with (3.25) to (3.29), it can be concluded that both direct and indirect space vector modulation ultimately result in the same expression for the duty cycles.

Based on the two stages space vector modulations, the current and voltage vectors for the whole six sectors are shown in Table 3.7. To synthesize each input current and output voltage vectors, two adjacent vectors are required. Therefore, there are four vectors used to synthesize both vectors.

Table 3.7 Modes for voltage and current sectors

	V1	V2	V3	V4	V5	V6
I1	<i>AAC</i>	<i>CAC</i>	<i>CAA</i>	<i>CCA</i>	<i>ACA</i>	<i>ACC</i>
I2	<i>BBC</i>	<i>CBC</i>	<i>CBB</i>	<i>CCB</i>	<i>BCB</i>	<i>BCC</i>
I3	<i>BBA</i>	<i>ABA</i>	<i>ABB</i>	<i>AAB</i>	<i>BAB</i>	<i>BAA</i>
I4	<i>CCA</i>	<i>ACA</i>	<i>ACC</i>	<i>AAC</i>	<i>CAC</i>	<i>CAA</i>
I5	<i>CCB</i>	<i>BCB</i>	<i>BCC</i>	<i>BBC</i>	<i>CBC</i>	<i>CBB</i>
I6	<i>AAB</i>	<i>BAB</i>	<i>BAA</i>	<i>BBA</i>	<i>ABA</i>	<i>ABB</i>

Table 3.8 Switching configuration for the combined matrix

	1	2	3	4	5	6
	V1, V6	V2, V1	V3, V2	V4, V3	V5, V4	V6, V5
1 I1, I6	AAC, AAB, ACC, ABB +9, -7, -3, +1	CAC, BAB, AAC, AAB -6, +4, +9, -7	CAA, BAA, CAC, BAB +3, -1, -6, +4	CCA, BBA, CAA, BAA -9, +7, +3, -1	ACA, ABA, CCA, BBA +6, -4, -9, +7	ACC, ABB, ACA, ABA -3, +1, +6, -4
2 I2, I1	BBC, AAC, BCC, ACC -8, +9, +2, -3	CBC, CAC, BBC, AAC +5, -6, -8, +9	CBB, CAA, CBC, CAC -2, +3, +5, -6	CCB, CCA, CBB, CAA +8, -9, -2, +3	BCB, ACA, CCB, CCA -4, +5, +7, -8	BCC, ACC, BCB, ACA +1, -2, -4, +5
3 I3, I2	BBA, BBC, BAA, BCC +7, -8, -1, +2	ABA, CBC, BBA, BBC -4, +5, +7, -8	ABB, CBB, ABA, CBC +1, -2, -4, +5	AAB, CCB, ABB, CBB -7, +8, +1, -2	BAB, BCB, AAB, CCB +4, -5, -7, +8	BAA, BCC, BAB, BCB -1, +2, +4, -5
4 I4, I3	CCA, BBA, CAA, BAA -9, +7, +3, -1	ACA, ABA, CCA, BBA +6, -4, -9, +7	ACC, ABB, ACA, ABA -3, +1, +6, -4	AAC, AAB, ACC, ABB +9, -7, -3, +1	CAC, BAB, AAC, AAB -6, +4, +9, -7	CAA, BAA, CAC, BAB +3, -1, -6, +4
5 I5, I4	CCB, CCA, CBB, CAA +8, -9, -2, +3	BCB, ACA, CCB, CCA -4, +5, +7, -8	BCC, ACC, BCB, ACA +1, -2, -4, +5	BBC, AAC, BCC, ACC -8, +9, +2, -3	CBC, CAC, BBC, AAC +5, -6, -8, +9	CBB, CAA, CBC, CAC -2, +3, +5, -6
6 I6, I5	AAB, CCB, ABB, CBB -7, +8, +1, -2	BAB, BCB, AAB, CCB +4, -5, -7, +8	BAA, BCC, BAB, BCB -1, +2, +4, -5	BBA, BBC, BAA, BCC +7, -8, -1, +2	ABA, CBC, BBA, BBC -4, +5, +7, -8	ABB, CBB, ABA, CBC +1, -2, -4, +5

Table 3.9 Modes result in zero voltage and current vectors

	0V1	0V2
0I1	<i>AAA</i>	<i>AAA</i>
0I2	<i>BBB</i>	<i>BBB</i>
0I3	<i>CCC</i>	<i>CCC</i>

Since each space vectors consists of 6 sectors, there are 36 input current and output voltage sector combinations. These are shown in Table 3.8, which has the same switching configuration derived based on direct space vector modulation and given in Table 3.4.

Table 3.10 Sequence of switching devices

	1	2	3
	V ₁ ,V ₆	V ₂ ,V ₁	V ₃ ,V ₂
1 I ₁ ,I ₆	CCC, ACC, AAC, AAB, ABB, BBB	BBB, BAB, AAB, AAC, CAC, CCC	CCC, CAC, CAA, BAA, BAB, BBB
2 I ₂ ,I ₁	BBB, BBC, BCC, ACC, AAC, AAA	AAA, AAC, CAC, CBC, BBC, BBB	BBB, CBB, CBC, CAC, CAA, AAA
3 I ₃ ,I ₂	AAA, BAA, BBA, BBC, BCC, CCC	CCC, CBC, BBC, BBA, ABA, AAA	AAA, ABA, ABB, CBB, CBC, CCC
4 I ₄ ,I ₃	CCC, CCA, CAA, BAA, BBA, BBB	BBB, BBA, ABA, ACA, CCA, CCC	CCC, ACC, ACA, ABA, ABB, BBB
5 I ₅ ,I ₄	BBB, CBB, CCB, CCA, BAA, AAA	AAA, ACA, CCA, CCB, BCB, BBB	BBB, BCB, BCC, ACC, ACA, AAA
6 I ₆ ,I ₅	AAA, AAB, ABB, CBB, CCB, CCC	CCC, CCB, BCB, BAB, AAB, AAA	AAA, BAA, BAB, BCB, BCC, CCC
	4	5	6
	V ₄ ,V ₃	V ₅ ,V ₄	V ₆ ,V ₅
1 I ₁ ,I ₆	CCC, CCA, CAA, BAA, BBA, BBB	BBB, BBA, ABA, ACA, CCA, CCC	CCC, ACC, ACA, ABA, ABB, BBB
2 I ₂ ,I ₁	BBB, CBB, CCB, CCA, BAA, AAA	AAA, ACA, CCA, CCB, BCB, BBB	BBB, BCB, BCC, ACC, ACA, AAA
3 I ₃ ,I ₂	AAA, AAB, ABB, CBB, CCB, CCC	CCC, CCB, BCB, BAB, AAB, AAA	AAA, BAA, BAB, BCB, BCC, CCC
4 I ₄ ,I ₃	CCC, ACC, AAC, AAB, ABB, BBB	BBB, BAB, AAB, AAC, CAC, CCC	CCC, CAC, CAA, BAA, BAB, BBB
5 I ₅ ,I ₄	BBB, BBC, BCC, ACC, AAC, AAA	AAA, AAC, CAC, CBC, BBC, BBB	BBB, CBB, CBC, CAC, CAA, AAA
6 I ₆ ,I ₅	AAA, BAA, BBA, BBC, BCC, CCC	CCC, CBC, BBC, BBA, ABA, AAA	AAA, ABA, ABB, CBB, CBC, CCC

Table 3.8 shows only the four active vectors, but in actual switching sequence the three zero vectors are included sequence. It can notice that these zero vectors are added at the two ends and in the middle of the sequence. For example the sequence when both input current and output voltage vectors lie on sector I, the sequence which result in the minimum switching transition is shown as

$$CCC \rightarrow ACC \rightarrow AAC \rightarrow AAA \rightarrow AAB \rightarrow ABB \rightarrow BBB$$

It is necessary to note that the middle zero vectors do not show in Table 3.10. AAA is added in the middle of the sequences of the first and fourth row; whereas BBB on third and six rows and CCC on the second and fifth rows. The complete procedure of finding the actual devices selected to construct Table 3.10 for all the possible output voltage and input current space vector combinations are presented in Appendix D.

Table 3.11 Neutral voltage in output voltage Sector I and input current sector II

		Vas	Vbs	Vcs	Vno
+9	AAC	<i>Vap</i>	<i>Vap</i>	<i>Vcp</i>	<i>Vno1</i>
-7	AAB	<i>Vap</i>	<i>Vap</i>	<i>Vbp</i>	<i>Vno2</i>
-3	ACC	<i>Vap</i>	<i>Vcp</i>	<i>Vcp</i>	<i>Vno3</i>
+1	ABB	<i>Vap</i>	<i>Vbp</i>	<i>Vbp</i>	<i>Vno4</i>
	AAA	<i>Vap</i>	<i>Vap</i>	<i>Vap</i>	<i>Vno5</i>
	BBB	<i>Vbp</i>	<i>Vbp</i>	<i>Vbp</i>	<i>Vno6</i>
	CCC	<i>Vcp</i>	<i>Vcp</i>	<i>Vcp</i>	<i>Vno7</i>

3.3.3 Common Mode Voltage Expression Based on Duty Cycle Space Vector

Modulation

An efficient mathematical approach for the analysis of matrix converter modulation techniques are developed based on a duty-cycle space vector [26]. This method uses the instantaneous space vector modulation. Consider a three phase time varying waveforms x_a , x_b and x_c . Transformed qd axis with a stationary reference frame transformation given in (3.62).

$$\begin{bmatrix} x_q \\ x_d \\ x_o \end{bmatrix} = \frac{2}{3} \begin{bmatrix} 1 & \cos\left(\frac{2\pi}{3}\right) & \cos\left(\frac{4\pi}{3}\right) \\ 0 & \sin\left(\frac{2\pi}{3}\right) & \sin\left(\frac{4\pi}{3}\right) \\ \frac{1}{2} & \frac{1}{2} & \frac{1}{2} \end{bmatrix} \begin{bmatrix} x_a \\ x_b \\ x_c \end{bmatrix} \quad (3.62)$$

From (3.62), x_q , x_d and x_o can be expressed as

$$x_q = \frac{2}{3} \left(x_a + x_b \cos\left(\frac{2\pi}{3}\right) + x_c \cos\left(\frac{4\pi}{3}\right) \right) \quad (3.63)$$

$$x_d = \frac{2}{3} \left(x_b \sin\left(\frac{2\pi}{3}\right) + x_c \sin\left(\frac{4\pi}{3}\right) \right) \quad (3.64)$$

$$x_o = \frac{1}{3} (x_a + x_b + x_c) \quad (3.65)$$

And the instantaneous space vector can be represented based on the two axis component as

$$\bar{x} = x_q + jx_d \quad (3.66)$$

Substituting (3.63) and (3.64) into (3.66)

$$\begin{aligned} \bar{x} &= \frac{2}{3} \left(x_a + x_b \left[\cos\left(\frac{2\pi}{3}\right) + j \sin\left(\frac{2\pi}{3}\right) \right] + x_c \left[\cos\left(\frac{4\pi}{3}\right) + j \sin\left(\frac{4\pi}{3}\right) \right] \right) \\ \bar{x} &= \frac{2}{3} \left(x_a + x_b e^{j\frac{2\pi}{3}} + x_c e^{j\frac{4\pi}{3}} \right) \end{aligned} \quad (3.67)$$

The inverse transformation matrix is obtained with a similar approach using the inverse stationary reference frame transformation matrix as given below

$$\begin{bmatrix} x_a \\ x_b \\ x_c \end{bmatrix} = \begin{bmatrix} 1 & 0 & 1 \\ \cos\left(\frac{2\pi}{3}\right) & \sin\left(\frac{2\pi}{3}\right) & 1 \\ \cos\left(\frac{4\pi}{3}\right) & \sin\left(\frac{4\pi}{3}\right) & 1 \end{bmatrix} \begin{bmatrix} x_q \\ x_d \\ x_o \end{bmatrix} \quad (3.68)$$

From (3.68), x_a , x_b and x_c can be computed as follows

$$x_a = x_q + x_o \quad (3.69)$$

$$x_b = x_q \cos\left(\frac{2\pi}{3}\right) + x_d \sin\left(\frac{2\pi}{3}\right) + x_o \quad (3.70)$$

$$x_c = x_q \cos\left(\frac{4\pi}{3}\right) + x_d \sin\left(\frac{4\pi}{3}\right) + x_o \quad (3.71)$$

Since x_q is expressed as the dot product of the space vector \bar{x} with the unit vector in the direction of zero axis.

$$x_q = \bar{x} \cdot e^{j0} \quad (3.72)$$

And the x_d is give as the dot product of the space vector \bar{x} with the unity vector in the direction of 90° .

$$x_d = \bar{x} \cdot e^{j\frac{\pi}{2}} \quad (3.73)$$

Substituting (12) into (9)

$$x_a = \bar{x} \cdot e^{j0} + x_o \quad (3.74)$$

And substituting (12) and (13) into (10)

$$x_b = \bar{x} \cdot \left(e^{j0} \cos\left(\frac{2\pi}{3}\right) + e^{j\frac{\pi}{2}} \sin\left(\frac{2\pi}{3}\right) \right) + x_o$$

$$x_b = \bar{x} \cdot e^{j\frac{2\pi}{3}} + x_o \quad (3.75)$$

Similarly substituting (12) and (13) into (11),

$$x_c = \bar{x} \cdot e^{j\frac{4\pi}{3}} + x_o \quad (3.76)$$

Therefore, the space vector can be represented using the following transformation

$$\begin{aligned} \bar{x} &= \frac{2}{3} \left(x_a + x_b e^{j\frac{2\pi}{3}} + x_c e^{j\frac{4\pi}{3}} \right) \\ x_o &= \frac{1}{3} (x_a + x_b + x_c) \end{aligned} \quad (3.77)$$

And the inverse transformation leads to

$$\begin{aligned}
 x_a &= \bar{x} \cdot e^{j0} + x_o \\
 x_b &= \bar{x} \cdot e^{j\frac{2\pi}{3}} + x_o \\
 x_c &= \bar{x} \cdot e^{j\frac{4\pi}{3}} + x_o
 \end{aligned} \tag{3.78}$$

In direct duty-cycle methods, instead of defining switching matrix, averaged matrix can be directly constructed from the known input voltage and output current and desired output voltage and input current [26, 37].

$$M_{ij} = ave(S_{ij}) = \begin{bmatrix} M_{aA} & M_{bA} & M_{cA} \\ M_{aB} & M_{bB} & M_{cB} \\ M_{aC} & M_{bC} & M_{cC} \end{bmatrix} \tag{3.79}$$

In order to prevent short circuit on the input side and ensure continuous output current

$$\begin{cases} M_{ij} \leq 1 \\ M_{aA} + M_{bA} + M_{cA} = 1 \\ M_{aB} + M_{bB} + M_{cB} = 1 \\ M_{aC} + M_{bC} + M_{cC} = 1 \end{cases} \tag{3.80}$$

Based on the transformation given in (3.77), the first three duty cycles in the first the matrix given in (17) can be represented by the duty-cycle space vector as follows

$$\bar{M}_A = \frac{2}{3} (M_{aA} + M_{bA} e^{j(2\pi/3)} + M_{cA} e^{j(4\pi/3)}) \tag{3.81}$$

$$\bar{M}_B = \frac{2}{3} (M_{aB} + M_{bB} e^{j(2\pi/3)} + M_{cB} e^{j(4\pi/3)}) \tag{3.82}$$

$$\bar{M}_C = \frac{2}{3} (M_{aC} + M_{bC} e^{j(2\pi/3)} + M_{cC} e^{j(4\pi/3)}) \tag{3.83}$$

And the inverse transformation can be obtained based on (3.78.) and the constraint given in (3.80)

$$\begin{aligned}
M_{aA} &= \frac{1}{3} + \bar{M}_A \cdot e^{j0} \\
M_{bA} &= \frac{1}{3} + \bar{M}_A \cdot e^{j(2\pi/3)} \\
M_{cA} &= \frac{1}{3} + \bar{M}_A \cdot e^{j(4\pi/3)}
\end{aligned} \tag{3.84}$$

Similarly, the second row on the matrix given in (3.79) can be obtained using the inverse transformation as

$$\begin{aligned}
M_{aB} &= \frac{1}{3} + \bar{M}_B \cdot e^{j0} \\
M_{bB} &= \frac{1}{3} + \bar{M}_B \cdot e^{j(2\pi/3)} \\
M_{cB} &= \frac{1}{3} + \bar{M}_B \cdot e^{j(4\pi/3)}
\end{aligned} \tag{3.85}$$

Finally, the inverse transformation corresponding to the third row can be given as

$$\begin{aligned}
M_{aC} &= \frac{1}{3} + \bar{M}_C \cdot e^{j0} \\
M_{bC} &= \frac{1}{3} + \bar{M}_C \cdot e^{j(2\pi/3)} \\
M_{cC} &= \frac{1}{3} + \bar{M}_C \cdot e^{j(4\pi/3)}
\end{aligned} \tag{3.86}$$

The input/output relationship of voltages and currents are related to the states of the nine averaged switches and represented as

$$\begin{bmatrix} V_{as} \\ V_{bs} \\ V_{cs} \end{bmatrix} = \begin{bmatrix} M_{aA} & M_{bA} & M_{cA} \\ M_{aB} & M_{bB} & M_{cB} \\ M_{aC} & M_{bC} & M_{cC} \end{bmatrix} \begin{bmatrix} V_{ap} \\ V_{bp} \\ V_{cp} \end{bmatrix} \tag{3.87}$$

$$\begin{bmatrix} I_{ap} \\ I_{bp} \\ I_{cp} \end{bmatrix} = \begin{bmatrix} M_{aA} & M_{bA} & M_{cA} \\ M_{aB} & M_{bB} & M_{cB} \\ M_{aC} & M_{bC} & M_{cC} \end{bmatrix}^T \begin{bmatrix} I_{as} \\ I_{bs} \\ I_{cs} \end{bmatrix} \tag{3.88}$$

Transforming the output three phase voltages to space vector using (3.77)

$$\bar{V}_s = \frac{2}{3} \left(V_{as} + V_{bs} e^{j\frac{2\pi}{3}} + V_{cs} e^{j\frac{4\pi}{3}} \right) \quad (3.89)$$

Substituting (3.87) into (3.89)

$$\bar{V}_s = \frac{2}{3} \left(\begin{array}{l} (M_{aA} V_{ap} + M_{bA} V_{bp} + M_{cA} V_{cp}) + \\ (M_{aB} V_{ap} + M_{bB} V_{bp} + M_{cB} V_{cp}) e^{j\frac{2\pi}{3}} + \\ (M_{aC} V_{ap} + M_{bC} V_{bp} + M_{cC} V_{cp}) e^{j\frac{4\pi}{3}} \end{array} \right) \quad (3.90)$$

The input three phase capacitor voltages can be represented in the terms of the input voltage space vector using the inverse transformation given in (3.78) for a balance voltage sets.

$$\begin{aligned} V_{ap} &= \bar{V}_p \cdot e^{j0} \\ V_{bp} &= \bar{V}_p \cdot e^{j\frac{2\pi}{3}} \\ V_{cp} &= \bar{V}_p \cdot e^{j\frac{4\pi}{3}} \end{aligned} \quad (3.91)$$

Substituting (3.91), (3.84), (3.85) and (3.86) into (3.90),

$$\bar{V}_s = \frac{\bar{V}_p}{2} (\bar{M}_A^* + \bar{M}_B^* e^{j\frac{2\pi}{3}} + \bar{M}_C^* e^{j\frac{4\pi}{3}}) + \frac{\bar{V}_p^*}{2} (\bar{M}_A + \bar{M}_B e^{j\frac{2\pi}{3}} + \bar{M}_C e^{j\frac{4\pi}{3}}) \quad (3.92)$$

Similarly, the input currents are transformed to instantaneous space vector

$$\bar{I}_p = \frac{2}{3} \left(I_{ap} + I_{bp} e^{j\frac{2\pi}{3}} + I_{cp} e^{j\frac{4\pi}{3}} \right) \quad (3.93)$$

From (3.93) and (3.88)

$$\bar{I}_p = \frac{2}{3} \begin{pmatrix} (M_{aA}I_{as} + M_{aB}I_{bs} + M_{aC}I_{cs}) + \\ (M_{bA}I_{as} + M_{bB}I_{bs} + M_{bC}I_{cs})e^{j\frac{2\pi}{3}} + \\ (M_{cA}I_{as} + M_{cB}I_{bs} + M_{cC}I_{cs})e^{j\frac{4\pi}{3}} \end{pmatrix} \quad (3.94)$$

Using the inverse transformation, the output current can be given in terms of the output current space vector as follows.

$$\begin{aligned} I_{as} &= \bar{I}_s \cdot e^{j0} \\ I_{bs} &= \bar{I}_s \cdot e^{j\frac{2\pi}{3}} \\ I_{cs} &= \bar{I}_s \cdot e^{j\frac{4\pi}{3}} \end{aligned} \quad (3.95)$$

Substituting (3.95), (3.84), (3.85) and (3.86)

$$\bar{I}_p = \frac{\bar{I}_s}{2} (\bar{M}_A + \bar{M}_B e^{j\frac{2\pi}{3}} + \bar{M}_C e^{j\frac{4\pi}{3}}) + \frac{\bar{I}_s^*}{2} (\bar{M}_A + \bar{M}_B e^{j\frac{4\pi}{3}} + \bar{M}_C e^{j\frac{2\pi}{3}}) \quad (3.96)$$

From (3.92) and (3.96), the following three vectors can be introduced

$$\bar{M}_D = \frac{1}{3} \left(\bar{M}_A + \bar{M}_B e^{j\frac{2\pi}{3}} + \bar{M}_C e^{j\frac{4\pi}{3}} \right) \quad (3.97)$$

$$\bar{M}_I = \frac{1}{3} \left(\bar{M}_A + \bar{M}_B e^{j\frac{4\pi}{3}} + \bar{M}_C e^{j\frac{2\pi}{3}} \right) \quad (3.98)$$

$$\bar{M}_0 = \frac{1}{3} (\bar{M}_A + \bar{M}_B + \bar{M}_C) \quad (3.99)$$

The three vectors, \bar{M}_D , \bar{M}_I and \bar{M}_0 might be considered as a direct, inverse and zero components of the duty-cycle space vector.

\bar{M}_A , \bar{M}_B and \bar{M}_C can be computed using the inverse transformation of (3.97) – (3.99).

$$\bar{M}_A = \frac{1}{3}(\bar{M}_D + \bar{M}_I + \bar{M}_O) \quad (3.100)$$

$$\bar{M}_B = \frac{1}{3}\left(\bar{M}_D e^{j\frac{4\pi}{3}} + \bar{M}_I e^{j\frac{2\pi}{3}} + \bar{M}_O\right) \quad (3.101)$$

$$\bar{M}_C = \frac{1}{3}\left(\bar{M}_D e^{j\frac{2\pi}{3}} + \bar{M}_I e^{j\frac{4\pi}{3}} + \bar{M}_O\right) \quad (3.102)$$

Substituting (3.100)-(3.102) into (3.92)

$$\bar{V}_s = \frac{3}{2}\bar{V}_p\bar{M}_I^* + \frac{3}{2}\bar{V}_p^*\bar{M}_D \quad (3.103)$$

Substituting (3.100)-(3.102) into (3.96)

$$\bar{I}_p = \frac{3}{2}\bar{I}_s\bar{M}_I + \frac{3}{2}\bar{I}_s^*\bar{M}_D \quad (3.104)$$

In a space vector modulation of a matrix converter, it is possible to control the output voltage space vector and the input current direction (or the input power factor). Note that it is not possible to control the magnitude of the input current. (3.106) is obtained by imposing the vector $\bar{I}_s\bar{M}_I + \bar{I}_s^*\bar{M}_D$ in the direction of the input current space vector [21, 26]. Therefore, the dot product of this vector with a unit vector perpendicular to the input current phase angle is zero.

$$\bar{V}_s = \frac{3}{2}\bar{V}_p\bar{M}_I^* + \frac{3}{2}\bar{V}_p^*\bar{M}_D \quad (3.105)$$

$$0 = (\bar{I}_s \bar{M}_I + \bar{I}_s^* \bar{M}_D) \cdot j\bar{\varphi} \quad (3.106)$$

$\bar{\varphi}$ is defined as a unit vector in direction of the input current space vector.

The solution for \bar{M}_D and \bar{M}_I is given in (3.107) and (3.108). The parameter λ is a real variable which reflects the degree of freedom which can be used to define different type of modulation strategy.

$$\bar{M}_D = \frac{\bar{V}_s \bar{\varphi}}{3(\bar{V}_p \cdot \bar{\varphi})} + \frac{\lambda}{\bar{V}_p^* \bar{I}_s^*} \quad (3.107)$$

$$\bar{M}_I = \frac{\bar{V}_s^* \bar{\varphi}}{3(\bar{V}_p \cdot \bar{\varphi})} - \frac{\lambda}{\bar{V}_p^* \bar{I}_s^*} \quad (3.108)$$

The vectors in (3.107) and (3.108) can be written in polar form as follows

$$\begin{aligned} \bar{V}_s &= |V_s| e^{j\theta_{vs}} \\ \bar{V}_p &= |V_p| e^{j\theta_{vp}} \\ \bar{I}_s &= |I_s| e^{j\theta_{is}} \\ \bar{I}_p &= |I_p| e^{j\theta_{ip}} \end{aligned} \quad (3.109)$$

Where θ_{ip} and θ_{vp} is the input current and voltage angles. θ_{vs} and θ_{is} are the output voltage and current, respectively. The output displacement angle, $\varphi_s = \theta_{vs} - \theta_{is}$. The voltage transfer ration is represented by q .

Substituting (3.109) into (3.107) and (3.108),

$$\bar{M}_D = \frac{1}{3} q e^{j(\theta_{vp} + \theta_{vs})} (1 + e^{-j\varphi_s} (\gamma - jr)) \quad (3.110)$$

$$\bar{M}_I = \frac{1}{3} q e^{j(\theta_{vp} - \theta_{vs})} (1 - e^{-j\varphi_s} (\gamma + jr)) \quad (3.111)$$

where

$$\gamma = \tan \varphi_p \sin \varphi_s + \frac{3\lambda}{V_s I_s} \quad (3.112)$$

$$r = \tan \varphi_p \cos \varphi_s \quad (3.113)$$

$$\varphi_p = \theta_{vp} - \theta_{ip} \quad (3.114)$$

From (3.100) to (3.102) the duty cycle space vector can be determined by adding an appropriate zero sequence components.

$$\bar{M}_{ij} = \bar{M}_D \bar{\alpha}_j^* + \bar{M}_I \bar{\alpha}_j + \bar{M}_o \quad (3.115)$$

where the unity vector $\bar{\alpha}_j$ can be given as.

$$\bar{\alpha}_j = \begin{cases} 1, & j = A \\ e^{j(2\pi/3)}, & j = B \\ e^{j(4\pi/3)}, & j = C \end{cases} \quad (3.116)$$

The duty cycle can be determined based on (3.115) and using the inverse transformation given in (3.78). It can be observed that M_{ij} is a duty cycle and it is a scalar term whereas the duty cycle space vector, \bar{M}_{ij} is a vector quantity.

$$M_{ij} = \frac{1}{3} + \bar{M}_{ij} \cdot \bar{\alpha}_k \quad (3.117)$$

Substituting (3.115) into (3.117), the expression for the duty cycles becomes

$$M_{ij} = \frac{1}{3} + (\overline{M}_D \overline{\alpha}_j^* + \overline{M}_I \overline{\alpha}_j + \overline{M}_o) \cdot \overline{\alpha}_k$$

$$M_{ij} = \frac{1}{3} + \overline{M}_o \cdot \overline{\alpha}_k + (\overline{M}_D \overline{\alpha}_j^* + \overline{M}_I \overline{\alpha}_j) \cdot \overline{\alpha}_k \quad (3.118)$$

It is necessary to note that, the duty cycle is a scalar terms since it is the result of the dot products of two vectors as seen in (3.118). In addition, it can also be expressed as a sum of two scalars as follows.

$$M_{ij} = M_{oj} + A_{ij} \quad (3.119)$$

The first scalar term is the component of the zero sequence space vectors and it is given as

$$M_{oj} = \frac{1}{3} + \overline{M}_o \cdot \overline{\alpha}_j \quad (3.120)$$

And the second terms which reflect the duty cycle space vector without the zero sequence component. These components can be defined as the duty cycle resulting from the active switching states and they are defined as

$$A_{ij} = (\overline{M}_D \overline{\alpha}_i^* + \overline{M}_I \overline{\alpha}_i) \cdot \overline{\alpha}_j \quad (3.121)$$

It is necessary to note that the above quantities linearly depend on \overline{M}_D and \overline{M}_I ; hence, they also depend on the output voltage transfer ratio and λ . Thus, A_{ij} are used to specify the parameter λ which result in the maximum output voltage transfer ratio for a given output current angle.

Since the modulation signals are average of the switching functions, the feasible value of the duty cycles is between 0 and 1. Applying this constraint on (3.119),

$$0 \leq M_{oj} + A_{ij} \leq 1 \quad (3.122)$$

It is possible to rewrite (3.122) in the following inequality,

$$-\min\{A_{ij}\} \leq M_{oj} \leq 1 - \max\{A_{ij}\} \quad (3.123)$$

Using (3.123), the following inequality holds true,

$$\max\{A_{ij}\} - \min\{A_{ij}\} \leq 1 \quad (3.124)$$

For each desired output phase voltage $V_{ref,j}$ the corresponding three active duty cycles used to synthesize it are A_{aj} , A_{bj} and A_{cj} . At any instant of time, the minimum and the maximum of the three active duty cycles are defined as $A_{j,min}$ and $A_{j,max}$, respectively.

$$\begin{aligned} A_{j,min} &= \min\{A_{aj}, A_{bj}, A_{cj}\} \\ A_{j,max} &= \max\{A_{aj}, A_{bj}, A_{cj}\} \end{aligned} \quad (3.125)$$

Substituting (3.121) into (3.124)

$$\begin{aligned} &\left| (\overline{M}_D \overline{\alpha}_{max}^* + \overline{M}_I \overline{\alpha}_{max}) \cdot \overline{\alpha}_j - (\overline{M}_D \overline{\alpha}_{min}^* + \overline{M}_I \overline{\alpha}_{min}) \cdot \overline{\alpha}_j \right| \leq 1 \\ &\left| \left(\overline{M}_D (\overline{\alpha}_{max}^* - \overline{\alpha}_{min}^*) + \overline{M}_I (\overline{\alpha}_{max} - \overline{\alpha}_{min}) \right) \cdot \overline{\alpha}_j \right| \leq 1 \\ &\left| (\overline{M}_D \Delta^* + \overline{M}_I \Delta) \cdot \overline{\alpha}_j \right| \leq 1 \end{aligned} \quad (3.126)$$

where

$$\Delta = \overline{\alpha}_{max} - \overline{\alpha}_{min} \quad (3.127)$$

Using the definition of $\bar{\alpha}$ given in (3.116), the difference between minimum and the maximum values are always $\sqrt{3}$. This is demonstrated as follow,

Case 1 $\bar{\alpha}_{\max} = \bar{\alpha}_A = 1$ and $\bar{\alpha}_{\min} = \bar{\alpha}_B = e^{j(2\pi/3)}$

$$|\Delta| = |\bar{\alpha}_{\max} - \bar{\alpha}_{\min}| = |1 - e^{j(2\pi/3)}| = \left| \frac{3}{2} + j \frac{\sqrt{3}}{2} \right| = \sqrt{3}$$

Case 2 $\bar{\alpha}_{\max} = \bar{\alpha}_B = e^{j(2\pi/3)}$ and $\bar{\alpha}_{\min} = \bar{\alpha}_C = e^{j(4\pi/3)}$

$$|\Delta| = |\bar{\alpha}_{\max} - \bar{\alpha}_{\min}| = |e^{j(2\pi/3)} - e^{j(4\pi/3)}| = |j\sqrt{3}| = \sqrt{3}$$

Case 2 $\bar{\alpha}_{\max} = \bar{\alpha}_C = e^{j(4\pi/3)}$ and $\bar{\alpha}_{\min} = \bar{\alpha}_A = 1$

$$|\Delta| = |\bar{\alpha}_{\max} - \bar{\alpha}_{\min}| = |e^{j(4\pi/3)} - 1| = \left| -\frac{3}{2} - j \frac{\sqrt{3}}{2} \right| = \sqrt{3}$$

From (3.126) the worst case is when the following scalar product is maximum.

$$\left\| (\bar{M}_D \Delta^* + \bar{M}_I \Delta) \right\| \leq 1 \quad (3.128)$$

Substituting (3.110) and (3.111) into (3.128)

$$\left\| (\bar{M}_D \Delta^* + \bar{M}_I \Delta) \right\| = \frac{2}{\sqrt{3}} q \left\| \cos(\theta_s - \theta_\Delta) + j\gamma \sin(\theta_s - \theta_\Delta - \varphi_s) - j\gamma \cos(\theta_s - \varphi_s - \theta_\Delta) \right\| \quad (3.129)$$

Cauchy-Swartz inequality: states that for any vector x and y

$$\|x + y\| \leq \|x\| \|y\| = \sqrt{x^2 + y^2} \quad (3.130)$$

Applying the property of Cauchy-Swartz inequality on (3.129),

$$\|\cos(\theta_s - \theta_\Delta) + j\gamma \sin(\theta_s - \theta_\Delta - \varphi_s) - jr \cos(\theta_s - \varphi_s - \theta_\Delta)\| \leq \sqrt{1 + \gamma^2 + r^2} \quad (3.131)$$

Substituting (3.131) and (3.129),

$$\|(\overline{M}_D \Delta^* + \overline{M}_I \Delta)\| = \frac{2}{\sqrt{3}} q \sqrt{1 + \gamma^2 + r^2} \quad (3.132)$$

Using (3.128) and (3.132)

$$\frac{2}{\sqrt{3}} q \sqrt{1 + \gamma^2 + r^2} \leq 1 \quad (3.133)$$

It can be rewritten as

$$q \leq \frac{\sqrt{3}}{2\sqrt{1 + \gamma^2 + r^2}} \quad (3.134)$$

From the matrix converter maximum allowable voltage transfer ratio,

$$q \leq \frac{\sqrt{3}}{2} \quad (3.135)$$

Based on (134) and (135), the condition for the maximum voltage transfer function is give as

$$\gamma = 0 \text{ and } r = 0 \quad (3.136)$$

Base on the condition given in (3.136) and substituting into (3.112), the necessary condition to obtain the maximum voltage transfer ratio is obtained if the parameter λ has the following value

$$\lambda = -\frac{1}{3}(1 - j \tan(\varphi_p) \sin(\varphi_s) V_s I_s) \quad (3.137)$$

φ_p and φ_s are the input and output power factors.

Substituting (3.137) into (3.110) and (3.111)

$$\bar{M}_D = \frac{\bar{V}_s}{3\bar{V}_p^*} (1 - j \tan(\varphi_p) \cos(\varphi_s) e^{-j\varphi_s}) \quad (3.138)$$

$$\bar{M}_I = \frac{\bar{V}_s}{3\bar{V}_p^*} (1 - j \tan(\varphi_p) \cos(\varphi_s) e^{j\varphi_s}) \quad (3.139)$$

The zero sequence components are necessary for the calculation of the duty-cycle and the basic idea is to search the minimum among the duty cycles for each input phase.

$$\delta_{oj} = \min(M_{ij}) \quad (3.140)$$

After the minimum duty cycle δ_{oj} is computed, substituting (3.119) into (3.140).

$$M_{oj} = \delta_{oj} - \min(A_{ij}) \quad (3.141)$$

Finally, the zero sequence components can be calculated as

$$\bar{M}_o = \frac{2}{3} \sum_{j=1}^3 M_{oj} \bar{\alpha}_j \quad (3.142)$$

To summarize the duty cycle space vector, consider the desired three phase output voltages are

$$\begin{aligned} V_{as_ref} &= V_{s_ref} \cos(\omega_s t + \theta_s) \\ V_{bs_ref} &= V_{s_ref} \cos(\omega_s t + \theta_s - \frac{2\pi}{3}) \\ V_{cs_ref} &= V_{s_ref} \cos(\omega_s t + \theta_s + \frac{2\pi}{3}) \end{aligned}$$

Space vector for the desired output voltage are found using the transformations given in (3.77). The desired output voltage vector can be represented as \bar{V}_{s_ref} . For the known output current angle, the output power factor can be represented as φ_s . Therefore, \bar{M}_D , \bar{M}_I and \bar{M}_o for the desired output voltage and input power factor φ_{p_ref} under the given output power factor can be determined as follow

Once, \bar{M}_D , \bar{M}_I and \bar{M}_o are determined the duty cycles can be calculated based on

$$\bar{M}_D = \frac{\bar{V}_{s_ref}}{3\bar{V}_p^*} (1 - j \tan(\varphi_{p_ref}) \cos(\varphi_s) e^{-j\varphi_s})$$

$$\bar{M}_I = \frac{\bar{V}_{s_ref}}{3\bar{V}_p^*} (1 - j \tan(\varphi_{p_ref}) \cos(\varphi_s) e^{j\varphi_s})$$

$$\bar{M}_o = \frac{2}{3} \sum_{j=1}^3 M_{oj} \bar{\alpha}_j$$

Once the duty cycle space vectors \bar{M}_D , \bar{M}_I and \bar{M}_o are determined, the duty cycles of each switch can be calculated as follows

$$M_{ij} = \frac{1}{3} + \bar{M}_o \cdot \bar{\alpha}_k + (\bar{M}_D \bar{\alpha}_j^* + \bar{M}_I \bar{\alpha}_j) \cdot \bar{\alpha}_k$$

$$M_{oj} = \frac{1}{3} + \bar{M}_o \cdot \bar{\alpha}_j$$

These expressions give the appropriate duty cycle for each switch to synthesize the desired output voltage and input current direction (or input power factor) simultaneously.

3.4 Simulation Results and Discussion

Simulation has been done using the carrier based modulation techniques and using a 60 Hz of input frequency, 30 Hz output frequency and 5 kHz switching frequencies and the results are demonstrated in Figure 3.13 to Figure 3.20.

Figure 3.13 shows the modulation signals used to generate phase 'a' output voltage. This modulation signal have basically consists of the dc component, the sum of the input and output frequencies, 90Hz and the difference between the two frequencies, 30Hz as seen in Figure 3.14. Unlike the conventional PWM technique for converters, the modulation signals do not directly used to generate the switching pulses rather the three signals Z_{1A} , Z_{2A} and Z_{3A} are first synthesized as seen in Figure 3.15. Since Z_{3A} is always unity the corresponding intermediate pulses P_{3A} is also ON and it is not shown in Figure 3.16. This figure only show the intermediate pulses P_{1A} and P_{2A} generated by comparing Z_{1A} and Z_{2A} , with triangle carrier.

After the intermediate signals are generated, actual switching signals are produced using (3.15) and presented in Figure 3.17. As seen from the results, only one switch is turned ON at each instant of time which avoids input voltage short circuit and there is a one switch which turns ON so that a current path is always provided. With similar approach, the modulation signals used to synthesize the output phase 'b' voltage are shown in Figure 3.18 and the actual switching signal which compiles both Kirchhoff's laws are given in Figure 3.19. And finally Figure 3.20 and Figure 3.21 show the modulation and actual switching signals which synthesize phase 'c' output voltage.

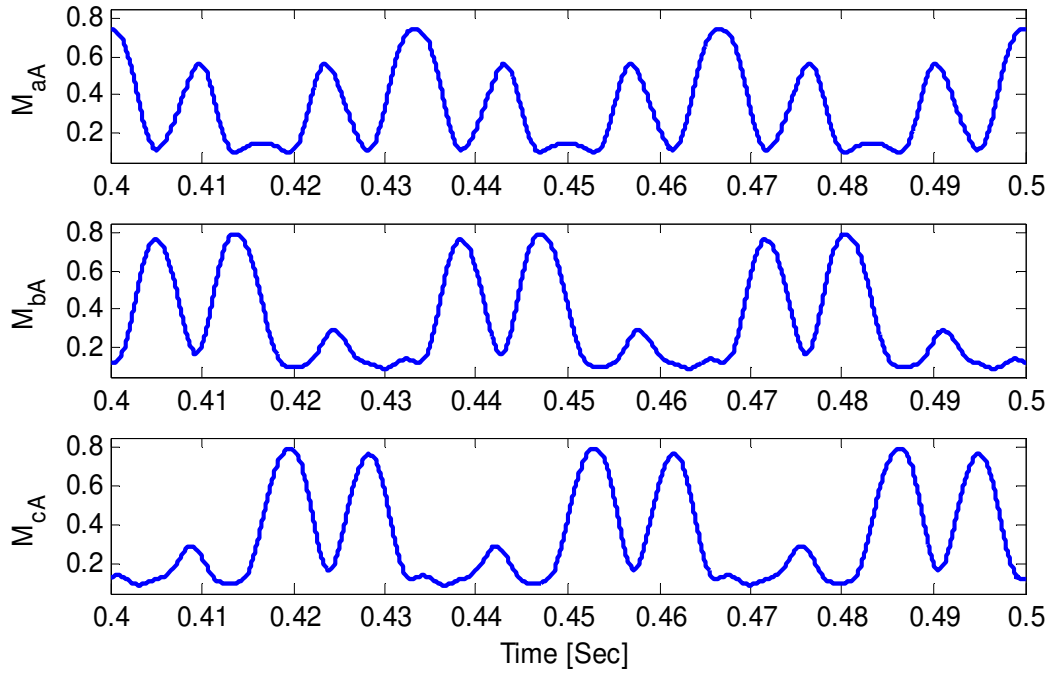


Figure 3.13 Modulation signals for output phase 'a' voltage

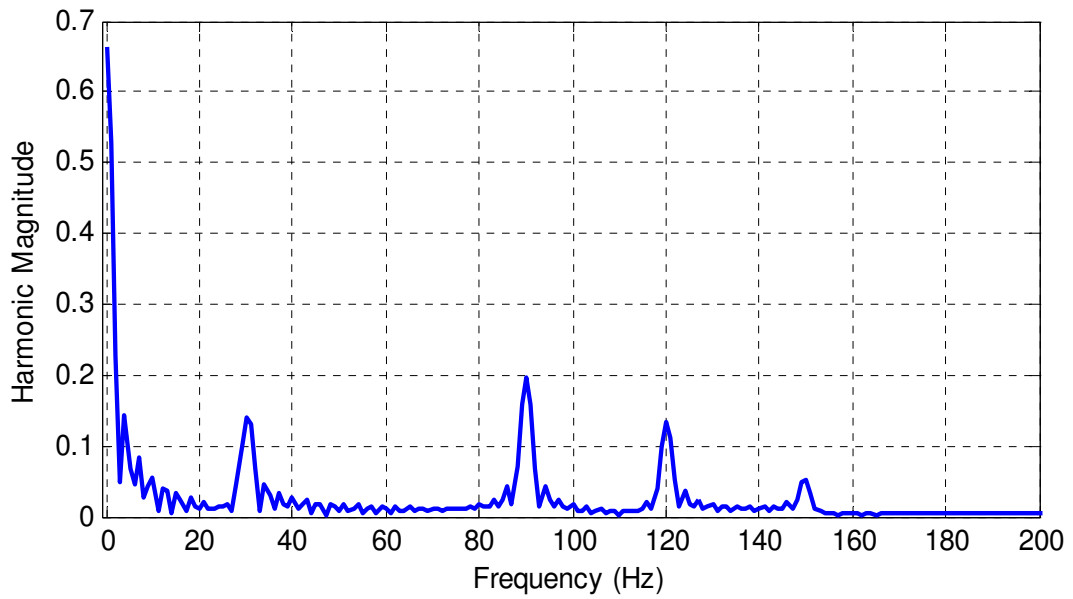


Figure 3.14 FFT for the modulation signal M_{aA}

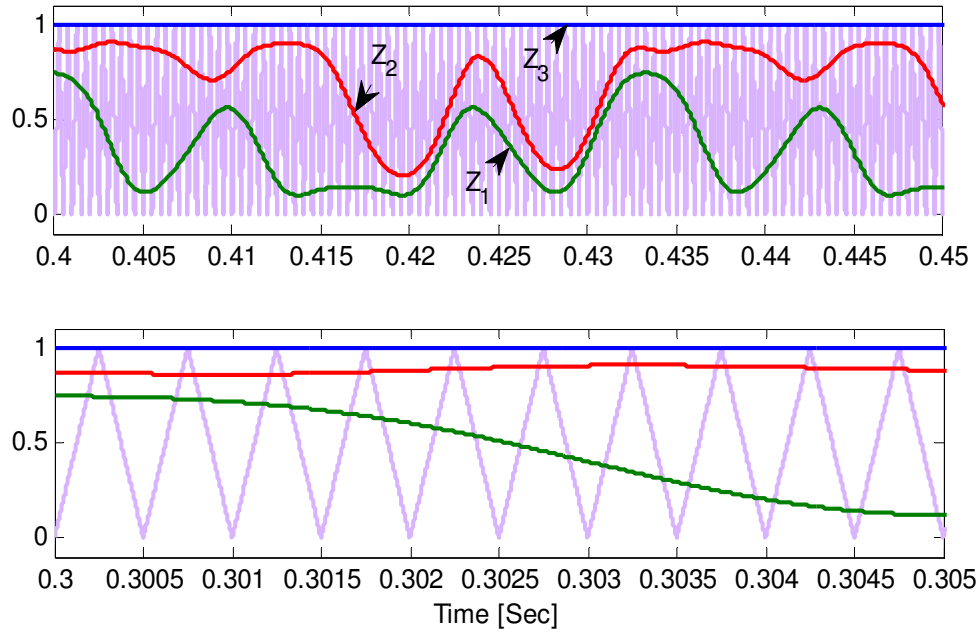


Figure 3.15 Carrier based pulse width modulation

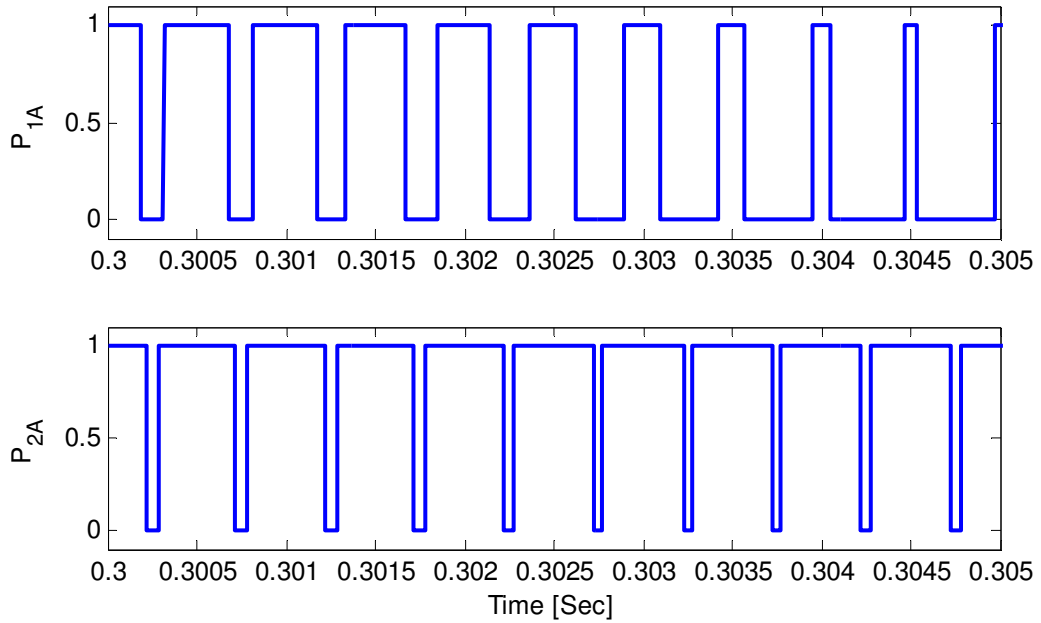


Figure 3.16 Intermediate signals used to generate switching signals

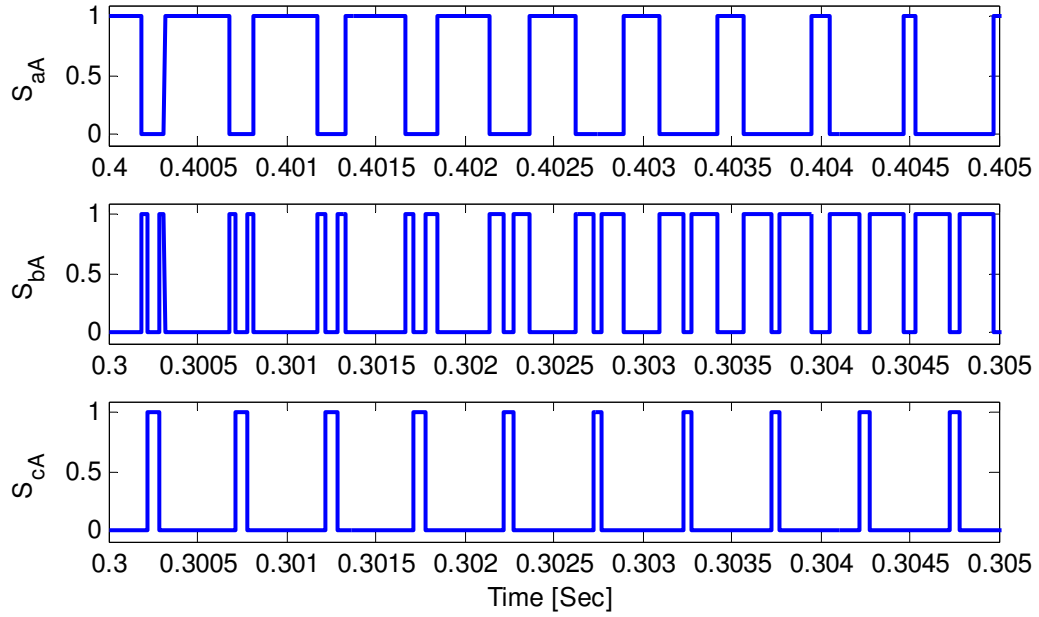


Figure 3.17 Switching signals for output phase 'a' voltage

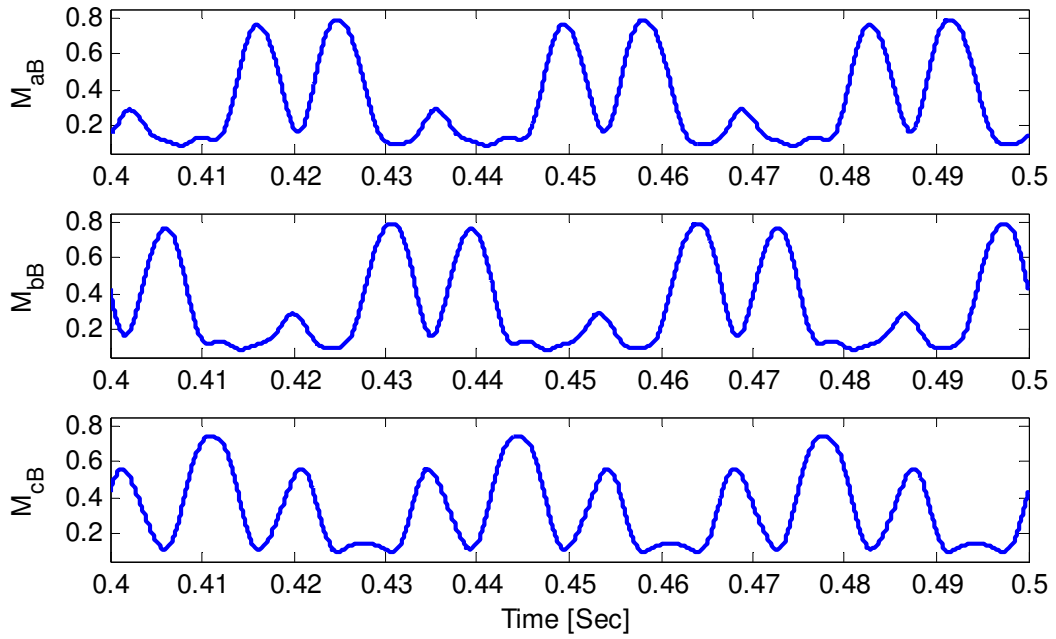


Figure 3.18 Modulation signals for output phase 'b' voltage

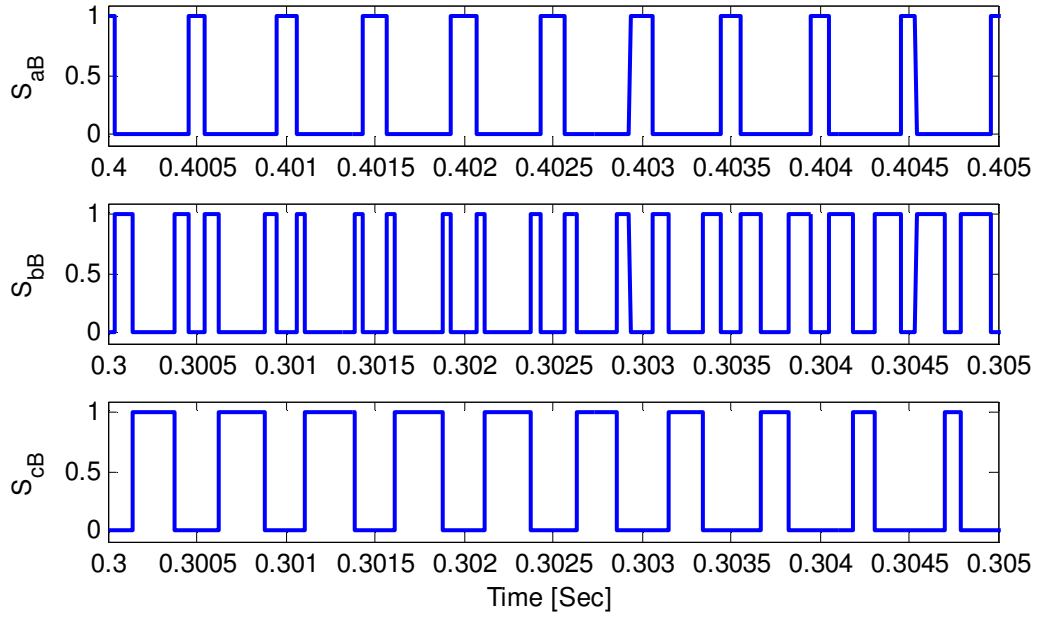


Figure 3.19 Switching signals for output phase 'b' voltage

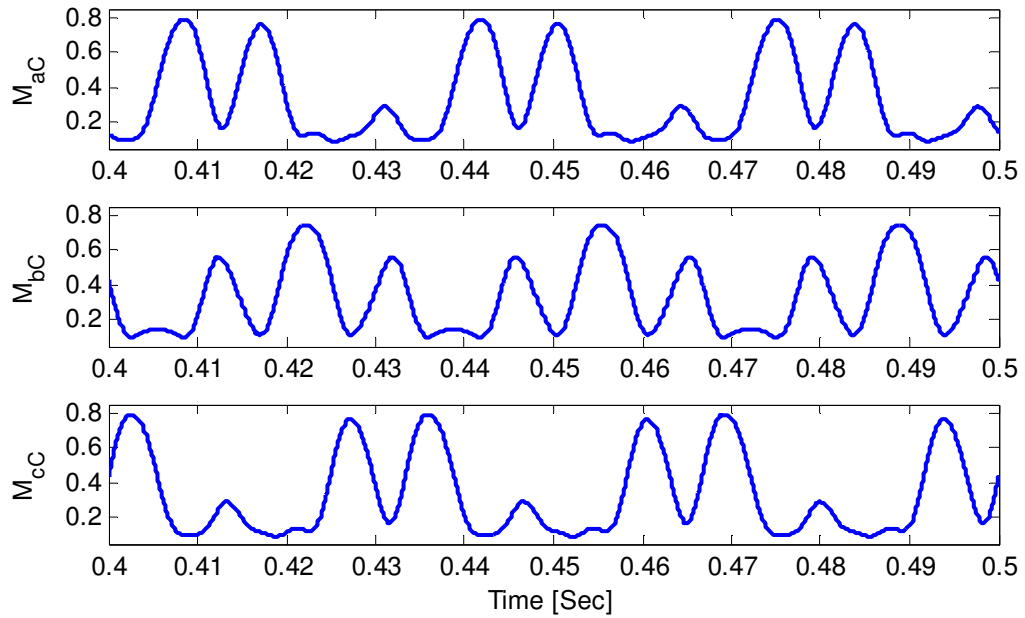


Figure 3.20 Modulation signals for output phase 'c' voltage

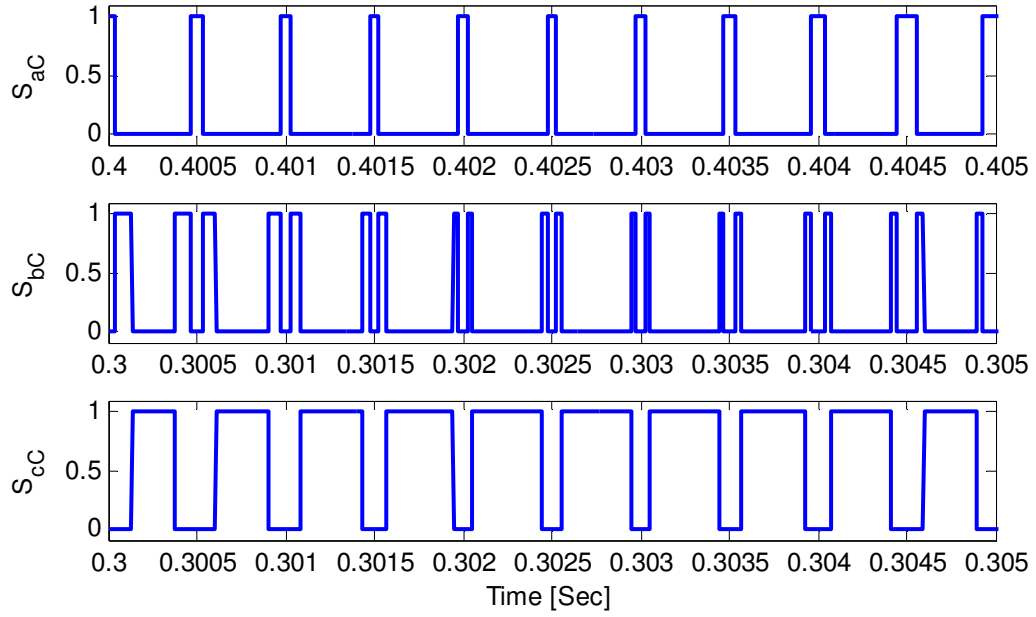


Figure 3.21 Switching signals for output phase 'c' voltage

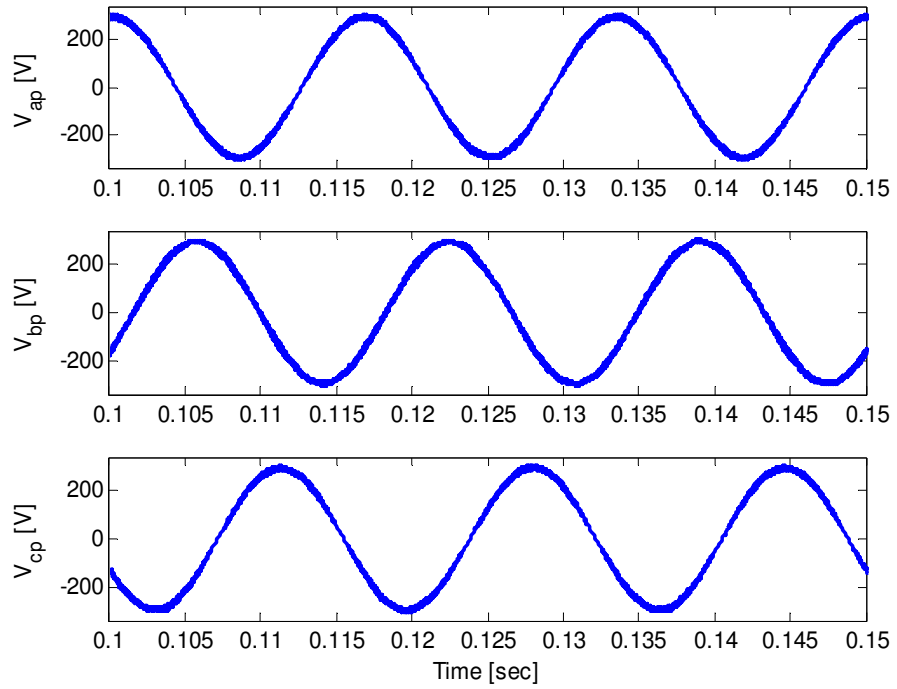


Figure 3.22 Input three phase voltages

The modulation signals generated using the methods discussed in this chapter is used to synthesize the desired three phase output voltage of $180V$ phase peak-to-peak with a frequency of $50Hz$. The input three phase voltages are $310V$ with a frequency of $60Hz$ as shown in Figure 3.22. As seen in Figure 3.23, the desired voltages are about $180V/50Hz$ and form balanced sets. The input power factor at the input terminal of the matrix converter is kept high to allow wide range of voltage transfer ratio. Figure 3.24 shows the input phase 'a' capacitor voltage and phase 'a' input matrix converter current which are in phase and hence unity input power factor operation at the input terminal. From Figure 3.23 in particular, it can be concluded that the developed carrier-based modulation scheme along with the technique used to generate the actual nine switching signal perfectly synthesizes the desired output voltage.

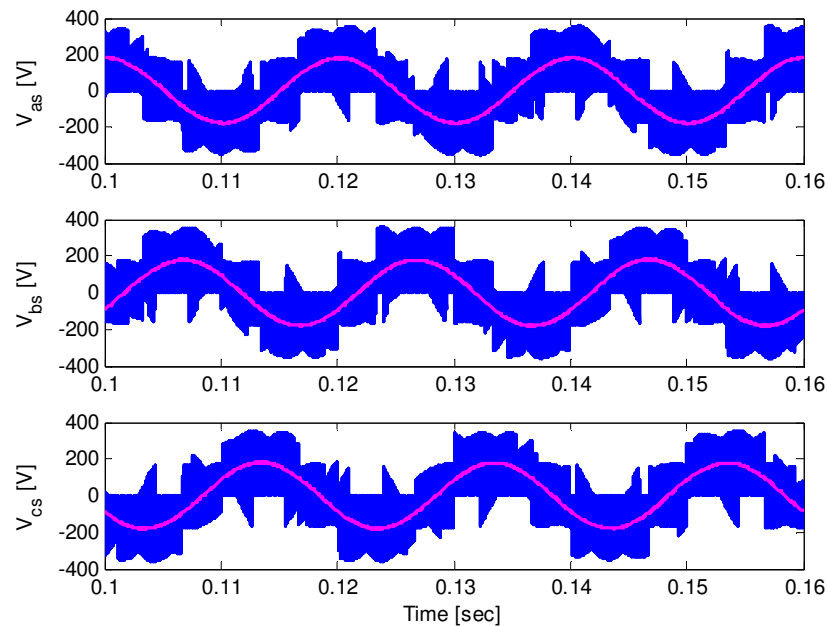


Figure 3.23 synthesized output three phase voltages

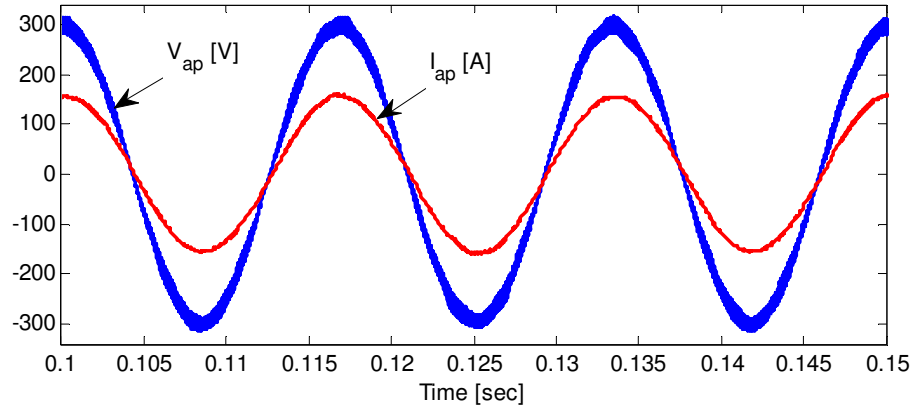


Figure 3.24 Phase 'a' input capacitor voltage and input matrix converter current with unity input power factor

3.5 Conclusion

The chapter presents both carrier-based and space vector modulation technique for three phase-to-three phase matrix converter. The resulting expressions of the modulation signals are simple and suitable for practical implementation. Besides, it is general that it can be used for unbalanced input voltages. It is interesting that this technique gives the same result as the complex and the more mathematically intensive approaches given in [3]. Detailed methodologies for generation of switching signals are also presented. The direct and indirect space vector modulations are clearly developed. The final result shows that it is possible to equivalently analyze the matrix converter into rectifier and inverter stages for the purpose of modulation and result in the same switching configuration as the direct space vector modulation. Although the space vector modulation does not require injection of third harmonic component, the common mode voltage is derived using space

vector which can be implemented in carrier based modulation. Computer simulation has also been done to verify the theoretical modulation technique and results demonstrate the generation of the switching signals which synthesize the output three phase voltage.

CHAPTER 4

INPUT FILTER DESIGN

4.1 Introduction

This chapter propose a new input filter design technique for a three phase to three phase matrix converter. The objective of the input filter is to mitigate the high frequency component of the switching signals from injecting into the ac mains. The type of input filter developed in this work is the conventional first order LC filter. For the purpose of specifying the switching signals which generate input current harmonics, a Fourier series of a switching signals are derived. This Fourier series analysis can possibly used to study the spectrum of the input current and output current waveforms. This Fourier series analysis is presented step by step following Appendix F. A harmonic balance technique is presented to independently study the fundamental and ripple component input and output waveforms. The complete derivations for the new input filter design methodology are set forth in detail. Since the input filter greatly affects the stability of a matrix converter system, the overall system stability under the designed input filter is studied. This analysis involves a small signal modeling and steady state analysis for a matrix converter feeding an RL load. Computer simulation has been done to show the performance of the proposed input filter design. These results also show that the designed filter meets the resonance frequency requirement as well as overall system stability criteria.

4.2 Fourier Series Analysis of Switching Signals of a Matrix Converter

This section present the Fourier series analysis of the switching signals of a three phase-to-three phase matrix converter. The expression of the modulation signals of a matrix converter which is the approximation of the switching function is given in (4.2).where $i = a, b$ or c and $j = A, B$ or C . In this analysis the common mode voltage is not included for the purpose of simplicity and without losing the generality.

$$M_{ij} = \frac{1}{3} + \frac{2V_{ip}V_{js}}{3V_p^2} \quad (4.1)$$

Define the phase ‘ i ’ input capacitor voltage and phase ‘ j ’ output voltages below where δ_{ip} and δ_{is} are the phase angles of the input and output voltages, respectively.

$$\begin{aligned} V_{ip} &= V_p \cos(\omega_p t + \delta_{ip}) \\ V_{js} &= V_s \cos(\omega_s t + \delta_{js}) \end{aligned} \quad (4.2)$$

Substituting (4.2) into (4.1)

$$M_{ij} = \frac{1}{3} + \frac{2V_s}{3V_p} \cos(\omega_p t + \delta_{ip}) \cos(\omega_s t + \delta_{js}) \quad (4.3)$$

Using the following trigonometric identity:

$$\cos(A) \cos(B) = \frac{1}{2} (\cos(A+B) + \cos(A-B))$$

Substituting the above trigonometric relation in (4.3), the modulation signal consists of two frequency components, one at the sum and the other on difference between the input and output frequencies as shown in Figure 2.14.

$$M_{ij} = \frac{1}{3} + \frac{V_s}{3V_p} \cos((\omega_p + \omega_s)t + \delta_{ip} + \delta_{js}) + \frac{V_s}{3V_p} \cos((\omega_p - \omega_s)t + \delta_{ip} - \delta_{js}) \quad (4.4)$$

The phase angles of the three phases input voltages are shown below considering a balanced source.

$$\delta_{ap} = \omega_p t, \quad \delta_{bp} = \omega_p t - \frac{2\pi}{3}, \quad \delta_{cp} = \omega_p t + \frac{2\pi}{3}$$

Similarly, the phase angles of the output voltages are

$$\delta_{As} = \omega_s t, \quad \delta_{Bs} = \omega_s t - \frac{2\pi}{3}, \quad \delta_{Cs} = \omega_s t + \frac{2\pi}{3}$$

The modulation signal corresponding to phase *a* input and phase *a* output voltage is represented as:

$$M_{aA} = \frac{1}{3} + \frac{V_s}{3V_p} (\cos(\omega_p - \omega_s)t + \cos(\omega_p + \omega_s)t) \quad (4.5)$$

Define the following rational numbers *a* and *b*. It is necessary to note that these constants may or may not be an integer based on input to output frequency.

$$\begin{aligned} a &= \frac{\omega_p}{\omega_s} - 1 \\ b &= \frac{\omega_p}{\omega_s} + 1 \end{aligned} \quad (4.6)$$

Substituting (4.6) into (4.5), and defining the output-to-input voltage transfer ratio, *q*

$$\begin{aligned} q &= \frac{V_s}{V_p} \\ M_{aA} &= \frac{1}{3} + \frac{q}{3} (\cos a \omega_s t + \cos b \omega_s t) \end{aligned} \quad (4.7)$$

From (4.7), the modulation signals can be considered as a^{th} and b^{th} harmonic components of output voltages. (4.7) can also be represented in terms of the input frequency and then it can be considered as harmonic components of input supply frequency rather than the output. Similarly, the other two modulation signals which synthesize the output phase 'a' voltage is given in (4.8) and (4.9), respectively.

$$M_{bA} = \frac{1}{3} + \frac{q}{3} (\cos(a\omega_s t - \beta) + \cos(b\omega_s t - \beta)) \quad (4.8)$$

$$M_{cA} = \frac{1}{3} + \frac{q}{3} (\cos(a\omega_s t + \beta) + \cos(b\omega_s t + \beta)) \quad (4.9)$$

The generalized expression for the modulation signals are shown below.

$$M_{ij} = \frac{1}{3} + \frac{V_s}{3V_p} (\cos(a\omega_s t + \theta_{ao}) + \cos(b\omega_s t + \theta_{bo})) \quad (4.10)$$

Where θ_{ao} and θ_{bo} the initial angles for the a^{th} and b^{th} harmonic component of the output voltage which are expressed in (4.11) and (4.12) respectively.

$$\theta_{ao} = \begin{cases} 0 & ; M_{aA}, M_{bB} \text{ and } M_{cC} \\ \frac{2\pi}{3} & ; M_{cA}, M_{aB} \text{ and } M_{bC} \\ -\frac{2\pi}{3} & ; M_{bA}, M_{cB} \text{ and } M_{aC} \end{cases} \quad (4.11)$$

The angle for the second harmonics are considered as

$$\theta_{bo} = \begin{cases} 0 & ; M_{aA}, M_{cB} \text{ and } M_{bC} \\ \frac{2\pi}{3} & ; M_{cA}, M_{bB} \text{ and } M_{aC} \\ -\frac{2\pi}{3} & ; M_{bA}, M_{aB} \text{ and } M_{cC} \end{cases} \quad (4.12)$$

The harmonic spectrum of a generalized carrier-based PWM wave can be expressed as (4.13) where the modulating signals consist of a^{th} and b^{th} harmonic and non-zero phase angles [58].

$$\begin{aligned}
f(x, y) = & \frac{A_{00}}{2} + \sum_{n=1}^{\infty} (A_{0n} \cos(ny) + B_{0n} \sin(ny)) \\
& + \sum_{m=1}^{\infty} (A_{m0} \cos(mx) + B_{m0} \sin(mx)) \\
& + \sum_{m=1}^{\infty} \sum_{\substack{n=-\infty \\ n \neq 0}}^{\infty} (A_{mn} \cos(mx + ny) + B_{mn} \sin(mx + ny))
\end{aligned} \tag{4.13}$$

Where m is carrier index variable which denotes the multiples of carrier frequency and n is base band index variable represents the multiples of fundamental frequency [53-54]. The first term in (4.13), $A_{00}/2$ denotes the dc offset of the PWM waveform. The first summation term defines the fundamental frequency component and baseband harmonics. The second summation term defines the carrier frequency components. And the double sum with defines the sideband harmonics around the carrier harmonic components. x and y which are defined as:

$$\begin{aligned}
y &= \omega_s t \\
x &= \omega_c t
\end{aligned} \tag{4.14}$$

The coefficients are defined below.

$$C_{mn} = A_{mn} + jB_{mn} = \frac{1}{2\pi^2} \int_{-\pi}^{\pi} \int_{-\pi}^{\pi} f(x, y) e^{j(mx+ny)} dx dy \tag{4.15}$$

With a similar approach, the switching signals of the matrix converter can also be represented in (4.16). The complex Fourier coefficients corresponding to the DC offset, the baseband harmonics and the side band harmonics around the carrier are computed calculated separately.

$$\begin{aligned}
S_{ij}(\omega_s, \omega_c) = & \frac{A_{00}}{2} + \sum_{n=1}^{\infty} (A_{0n} \cos(n\omega_s t) + B_{0n} \sin(n\omega_s t)) \\
& + \sum_{m=1}^{\infty} (A_{m0} \cos(m\omega_c t) + B_{m0} \sin(m\omega_c t)) \\
& + \sum_{m=1}^{\infty} \sum_{\substack{n=-\infty \\ n \neq 0}}^{\infty} (A_{mn} \cos(m\omega_c t + n\omega_s t) + B_{mn} \sin(m\omega_c t + n\omega_s t))
\end{aligned} \tag{4.16}$$

The coefficient of the DC offset can be computed when $m = 0$ and $n = 0$ and using (4.16)

$$C_{00} = \frac{1}{2\pi^2} \int_{-\pi}^{\pi} \int_{-\pi M_{ij}}^{\pi M_{ij}} e^{j(0x+0y)} dx dy$$

Substituting (4.10) and evaluating the double integrals,

$$C_{00} = \frac{2}{3} + \frac{2q}{3\pi a} \sin(a\pi) \cos(\theta_{ao}) + \frac{2q}{3\pi b} \sin(b\pi) \cos(\theta_{bo}) \tag{4.17}$$

Since the above expression only contains a real part, the imaginary component B_{00} becomes zero.

$$A_{00} = \frac{2}{3} + \frac{2q}{3\pi a} \sin(a\pi) \cos(\theta_{ao}) + \frac{2q}{3\pi b} \sin(b\pi) \cos(\theta_{bo}) \tag{4.18}$$

If the ratio of the input to output frequency is integer, the coefficients are simplified as follows.

$$A_{00} = C_{00} = \frac{2}{3}$$

The coefficient for the base band harmonics computed when $m = 0$ and $n > 0$

$$C_{0n} = \frac{1}{2\pi^2} \int_{-\pi}^{\pi} \int_{-\pi M_{ij}}^{\pi M_{ij}} e^{j(0x+ny)} dx dy$$

Substituting (4.10) and evaluating the inner integral

$$C_{0n} = \frac{1}{3\pi} \int_{-\pi}^{\pi} e^{jny} dy + \frac{q}{3\pi} \int_{-\pi}^{\pi} (\cos(ay + \theta_{ao}) + \cos(by + \theta_{bo})) e^{jny} dy$$

Since integral of the exponential function over a period gives a Sinc function

$$\int_{-\pi}^{\pi} e^{jny} dy = \int_{-\pi}^{\pi} e^{-jny} dy = \frac{2\pi \sin(n\pi)}{n\pi}$$

The cosine function can be represented in terms of the exponential function as follows.

$$\cos(by + \theta_{bo}) = \frac{1}{2} \left(e^{j(by + \theta_{bo})} + e^{-j(by + \theta_{bo})} \right)$$

The integral of this function over the period is

$$\int_{-\pi}^{\pi} \cos(ay + \theta_{ao}) e^{jny} dy = e^{j\theta_{ao}} \frac{\pi \sin((a+n)\pi)}{(a+n)\pi} + e^{-j\theta_{ao}} \frac{\pi \sin((a-n)\pi)}{(a-n)\pi}$$

Similarly,

$$\int_{-\pi}^{\pi} \cos(by + \theta_{bo}) e^{jny} dy = e^{j\theta_{bo}} \frac{\pi \sin((b+n)\pi)}{(b+n)\pi} + e^{-j\theta_{bo}} \frac{\pi \sin((b-n)\pi)}{(b-n)\pi}$$

Therefore the final expression for the coefficient becomes

$$C_{0n} = \frac{2 \sin(n\pi)}{3 n\pi} + \frac{q}{3} \left(e^{j\theta_{ao}} \frac{\sin((a+n)\pi)}{(a+n)\pi} + e^{-j\theta_{ao}} \frac{\sin((a-n)\pi)}{(a-n)\pi} \right) + \frac{q}{3} \left(e^{j\theta_{bo}} \frac{\sin((b+n)\pi)}{(b+n)\pi} + e^{-j\theta_{bo}} \frac{\sin((b-n)\pi)}{(b-n)\pi} \right) \quad (4.19)$$

The coefficient of the side band dominant harmonics which are the a^{th} and b^{th} harmonics can be determined from (4.19) as follows:

For $n = a$

$$C_{0a} = \frac{2 \sin(a\pi)}{3 a\pi} + \frac{q}{3} \left(e^{j\theta_{ao}} \frac{\sin(2a\pi)}{2a\pi} + e^{-j\theta_{ao}} \right) + \frac{q}{3} \left(e^{j\theta_{bo}} \frac{\sin((b+a)\pi)}{(b+a)\pi} + e^{-j\theta_{bo}} \frac{\sin((b-a)\pi)}{(b-a)\pi} \right)$$

For $n = b$

$$C_{0b} = \frac{2 \sin(b\pi)}{3 b\pi} + \frac{q}{3} \left(e^{j\theta_{ao}} \frac{\sin((a+b)\pi)}{(a+b)\pi} + e^{-j\theta_{ao}} \frac{\sin((a-b)\pi)}{(a-b)\pi} \right) + \frac{q}{3} \left(e^{j\theta_{bo}} \frac{\sin(2b\pi)}{2b\pi} + e^{-j\theta_{bo}} \right)$$

The third terms in (4.16) are the carrier harmonics when $m > 0$ and $n = 0$ and the coefficients can be computed as follows.

$$C_{m0} = \frac{1}{2\pi^2} \int_{-\pi}^{\pi} \int_{-\pi M_{ij}}^{\pi M_{ij}} e^{j(mx+0y)} dx dy$$

After evaluating the inner integral, it is possible to split into two terms

$$C_{mo} = \frac{e^{\frac{j m \pi}{3}}}{j 2 m \pi^2} \int_{-\pi}^{\pi} e^{\frac{j m \pi}{3} q \cos(ay + \theta_{ao})} e^{\frac{j m \pi}{3} q \cos(by + \theta_{bo})} dy - \frac{e^{-\frac{j \pi}{3}}}{j 2 m \pi^2} \int_{-\pi}^{\pi} e^{-\frac{j m \pi}{3} q \cos(ay + \theta_{ao})} e^{-\frac{j m \pi}{3} q \cos(by + \theta_{bo})} dy$$

Define the following two terms and the integrals are done separately,

$$C_{mo} = \frac{e^{\frac{j m \pi}{3}}}{j 2 m \pi^2} G - \frac{e^{-\frac{j \pi}{3}}}{j 2 m \pi^2} G^*$$

$$G = \int_{-\pi}^{\pi} \left(J_o\left(\frac{\pi n}{3} q\right) + 2 \sum_{k=1}^{\infty} j^k J_k\left(\frac{\pi n}{3} q\right) \cos(aky + k\theta_{ao}) \right) \left(J_o\left(\frac{\pi n}{3} q\right) + 2 \sum_{h=1}^{\infty} j^h J_h\left(\frac{\pi n}{3} q\right) \cos(bhy + h\theta_{bo}) \right) dy \quad (4.20)$$

$$G^* = \int_{-\pi}^{\pi} \left(J_o\left(\frac{\pi n}{3} q\right) + 2 \sum_{k=1}^{\infty} j^{-k} J_k\left(\frac{\pi n}{3} q\right) \cos(aky + k\theta_{ao}) \right) \left(J_o\left(\frac{\pi n}{3} q\right) + 2 \sum_{h=1}^{\infty} j^{-h} J_h\left(\frac{\pi n}{3} q\right) \cos(bhy + h\theta_{bo}) \right) dy \quad (4.21)$$

Using Jacobi-Anger expansion $e^{\pm j \xi \cos(\theta)}$ can be given in Bessel series expressions as [58]:

$$e^{\pm j \xi \cos(\theta)} = J_o(\xi) + 2 \sum_{k=1}^{\infty} j^{\pm k} J_k(\xi) \cos(k\theta) \quad (4.22)$$

Applying (4.22) on (4.20) and (4.21)

$$\begin{aligned}
G &= \int_{-\pi}^{\pi} \left(\underbrace{J_o\left(\frac{\pi n}{3}q\right)J_o\left(\frac{\pi n}{3}q\right)}_{G_1} + \underbrace{2J_o\left(\frac{\pi n}{3}q\right)\sum_{h=1}^{\infty} j^h J_h\left(\frac{\pi n}{3}q\right)\cos(by + h\theta_{bo})}_{G_2} + \right. \\
&\quad \left. \underbrace{2J_o\left(\frac{\pi n}{3}q\right)\sum_{k=1}^{\infty} j^k J_k\left(\frac{\pi n}{3}q\right)\cos(aky + k\theta_{ao})}_{G_3} + \right. \\
&\quad \left. \underbrace{4\sum_{k=1}^{\infty}\sum_{h=1}^{\infty} j^{h+k} J_h\left(\frac{\pi}{3}q\right)J_k\left(\frac{\pi}{3}q\right)\cos(bhy + h\theta_{bo})\cos(aky + \theta_{ao})}_{G_4} \right) dy \\
G^* &= \int_{-\pi}^{\pi} \left(\underbrace{J_o\left(\frac{\pi n}{3}q\right)J_o\left(\frac{\pi n}{3}q\right)}_{G_1^*} + \underbrace{2J_o\left(\frac{\pi n}{3}q\right)\sum_{h=1}^{\infty} j^{-h} J_h\left(\frac{\pi n}{3}q\right)\cos(bhy + h\theta_{bo})}_{G_2^*} + \right. \\
&\quad \left. \underbrace{2J_o\left(\frac{\pi n}{3}q\right)\sum_{k=1}^{\infty} j^{-k} J_k\left(\frac{\pi n}{3}q\right)\cos(aky + k\theta_{ao})}_{G_3^*} + \right. \\
&\quad \left. \underbrace{4\sum_{k=1}^{\infty}\sum_{h=1}^{\infty} j^{-h-k} J_h\left(\frac{\pi}{3}q\right)J_k\left(\frac{\pi}{3}q\right)\cos(bhy + h\theta_{bo})\cos(aky + k\theta_{ao})}_{G_4^*} \right) dy
\end{aligned}$$

The expressions given in the above expressions consists of four terms, each of them are evaluated independently, the first terms can be given as

$$\begin{aligned}
C_{m01} &= \frac{e^{\frac{jm\pi}{3}}}{j2m\pi^2} G_1 - \frac{e^{-\frac{jm\pi}{3}}}{j2m\pi^2} G_1^* \\
C_{m01} &= \frac{2}{3} J_o\left(\frac{\pi n}{3}q\right)J_o\left(\frac{\pi n}{3}q\right) \frac{\sin\left(\frac{m\pi}{3}\right)}{\frac{m\pi}{3}} \tag{4.23}
\end{aligned}$$

And the second term is evaluated and is given in (4.24)

$$C_{m02} = \frac{2J_o\left(\frac{\pi n}{3}q\right)}{j2m\pi^2} \sum_{h=1}^{\infty} J_h\left(\frac{\pi n}{3}q\right) \left(e^{\frac{jm\pi}{3}} j^h - e^{-\frac{jm\pi}{3}} j^{-h} \right) \int_{-\pi}^{\pi} \cos(bhy + h\theta_{bo}) dy$$

Using the definition of the exponential functions

$$j^h = e^{j\pi/2^h}$$

$$e^{\frac{jm\pi}{3}} j^h - e^{-\frac{jm\pi}{3}} j^{-h} = e^{j\left(\frac{m\pi}{3} + \frac{h\pi}{2}\right)} - e^{-j\left(\frac{m\pi}{3} + \frac{h\pi}{2}\right)} = j2 \sin\left(\frac{m\pi}{3} + \frac{h\pi}{2}\right)$$

$$C_{m02} = \frac{2J_o\left(\frac{\pi n}{3}q\right)}{m\pi^2} \sum_{h=1}^{\infty} J_h\left(\frac{\pi n}{3}q\right) \sin\left(\frac{m\pi}{3} + \frac{h\pi}{2}\right) \frac{1}{hb} \sin(\pi hb) \cos(h\theta_{bo}) \quad (4.24)$$

Similarly the third terms,

$$C_{m03} = \frac{2J_o\left(\frac{\pi n}{3}q\right)}{m\pi^2} \sum_{h=1}^{\infty} J_h\left(\frac{\pi n}{3}q\right) \sin\left(\frac{m\pi}{3} + \frac{k\pi}{2}\right) \frac{1}{ak} \sin(\pi ka) \cos(k\theta_{ao}) \quad (4.25)$$

And finally the fourth term can be expressed as given in (4.26)

$$C_{m04} = \frac{4}{m\pi^2} \sum_{k=1}^{\infty} \sum_{h=1}^{\infty} J_h\left(\frac{\pi}{3}q\right) J_k\left(\frac{\pi}{3}q\right) R_4 \sin\left(\frac{\pi}{3}m + \frac{\pi}{2}(h+k)\right) \quad (4.26)$$

Where

$$R_4 = \frac{1}{2} \frac{\cos(\theta_{ao} + \theta_{bo})}{a+b} \sin((a+b)\pi) + \frac{1}{2} \frac{\cos(\theta_{ao} - \theta_{bo})}{a-b} \sin((a-b)\pi) \quad (4.27)$$

The last group consisting of the double summation determine the carrier harmonics $m > 0$ and $n \neq 0$.

$$C_{mn} = \frac{1}{2\pi^2} \int_{-\pi}^{\pi} \int_{-\pi M_{ij}}^{\pi M_{ij}} e^{j(mx+ny)} dx dy$$

$$C_{mn} = \frac{e^{\frac{jm\pi}{3}}}{j2m\pi^2} \int_{-\pi}^{\pi} e^{jny} e^{\frac{jm\pi}{3}q \cos(ay+\theta_{ao})} e^{\frac{jm\pi}{3}q \cos(by+\theta_{bo})} dy -$$

$$\frac{e^{-\frac{j\pi}{3}}}{j2m\pi^2} \int_{-\pi}^{\pi} e^{jny} e^{-\frac{jm\pi}{3}q \cos(ay+\theta_{ao})} e^{-\frac{jm\pi}{3}q \cos(by+\theta_{bo})} dy$$

Using the similar approach used in the previous expression,

$$C_{m0} = \frac{e^{\frac{j\pi}{3}}}{j2m\pi^2} G - \frac{e^{-\frac{j\pi}{3}}}{j2m\pi^2} G^*$$

Where

$$G = \int_{-\pi}^{\pi} e^{jny} \left(\underbrace{J_o\left(\frac{\pi n}{3}q\right)J_o\left(\frac{\pi n}{3}q\right)}_{G_1} + \underbrace{2J_o\left(\frac{\pi n}{3}q\right)\sum_{h=1}^{\infty} j^h J_h\left(\frac{\pi n}{3}q\right)\cos(by + \theta_{bo})}_{G_2} + \right. \\ \left. \underbrace{2J_o\left(\frac{\pi n}{3}q\right)\sum_{k=1}^{\infty} j^k J_k\left(\frac{\pi n}{3}q\right)\cos(ay + \theta_{ao})}_{G_3} + \right. \\ \left. \underbrace{4\sum_{k=1}^{\infty}\sum_{h=1}^{\infty} j^{h+k} J_h\left(\frac{\pi}{3}q\right)J_k\left(\frac{\pi}{3}q\right)\cos(by + \theta_{bo})\cos(ay + \theta_{ao})}_{G_4} \right) dy$$

$$G^* = \int_{-\pi}^{\pi} e^{jny} \left(\underbrace{J_o\left(\frac{\pi n}{3}q\right)J_o\left(\frac{\pi n}{3}q\right)}_{G_1^*} + \underbrace{2J_o\left(\frac{\pi n}{3}q\right)\sum_{h=1}^{\infty} j^{-h} J_h\left(\frac{\pi n}{3}q\right)\cos(by + \theta_{bo})}_{G_2^*} + \right. \\ \left. \underbrace{2J_o\left(\frac{\pi n}{3}q\right)\sum_{k=1}^{\infty} j^{-k} J_k\left(\frac{\pi n}{3}q\right)\cos(ay + \theta_{ao})}_{G_3^*} + \right. \\ \left. \underbrace{4\sum_{k=1}^{\infty}\sum_{h=1}^{\infty} j^{-h-k} J_h\left(\frac{\pi}{3}q\right)J_k\left(\frac{\pi}{3}q\right)\cos(by + \theta_{bo})\cos(ay + \theta_{ao})}_{G_4^*} \right) dy$$

Evaluating the first term,

$$C_{mn1} = \frac{e^{\frac{jn\pi}{3}}}{j2m\pi^2} G_1 - \frac{e^{-\frac{jn\pi}{3}}}{j2m\pi^2} G_1^*$$

$$C_{mn1} = \frac{2}{3} J_o\left(\frac{\pi n}{3}q\right)J_o\left(\frac{\pi n}{3}q\right) \frac{\sin\left(\frac{m\pi}{3}\right)}{\frac{m\pi}{3}} \frac{\sin(n\pi)}{n\pi} \quad (4.28)$$

The second term becomes,

$$\begin{aligned}
C_{mn2} &= \frac{e^{\frac{jm\pi}{3}}}{j2m\pi^2} \int_{-\pi}^{\pi} 2J_o\left(\frac{\pi n}{3}q\right) \sum_{h=1}^{\infty} j^h J_h\left(\frac{\pi n}{3}q\right) \cos(by + \theta_{bo}) - \\
&\quad \frac{e^{\frac{jm\pi}{3}}}{j2m\pi^2} \int_{-\pi}^{\pi} 2J_o\left(\frac{\pi n}{3}q\right) \sum_{h=1}^{\infty} j^{-h} J_h\left(\frac{\pi n}{3}q\right) \cos(by + \theta_{bo}) \\
C_{mn2} &= \frac{2J_o\left(\frac{\pi n}{3}q\right)}{m\pi} \sum_{h=1}^{\infty} J_h\left(\frac{\pi n}{3}q\right) R_{mn2} \sin\left(\frac{m\pi}{3} + \frac{h\pi}{2}\right)
\end{aligned} \tag{4.29}$$

Similarly,

$$C_{mn3} = \frac{2J_o\left(\frac{\pi n}{3}q\right)}{m\pi} \sum_{k=1}^{\infty} J_k\left(\frac{\pi n}{3}q\right) R_{mn3} \sin\left(\frac{m\pi}{3} + \frac{k\pi}{2}\right) \tag{4.30}$$

Where

$$R_{mn3} = e^{j\theta_{ao}} \frac{\sin((n+ak)\pi)}{(n+ak)\pi} + e^{-j\theta_{ao}} \frac{\sin((n-ak)\pi)}{(n-ak)\pi} \tag{4.31}$$

And the fourth term can be evaluated as follows

$$\begin{aligned}
C_{mn4} &= \frac{1}{j2m\pi^2} 4 \sum_{k=1}^{\infty} \sum_{h=1}^{\infty} j^{h+k} J_h\left(\frac{\pi}{3}q\right) J_k\left(\frac{\pi}{3}q\right) \int_{-\pi}^{\pi} e^{jny} \cos(ay + \theta_{ao}) \cos(by + \theta_{bo}) \\
C_{mn4} &= \frac{4}{m\pi} \sum_{k=1}^{\infty} \sum_{h=1}^{\infty} J_h\left(\frac{\pi}{3}q\right) J_k\left(\frac{\pi}{3}q\right) R_{mn4} \sin\left(\frac{\pi}{3}m + \frac{\pi}{2}(h+k)\right)
\end{aligned} \tag{4.32}$$

Where

$$\begin{aligned}
R_{mn4} &= e^{j(\theta_{bo} + \theta_{ao})} \frac{\sin((n+bh+ak)\pi)}{(n+bh+ak)\pi} + e^{j(\theta_{bo} - \theta_{ao})} \frac{\sin((n+bh-ak)\pi)}{(n+bh-ak)\pi} + \\
&\quad e^{-j(\theta_{bo} - \theta_{ao})} \frac{\sin((n-bh+ak)\pi)}{(n-bh+ak)\pi} + e^{-j(\theta_{bo} + \theta_{ao})} \frac{\sin((n-bh-ak)\pi)}{(n-bh-ak)\pi}
\end{aligned} \tag{4.32}$$

Combining (4.28), (4.29), (4.30) and (4.32) the coefficient of the Fourier series is finally combined as follows.

$$C_{mn} = \frac{2}{m\pi} \sum_{m=1}^{\infty} \sum_{n=-\infty}^{\infty} \left\{ \begin{aligned} & J_o\left(\frac{\pi n}{3}q\right)J_o\left(\frac{\pi n}{3}q\right)\sin\left(\frac{m\pi}{3}\right)\frac{\sin(n\pi)}{n\pi} + \\ & \sum J_o\left(\frac{\pi n}{3}q\right)J_h\left(\frac{\pi n}{3}q\right)R_{mn2}\sin\left(\frac{m\pi}{3} + \frac{h\pi}{2}\right) + \\ & \sum J_o\left(\frac{\pi n}{3}q\right)J_k\left(\frac{\pi n}{3}q\right)R_{mn3}\sin\left(\frac{m\pi}{3} + \frac{k\pi}{2}\right) + \\ & \sum J_h\left(\frac{\pi}{3}q\right)J_k\left(\frac{\pi}{3}q\right)R_{mn4}\sin\left(\frac{\pi}{3}m + \frac{\pi}{2}(h+k)\right) \end{aligned} \right. \quad (4.33)$$

4.3 Input Filter Parameters Specification

A typical connection of an input filter for the matrix converter is shown in Figure 3.1. In matrix converter with a harmonic of current-source characteristics, the second order LC filter is preferred [57]. The current and voltage relationships of the filter are

$$V_i(s) = \frac{sRL}{R + sL} I_i(s) + V_p(s) \quad (4.34)$$

$$sC_f V_i(s) = I_i(s) - I_p(s) \quad (4.35)$$

The input voltage can be expressed in terms of only the current as

$$V_i(s) = \frac{1}{sC_f} [I_i(s) - I_p(s)] \quad (4.36)$$

Substituting (4.36) into (4.34)

$$I_i(s) = \frac{s^2 L_f C_f + s R_f C_f}{s^2 R_f L_f C_f + s L_f + R_f} V_i(s) + \frac{s L_f + R_f}{s^2 R_f L_f C_f + s L_f + R_f} I_p(s)$$

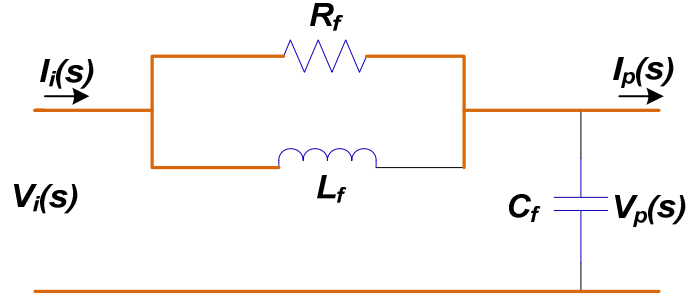


Figure 4.1 Schematics of input filter circuit

The input current transfer function related to input voltage is given as:

$$\frac{I_i(s)}{V_i(s)} = \frac{s^2 \frac{1}{R_f} + s \frac{1}{L_f}}{s^2 + \frac{1}{R_f C_f} s + \frac{1}{L_f C_f}} \quad (4.37)$$

And the input current transfer function related to output current is

$$\frac{I_i(s)}{I_p(s)} = \frac{s \frac{1}{R_f C_f} + \frac{1}{L_f C_f}}{s^2 + \frac{1}{R_f C_f} s + \frac{1}{L_f C_f}} \quad (4.38)$$

Considering the denominators of the above two transfer functions, and compare with the second order Butterworth filter,

$$s^2 + \frac{1}{R_f C_f} s + \frac{1}{L_f C_f} \approx s^2 + 2\xi\omega_n s + \omega_n^2 \quad (4.39)$$

Thus the characteristic frequency ω_n and damping factor ξ are given as:

$$\omega_n = \frac{1}{\sqrt{L_f C_f}} \quad (4.40)$$

$$\xi = \frac{1}{2R_f} \sqrt{L_f C_f} \quad (4.41)$$

4.3.1 Harmonic Balance Technique

The schematic of a three phase matrix converter feeding an RL load is shown in Figure 4.2. This typical topology is used to illustrate the design methodology proposed in this thesis. As shown in the figure, a linear load is connected to the matrix converter output terminal in which the output currents are considered to be pure sinusoidal and balanced three phase. The harmonics present in the input current are totally due to the switching. To demonstrate the dominant input current harmonics, one phase of the input current and the corresponding three switching signals are considered for analysis.

The switching signals which generate the input phase ‘a’ current from a three phase output current can be represented in terms of the dominant harmonics as follows.

$$S_{aA} = \frac{1}{3} + C_{1aA} \cos(\omega_x t) + C_{2aA} \cos(\omega_y t) + C_{3aA} \cos(\omega_c - \omega_x)t + C_{4aA} \cos(\omega_c - \omega_y)t + C_{5aA} \cos(\omega_c)t + C_{6aA} \cos(\omega_c + \omega_x)t + C_{7aA} \cos(\omega_c + \omega_y)t \quad (4.42)$$

$$S_{aB} = \frac{1}{3} + C_{1aB} \cos(\omega_x t + \beta) + C_{2aB} \cos(\omega_y t - \beta) + C_{3aB} \cos(\omega_c - \omega_x)t - \beta) + C_{4aB} \cos(\omega_c - \omega_y)t + \beta) + C_{5aB} \cos(\omega_c)t + C_{6aB} \cos((\omega_c + \omega_x)t + \beta) + C_{7aB} \cos((\omega_c + \omega_y)t - \beta) \quad (4.43)$$

$$S_{aC} = \frac{1}{3} + C_{1aC} \cos(\omega_x t - \beta) + C_{2aC} \cos(\omega_y t + \beta) + C_{3aC} \cos((\omega_c - \omega_x)t + \beta) + C_{4aC} \cos((\omega_c - \omega_y)t - \beta) + C_{5aC} \cos(\omega_c)t + C_{6aC} \cos((\omega_c + \omega_x)t - \beta) + C_{7aC} \cos((\omega_c + \omega_y)t + \beta) \quad (4.44)$$

Where

$$\omega_x = \omega_p - \omega_s \quad \omega_y = \omega_p + \omega_s$$

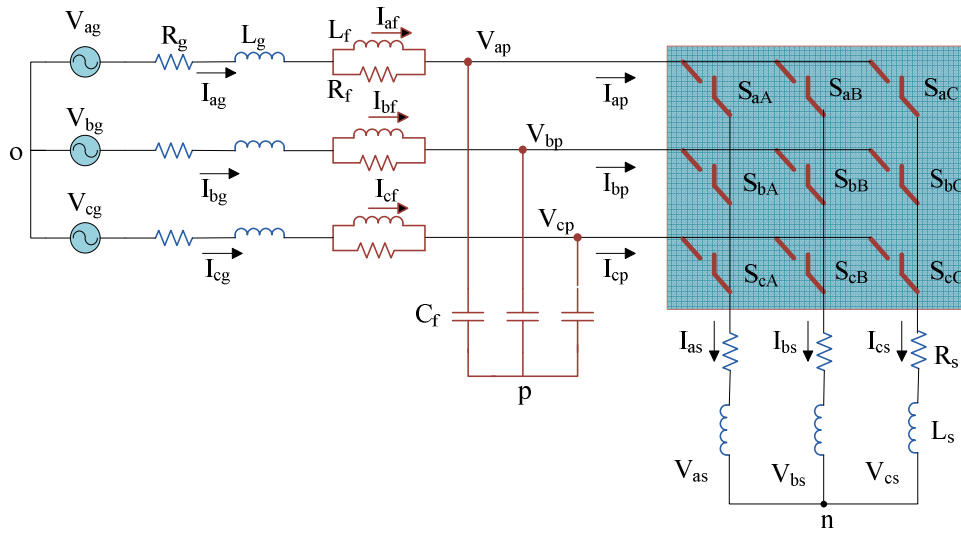


Figure 4.2 A matrix converter feeding an RL load

The output three phase currents with amplitude I_s and phase angle of θ_s are represented as follows

$$\begin{aligned}
 I_{as} &= I_s \cos(\omega_s t + \theta_s) \\
 I_{bs} &= I_s \cos(\omega_s t - \frac{2\pi}{3} + \theta_s) \\
 I_{cs} &= I_s \cos(\omega_s t + \frac{2\pi}{3} + \theta_s)
 \end{aligned} \tag{4.45}$$

The mapping between the input and output currents of a matrix converter is shown below.

$$I_{ap} = S_{aA} I_{as} + S_{aB} I_{bs} + S_{aC} I_{cs} \tag{4.46}$$

The input current can be obtained by substituting the switching signal expressions given in (4.42-4.44) into (4.46). The Fast Fourier Transform (FFT) of the input current are plotted in Figure 4.3. And it has been observed that the dominant harmonic components of the input current are occurred at $\omega_c - \omega_p$ and $\omega_c + \omega_p$.

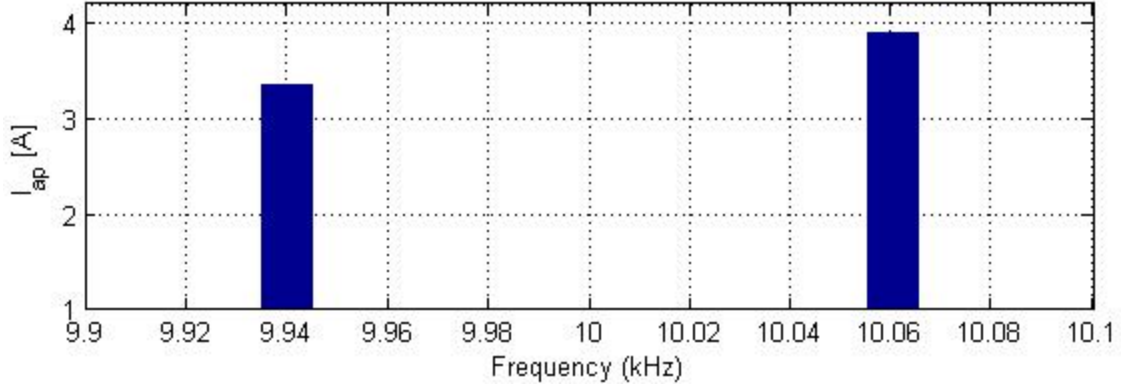


Figure 4.3 Dominant harmonics components of the input current

This input current ripple, I_{apr} can be given as:

$$I_{ap,ripp} = \frac{1}{2}(C_{3aA} + C_{4aA} + C_{3aB} + C_{4aB} + C_{3aC} + C_{4aC})I_s \cos(\omega_c - \omega_p)t + \frac{1}{2}(C_{6aA} + C_{7aA} + C_{6aB} + C_{7aB} + C_{6aC} + C_{7aC})I_s \cos(\omega_c + \omega_p)t + \quad (4.47)$$

For analysis one of the ripple components of the input current is considered which is shown below.

$$I_{apr} = I_{pr} \cos(\omega_c + \omega_p)t \quad (4.48)$$

Where I_{pr} is the magnitude of the ripple which is given in terms of the output current and Fourier coefficient of the switching signals.

$$I_{pr} = \frac{1}{2}(C_{6aA} + C_{7aA} + C_{6aB} + C_{7aB} + C_{6aC} + C_{7aC})I_s \quad (4.49)$$

The phase 'a' input current of the matrix converter consisting of a fundamental component and a ripple part is represented as.

$$I_{ap} = I_p \cos(\omega_p t + \theta_i) + I_{pr} \cos(\omega_c + \omega_p)t + \theta_{ir} \quad (4.50)$$

Similarly, the phase 'a' input capacitor voltage, the filter current and source current have the same ripple component as that of the input current.

$$V_{apr} = V_p \cos(\omega_p t + \theta_v) + V_{pr} \cos((\omega_c + \omega_p)t + \theta_{vr}) \quad (4.51)$$

$$I_{ afr } = I_f \cos(\omega_p t + \theta_f) + I_{ fr } \cos((\omega_c + \omega_p)t + \theta_{fr}) \quad (4.52)$$

$$I_{ ag,r } = I_g \cos(\omega_p t + \theta_g) + I_{ gr } \cos((\omega_c + \omega_p)t + \theta_{gr}) \quad (4.53)$$

The three phase ac source is considered to be pure sinusoidal and balanced.

$$\begin{aligned} V_{ag} &= V_g \cos(\omega_p t) \\ V_{bg} &= V_g \cos(\omega_p t - \frac{2\pi}{3}) \\ V_{cg} &= V_g \cos(\omega_p t + \frac{2\pi}{3}) \end{aligned} \quad (4.54)$$

The dynamic source current shown in Figure 4.2 are given as.

$$\begin{aligned} V_{ag} &= R_g I_{ag} + L_g pI_{ag} + R_f (I_{ag} - I_{af}) + V_{ap} \\ V_{bg} &= R_g I_{bg} + L_g pI_{bg} + R_f (I_{bg} - I_{bf}) + V_{bp} \\ V_{cg} &= R_g I_{cg} + L_g pI_{cg} + R_f (I_{cg} - I_{cf}) + V_{cp} \end{aligned} \quad (4.55)$$

The filter capacitor dynamics are given as

$$\begin{aligned} C_f pV_{ap} &= I_{ag} - I_{ap} \\ C_f pV_{bp} &= I_{bg} - I_{bp} \\ C_f pV_{cp} &= I_{cg} - I_{cp} \end{aligned} \quad (4.56)$$

The three phase dynamics equation of the filter inductor are expressed as

$$\begin{aligned} L_f pI_{af} &= R_f (I_{ag} - I_{af}) \\ L_f pI_{bf} &= R_f (I_{bg} - I_{bf}) \\ L_f pI_{cf} &= R_f (I_{cg} - I_{cf}) \end{aligned} \quad (4.57)$$

Since the input capacitor voltage, filter current and source current consists of a fundamental and ripple part. Using Harmonic Balance Technique it is possible to separate the fundamental and ripple dynamic of the input side. Before applying this technique, it is necessary to transform input side dynamics into synchronous reference frame using the transformation matrix given in 4.58.

$$K = \begin{bmatrix} \cos(\theta_p) & \cos(\theta_p - \frac{2\pi}{3}) & \cos(\theta_p + \frac{2\pi}{3}) \\ \sin(\theta_p) & \sin(\theta_p - \frac{2\pi}{3}) & \sin(\theta_p + \frac{2\pi}{3}) \\ \cos(\theta_r) & \cos(\theta_r - \frac{2\pi}{3}) & \cos(\theta_r + \frac{2\pi}{3}) \\ \sin(\theta_r) & \sin(\theta_r - \frac{2\pi}{3}) & \sin(\theta_r + \frac{2\pi}{3}) \end{bmatrix} \quad (4.58)$$

The transformed qd equation for the fundamental component of the source current dynamics is given in (4.59). I_{qg1} and I_{dg1} are the q -axis and d -axis components of the fundamental component of the source current.

$$\begin{aligned} V_{qg} &= R_g I_{qg1} + L_g p I_{qg1} + \omega_p L_g I_{dg1} + R_f (I_{qg1} - I_{qf1}) + V_{qp1} \\ V_{dg} &= R_g I_{dg1} + L_g p I_{dg1} - \omega_p L_g I_{qg1} + R_f (I_{dg1} - I_{df1}) + V_{dp1} \end{aligned} \quad (4.59)$$

The dynamics equations for the fundamental q -axis and d -axis filter current, I_{qf1} and I_{df1} are given as

$$\begin{aligned} L_f p I_{qf1} + \omega_p L_f I_{df1} &= R_f (I_{qg1} - I_{qf1}) \\ L_f p I_{df1} - \omega_p L_f I_{qf1} &= R_f (I_{dg1} - I_{df1}) \end{aligned} \quad (4.60)$$

Similarly, the input capacitor voltage

$$\begin{aligned} C_f p V_{qp1} + \omega_p C_f V_{dp1} &= I_{qg1} - I_{qf1} \\ C_f p V_{dp1} - \omega_p C_f V_{qp1} &= I_{dg1} - I_{df1} \end{aligned} \quad (4.61)$$

Similarly, the ripple dynamic equations for the source current are given below where I_{qgr} and I_{dgr} are the q-axis and d-axis ripple components of the source current. I_{qfr} and I_{dfr} are the corresponding filter current ripples. Similarly, V_{qpr} and V_{dpr} stand for the ripple axes components of the input capacitor voltages.

$$\begin{aligned} 0 &= R_g I_{qgr} + L_g p I_{qgr} + (\omega_c + \omega_p) L_g I_{dgr} + R_f (I_{qgr} - I_{qfr}) + V_{qpr} \\ 0 &= R_g I_{dgr} + L_g p I_{dgr} - (\omega_c + \omega_p) L_g I_{qgr} + R_f (I_{dgr} - I_{dfr}) + V_{dpr} \end{aligned} \quad (4.62)$$

The ripple dynamics for the filter current in synchronous reference frame are expressed in (4.63).

$$\begin{aligned} L_f p I_{qfr} + (\omega_c + \omega_p) L_f I_{dfr} &= R_f (I_{qgr} - I_{qfr}) \\ L_f p I_{dfr} - (\omega_c + \omega_p) L_f I_{qfr} &= R_f (I_{dgr} - I_{dfr}) \end{aligned} \quad (4.63)$$

Similarly, the input capacitor voltage dynamics are given as

$$\begin{aligned} C_f p V_{qpr} + (\omega_c + \omega_p) C_f V_{dpr} &= I_{qgr} - I_{qpr} \\ C_f p V_{dpr} - (\omega_c + \omega_p) C_f V_{qpr} &= I_{dgr} - I_{dpr} \end{aligned} \quad (4.64)$$

At steady state where the time derivatives, $p = 0$ the expression given from (4.62) to (4.64) becomes,

$$\begin{aligned} 0 &= (R_g + R_f) I_{qgr} + (\omega_c + \omega_p) L_g I_{dgr} - R_f I_{qfr} + V_{qpr} \\ 0 &= (R_g + R_f) I_{dgr} - (\omega_c + \omega_p) L_g I_{qgr} - R_f I_{dfr} + V_{dpr} \end{aligned} \quad (4.65)$$

$$\begin{aligned} (\omega_c + \omega_p) L_f I_{dfr} &= R_f (I_{qgr} - I_{qfr}) \\ -(\omega_c + \omega_p) L_f I_{qfr} &= R_f (I_{dgr} - I_{dfr}) \end{aligned} \quad (4.66)$$

$$\begin{aligned} (\omega_c + \omega_p) C_f V_{dpr} &= I_{qgr} - I_{qpr} \\ -(\omega_c + \omega_p) C_f V_{qpr} &= I_{dgr} - I_{dpr} \end{aligned} \quad (4.67)$$

From (4.66), the q-axis and d-axis filter current can be expressed in terms of the source currents as follow.

$$I_{qfr} = \frac{R_f^2}{R_f^2 + (\omega_c + \omega_p)^2 L_f^2} I_{qgr} - \frac{(\omega_c + \omega_p) L_f R_f}{R_f^2 + (\omega_c + \omega_p)^2 L_f^2} I_{dgr} \quad (4.68)$$

$$I_{dfr} = \frac{(\omega_c + \omega_p) L_f R_f}{R_f^2 + (\omega_c + \omega_p)^2 L_f^2} I_{qgr} + \frac{R_f^2}{R_f^2 + (\omega_c + \omega_p)^2 L_f^2} I_{dgr} \quad (4.69)$$

Since the input current ripple component is a function of the output current and the Fourier coefficient, (4.67) can be modified as given (4.70). K_{ripp} is a coefficient computed from the coefficients of the switching signal components which result in the particular input current ripple.

$$(\omega_c + \omega_p) C_f V_{dpr} = I_{qgr} - K_{ripp} I_{qs} \quad (4.70)$$

$$-(\omega_c + \omega_p) C_f V_{qpr} = I_{dgr} - K_{ripp} I_{ds} \quad (4.71)$$

Substituting (4.68) and (4.69) into (4.65),

$$0 = \left(R_g + R_f - \frac{R_f^3}{R_f^2 + (\omega_c + \omega_p)^2 L_f^2} \right) I_{qgr} + \left((\omega_c + \omega_p) L_g + \frac{(\omega_c + \omega_p) L_f R_f^2}{R_f^2 + (\omega_c + \omega_p)^2 L_f^2} \right) I_{dgr} + V_{qpr} \quad (4.72)$$

$$0 = \left(R_g + R_f - \frac{R_f^3}{R_f^2 + (\omega_c + \omega_p)^2 L_f^2} \right) I_{dgr} - \left((\omega_c + \omega_p) L_g + \frac{(\omega_c + \omega_p) L_f R_f^2}{R_f^2 + (\omega_c + \omega_p)^2 L_f^2} \right) I_{qgr} + V_{dpr} \quad (4.73)$$

Since the filter parameters are selected based on the specified maximum allowable source current and input capacitor voltage ripples, I_{gr} and V_{pr} .

$$I_{qgr}^2 + I_{dgr}^2 = I_{gr}^2 \quad (4.74)$$

$$V_{qpr}^2 + V_{dpr}^2 = V_{pr}^2 \quad (4.75)$$

Solving the six non-linear equations given (4.70) - (4.75), it is possible to determine the six unknowns, I_{qg} , I_{dg} , V_{qp} , V_{dp} , L_f and C_f . It is necessary to note that these variables are computed for a specified value of damping resistor and rated output current. However, the designed filter is later proved to work for output currents lower than the rated value. Besides, the chosen damping resistor is valid regarding the stability of the overall system. The rated output current is chosen to be $15A$ with phase angle of -30° and damping resistor value of 30Ω . The maximum allowable source current and input capacitor voltage ripples are selected to be $0.27A$ and $12.5V$, respectively. The filter inductor and capacitor are calculated to be $7.46mH$ and $10\mu F$ respective.

4.3.2 Stability Analysis for Matrix converter feeding an RL load

The stability of the system shown in Figure 4.2 are studied stability of the system under chosen filter parameters. This analysis is necessary to properly choose the damping resistor which determines the filter inductor and capacitor. The dynamic equations of the overall system are summarized as follows:

$$\begin{aligned} V_{qg} &= R_g I_{qg} + L_g p I_{qg} + \omega_p L_g I_{dg} + R_f (I_{qg} - I_{qf}) + V_{qp} \\ V_{dg} &= R_g I_{dg} + L_g p I_{dg} - \omega_p L_g I_{qg} + R_f (I_{dg} - I_{df}) + V_{dp} \end{aligned} \quad (4.76)$$

$$\begin{aligned}
L_f pI_{qf} + \omega_p L_g I_{df} &= R_f (I_{qg} - I_{qf}) \\
L_f pI_{df} - \omega_p L_g I_{qf} &= R_f (I_{dg} - I_{df})
\end{aligned} \tag{4.77}$$

$$\begin{aligned}
C_f pV_{qp} + \omega_p C_f V_{dp} &= I_{qg} - I_{qp} \\
C_f pV_{dp} - \omega_p C_f V_{qp} &= I_{dg} - I_{dp}
\end{aligned} \tag{4.78}$$

The dynamics of digital filter in synchronous reference frame are

$$\begin{aligned}
pV_{qf} &= \frac{1}{\tau} (V_{qp} - V_{qf}) \\
pV_{df} &= \frac{1}{\tau} (V_{dp} - V_{df})
\end{aligned} \tag{4.79}$$

The output current dynamics are given in qd reference frame as given below where V_{qs} and V_{ds} are the output voltages where as I_{qs} and I_{ds} are the output current axes components.

$$\begin{aligned}
V_{qs} &= R_s I_{qs} + L_s pI_{qs} + \omega_s I_{ds} \\
V_{ds} &= R_s I_{ds} + L_s pI_{ds} - \omega_s I_{qs}
\end{aligned} \tag{4.80}$$

The mapping between the input and output of the matrix converter current and voltage relations are given as

$$\begin{aligned}
I_{dp} &= M_{qd} I_{qs} + M_{dd} I_{ds} \\
I_{qp} &= M_{qq} I_{qs} + M_{dq} I_{ds}
\end{aligned} \tag{4.81}$$

The modulation signal components, M_{qq} , M_{qd} , M_{dq} and M_{dd} are discussed in detail in the subsequent chapters. The output voltage is also written in terms of the input capacitor voltage as follow.

$$\begin{aligned}
V_{qs} &= M_{qq} V_{qp} + M_{qd} V_{dp} \\
V_{ds} &= M_{dq} V_{qp} + M_{dd} V_{dp}
\end{aligned} \tag{4.82}$$

The stability study involves the small signal modeling and steady state analysis for system shown in the Figure 4.2. The linearization of the system dynamics around steady state operating point leads to the following small signal model of the system.

$$p\Delta I_{qg} = \frac{1}{L_g} \left(\Delta V_{qg} - (R_g + R_f) \Delta I_{qg} + R_f \Delta I_{qf} - \omega_p L_g \Delta I_{dg} - \Delta V_{qp} \right)$$

$$p\Delta I_{dg} = \frac{1}{L_g} \left(\Delta V_{dg} - (R_g + R_f) \Delta I_{dg} + R_f \Delta I_{df} + \omega_p L_g \Delta I_{qg} - \Delta V_{dp} \right)$$

$$p\Delta I_{qf} = \frac{1}{L_f} \left(R_f \Delta I_{qg} - R_f \Delta I_{qf} - \omega_p L_f \Delta I_{df} \right)$$

$$p\Delta I_{df} = \frac{1}{L_f} \left(R_f \Delta I_{qg} - R_f \Delta I_{qf} - \omega_p L_f \Delta I_{df} \right)$$

$$p\Delta I_{qf} = \frac{1}{L_f} \left(R_f \Delta I_{qg} - R_f \Delta I_{qf} - \omega_p L_f \Delta I_{df} \right)$$

$$p\Delta V_{qp} = \frac{1}{C_f} \left(\Delta I_{qg} - \omega_p C_f \Delta V_{dp} - M_{qqo} \Delta I_{qs} - M_{dqo} \Delta I_{ds} - I_{qso} \Delta M_{qq} - I_{dso} \Delta M_{dq} \right)$$

$$p\Delta V_{dp} = \frac{1}{C_f} \left(\Delta I_{dg} + \omega_p C_f \Delta V_{qp} - M_{qdo} \Delta I_{qs} - M_{ddo} \Delta I_{ds} - I_{qso} \Delta M_{qd} - I_{dso} \Delta M_{dd} \right)$$

$$p\Delta V_{qf} = \frac{1}{\tau} (\Delta V_{qp} - \Delta V_{qf})$$

$$p\Delta V_{df} = \frac{1}{\tau} (\Delta V_{dp} - \Delta V_{df})$$

$$p\Delta I_{qs} = \frac{1}{L_o} \left(M_{qqo} \Delta V_{qp} + M_{qdo} \Delta V_{dp} - R_s \Delta I_{qs} - \omega_s L_s \Delta I_{ds} + V_{qpo} \Delta M_{qq} + V_{dpo} \Delta M_{qd} \right)$$

$$p\Delta I_{ds} = \frac{1}{L_s} \left(M_{dqo} \Delta V_{qp} + M_{ddo} \Delta V_{dp} - R_s \Delta I_{ds} + \omega_s L_s \Delta I_{qs} + V_{qpo} \Delta M_{dq} + V_{dpo} \Delta M_{dd} \right)$$

The characteristic matrix is shown (4.83) and it depends on the operating points.

$$A = \begin{bmatrix} -\frac{R_g + R_f}{L_g} & -\omega_p & \frac{R_f}{L_g} & 0 & -\frac{1}{L_g} & 0 & 0 & 0 & 0 & 0 \\ \omega_p & -\frac{R_g + R_f}{L_g} & 0 & \frac{R_f}{L_g} & 0 & -\frac{1}{L_g} & 0 & 0 & 0 & 0 \\ \frac{R_f}{L_f} & 0 & -\frac{R_f}{L_f} & -\omega_p & 0 & 0 & 0 & 0 & 0 & 0 \\ 0 & \frac{R_f}{L_f} & \omega_p & -\frac{R_f}{L_f} & 0 & 0 & 0 & 0 & 0 & 0 \\ \frac{1}{C_f} & 0 & 0 & 0 & 0 & -\omega_p & y_1 & y_2 & z_1 & z_2 \\ 0 & \frac{1}{C_f} & 0 & 0 & \omega_p & 0 & y_3 & y_4 & z_3 & z_3 \\ 0 & 0 & 0 & 0 & \frac{1}{\tau} & 0 & -\frac{1}{\tau} & 0 & 0 & 0 \\ 0 & 0 & 0 & 0 & 0 & \frac{1}{\tau} & 0 & -\frac{1}{\tau} & 0 & 0 \\ 0 & 0 & 0 & 0 & -x_1 & -x_2 & x_1 & x_2 & -\frac{R_s}{L_s} & -\omega_s \\ 0 & 0 & 0 & 0 & -x_3 & -x_4 & x_3 & x_4 & \omega_s & -\frac{R_s}{L_s} \end{bmatrix} \quad (4.83)$$

The constants represented in the matrix are computed at the steady state operation.

$$x_1 = -\frac{V_{qso} V_{qpo}}{V_{po}^2}$$

$$x_2 = -\frac{V_{qso} V_{dpo}}{V_{po}^2}$$

$$x_3 = -\frac{V_{dso} V_{qpo}}{V_{po}^2}$$

$$x_4 = -\frac{V_{dso} V_{dpo}}{V_{po}^2}$$

$$y_1 = -y_4 = \frac{1}{C_f} \frac{(V_{qpo}^2 - V_{dpo}^2)k}{V_{po}^4}$$

$$y_2 = y_3 = \frac{1}{C_f} \frac{2V_{qpo} V_{dpo} k}{V_{po}^4}$$

$$k = V_{qso} I_{qso} + V_{dso} I_{dso}$$

Table 4.1 System parameters

$V_s = 160V \quad f_s = 50Hz$			
$R_s = 10\Omega$		$L_s = 20mH \text{ for } I_s = 15A \text{ with } -30^\circ$	
$R_s = 30\Omega$		$L_s = 60mH \text{ for } I_s = 5A \text{ with } -30^\circ$	
$V_g = 230V$	$f_p = 60Hz$	$R_g = 0.5\Omega,$	$L_g = 1mH$
$R_f = 30\Omega$	$L_f = 7.46mH$	$C_f = 10\mu F$	

The steady state variables are computed step-by-step as follows for the given parameter
 For varies damping resistance the operating points are computed to analyze the Eigen
 value of the characteristic matrix given above. The operating points by solving the
 quadratic equation shown in (4.84)

$$aM_{dd}^2 + bM_{dd} + c = 0 \quad (4.82)$$

$$M_{dq} = M_x - g_1 g_2 M_{dd}$$

$$M_{qd} = M_{dd} \frac{V_{qs}}{V_{ds}}$$

$$M_{qq} = \frac{M_{dq}}{M_{dd}} M_{qd}$$

$$V_{qp} = k_1 V_{qg} + g_1 (M_{qd} I_{qs} + M_{dd} I_{ds})$$

$$I_{qg} = \beta_3 \beta_4 (V_{qg} - V_{qp})$$

$$I_{dg} = \rho I_{qg}$$

$$V_{dp} = \beta_4 (V_{qg} - V_{qp})$$

$$I_{qf} = \beta_1 I_{qg}$$

$$I_{df} = \beta_2 I_{qg}$$

4.4 Simulation Results and Discussion

Using the system parameter given in Table 4.1 which is based on the designed filter, simulations are done to examine the effect of the damping resistor on the system stability as well as to verify the filter designed based on the proposed method in mitigating the harmonic in the input current. Figure 4.4 show the stability limit of the studied system in terms of the voltage transfer ratio and digital filter time constant. It is observed that higher filter time constant results in wider range of stability region. The figure also shows that to operate in higher voltage gain, the corresponding digital filter should have higher time constant to keep the overall system stable. The effect of the damping resistance on the system stability is shown in Figure 4.5 by analyzing the dominant Eigen value for each value of damping resistances. Note that this dominant Eigen value varies with the damping resistance and therefore it is necessary to particularly selected dominant Eigen value as the resistance vary. It is seen that with the select damping resistance, $R_f = 30\Omega$, the system is stable even in lower digital time constant. It can also be observed from the figure that, lower resistance leads to a better system stability; however, the low value of damping resistance will lead to higher power loss in the filter.

Simulations are also done to observe the resulting input and output waveforms of the matrix converter –RL load system. A sinusoidal input voltage with input unity power factor is considered for simulation as shown in Figure 4.6. As seen in the Figure 4.7, the designed input filter maintained sufficiently high power factor at the input terminal of the converter which allows wide range of output voltage operation.

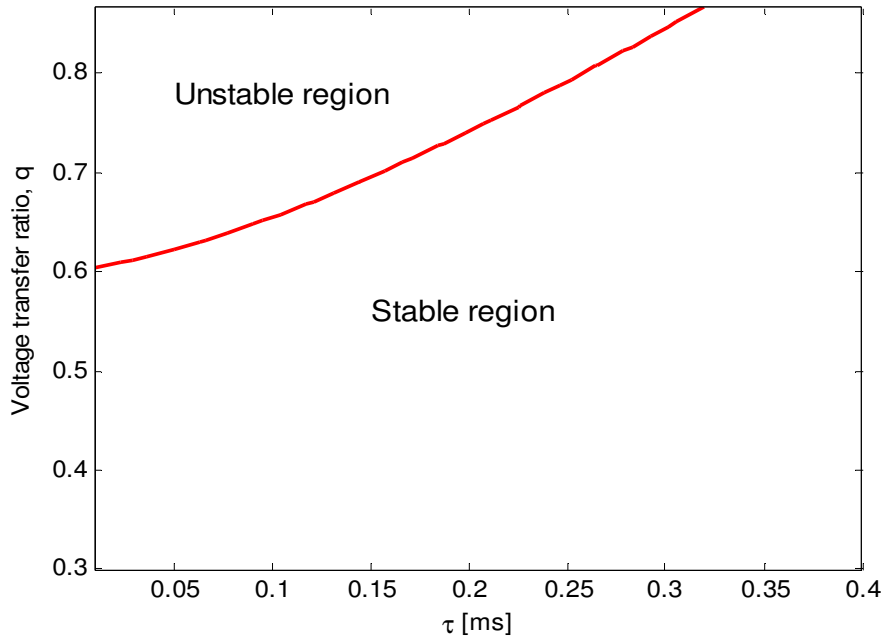


Figure 4.4 Stability limit of a matrix converter with RL load

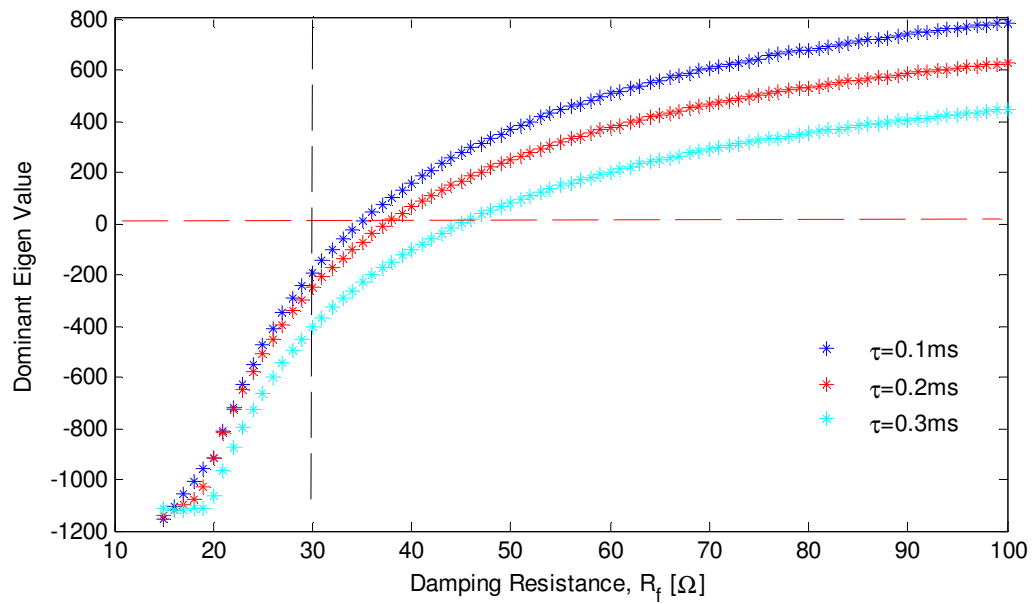


Figure 4.5 Dominant Eigen Values for various damping resistance

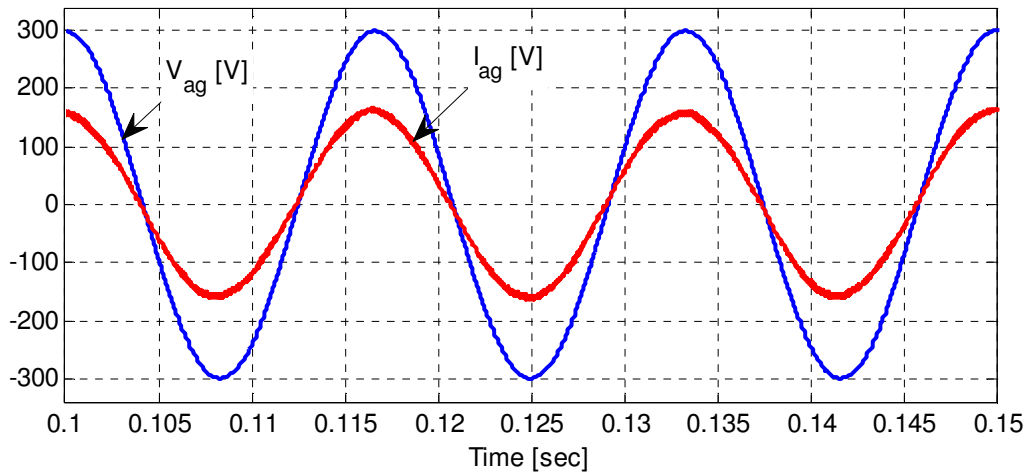


Figure 4.6 Phase 'a' source voltage and current

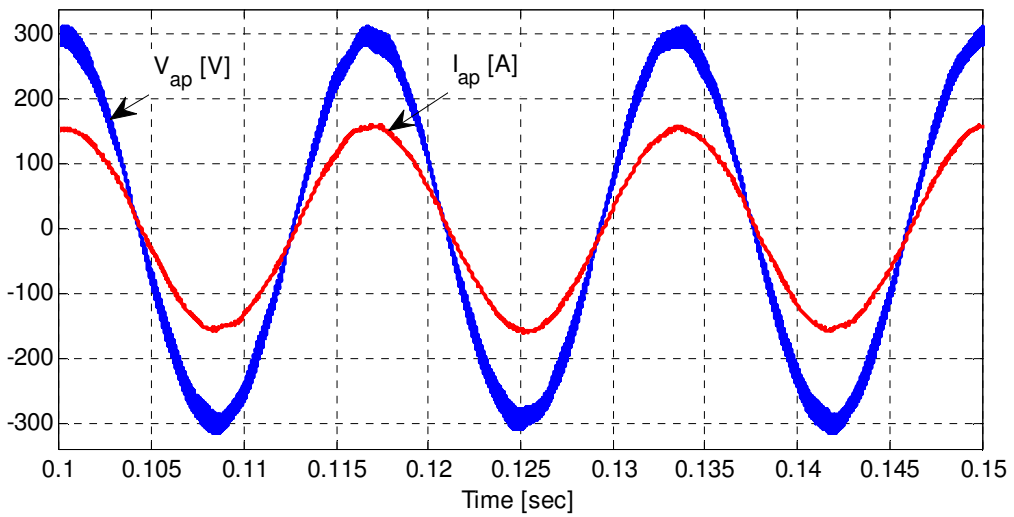


Figure 4.7 Phase 'a' input capacitor voltage and current of the MC

The source current shown in figure above are magnified by twenty times. The averaged output voltage and current with 10 times magnified are shown in Figure 4.8. The input current of the converter before and source current which is after the filter is shown in Figure 4.9.

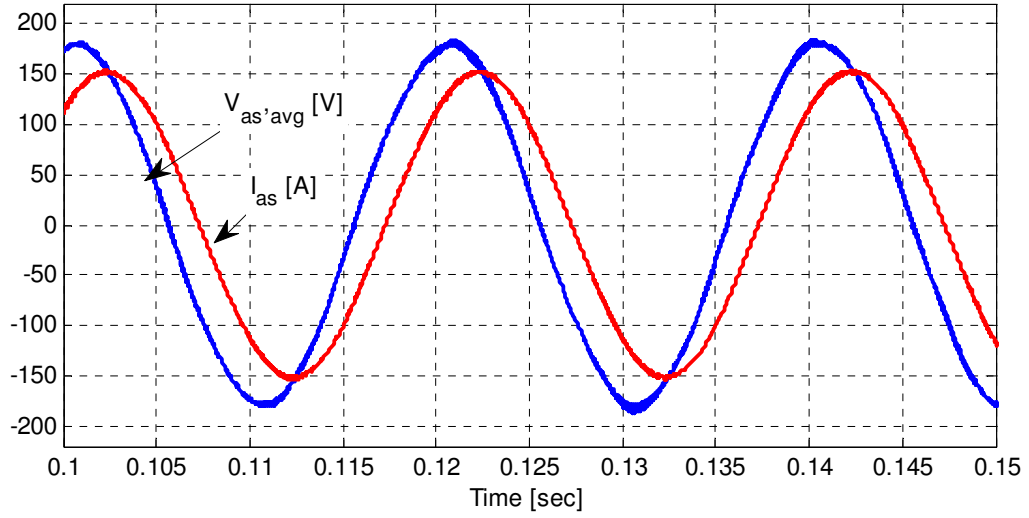


Figure 4.8 Phase 'a' output voltage and current

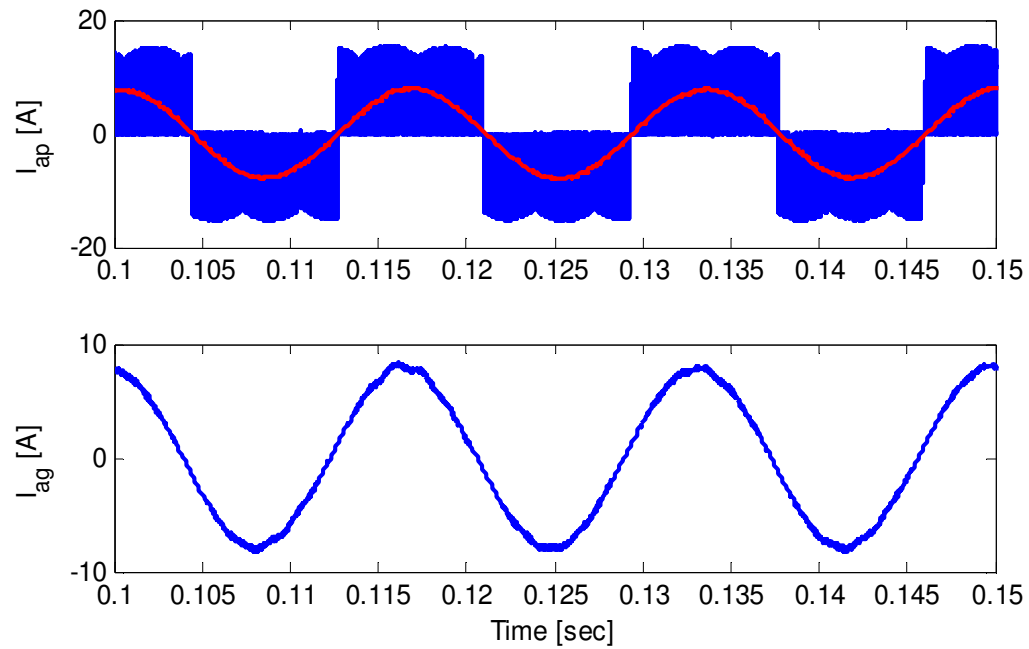


Figure 4.9 Input current and source current

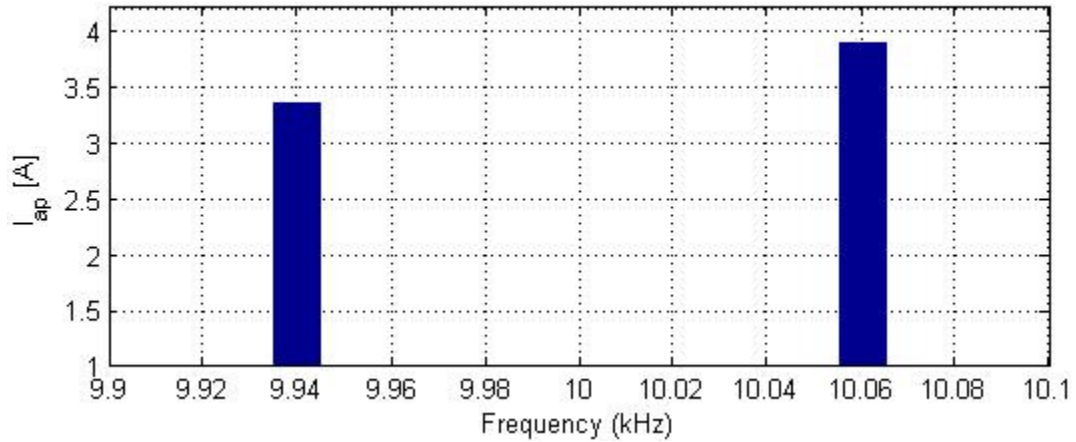


Figure 4.10 FFT of input current of the MC

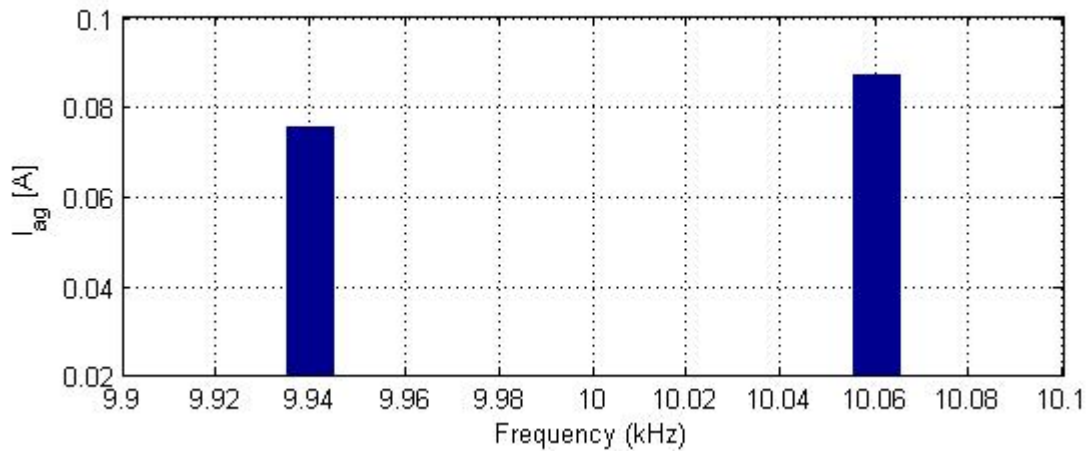


Figure 4.11 FFT of the source current

The harmonic content of Figure 4.9 are presented in the above two figures. The dominant harmonic of the input current is as high as 4A and the next dominant harmonics is around 3.4A. As observed in Figure 4.11, these harmonics are greatly reduced in the source current due to the input filter. From this result it can be concluded that even if the proposed filter parameter considered only one of the dominant harmonics, it also mitigates the other harmonics.

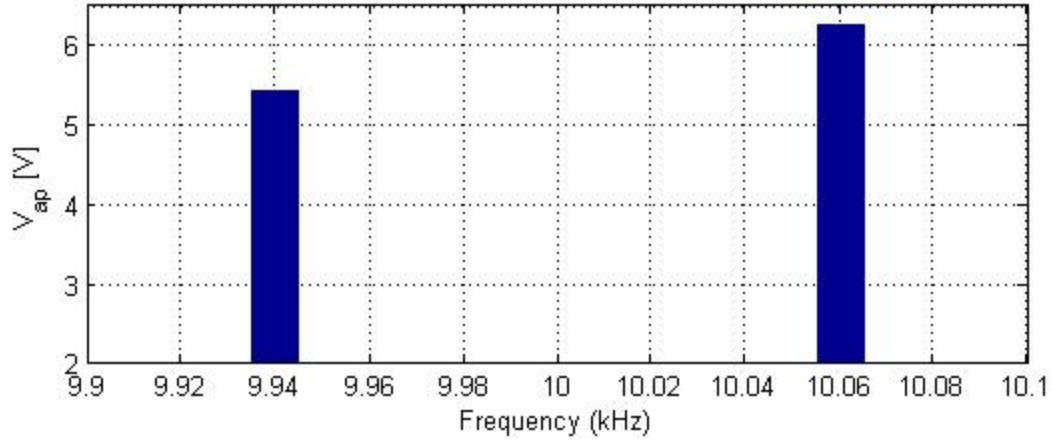


Figure 4.12 FFT of the input capacitor voltage

Figure 4.12 shows the harmonic component of the input capacitor voltage. With the designed input filter, the input capacitor voltage and source current ripples meet the specified maximum allowable ripples as demonstrated in Figure 4.11 and Figure 4.12.

The stability of the system under the determined filter capacitor and inductor values for an output current of 5A is studied. As observed in Figure 4.13, the damping resistance does not affect the system stability under low output current. And therefore, the filter designed based on output rated current can also work for lower current operation.

The Bode plot of the filter transfer function given in (4.38) is shown in Figure 4.14. This figure shows that the gain at the resonance frequency, 583Hz is near to zero and therefore, it can be concluded that the chosen filter parameters can also result in very less oscillation at the characteristic frequency.

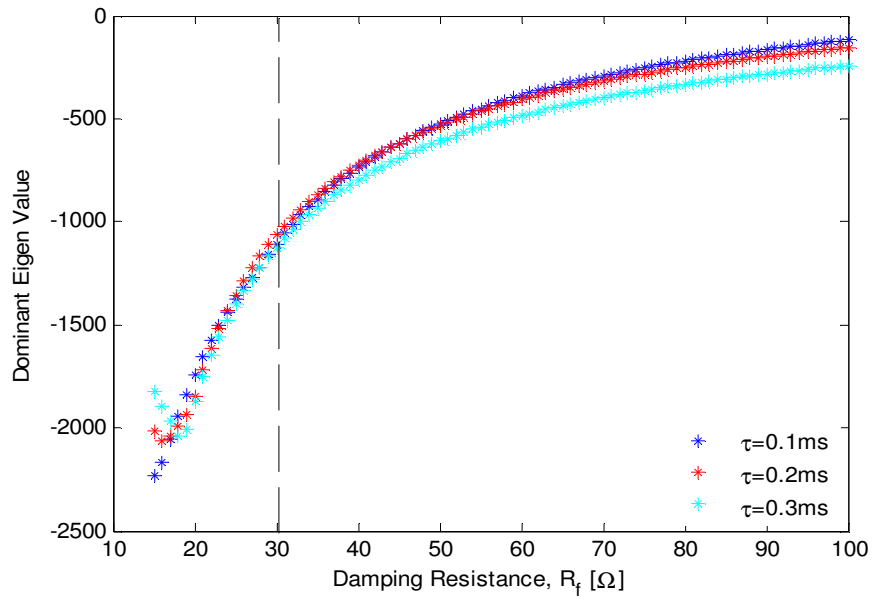


Figure 4.13 Stability limit for a load current of 5A

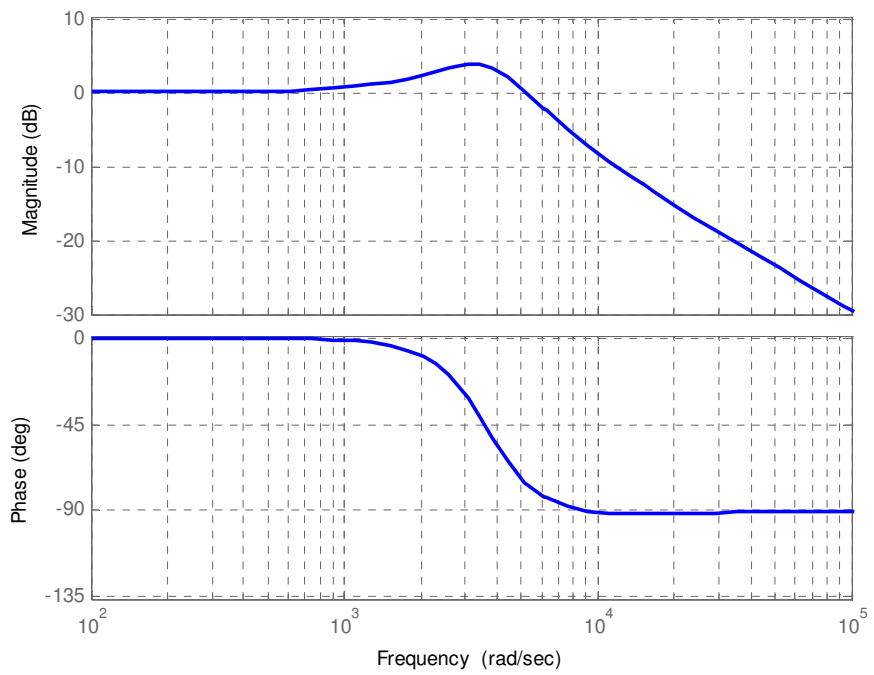


Figure 4.14 Bode plot of the designed input filter

4.5 Conclusion

This chapter propose a new input filter design for a matrix converter which mitigate unwanted harmonic generated by the high frequency switching. A harmonic balance technique is set forth which enables an independent analysis for the ripple component of the current and voltage waveform. The filter inductor and capacitor are determined based on the specified maximum allowable source current and input capacitor voltage ripples under a given damping resistance and output rated current. Stability of the overall system is studied with the help of small signal modelling and steady state analysis. Simulation results shows that the system is stable under the chosen damping resistor even with a low digital low pass filter's time constant. Moreover, the designed filter parameters which are determined based on the rated output current perfectly works lower output currents. Although the analysis is consider only one dominant harmonic component of the input current, the resulting filter are capable of mitigating lower harmonics as well. It is also observed that the proposed approach maintained a high power factor at the input terminal of the matrix converter which allows wider control range of a matrix converter. Based on the transfer function of the filter, the chosen damping resistance is sufficiently damp the oscillation near the resonant frequency and besides this resonance frequency is far from the fundamental and sufficiently lower that the switching frequency. Finally, this new approach can be implemented when the source voltage contained harmonics although this work assumes a pure ac source.

CHAPTER 5

DYNAMIC AND STEADY STATE MODELLING OF MATRIX CONVERTER SYSTEMS

5.1 Introduction

This chapter presents the complete modelling of a matrix converter feeding a passive RL load. It also gives a detailed steady state analysis supported by a computer simulation. The model implements the carrier based modulation strategies developed in the chapter 3. The dynamic and steady state performance analysis of a matrix converter fed induction motor are presented in this chapter. A new generalized steady state analysis which can be implemented for matrix converter based drives operating in both unity and non unity input power factor operations. The motivation behind this analysis is that most of the literature gives a steady state operating points computed under unity input power factor operation. With the help of this generalized analysis, it is possible to study the performance of the drive under lagging, unity or leading input power factor. Moreover, this analysis is used to evaluate the operating points for the stability study of the drive system. Computer simulation results obtained using a MATLAB/Simulink platform have been provided to verify the starting transient, dynamic response and the steady state performance of the drive.

5.2 Matrix Converter Feeding an RL Load

5.2.1 Dynamic Modelling

The topology of the overall system which comprises a three phase power supply, an input LC filter, digital low pass filter, modulation signal and switching signal generation blocks and three phase-to-phase AC/AC matrix converter feeding a passive load is schematically shown in Figure 5.1. The digital low pass filter is implemented in synchronous reference frame; therefore, the measured input capacitor voltages first transformed to qd synchronous reference frame and then transformed back to abc after the low pass filter. These filtered capacitor voltages are then used to determine the appropriate modulation signals which are compared with high frequency triangular carrier signal to generate the actual switching pulses. The modulation scheme used throughout the modelling is carrier-based PWM or duty-cycle technique.

Complying with the Kirchhoff's voltage and current laws, the switching functions are constrained as follows.

$$\begin{aligned} S_{aA} + S_{bA} + S_{cA} &= 1 \\ S_{aB} + S_{bB} + S_{cB} &= 1 \\ S_{aC} + S_{bC} + S_{cC} &= 1 \end{aligned} \tag{5.1}$$

The three phase voltage equations for the input side of the MC are given in (5.2) assuming the common mode voltage between point p and o shown in Figure 5.1 are zero. The term p represents the time derivatives (d/dt).

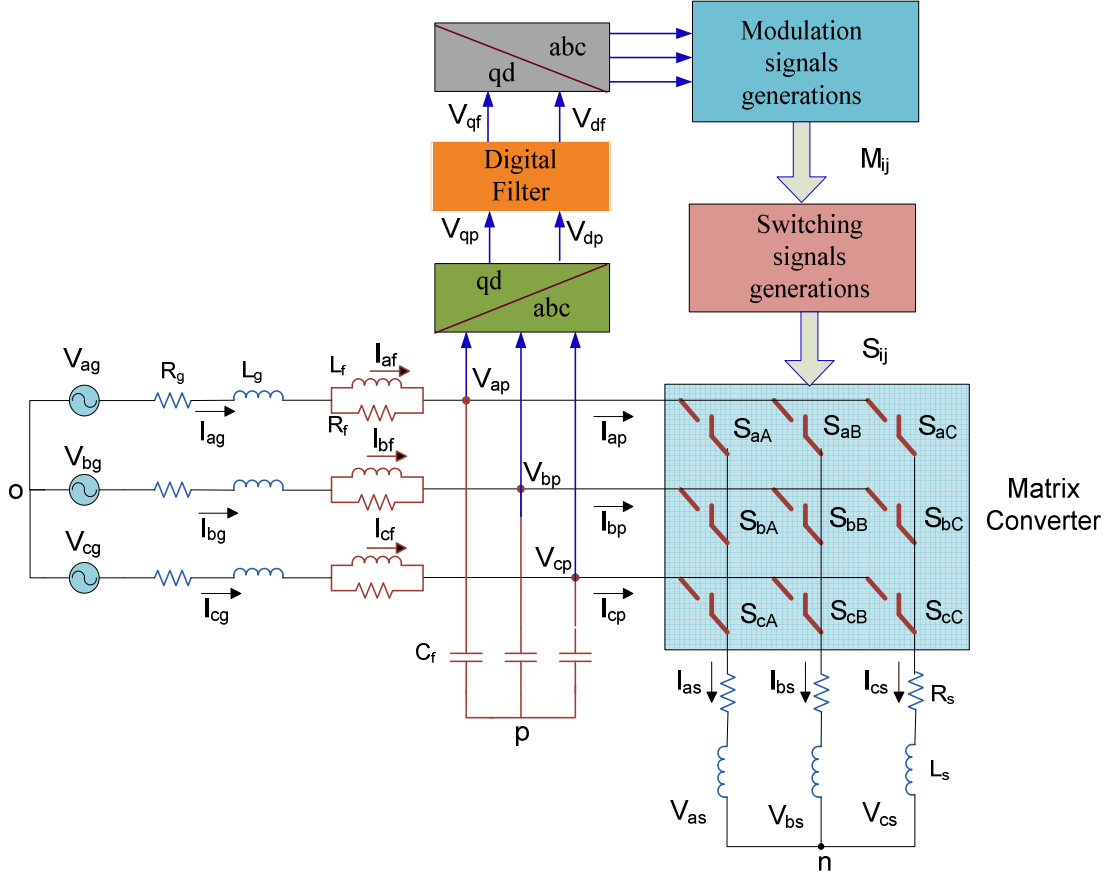


Figure 5.1 Schematic diagram of AC/AC matrix converter feeding an RL load

The dynamic equations for the filter capacitor voltages are expressed in (5.4). Where I_{ag} , I_{bg} and I_{cg} are the three phase source current while I_{ap} , I_{bp} and I_{cp} are the three phase input current of the matrix converter. V_{ap} , V_{bp} and V_{cp} represent the input three phase capacitor voltages.

$$\begin{aligned}
 C_f pV_{ap} &= I_{ag} - I_{ap} \\
 C_f pV_{bp} &= I_{bg} - I_{bp} \\
 C_f pV_{cp} &= I_{cg} - I_{cp}
 \end{aligned} \tag{5.4}$$

The mapping of the input phase voltages and output phase voltages of the converter are related as in (5.5). V_{as} , V_{bs} and V_{cs} are the output three phase voltages.

$$\begin{aligned}
V_{as} + V_{np} &= S_{aA} V_{ap} + S_{bA} V_{bp} + S_{cA} V_{cp} \\
V_{bs} + V_{np} &= S_{aB} V_{ap} + S_{bB} V_{bp} + S_{cB} V_{cp} \\
V_{cs} + V_{np} &= S_{aC} V_{ap} + S_{bC} V_{bp} + S_{cC} V_{cp}
\end{aligned} \tag{5.5}$$

For a balanced output voltage, the sum of the output phase voltages becomes zero.

Summing all the rows in (5.5), the expression for V_{np} is given by (5.6).

$$V_{np} = \frac{1}{3} \left(\begin{aligned} &S_{aA} V_{ap} + S_{bA} V_{bp} + S_{cA} V_{cp} + S_{aB} V_{ap} + \\ &S_{bB} V_{bp} + S_{cB} V_{cp} + S_{aC} V_{ap} + S_{bC} V_{bp} + S_{cC} V_{cp} \end{aligned} \right) \tag{5.6}$$

The input and output phase currents are related by switching function given by (5.7)

where I_{as} , I_{bs} and I_{cs} are the output currents.

$$\begin{aligned}
I_{ap} &= S_{aA} I_{as} + S_{aB} I_{bs} + S_{aC} I_{cs} \\
I_{bp} &= S_{bA} I_{as} + S_{bB} I_{bs} + S_{bC} I_{cs} \\
I_{cp} &= S_{cA} I_{as} + S_{cB} I_{bs} + S_{cC} I_{cs}
\end{aligned} \tag{5.7}$$

The output RL load voltage equations are expressed in (5.8) where R_s and L_s are respectively the resistance and inductance of the passive load.

$$\begin{aligned}
V_{as} &= R_s I_{as} + L_s p I_{as} \\
V_{bs} &= R_s I_{bs} + L_s p I_{bs} \\
V_{cs} &= R_s I_{cs} + L_s p I_{cs}
\end{aligned} \tag{5.8}$$

The expression for the digital low pass filter is given in the synchronous reference frame since it does not introduce any phase angle and attenuation on the fundamental component of the input voltage [40]. V_{qf} and V_{df} are the q-axis and d-axis of the filtered capacitor voltages and τ represents the time constant of the digital low pass filter.

$$\begin{aligned}
pV_{qf} &= \frac{1}{\tau} (V_{qp} - V_{qf}) \\
pV_{df} &= \frac{1}{\tau} (V_{dp} - V_{df})
\end{aligned} \tag{5.9}$$

Adding a zero sequence (common mode) voltage, V_{no} on the modulation signals which is expressed as in (5.10), the expression for the modulation signals are given as in (5.11) [8.]

$$V_{no} = \frac{1}{4}V_p \cos(3\omega_p t) - \frac{1}{6}V_s \cos(3\omega_s t) \quad (5.10)$$

$$M_{ij} = \frac{1}{3} \left(1 + \frac{2V_{ip}}{V_p^2} (V_{js} + V_{no}) + \frac{4q}{3\sqrt{3}} \sin(\omega_p t) \sin(3\omega_p t) \right) \quad (5.11)$$

There are two transformations carried out in this analysis: the input side and output side transformations $K(\theta_p)$ and $K(\theta_s)$. θ_{op} and θ_{os} are their corresponding initial angle of the reference frames.

$$K(\theta_s) = \frac{2}{3} \begin{bmatrix} \cos(\theta_s) & \cos(\theta_s - \frac{2\pi}{3}) & \cos(\theta_s + \frac{2\pi}{3}) \\ \sin(\theta_s) & \sin(\theta_s - \frac{2\pi}{3}) & \sin(\theta_s + \frac{2\pi}{3}) \\ \frac{1}{2} & \frac{1}{2} & \frac{1}{2} \end{bmatrix} \quad (5.12)$$

$$K(\theta_p) = \frac{2}{3} \begin{bmatrix} \cos(\theta_p) & \cos(\theta_p - \frac{2\pi}{3}) & \cos(\theta_p + \frac{2\pi}{3}) \\ \sin(\theta_p) & \sin(\theta_p - \frac{2\pi}{3}) & \sin(\theta_p + \frac{2\pi}{3}) \\ \frac{1}{2} & \frac{1}{2} & \frac{1}{2} \end{bmatrix} \quad (5.13)$$

where

$$\theta_p = \omega_p t + \theta_{op} \quad \theta_s = \omega_s t + \theta_{os}$$

All the currents are transformed using the above two transformations using the relations given in (5.14).

$$\begin{aligned}
I_{qdg} &= K(\theta_p) I_{abcg} \\
I_{qdf} &= K(\theta_p) I_{abcf} \\
I_{qdp} &= K(\theta_p) S^T K^{-1}(\theta_s) I_{abcs} \\
I_{qds} &= K(\theta_s) I_{abcs}
\end{aligned} \tag{5.14}$$

I_{af} , I_{bf} and I_{cf} are the three phase current flowing through the filter inductor. Note that the currents shown below are a vector of three elements

$$I_{qdg} = \begin{bmatrix} I_{qg} \\ I_{dg} \\ I_{og} \end{bmatrix} \quad I_{qdf} = \begin{bmatrix} I_{qf} \\ I_{df} \\ I_{of} \end{bmatrix} \quad I_{qdp} = \begin{bmatrix} I_{qp} \\ I_{dp} \\ I_{op} \end{bmatrix} \quad I_{qds} = \begin{bmatrix} I_{qs} \\ I_{ds} \\ I_{os} \end{bmatrix}$$

where

I_{qg} - the q-axis source current

I_{dg} - the d-axis source current

I_{qf} - the q-axis filter current

I_{dg} - the d-axis source current

I_{qp} - the q-axis input current of the matrix converter

I_{dp} - the d-axis input current of the matrix converter

I_{qs} - the q-axis output current

I_{qs} - the d-axis output current

$$I_{abcg} = \begin{bmatrix} I_{ag} \\ I_{bg} \\ I_{cg} \end{bmatrix} \quad I_{abcf} = \begin{bmatrix} I_{af} \\ I_{bf} \\ I_{cf} \end{bmatrix}$$

$$I_{abc p} = \begin{bmatrix} I_{ap} \\ I_{bp} \\ I_{cp} \end{bmatrix} \quad I_{abcs} = \begin{bmatrix} I_{as} \\ I_{bs} \\ I_{cs} \end{bmatrix}$$

Similarly, the voltages are transformed to synchronous qd axis as follows.

$$\begin{aligned}
 V_{qdg} &= K(\theta_p)V_{abcg} \\
 V_{qdp} &= K(\theta_p)V_{abc p} \\
 V_{qds} &= K(\theta_s)SK^{-1}(\theta_p)V_{abc p}
 \end{aligned} \tag{5.15}$$

where

$$V_{qdg} = \begin{bmatrix} V_{qg} \\ V_{dg} \\ V_{og} \end{bmatrix} \quad V_{qdp} = \begin{bmatrix} V_{qp} \\ V_{dp} \\ V_{op} \end{bmatrix} \quad V_{qds} = \begin{bmatrix} V_{qs} \\ V_{ds} \\ V_{os} \end{bmatrix}$$

And

V_{qg}, V_{dg} - the q-axis and d-axis source voltages

V_{qp}, V_{dp} - the q-axis and d-axis input capacitor voltages

V_{qs}, V_{ds} - the q-axis and d-axis output voltages

$$V_{qdg} = \begin{bmatrix} V_{ag} \\ V_{bg} \\ V_{cg} \end{bmatrix} \quad V_{qdp} = \begin{bmatrix} V_{ap} \\ V_{bp} \\ V_{cp} \end{bmatrix} \quad V_{qds} = \begin{bmatrix} V_{as} \\ V_{bs} \\ V_{cs} \end{bmatrix}$$

Using (5.14) and (5.15) the synchronous reference frame source voltage expression is given as

$$\begin{aligned}
 V_{qg} &= R_g I_{qg} + L_g pI_{qg} + \omega_p L_g I_{dg} + R_f (I_{qg} - I_{qf}) + V_{qp} \\
 V_{dg} &= R_g I_{dg} + L_g pI_{dg} - \omega_p L_g I_{qg} + R_f (I_{dg} - I_{df}) + V_{dp}
 \end{aligned} \tag{5.16}$$

The qd axis voltage is expressed as

$$\begin{aligned}
 L_f pI_{qf} + \omega_p L_g I_{df} &= R_f (I_{qg} - I_{qf}) \\
 L_f pI_{df} - \omega_p L_g I_{qf} &= R_f (I_{dg} - I_{df})
 \end{aligned} \tag{5.17}$$

Similarly, the capacitor dynamics in qd is shown below

$$\begin{aligned} C_f pV_{qp} + \omega_p C_f V_{dp} &= I_{qg} - I_{qp} \\ C_f pV_{dp} - \omega_p C_f V_{qp} &= I_{dg} - I_{dp} \end{aligned} \quad (5.18)$$

The mapping between the input and output current is done using the four components of a modulation signals. The detailed derivation for the expression given in (5.19-5.23) is given in Appendix E.

$$\begin{aligned} I_{dp} &= M_{qd} I_{qs} + M_{dd} I_{ds} \\ I_{qp} &= M_{qq} I_{qs} + M_{dq} I_{ds} \end{aligned} \quad (5.19)$$

The expressions of the synchronous frame modulation signals are shown as follows,

$$\begin{aligned} M_{qq} &= M \cos(\delta_{ss}) \cos(\delta_{pp}) & M_{qd} &= -M \cos(\delta_{ss}) \sin(\delta_{pp}) \\ M_{dq} &= -M \sin(\delta_{ss}) \cos(\delta_{pp}) & M_{dd} &= M \sin(\delta_{ss}) \sin(\delta_{pp}) \end{aligned} \quad (5.20)$$

where δ_{op} and δ_{os} are the phase angle of the capacitor and output voltages respectively.

$$\delta_{ss} = \delta_{os} - \theta_{os} \quad \delta_{pp} = \delta_{op} - \theta_{op} \quad (5.21)$$

The modulation index of the matrix converter is related to each component of the modulation signals as follows

$$M^2 = M_{qq}^2 + M_{qd}^2 + M_{dq}^2 + M_{dd}^2 \quad (5.22)$$

The input output voltage mapping in qd is represented in (5.23)

$$\begin{aligned} V_{qs} &= M_{qq} V_{qp} + M_{qd} V_{dp} \\ V_{ds} &= M_{dq} V_{qp} + M_{dd} V_{dp} \end{aligned} \quad (5.23)$$

Finally, the output voltage of the converter given

$$\begin{aligned} V_{qs} &= R_s I_{qs} + L_s pI_{qs} + \omega_s I_{ds} \\ V_{ds} &= R_s I_{ds} + L_s pI_{ds} - \omega_s I_{qs} \end{aligned} \quad (5.24)$$

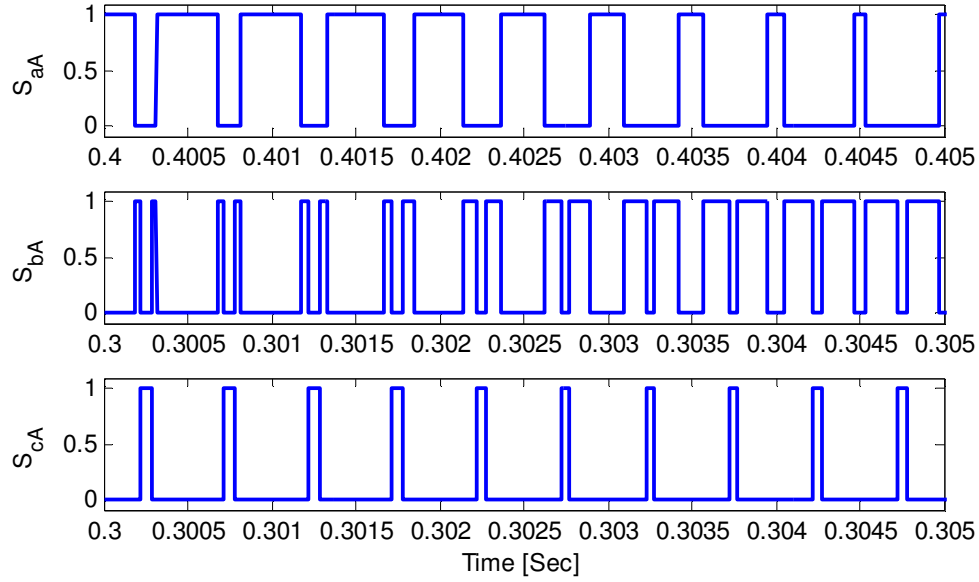


Figure 5.2 Switching pulses for phase ‘a’ output voltage

5.2.2 Dynamic Simulation Results and Discussion

Based on the model equation derived in the previous section and with the parameters given in Table 5.1, simulations are given in Figure 5.2 to 5.8. The switching signals used to synthesize output phase ‘a’ voltage are shown in Figure 5.2 where at any instant of time one and only one device turns ON. The output line-to-line voltages are given in Figure 5.3 with an average sinusoidal waveform. Similarly, the three phase voltages are all sinusoidal average voltages and balanced as seen in Figure 5.5. The input phase capacitor voltage containing small ripple are shown in Figure 5.5 and are filtered by the digital low pass filter before they are used to generate a modulation signals.

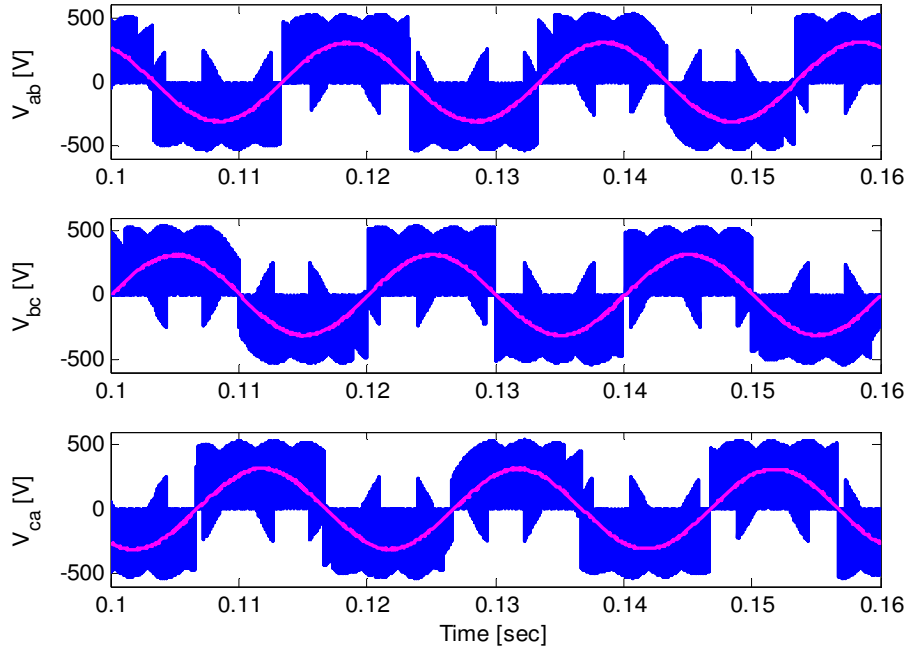


Figure 5.3 MC output line-to-line voltages

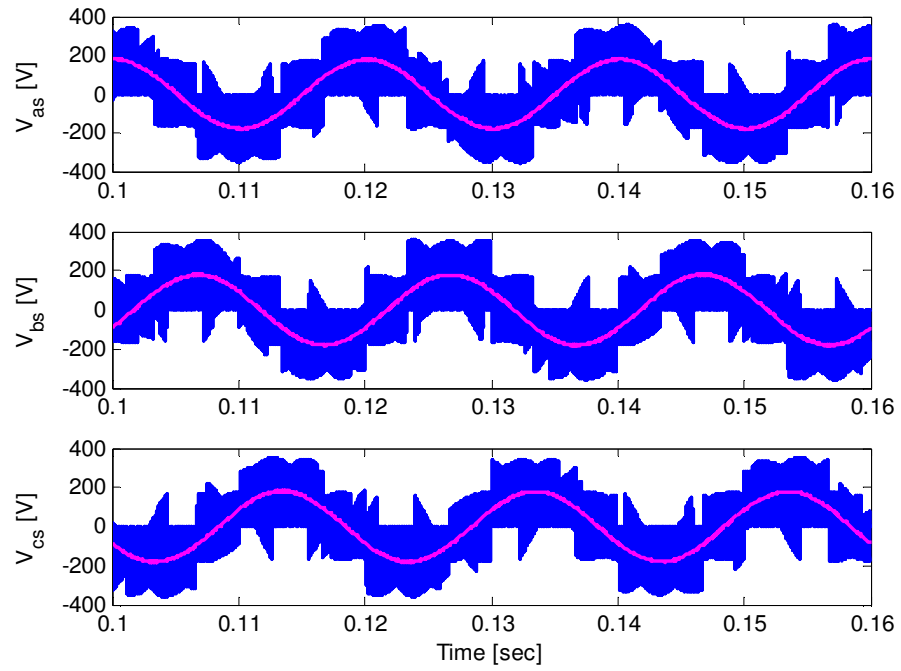


Figure 5.4 MC output three phase voltages

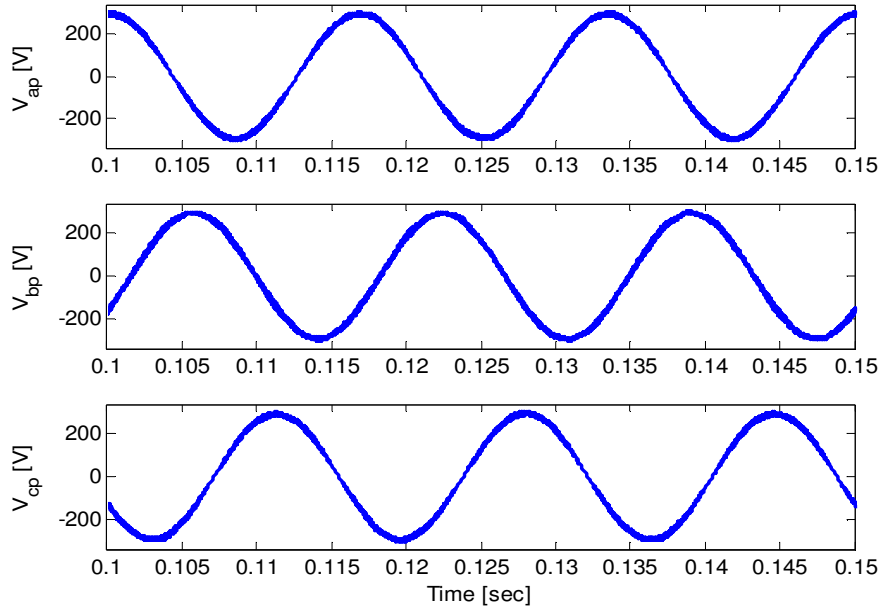


Figure 5.5 Input three phase capacitor voltages

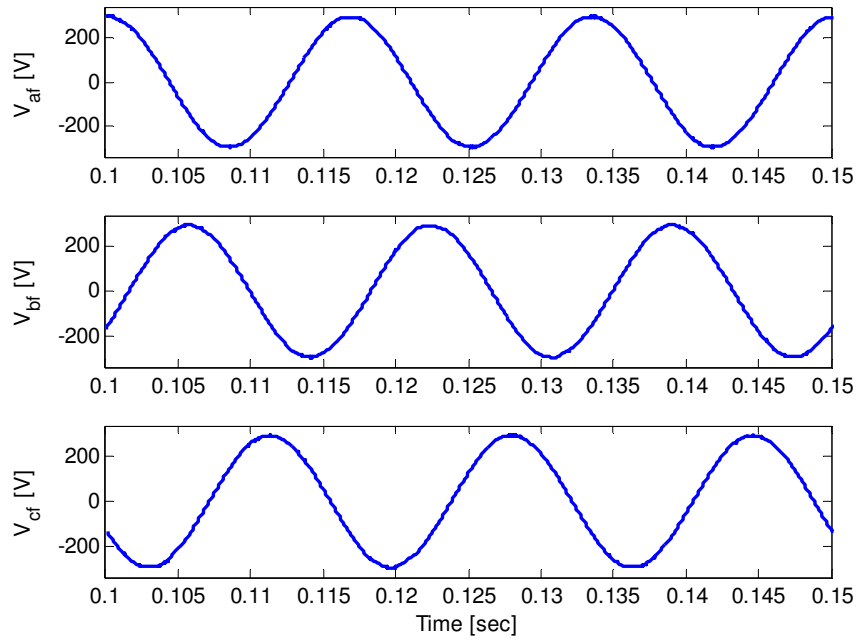


Figure 5.6 Filtered three phase capacitor voltages

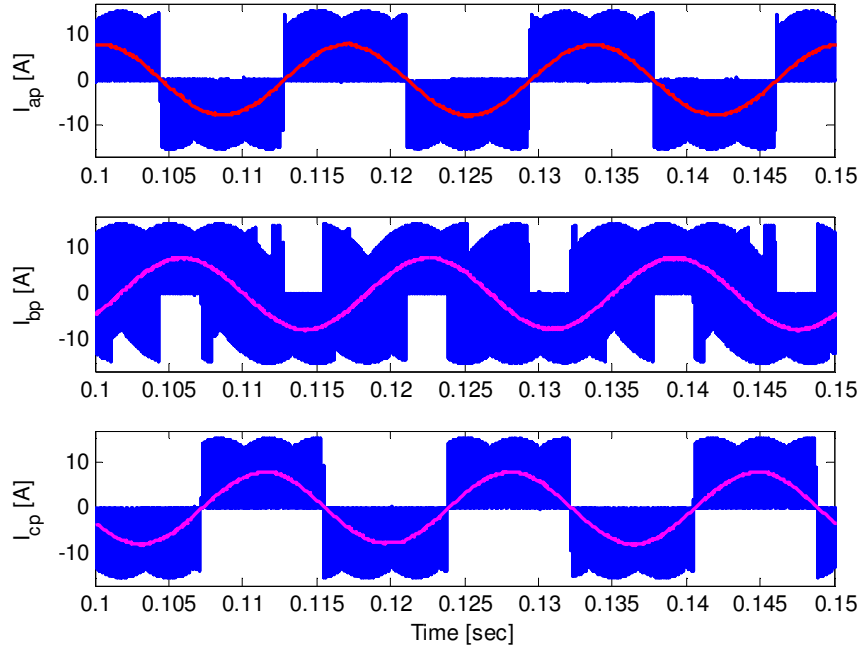


Figure 5.7 MC three phase input current

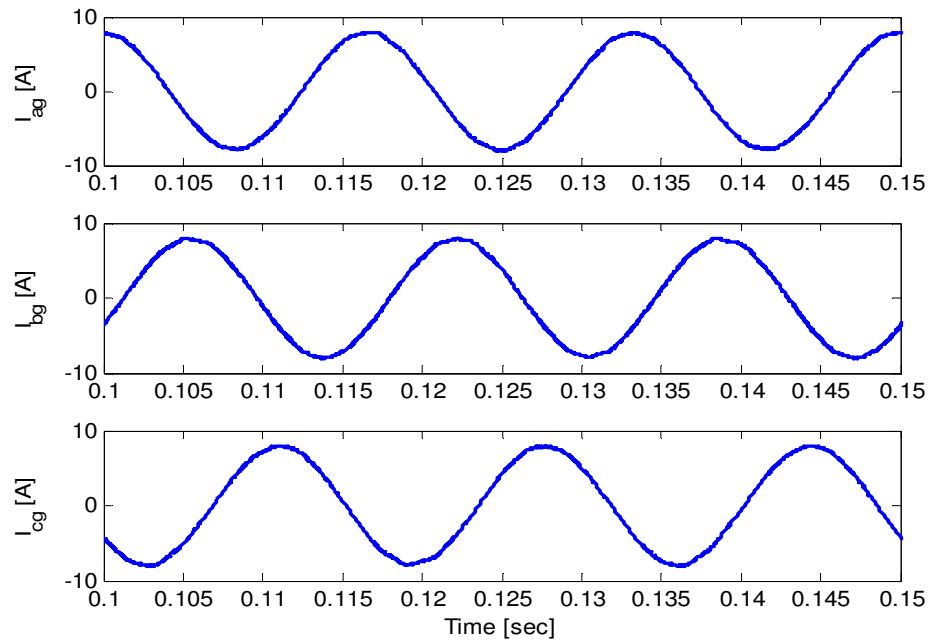


Figure 5.8 Three phase source currents

These filtered input voltages are given in Figure 5.6. The input current of the matrix converter and the source current after the input low pass filter is show in Figure 5.7 and 5.8 respectively.

5.2.3 Generalized Steady State Analysis

The generalized steady state analysis proposed in this thesis is presented in this section. To determine the steady state analysis, the dynamic equations given in abc are transformed into qd synchronous reference frames. At steady state the q-axis and d-axis voltage equations of the source are expressed as

$$\begin{aligned} V_{qg} &= R_g I_{qg} + \omega_p L_g I_{dg} + R_f (I_{qg} - I_{qf}) + V_{qp} \\ V_{dg} &= R_g I_{dg} - \omega_p L_g I_{qg} + R_f (I_{dg} - I_{df}) + V_{dp} \end{aligned} \quad (5.25)$$

The voltage equations for the inductor voltage at steady state are

$$\begin{aligned} \omega_p L_f I_{df} &= R_f (I_{qg} - I_{qf}) \\ -\omega_p L_f I_{qf} &= R_f (I_{dg} - I_{df}) \end{aligned} \quad (5.26)$$

The q-axis and d-axis voltage equations for the inductor voltage at steady state is given as

$$\begin{aligned} \omega_p C_f V_{dp} &= I_{qg} - M_{qq} I_{qs} - M_{dq} I_{ds} \\ -\omega_p C_f V_{qp} &= I_{dg} - M_{qd} I_{qs} - M_{dd} I_{ds} \end{aligned} \quad (5.27)$$

The active and reactive power drawn from the source can be represented in terms of the synchronous reference frame voltages and currents as follows:

$$\begin{aligned}
P_g &= \frac{3}{2}(V_{qg} I_{qg} + V_{dg} I_{dg}) \\
Q_g &= \frac{3}{2}(V_{qg} I_{dg} - V_{dg} I_{qg})
\end{aligned} \tag{5.28}$$

Aligning the input side reference frame angle to the d -axis of the source voltage, the d -axis of the source voltage becomes zero and the q -axis source voltage is equal to the magnitude of the phase voltage. The expressions for the active and reactive power are modified as shown in (5.29).

$$P_g = \frac{3}{2} V_g I_{qg} \quad Q_g = \frac{3}{2} V_g I_{dg} \tag{5.29}$$

Considering the output sides, the steady state synchronous reference frame voltage equations are

$$\begin{aligned}
V_{qs} &= R_s I_{qs} + \omega_s L_s I_{ds} \\
V_{ds} &= R_s I_{ds} - \omega_s L_s I_{qs}
\end{aligned} \tag{5.30}$$

The corresponding q -axis and d -axis load current can be computed from the respective voltages using expression (5.31)

$$\begin{aligned}
I_{qs} &= \frac{R_s}{R_s^2 + \omega_s^2 L_s^2} V_{qs} - \frac{\omega_s L_s}{R_s^2 + \omega_s^2 L_s^2} V_{ds} \\
I_{ds} &= \frac{\omega_s L_s}{R_s^2 + \omega_s^2 L_s^2} V_{qs} + \frac{R_s}{R_s^2 + \omega_s^2 L_s^2} V_{ds}
\end{aligned} \tag{5.31}$$

Since this particular approaches is a generalized method of steady state analysis, it can be used when the whole system operate a unity, lagging or leading power factor at the source side. By specifying the operating input power factor (pf), based on (5.29) the

relation between the q-axis and d-axis components of the source current can easily be represented as shown below.

$$I_{dg} = \rho I_{qg} \quad (5.32)$$

where ρ is the ratio of the reactive power to the active power

The qd components of the inductor current can also be represented in terms of the q-axis source current by simultaneously solving (5.26).

$$\begin{aligned} I_{qf} &= \beta_1 I_{qg} \\ I_{df} &= \beta_2 I_{qg} \end{aligned} \quad (5.33)$$

The constants which are function of the input frequency, input power factor, filter inductor and damping resistor are represented below.

$$\begin{aligned} \beta_1 &= \frac{R_f - \rho \omega_p L_f}{R_f^2 + \omega_p^2 L_f^2} R_f \\ \beta_2 &= \frac{\rho R_f + \omega_p L_f}{R_f^2 + \omega_p^2 L_f^2} R_f \end{aligned} \quad (5.34)$$

Substituting (5.33) into (5.25), all the input side voltages and currents can be represented in terms of only the q-axis capacitor voltage which is represented by (5.35)

$$\begin{aligned} I_{qg} &= \beta_3 \beta_4 (V_{qg} - V_{qp}) \\ V_{dp} &= \beta_4 (V_{qg} - V_{qp}) \end{aligned} \quad (5.35)$$

where the expressions of the above constants are given in (5.36) and it is seen that all these constants so far does not depend on the filter capacitor parameter.

$$\beta_3 = \frac{1}{(\omega_p L_g + R_f \beta_2 - \rho(R_g + R_f))} \quad (5.36)$$

$$\beta_4 = \frac{1}{\beta_3(R_g + R_f(1 - \beta_1)) + \rho\omega_p L_g}$$

The input and output voltage now are related by the four components of the modulation signals.

$$\begin{aligned} V_{qs} &= M_{qq} V_{qp} + M_{qd} V_{dp} \\ V_{ds} &= M_{dq} V_{qp} + M_{dd} V_{dp} \end{aligned} \quad (5.37)$$

Similarly, the input current components are related to the output voltages by these modulation signal components.

$$\begin{aligned} I_{qp} &= M_{qq} I_{qs} + M_{dq} I_{ds} \\ I_{dp} &= M_{qd} I_{qs} + M_{dd} I_{ds} \end{aligned} \quad (5.38)$$

These four components of the modulation signals are represented in (5.39) where M is the modulation index, δ_{ss} is the phase angle difference between the output voltage and output side reference frame. And δ_{pp} is the phase angle difference between the input capacitor voltage and input side reference frame. The complete derivation is given in Appendix IV.

$$\begin{aligned} M_{qq} &= M \cos(\delta_{ss}) \cos(\delta_{pp}) \\ M_{qd} &= -M \cos(\delta_{ss}) \sin(\delta_{pp}) \\ M_{dq} &= -M \sin(\delta_{ss}) \cos(\delta_{pp}) \\ M_{dd} &= M \sin(\delta_{ss}) \sin(\delta_{pp}) \\ M^2 &= M_{qq}^2 + M_{qd}^2 + M_{dq}^2 + M_{dd}^2 \end{aligned} \quad (5.39)$$

Defining constants k_I and g_I as given in (5.40), V_{qp} can be represented in terms of the other variables.

$$k_1 = \frac{\rho\beta_3\beta_4}{\rho\beta_3\beta_4 - \omega_p C_f} \quad (5.40)$$

$$g_1 = -\frac{1}{\rho\beta_3\beta_4 - \omega_p C_f}$$

$$V_{qp} = k_1 V_{qg} + g_1 (M_{qd} I_{qs} + M_{dd} I_{ds}) \quad (5.41)$$

The four non-linear equation and four variables, M_{qq} , M_{qd} , M_{dq} and M_{dd} , are shown in (5.42). Eliminating three of the four unknowns, first M_{qq} then M_{dq} and later M_{qd} , makes the computation easier and it does not need mathematical tools.

$$M_{qq} M_{dd} = M_{qd} M_{dq}$$

$$V_{qs} = (M_{qq} - M_{qd} \beta_4) (k_1 V_{qg} + g_1 (M_{qd} I_{qs} + M_{dd} I_{ds})) + M_{qd} \beta_4 V_{qg}$$

$$V_{ds} = (M_{dq} - M_{dd} \beta_4) (k_1 V_{qg} + g_1 (M_{qd} I_{qs} + M_{dd} I_{ds})) + M_{dd} \beta_4 V_{qg} \quad (5.42)$$

$$g_2 (k_1 V_{qg} + g_1 (M_{qd} I_{qs} + M_{dd} I_{ds})) = g_2 V_{qg} - M_{qq} I_{qs} - M_{dq} I_{ds}$$

The final quadratic equation which is a function of M_{dd} is shown (5.43). Once M_{dd} is computed all the other variables are determined by back substitution.

$$aM_{dd}^2 + bM_{dd} + c = 0 \quad (5.43)$$

The coefficients of the quadratic equations are given as follows.

$$a = g_1 (g_1 g_2 + \beta_4) (V_{qs} I_{qs} + V_{ds} I_{ds})$$

$$b = (k_1 (g_1 g_2 + \beta_4 + k_1 g_1 g_2) - (\beta_4 + g_1 g_2)) V_{qg} V_{ds}$$

$$c = V_{ds}^2 - k_1 M_x V_{ds} V_{qg} \quad (5.46)$$

$$g_2 = \beta_3 \beta_4 - \omega_p C_f \beta_4$$

$$M_x = \frac{g_2 V_{qg} V_{ds} (1 - k_1)}{V_{qs} I_{qs} + V_{ds} I_{ds}}$$

5.2.4 Steady State Simulation Results and Discussions

In order to verify the analysis, simulation of a MC system with the parameters given in Table 5.1 is performed. Figure 5.9 to Figure 5.13 shows the steady state simulation results of a matrix converter supplying an RL load. The output power factor is always a lagging power factor since it is an RL load and the value of this power factor depends on the load parameters. The graphs presented in this section are obtained by varying the output power factor possibly from near to 0 to 1 at the same time three cases of the input power factors are taken. The output active power and reactive power combinations are seen in Figure 3.9. It has been observed that the output powers are independent of the input power factor.

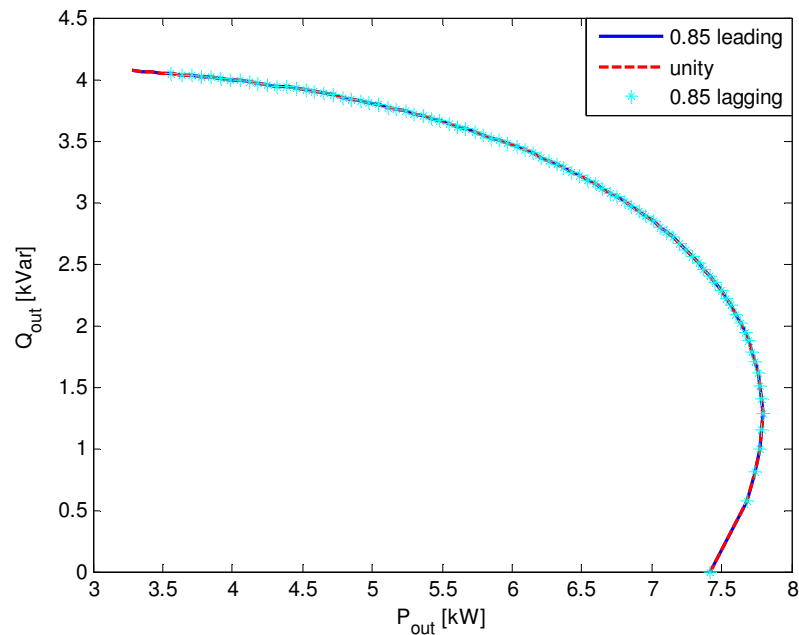


Figure 5.9 Output active and reactive power for possible output power factor operations

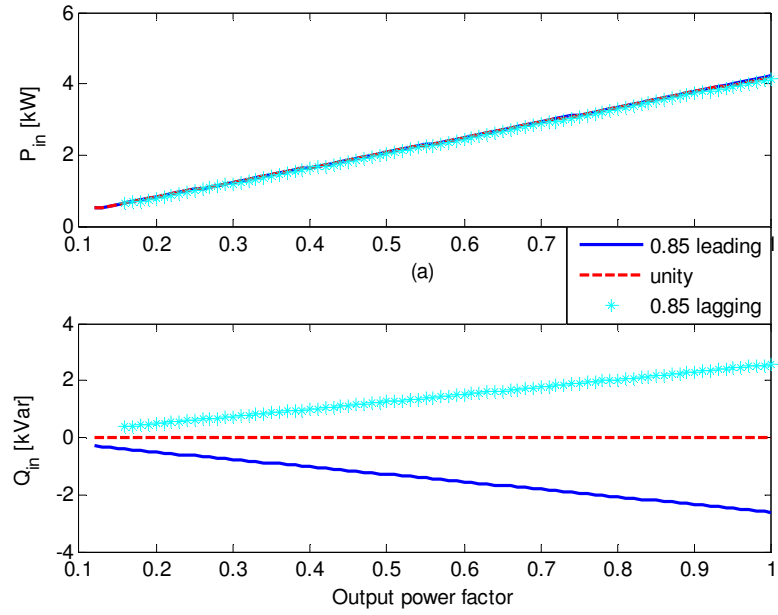


Figure 5.10 Input active and reactive powers

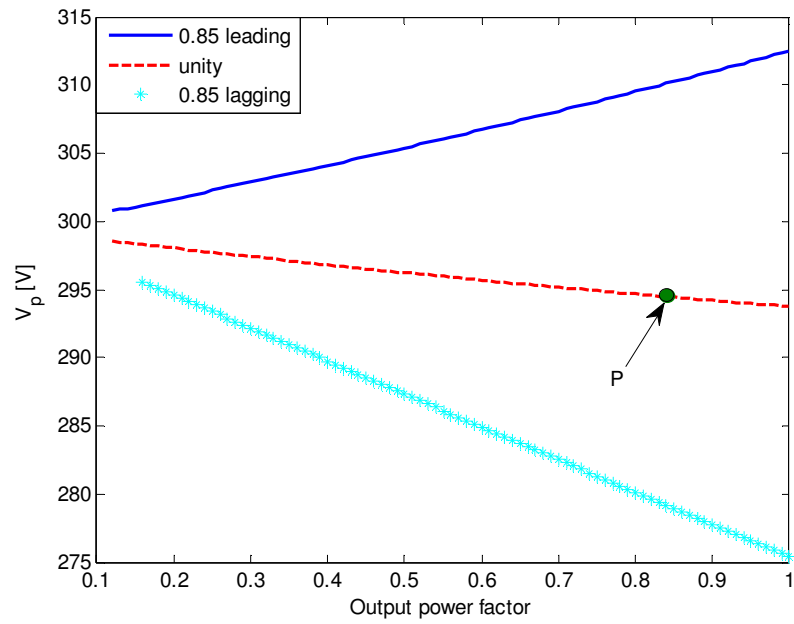


Figure 5.11 Magnitude of input capacitor voltage

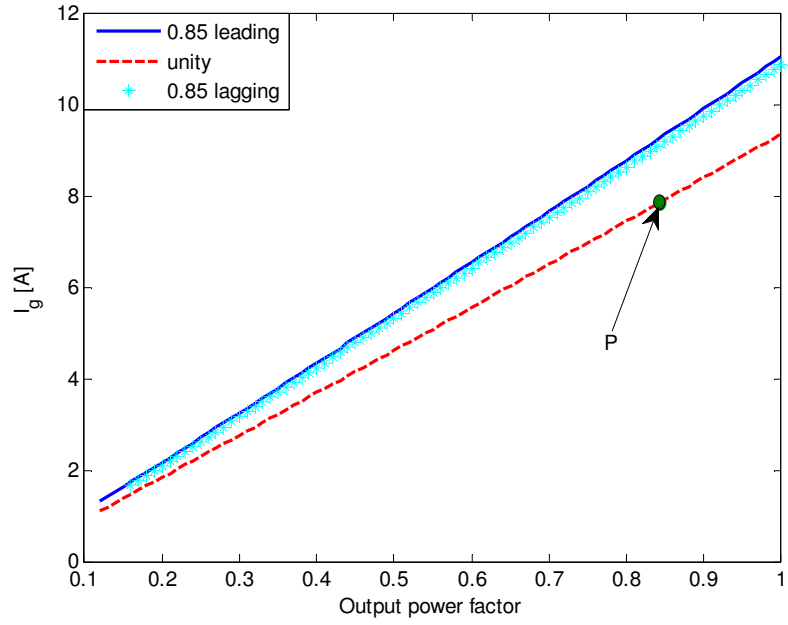


Figure 5.12 Magnitude of source current

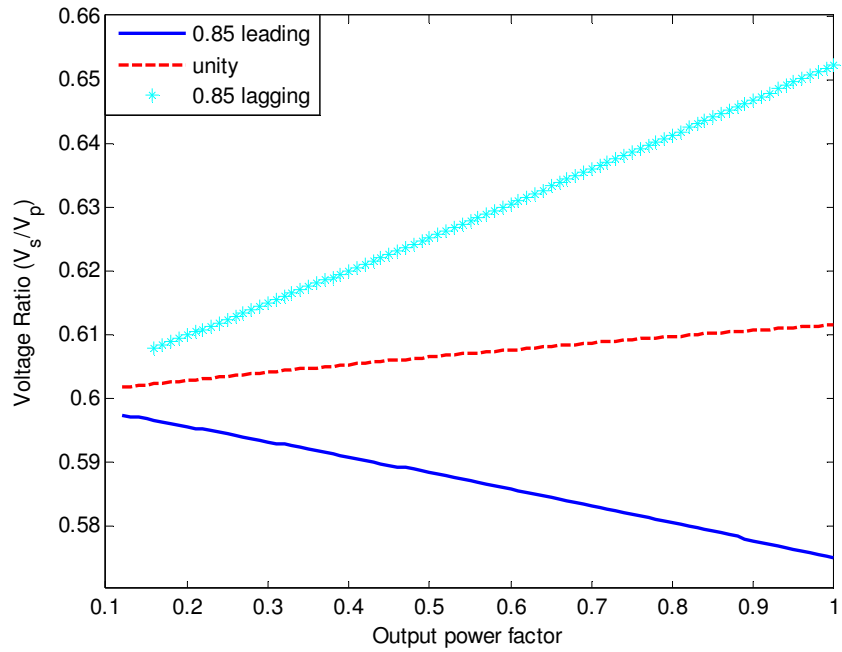


Figure 5.13 Converter output to input voltage ratio

5.3 Modelling of Matrix Converter Fed Induction Machine

5.3.1 Dynamic Modelling

A typical schematic of a MC converter fed induction motor is show in Figure 5.15. The modeling in the case is similar with the model presented in the previous section. In this case the load is an induction machine. The input side dynamic equations are shown below.

$$\begin{aligned} V_{qg} &= R_g I_{qg} + L_g pI_{qg} + \omega_p L_g I_{dg} + R_f (I_{qg} - I_{qf}) + V_{qp} \\ V_{dg} &= R_g I_{dg} + L_g pI_{dg} - \omega_p L_g I_{qg} + R_f (I_{dg} - I_{df}) + V_{dp} \end{aligned} \quad (5.47)$$

The qd axis voltage is expressed as

$$\begin{aligned} L_f pI_{qf} + \omega_p L_g I_{df} &= R_f (I_{qg} - I_{qf}) \\ L_f pI_{df} - \omega_p L_g I_{qf} &= R_f (I_{dg} - I_{df}) \end{aligned} \quad (5.48)$$

Similarly, the capacitor dynamics in qd is shown below

$$\begin{aligned} C_f pV_{qp} + \omega_p C_f V_{dp} &= I_{qg} - I_{qf} \\ C_f pV_{dp} - \omega_p C_f V_{qp} &= I_{dg} - I_{df} \end{aligned} \quad (5.49)$$

The q-axis and d-axis stator voltages are in synchronous reference frame is expressed as

(5.50)

$$\begin{aligned} V_{qs} &= R_s I_{qs} + p\lambda_{qs} + \omega_s \lambda_{ds} \\ V_{ds} &= R_s I_{ds} + p\lambda_{ds} - \omega_s \lambda_{qs} \end{aligned} \quad (5.50)$$

$$\begin{aligned}\lambda'_{qr} &= L_m I_{qs} + L_r I'_{qr} \\ \lambda'_{dr} &= L_m I_{ds} + L_r I'_{dr}\end{aligned}\tag{5.53}$$

The electromagnetic torque is expressed in terms of the stator flux linkage and stator current as given in (5.54). This torque is positive for motor action and negative in generating mode.

$$T_e = \frac{3P}{4} (\lambda_{ds} I_{qs} - \lambda_{qs} I_{ds})\tag{5.54}$$

The rotor speed and electromagnetic torque of a P pole machine are related by (5.55) where J is the inertia of the rotor and connected mechanical load expressed in kgm². T_L is the load torque.

$$p\omega_r = \frac{P}{2J} (T_e - T_L)\tag{5.55}$$

5.3.2 Dynamic Simulation Results and Discussion

Simulation of the system is developed based on the model equations (5.48) to (5.55) using the parameters given in Table 5.1. The motor starts at no load so as to observe the starting transient and then a 25 Nm load torque are applied after 0.5 s to show the dynamic response of the system. At starting, the motor experiences high electromagnetic torque with rising rotor speed until they both reach their steady values after 0.3 s as seen in Figure 5.15. These figures also show the responses for a step change of load at 0.6 s. The output line-to-line and phase voltages of the converter are both average sinusoidal waveforms as shown in Figure 5.16.

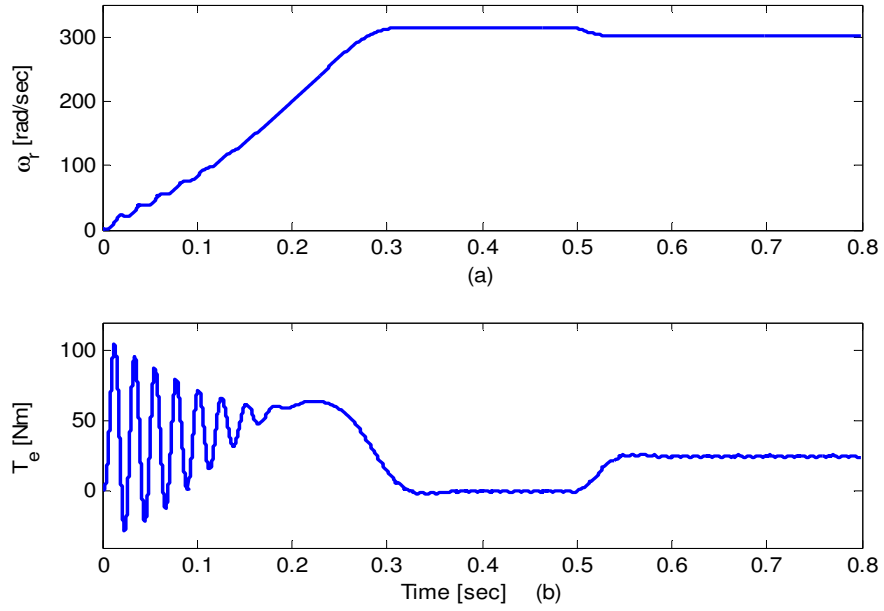


Figure 5.15 Starting transient and dynamic response of (a) rotor speed and (b) electromagnetic torque

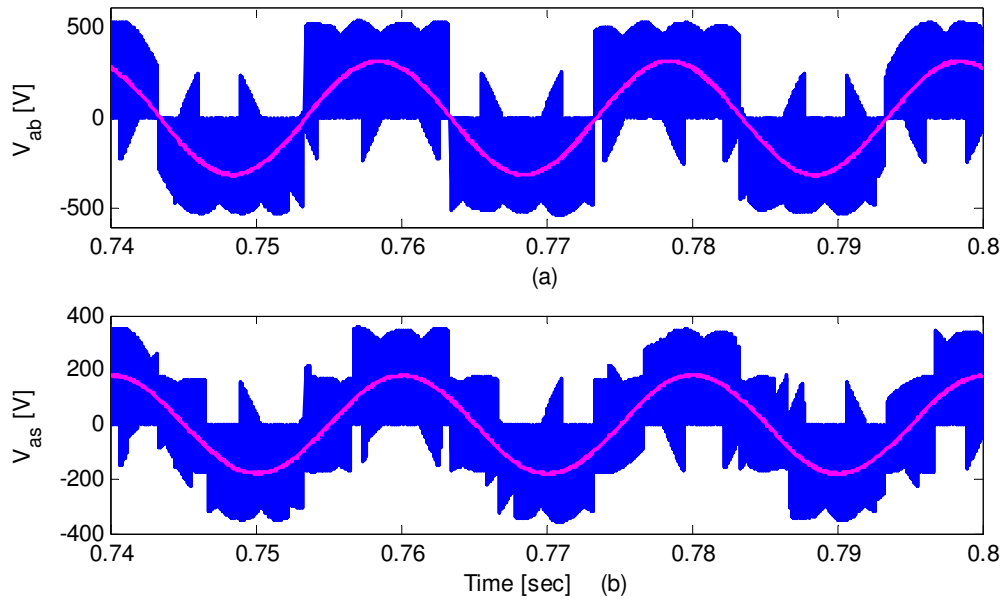


Figure 5.16 MC output (a) line-to-line voltage (b) phase voltage

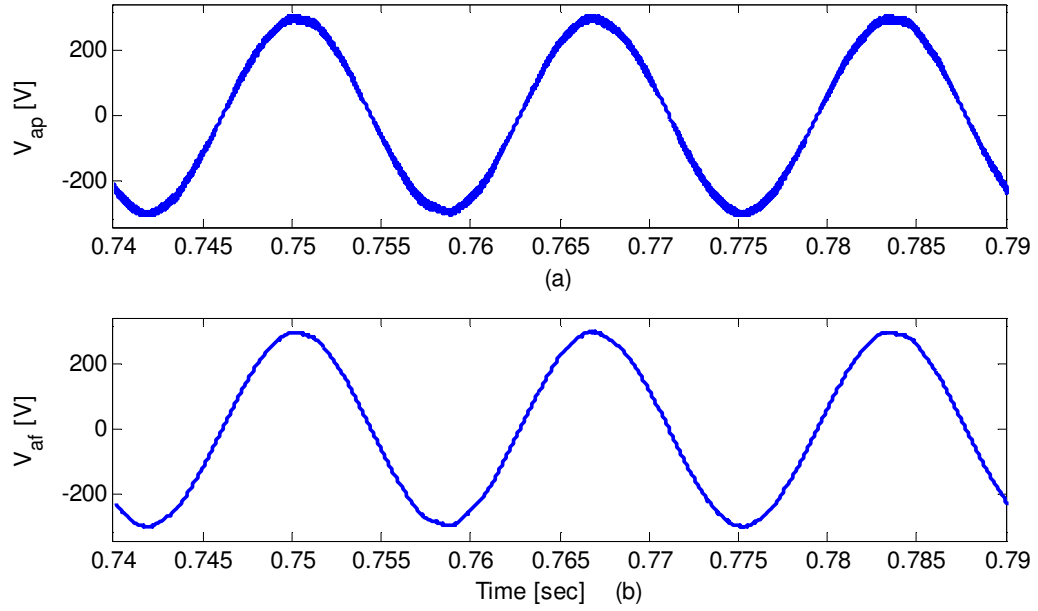


Figure 5.17 (a) Input capacitor phase voltage (b) filtered capacitor voltage

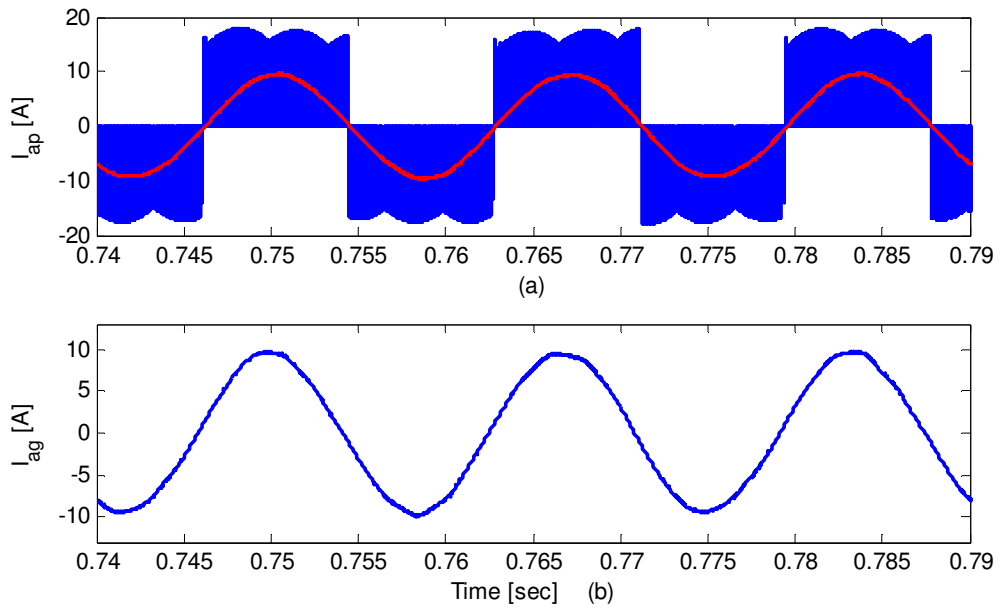


Figure 5.18 (a) MC input phase current (b) source phase current

The input capacitor voltages before and after the digital filter are given in Figure 5.17. It clearly verify that the digital low pass filter implemented in qd-synchronous

reference frame eliminate higher order harmonics resulting in a relatively pure sinusoidal voltage which is used to generate the modulation signals.

5.3.3 Generalized Steady State Analysis

This section presents a generalized steady state analysis for matrix converter fed induction machine. With similar approaches shown in section 5.1.3, steady state the q-axis and d-axis voltage equations of the source are expressed as

$$\begin{aligned} V_{qg} &= R_g I_{qg} + \omega_p L_g I_{dg} + R_f (I_{qg} - I_{qf}) + V_{qp} \\ V_{dg} &= R_g I_{dg} - \omega_p L_g I_{qg} + R_f (I_{dg} - I_{df}) + V_{dp} \end{aligned} \quad (5.56)$$

And the voltage equations for the inductor voltage at steady state

$$\begin{aligned} \omega_p L_f I_{df} &= R_f (I_{qg} - I_{qf}) \\ -\omega_p L_f I_{qf} &= R_f (I_{dg} - I_{df}) \end{aligned} \quad (5.57)$$

The q-axis and d-axis voltage equations for the inductor voltage at steady state is given as

$$\begin{aligned} \omega_p C_f V_{dp} &= I_{qg} - M_{qq} I_{qs} - M_{dq} I_{ds} \\ -\omega_p C_f V_{qp} &= I_{dg} - M_{qd} I_{qs} - M_{dd} I_{ds} \end{aligned} \quad (5.58)$$

The active and reactive power of the drawn from the source can be represented in terms of the synchronous reference frame voltages and currents as follows.

$$\begin{aligned} P_g &= \frac{3}{2} (V_{qg} I_{qg} + V_{dg} I_{dg}) \\ Q_g &= \frac{3}{2} (V_{qg} I_{dg} - V_{dg} I_{qg}) \end{aligned} \quad (5.59)$$

The q-axis and d-axis stator voltages are given as:

$$\begin{aligned} V_{qs} &= R_s I_{qs} + \omega_s \lambda_{ds} \\ V_{ds} &= R_s I_{ds} - \omega_s \lambda_{qs} \end{aligned} \quad (5.60)$$

Rotor voltage steady state equations

$$\begin{aligned} V_{qr}' &= 0 = R_r' I_{qr}' + (\omega_s - \omega_r) \lambda_{dr}' \\ V_{dr}' &= 0 = R_r' I_{dr}' - (\omega_s - \omega_r) \lambda_{qr}' \end{aligned} \quad (5.61)$$

The expressions for q-axis and d-axis stator flux linkages are given as:

$$\begin{aligned} \lambda_{qs} &= L_s I_{qs} + L_m I_{qr}' \\ \lambda_{ds} &= L_s I_{ds} + L_m I_{dr}' \end{aligned} \quad (5.62)$$

The q-axis and d-axis rotor flux linkages are expressed as:

$$\begin{aligned} \lambda_{qr}' &= L_m I_{qs} + L_r' I_{qr}' \\ \lambda_{dr}' &= L_m I_{ds} + L_r' I_{dr}' \end{aligned} \quad (5.63)$$

In matrix form

$$\begin{bmatrix} V_{qs} \\ V_{ds} \\ 0 \\ 0 \end{bmatrix} = \begin{bmatrix} R_s & \omega_s L_s & 0 & \omega_s L_m \\ -\omega_s L_s & R_s & -\omega_s L_m & 0 \\ 0 & s\omega_s L_m & R_r & s\omega_s L_r \\ -s\omega_s L_m & 0 & -s\omega_s L_r & R_r \end{bmatrix} \begin{bmatrix} I_{qs} \\ I_{ds} \\ I_{qr}' \\ I_{dr}' \end{bmatrix} \quad (5.64)$$

The electronic torque is expressed in terms of the stator flux linkage and stator current as given in (5.64). This torque is positive for motor action and negative in generating mode.

$$T_e = \frac{3P}{4} (\lambda_{ds} I_{qs} - \lambda_{qs} I_{ds}) \quad (5.65)$$

The rotor speed and electromagnetic torque of a P pole machine are related by (5.65) where J is the inertia of the rotor and connected mechanical load expressed in kgm^2 . T_L is the load torque.

$$p\omega_r = \frac{P}{2J}(T_e - T_L) \quad (5.66)$$

The steady state variables are computed step-by-step as follows:

$$aM_{dd}^2 + bM_{dd} + c = 0 \quad (5.67)$$

$$M_{dq} = M_x - g_1 g_2 M_{dd}$$

$$M_{qd} = M_{dd} \frac{V_{qs}}{V_{ds}}$$

$$M_{qq} = \frac{M_{dq}}{M_{dd}} M_{qd}$$

$$V_{qp} = k_1 V_{qg} + g_1 (M_{qd} I_{qs} + M_{dd} I_{ds})$$

$$I_{qg} = \beta_3 \beta_4 (V_{qg} - V_{qp})$$

$$I_{dg} = \rho I_{qg}$$

$$V_{dp} = \beta_4 (V_{qg} - V_{qp})$$

$$I_{qf} = \beta_1 I_{qg}$$

$$I_{df} = \beta_2 I_{qg}$$

$$I_{qs} = m_1 V_{qs} - m_2 V_{ds}$$

$$I_{ds} = m_2 V_{qs} + m_1 V_{ds}$$

The constants used in the above expressions are given below:

$$a = g_1 (g_1 g_2 + \beta_4) (V_{qs} I_{qs} + V_{ds} I_{ds})$$

$$b = (k_1 (g_1 g_2 + \beta_4 + k_1 g_1 g_2) - (\beta_4 + g_1 g_2)) V_{qg} V_{ds}$$

$$c = V_{ds}^2 - k_1 M_x V_{ds} V_{qg}$$

$$M_x = \frac{g_2 V_{qg} V_{ds} (1 - k_1)}{V_{qs} I_{qs} + V_{ds} I_{ds}}$$

$$g_1 = -\frac{1}{\rho \beta_3 \beta_4 - \omega_p C_f}$$

$$g_2 = \beta_3 \beta_4 - \omega_p C_f \beta_4$$

$$\beta_1 = \frac{R_f - \rho \omega_p L_f}{R_f^2 + \omega_p^2 L_f^2} R_f$$

$$\beta_2 = \frac{\rho R_f + \omega_p L_f}{R_f^2 + \omega_p^2 L_f^2} R_f$$

$$\beta_3 = \frac{1}{(\omega_p L_g + R_f \beta_2 - \rho (R_g + R_f))}$$

$$\beta_4 = \frac{1}{\beta_3 (R_g + R_f (1 - \beta_1) + \rho \omega_p L_g)}$$

$$m_1 = \frac{1}{\Delta} (R_s R_r^2 + R_s s^2 \omega_s^2 L_r^2 + s^2 \omega_s^2 L_m^2 R_r)$$

$$k_1 = \frac{\rho \beta_3 \beta_4}{\rho \beta_3 \beta_4 - \omega_p C_f}$$

$$m_2 = \frac{\omega_s}{\Delta} (L_s R_r^2 + \omega_s^2 L_s s^2 L_r^2 - s^2 \omega_s^2 L_m^2 L_r)$$

$$\rho = \tan(\cos^{-1}(pf))$$

5.3.4 Steady State Simulation Results and Discussions

To verify the steady state performance of the induction motor drive, calculations are done based on the model equations (5.56) to (5.67) with the parameters given in Table 5.1. Figures 5.19 - 5.19 are drawn considering lagging, unity and leading input power factor operations. The torque-slip characteristics of the motor are shown in Figure 5.19 for different input power factor operations. This figure also shows that the electromagnetic torque does not depend on the input power factor. Figure 5.20 gives the magnitudes of the input capacitor voltage and source current. It can be observed that when the drive operates at lagging input power factor, the speed range is very narrow because of the limit in the matrix converter voltage transfer ratio. However, when the overall system operates in leading and unity power factor, the matrix converter voltage is below the maximum allowable limit in all possible speed ranges as seen in Figure 5.22. The fundamental reason is demonstrate in Figure 5.20, when the system operate in leading power factor mode, the magnitude of the input capacitor voltage will significantly increased to inject reactive power to the source. As a result, it is possible to keep the output stator voltage at the required value within the limit. On the other hand, in lagging power factor operation, the capacitor voltage relatively lower value. Therefore, it is not possible to get the specified stator voltage for wide load ranges; otherwise it goes to unwanted over modulation region. The input active and reactive powers are shown in Figure 5.21.

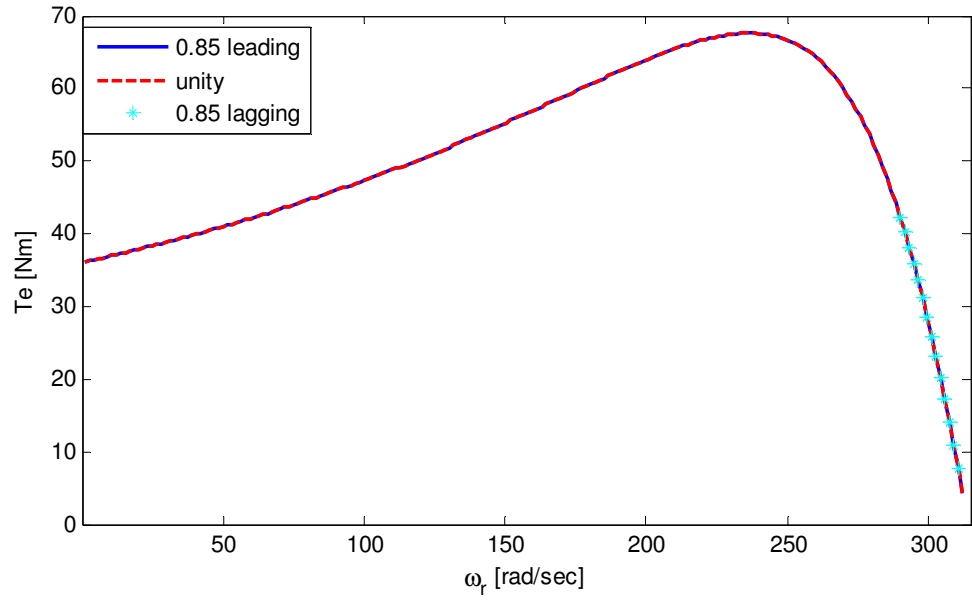


Figure 5.19 Steady state torque-slip characteristics of an induction machine

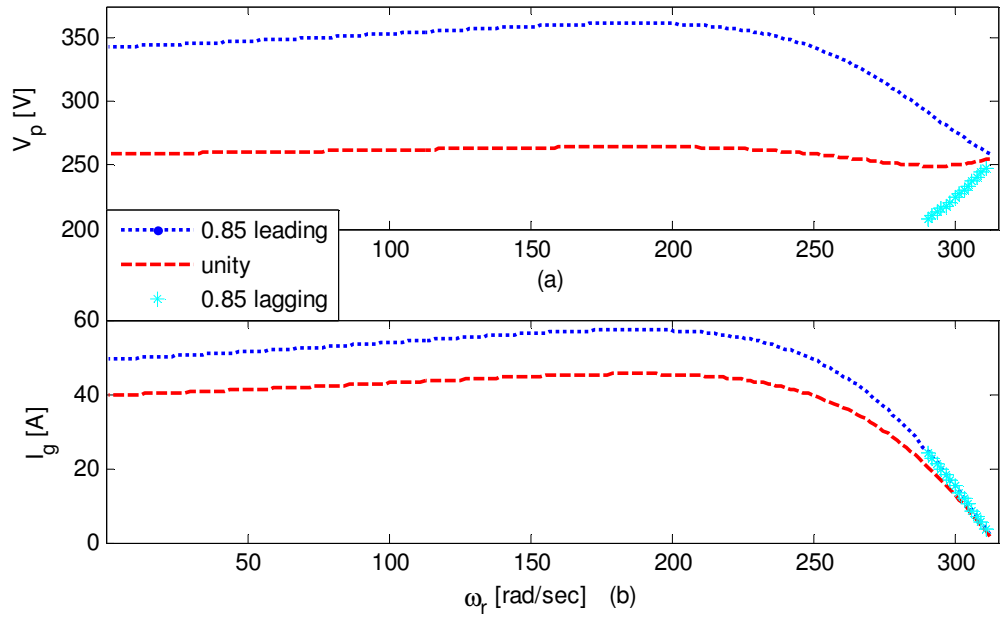


Figure 5.20 Magnitude of capacitor voltage and (b) magnitude of source current

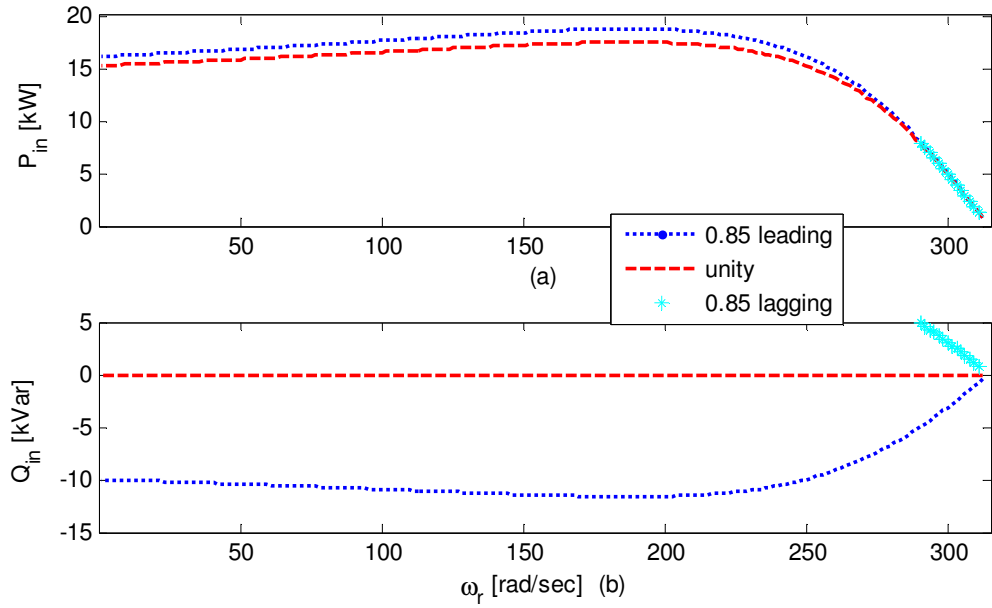


Figure 5.21 (a) Active power and (b) reactive power drawn from the source

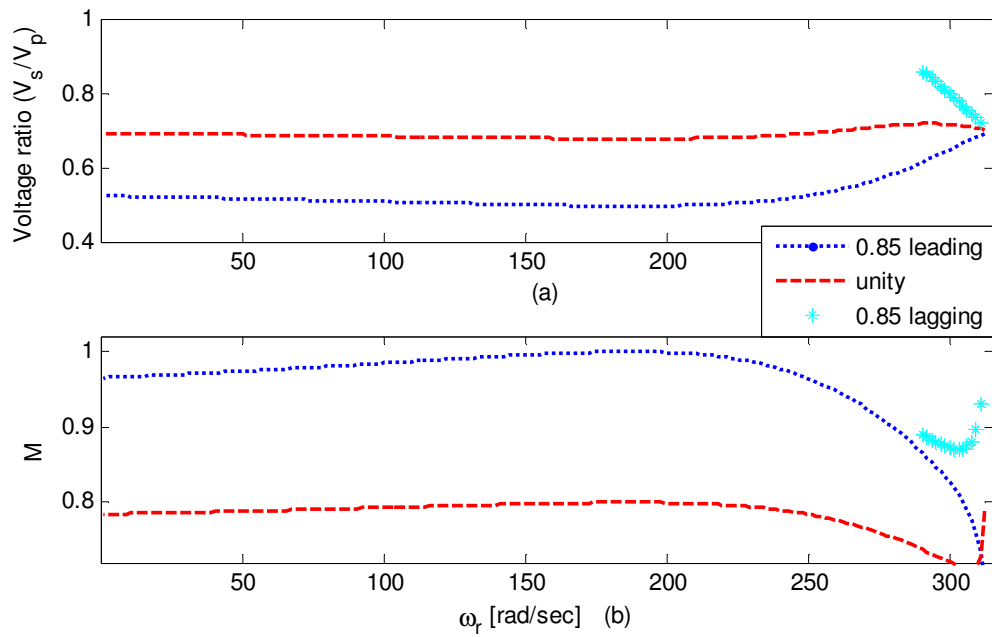


Figure 5.22 Effect of input and output power factors on (a) voltage ratio and (b) magnitude of modulation index

Table 5.1 System Parameters

RL Load parameters				
$V_s = 220V(rms)$	$f_s = 50Hz$	$R_s = 10\Omega$	$L_s = 20mH$	
Source and filter parameters				
$V_g = 380V(rms)$	$f_p = 60Hz$	$R_g = 0.5\Omega,$	$L_g = 1mH$	
$R_f = 30\Omega$	$L_f = 7.46mH$	$C_f = 10\mu F$		
Induction machine parameters				
$V_s = 220Vrms$	$f_s = 50Hz$	$R_s = 0.531\Omega$	$R_r = 0.408\Omega$	
$L_s = 87.22mH$	$L_r = 87.22mH$	$L_m = 85.7mH$	$J = 0.04kg.m^2$	$P = 4$

5.4 Conclusion

A modeling of the AC/AC matrix converter feeding an RL load is presented. A new generalized steady state analysis is developed which avoid the constraint of operating at input unity power factor. Simulation has been done to verify the theoretical analysis. Results show that with matrix converter, it is possible to control the input and output power factor independently. With a similar approach, dynamic and steady state analysis are developed for matrix converter fed induction motor system. Computer simulation results clearly show the starting transient and the dynamic response to a sudden change of the load during the steady state operation. The steady state analysis of the complete system is also laid out clearly along with the plots of the performance characteristics of the system.

CHAPTER 6

STABILITY ANALYSIS FOR A MATRIX CONVERTER FED INDUCTION MOTOR

6.1 Introduction

This chapter investigates issues related to instabilities in a matrix converter fed drive system. The presence of the input LC filter along with the direct coupling nature of the matrix converter may lead to unstable operation when the power delivered exceeds a certain limit value.

A new generalized model for stability analysis based on a small signal modeling is proposed, for matrix converter fed induction motor drive system. A small signal model of the overall drive system is also presented in synchronous reference frame. It is necessary to note that the stability analysis does not include the mechanical dynamics as a result it can also be known as electrical stability analysis. The stability of the system is evaluated by analyzing the migration of eigen values of the system, which is linearized around the operating point. The generalized steady state analysis is also presented to provide the operating points for stability analysis as well as to study the steady state performance of the system under constant Volt per Hertz (V/F) operation.

This approach considers the analysis when the drive system operates at unity as well as non-unity input power factor at the source side. With the help of this model, different factors which affect the matrix converter stability are analyzed including stator and rotor resistance variation due to motor heating and the impact of non-zero reactive power at the source side. The paper also presents a complete and a general steady state analysis in the $q-d$ synchronous reference frame when the whole drive system operates under a constant Volt/Hertz operation. Computer simulations are carried out to verify theoretical analysis on stability as well as on the steady state performance characteristics

6.2 Modeling of the Drive System

The complete modelling of the studied system shown in Figure 6.1 is presented section 5.3. The input voltage equations in a synchronous reference frame are shown as.

$$\begin{aligned} V_{qg} &= R_g I_{qg} + L_g pI_{qg} + \omega_p L_g I_{dg} + R_f (I_{qg} - I_{qf}) + V_{qp} \\ V_{dg} &= R_g I_{dg} + L_g pI_{dg} - \omega_p L_g I_{qg} + R_f (I_{dg} - I_{df}) + V_{dp} \end{aligned} \quad (6.1)$$

The voltage drop in the filter inductor can be represented as

$$\begin{aligned} L_f pI_{qf} + \omega_p L_g I_{df} &= R_f (I_{qg} - I_{qf}) \\ L_f pI_{df} - \omega_p L_g I_{qf} &= R_f (I_{dg} - I_{df}) \end{aligned} \quad (6.2)$$

The dynamic equation of filter capacitor is given by,

$$\begin{aligned} C_f pV_{qp} + \omega_p C_f V_{dp} &= I_{qg} - I_{qf} \\ C_f pV_{dp} - \omega_p C_f V_{qp} &= I_{dg} - I_{df} \end{aligned} \quad (6.3)$$

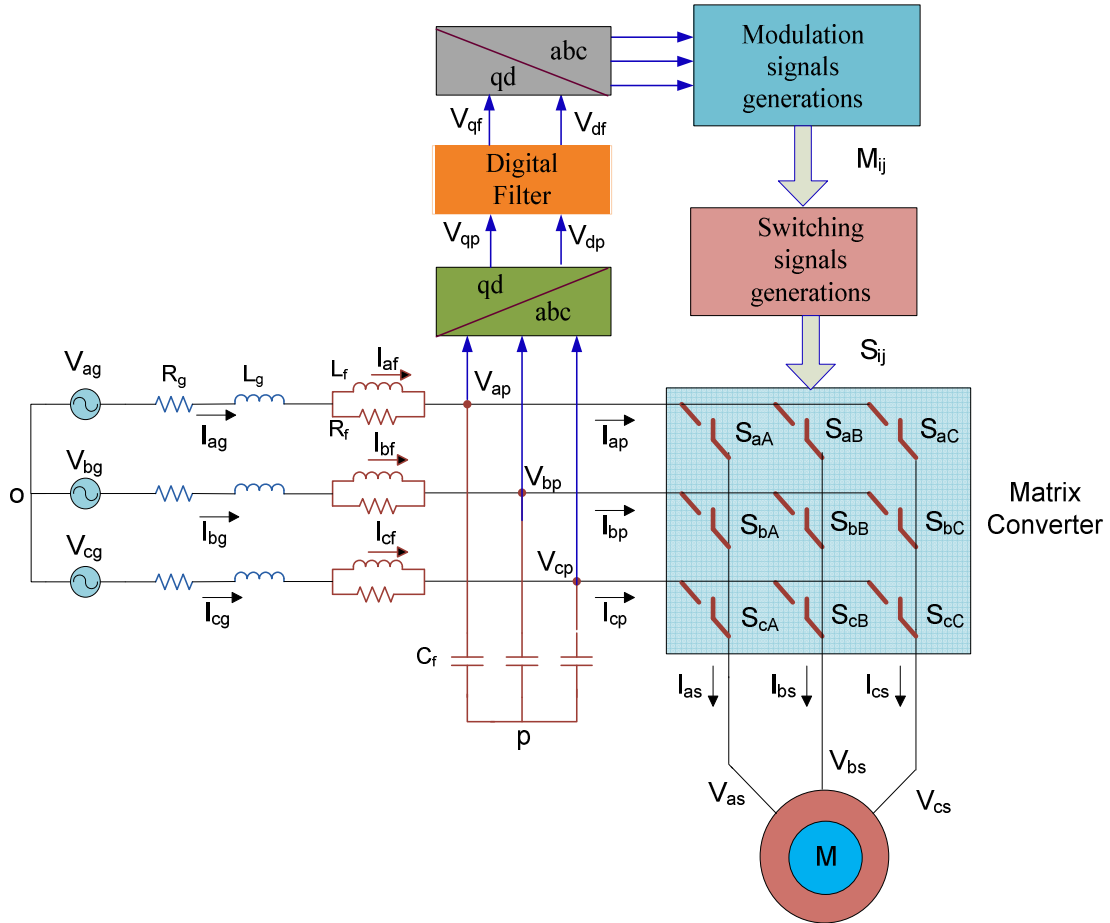


Figure 6.1 Schematic diagram of the AC/AC matrix converter fed induction motor

The q-axis and d-axis stator voltages are

$$\begin{aligned} V_{qs} &= R_s I_{qs} + p\lambda_{qs} + \omega_s \lambda_{ds} \\ V_{ds} &= R_s I_{ds} + p\lambda_{ds} - \omega_s \lambda_{qs} \end{aligned} \quad (6.4)$$

In squirrel cage type induction machine with shorted rotor, the rotor voltages are zero and expressed as

$$\begin{aligned} V_{qr} &= 0 = R_r I_{qr} + p\lambda_{qr} + (\omega_s - \omega_r)\lambda_{dr} \\ V_{dr} &= 0 = R_r I_{dr} + p\lambda_{dr} - (\omega_s - \omega_r)\lambda_{qr} \end{aligned} \quad (6.5)$$

The expressions for q-axis and d-axis stator flux linkages are given as:

$$\begin{aligned}\lambda_{qs} &= L_s I_{qs} + L_m I_{qr} \\ \lambda_{ds} &= L_s I_{ds} + L_m I_{dr}\end{aligned}\tag{6.6}$$

The q-axis and d-axis rotor flux linkages are expressed as:

$$\begin{aligned}\lambda_{qr} &= L_m I_{qs} + L_r I_{qr} \\ \lambda_{dr} &= L_m I_{ds} + L_r I_{dr}\end{aligned}\tag{6.7}$$

The electronic torque is expressed in terms of the stator flux linkage and stator current as given in (4.54). This torque is positive for motor action and negative in generating mode.

$$T_e = \frac{3P}{4} (\lambda_{ds} I_{qs} - \lambda_{qs} I_{ds})\tag{6.8}$$

The rotor speed and electromagnetic torque of a P pole machine are related by (6.9) where J is the inertia of the rotor and connected mechanical load expressed in kgm^2 . T_L is the load torque.

$$p\omega_r = \frac{P}{2J} (T_e - T_L)\tag{6.9}$$

The digital filter dynamics in synchronous reference frame are

$$\begin{aligned}pV_{qf} &= \frac{1}{\tau} (V_{qp} - V_{qf}) \\ pV_{df} &= \frac{1}{\tau} (V_{dp} - V_{df})\end{aligned}\tag{6.9}$$

The mapping between the input current and output current using the components of the modulation signals are

$$\begin{aligned}I_{qp} &= M_{qq} I_{qs} + M_{dq} I_{ds} \\ I_{dp} &= M_{qd} I_{qs} + M_{dd} I_{ds}\end{aligned}\tag{6.10}$$

Similarly, the output voltage can be expressed in terms of the input voltage and modulation signals as follow.

$$\begin{aligned} V_{qs} &= M_{qq}V_{qp} + M_{qd}V_{dp} \\ V_{ds} &= M_{dq}V_{qp} + M_{dd}V_{dp} \end{aligned} \quad (6.11)$$

Equation in (6.1) can be rearranged as follows

$$\begin{aligned} pI_{qg} &= \frac{1}{L_g} (V_{qg} - (R_g + R_f)I_{qg} + R_f I_{qf} - \omega_p L_g I_{dg} - V_{qp}) \\ pI_{dg} &= \frac{1}{L_g} (V_{dg} - (R_g + R_f)I_{dg} + R_f I_{df} + \omega_p L_g I_{qg} - V_{dp}) \end{aligned} \quad (6.12)$$

Similarly, the filter current dynamics can be expressed as

$$\begin{aligned} pI_{qf} &= \frac{1}{L_f} (R_f I_{qg} - R_f I_{qf} - \omega_p L_f I_{df}) \\ pI_{df} &= \frac{1}{L_f} (R_f I_{dg} + \omega_p L_f I_{qf} - R_f I_{df}) \end{aligned} \quad (6.13)$$

Substituting (6.10) into (6.3)

$$\begin{aligned} pV_{qp} &= \frac{1}{C_f} (I_{qg} - \omega_p C_f V_{dp} - M_{qq}I_{qs} - M_{dq}I_{ds}) \\ pV_{dp} &= \frac{1}{C_f} (I_{dg} + \omega_p C_f V_{qp} - M_{qd}I_{qs} - M_{dd}I_{ds}) \end{aligned} \quad (6.14)$$

$$\begin{aligned} pV_{qf} &= \frac{1}{\tau} (V_{qp} - V_{qf}) \\ pV_{df} &= \frac{1}{\tau} (V_{dp} - V_{df}) \end{aligned} \quad (6.15)$$

The q-axis stator and the rotor currents can be written in terms of the stator and rotor flux linkages as follows.

$$I_{qs} = \frac{r_s}{D} (L_r \lambda_{qs} - L_m \lambda_{qr}) \quad (6.16)$$

$$I_{qr} = \frac{r_r}{D} (-L_m \lambda_{qs} + L_s \lambda_{qr}) \quad (6.17)$$

where the

$$D = L_s L_r - L_m^2 \quad (6.18)$$

Similarly, the d-axis stator and the rotor currents can be written in terms of the stator and rotor flux linkages as follows.

$$I_{ds} = \frac{r_s}{D} (L_r \lambda_{ds} - L_m \lambda_{dr}) \quad (6.19)$$

$$I_{dr} = \frac{r_r}{D} (-L_m \lambda_{ds} + L_s \lambda_{dr}) \quad (6.20)$$

Substituting (6.16-6.19) into (6.4) and (6.5), the induction motor dynamics can be written in terms of only the stator flux linkages. From the stator voltage equations, the dynamics of the stator flux linkage can be written as

$$\begin{aligned} p\lambda_{qs} &= M_{qq} V_{qp} + M_{qd} V_{dp} - \frac{r_s L_r}{D} \lambda_{qs} + \frac{r_s L_m}{D} \lambda_{qr} - \omega_e \lambda_{ds} \\ p\lambda_{ds} &= M_{dq} V_{qp} + M_{dd} V_{dp} - \frac{r_s L_r}{D} \lambda_{ds} + \frac{r_s L_m}{D} \lambda_{dr} + \omega_e \lambda_{qs} \end{aligned} \quad (6.21)$$

Similarly, the rotor flux dynamics can be represented as

$$\begin{aligned} p\lambda_{qr} &= \frac{r_r L_m}{D} \lambda_{qs} - \frac{r_r L_s}{D} \lambda_{qr} - \omega_{so} \lambda_{dr} \\ p\lambda_{dr} &= \frac{r_r L_m}{D} \lambda_{ds} - \frac{r_r L_s}{D} \lambda_{dr} + \omega_{so} \lambda_{qr} \end{aligned} \quad (6.22)$$

6.3 Small Signal Analysis

This section discusses the stability of the model given in Figure 6.1. The small signal analysis of the system is done to determine the stability limit under constant volts per hertz (V/f) operation. To determine the small signal model of the system, it should be first linearized around the operating point. Therefore each state are defined by the operating points

$$X = X_o + \Delta X \quad (6.23)$$

And the inputs and the disturbances are

$$U = U_o + \Delta U \quad (6.48)$$

where

$$U = \begin{bmatrix} M_{qq} \\ M_{qd} \\ M_{dq} \\ M_{dd} \end{bmatrix} \quad U_o = \begin{bmatrix} M_{qqo} \\ M_{qdo} \\ M_{dqo} \\ M_{ddo} \end{bmatrix} \quad \Delta U = \begin{bmatrix} \Delta M_{qq} \\ \Delta M_{qd} \\ \Delta M_{dq} \\ \Delta M_{dd} \end{bmatrix}$$

$$X = [I_{qg} \quad I_{dg} \quad I_{qf} \quad I_{df} \quad V_{qp} \quad V_{dp} \quad V_{qf} \quad V_{df} \quad \lambda_{qs} \quad \lambda_{ds} \quad \lambda_{qr} \quad \lambda_{dr}]^T$$

$$X_o = [I_{qgo} \quad I_{dgo} \quad I_{qfo} \quad I_{dfo} \quad V_{qpo} \quad V_{dpo} \quad V_{qfo} \quad V_{dfo} \quad \lambda_{qso} \quad \lambda_{dso} \quad \lambda_{qro} \quad \lambda_{dro}]^T$$

$$\Delta X = [\Delta I_{qg} \quad \Delta I_{dg} \quad \Delta I_{qf} \quad \Delta I_{df} \quad \Delta V_{qp} \quad \Delta V_{dp} \quad \Delta V_{qf} \quad \Delta V_{df} \quad \Delta \lambda_{qs} \quad \Delta \lambda_{ds} \quad \Delta \lambda_{qr} \quad \Delta \lambda_{dr}]^T$$

The linearization of the system dynamics around steady state operating point leads to the following small signal model of the system.

$$p\Delta I_{qg} = \frac{1}{L_g} (\Delta V_{qg} - (R_g + R_f)\Delta I_{qg} + R_f\Delta I_{qf} - \omega_p L_g \Delta I_{dg} - \Delta V_{qp}) \quad (6.24)$$

$$p\Delta I_{dg} = \frac{1}{L_g} (\Delta V_{dg} - (R_g + R_f)\Delta I_{dg} + R_f\Delta I_{df} + \omega_p L_g \Delta I_{qg} - \Delta V_{dp}) \quad (6.25)$$

$$p\Delta I_{qf} = \frac{1}{L_f} (R_f\Delta I_{qg} - R_f\Delta I_{qf} - \omega_p L_f \Delta I_{df}) \quad (6.26)$$

$$p\Delta I_{df} = \frac{1}{L_f} (R_f\Delta I_{dg} + \omega_p L_f \Delta I_{qf} - R_f\Delta I_{df}) \quad (6.27)$$

$$p\Delta V_{qp} = \frac{1}{C_f} (\Delta I_{qg} - \omega_p C_f \Delta V_{dp} - M_{qqo}\Delta I_{qs} - M_{dqo}\Delta I_{ds} - I_{qso}\Delta M_{qq} - I_{dso}\Delta M_{dq}) \quad (6.28)$$

$$p\Delta V_{dp} = \frac{1}{C_f} (\Delta I_{dg} + \omega_p C_f \Delta V_{qp} - M_{qdo}\Delta I_{qs} - M_{ddo}\Delta I_{ds} - I_{qso}\Delta M_{qd} - I_{dso}\Delta M_{dd}) \quad (6.29)$$

$$p\Delta V_{qf} = \frac{1}{\tau} (\Delta V_{qp} - \Delta V_{qf}) \quad (6.30)$$

$$p\Delta V_{df} = \frac{1}{\tau} (\Delta V_{dp} - \Delta V_{df}) \quad (6.31)$$

$$p\Delta \lambda_{qs} = M_{qq}\Delta V_{qp} + M_{qd}\Delta V_{dp} + V_{qp0}\Delta M_{qq} + V_{dp0}\Delta M_{qd} - \frac{r_s L_r}{D} \Delta \lambda_{qs} + \frac{r_s L_m}{D} \Delta \lambda_{qr} - \omega_e \Delta \lambda_{ds} \quad (6.32)$$

$$p\Delta\lambda_{ds} = M_{dq}\Delta V_{qp} + M_{dd}\Delta V_{dp} + V_{qpo}\Delta M_{dq} + V_{dpo}\Delta M_{dd} - \frac{r_s L_r}{D}\Delta\lambda_{ds} + \frac{r_s L_m}{D}\Delta\lambda_{dr} + \omega_e\Delta\lambda_{qs} \quad (6.33)$$

$$p\Delta\lambda_{qr} = \frac{r_r L_m}{D}\Delta\lambda_{qs} - \frac{r_r L_s}{D}\Delta\lambda_{qr} - \omega_{so}\Delta\lambda_{dr} \quad (6.34)$$

$$p\Delta\lambda_{dr} = \frac{r_r L_m}{D}\Delta\lambda_{ds} - \frac{r_r L_s}{D}\Delta\lambda_{dr} + \omega_{so}\Delta\lambda_{qr} \quad (6.35)$$

By resolving (6.24)-(6.35), the state equations is given as

$$pX = AX + BU$$

In the above state space representation, the inputs are the modulation signals. Since the operating conditions are computed for a specified stator voltage of the induction motor, it is possible to change the inputs from the modulation signals to the stator voltage. Define the four components of the components of the modulation signals as follows. It is necessary to note that these modulation signals depend on the filtered capacitor voltage and output voltage.

$$M_{qq} = \frac{V_{qs}V_{qf}}{V_{qf}^2 + V_{df}^2} \quad (6.36)$$

$$M_{qd} = \frac{V_{qs}V_{df}}{V_{qf}^2 + V_{df}^2} \quad (6.37)$$

$$M_{dq} = \frac{V_{ds}V_{qf}}{V_{qf}^2 + V_{df}^2} \quad (6.38)$$

$$M_{dd} = \frac{V_{ds}V_{df}}{V_{qf}^2 + V_{df}^2} \quad (6.39)$$

Applying small signal analysis on (6.36)-(6.39), the operating point modulation signals can separately represented in terms of the operating point filter input capacitor voltage and output voltage.

$$M_{qqo} = \frac{V_{qso} V_{qfo}}{V_{fo}^2} \quad (6.40)$$

$$M_{qdo} = \frac{V_{qso} V_{dfo}}{V_{fo}^2} \quad (6.41)$$

$$M_{dqo} = \frac{V_{dso} V_{qfo}}{V_{fo}^2} \quad (6.42)$$

$$M_{ddo} = \frac{V_{dso} V_{dfo}}{V_{fo}^2} \quad (6.43)$$

At steady state, the input capacitor voltage before and after low pass filter is the same. Substituting (6.44)-(6.47) into (6.28), (6.29), (6.32) and (6.33), the system characteristic matrix is given in (6.50).

$$\Delta M_{qq} = \frac{V_{qso} (V_{dfo}^2 - V_{qfo}^2)}{(V_{qfo}^2 + V_{dfo}^2)^2} \Delta V_{qf} - \frac{2V_{qso} V_{qfo} V_{dfo}}{(V_{qfo}^2 + V_{dfo}^2)^2} \Delta V_{df} + \frac{V_{qfo}}{V_{qfo}^2 + V_{dfo}^2} \Delta V_{qs} \quad (6.44)$$

$$\Delta M_{qd} = -\frac{2\mathcal{W}_{qso} V_{qfo} V_{dfo}}{(V_{qfo}^2 + V_{dfo}^2)^2} \Delta V_{qf} + \frac{\mathcal{W}_{qso} (V_{qfo}^2 - V_{dfo}^2)}{(V_{qfo}^2 + V_{dfo}^2)^2} \Delta V_{df} + \frac{\mathcal{W}_{dfo}}{V_{qfo}^2 + V_{dfo}^2} \Delta V_{qs} \quad (6.45)$$

$$\Delta M_{dq} = \frac{\mathcal{W}_{dso} (V_{dfo}^2 - V_{qfo}^2)}{(V_{qfo}^2 + V_{dfo}^2)^2} \Delta V_{qf} - \frac{2\mathcal{W}_{dso} V_{qfo} V_{dfo}}{(V_{qfo}^2 + V_{dfo}^2)^2} \Delta V_{df} + \frac{\mathcal{W}_{qfo}}{V_{qfo}^2 + V_{dfo}^2} \Delta V_{ds} \quad (6.46)$$

$$\Delta M_{dd} = -\frac{2\mathcal{W}_{dso} V_{qfo} V_{dfo}}{(V_{qfo}^2 + V_{dfo}^2)^2} \Delta V_{qf} + \frac{\mathcal{W}_{dso} (V_{qfo}^2 - V_{dfo}^2)}{(V_{qfo}^2 + V_{dfo}^2)^2} \Delta V_{df} + \frac{\mathcal{W}_{dfo}}{V_{qfo}^2 + V_{dfo}^2} \Delta V_{ds} \quad (6.47)$$

$$A = \begin{bmatrix} -\frac{R_g + R_f}{L_g} & -\omega_p & \frac{R_f}{L_g} & 0 & -\frac{1}{L_g} & 0 & 0 & 0 & 0 & 0 & 0 & 0 \\ \omega_p & -\frac{R_g + R_f}{L_g} & 0 & \frac{R_f}{L_g} & 0 & -\frac{1}{L_g} & 0 & 0 & 0 & 0 & 0 & 0 \\ \frac{R_f}{L_f} & 0 & -\frac{R_f}{L_f} & -\omega_p & 0 & 0 & 0 & 0 & 0 & 0 & 0 & 0 \\ 0 & \frac{R_f}{L_f} & \omega_p & -\frac{R_f}{L_f} & 0 & 0 & 0 & 0 & 0 & 0 & 0 & 0 \\ \frac{1}{C_f} & 0 & 0 & 0 & 0 & -\omega_p & y_1 & y_2 & \frac{x_1}{C_f} & \frac{x_2}{C_f} & 0 & 0 \\ 0 & \frac{1}{C_f} & 0 & 0 & \omega_p & 0 & y_3 & y_4 & \frac{x_3}{C_f} & \frac{x_4}{C_f} & 0 & 0 \\ 0 & 0 & 0 & 0 & \frac{1}{\tau} & 0 & -\frac{1}{\tau} & 0 & 0 & 0 & 0 & 0 \\ 0 & 0 & 0 & 0 & 0 & \frac{1}{\tau} & 0 & -\frac{1}{\tau} & 0 & 0 & 0 & 0 \\ 0 & 0 & 0 & 0 & -x_1 & -x_2 & x_1 & x_2 & -\frac{R_s L_r}{D} & -\omega_e & \frac{R_s L_m}{D} & 0 \\ 0 & 0 & 0 & 0 & -x_3 & -x_4 & x_3 & x_4 & \omega_e & -\frac{R_s L_r}{D} & 0 & \frac{R_s L_m}{D} \\ 0 & 0 & 0 & 0 & 0 & 0 & 0 & 0 & \frac{R_r L_m}{D} & 0 & -\frac{R_r L_s}{D} & -\omega_{so} \\ 0 & 0 & 0 & 0 & 0 & 0 & 0 & 0 & 0 & \frac{R_r L_m}{D} & \omega_{so} & -\frac{R_r L_s}{D} \end{bmatrix}$$

(6.50)

The constants represented in the matrix are computed at the steady state operation.

$$x_1 = -\frac{V_{qso} V_{qpo}}{V_{po}^2}$$

$$x_2 = -\frac{V_{qso} V_{dpo}}{V_{po}^2}$$

$$x_3 = -\frac{V_{dso} V_{qpo}}{V_{po}^2}$$

$$x_4 = -\frac{V_{dso} V_{dpo}}{V_{po}^2}$$

$$y_1 = -y_4 = \frac{1}{C_f} \frac{(V_{qpo}^2 - V_{dpo}^2)k}{V_{po}^4}$$

$$y_2 = y_3 = \frac{1}{C_f} \frac{2V_{qpo} V_{dpo} k}{V_{po}^4}$$

$$k = V_{qso} I_{qso} + V_{dso} I_{dso}$$

The eigen-values can be found by evaluating the determinant of $|SI - A| = 0$, where the matrix A is given in (6.50). There are 12 eigen values in which 10 of them always have negative real parts regardless of the operating points; therefore, the rest two identical dominant eigen values are used for determining stability limits. The graphs shown in this section are obtained by varying the output and slip frequencies and collecting the operating points which give zero real part of the dominant eigen values. It is necessary to note that this eigen-value depends on the operating points. In [40], it is assumed that the initial angles of the capacitor and reference voltages are zero, but in this analysis there is no assumption made so that it is possible to study the effect non-zero reactive power at the source on the stability of the system.

6.4 Simulation Results and Discussions

A matrix converter-induction motor system with parameters given in Table I, are considered and the results of the stability analysis are given in Figure 6.2 to Figure 6.6 in which the regions above the curves are the instability regions. As seen in Figure 6.2, a significant improvement can be achieved using a low pass filter to the input capacitor voltage. The influences of each factor on the stability are analyzed by adjusting only one of them and keeping the other factors constant. As seen in Figure 6.3, in some regions of load there is a limit on the maximum allowable output frequency to keep the system stable. The figure also demonstrates that it is possible to improve the output frequency limit by increasing the filter time constant, though the higher the time constant, the slower the system response would be. The effect of the damping resistance is also

observed in Figure 6.4 Choosing a lower resistance value draws the high frequency components of the input current and hence improves the stability of the system. However, if this resistance is too small, the power loss in the damping resistance becomes very significant at a low frequency.

The impact of the stator and rotor resistance variation on drive stability analysis is also considered in this paper. For demonstration, the rotor resistance is varied by 40% and 80% while the stator resistance increases by 20% and 40% since the rotor heating affects the value of rotor resistance more than the value of stator resistance. Hence $R_{s2} = 1.2R_s$, $R_{s3} = 1.4R_s$, $R_{r2} = 1.4R_r$, and $R_{r3} = 1.8R_r$ are selected for the analysis. From the result seen in Figure 6.5, these resistance variations expand the stability margins. It was noted that the rotor resistance variation is crucial in the design of high performance induction motor control algorithms where the flux observers require the exact knowledge of the rotor resistance [74]. However, regarding the stability of the system, it is not a crucial issue. In Figure 6.6, the impact of non-zero reactive power on the matrix converter stability is given. The result clearly shows that the system has better stability region when the matrix converter operates with a leading power factor than with a lagging power factor under the given input filter parameters. Therefore, in applications where the matrix converter is used as a reactive power compensator, the stability region is improved. However, when the converter operates at source lagging power, the drive system becomes more stable with increasing in power factor.

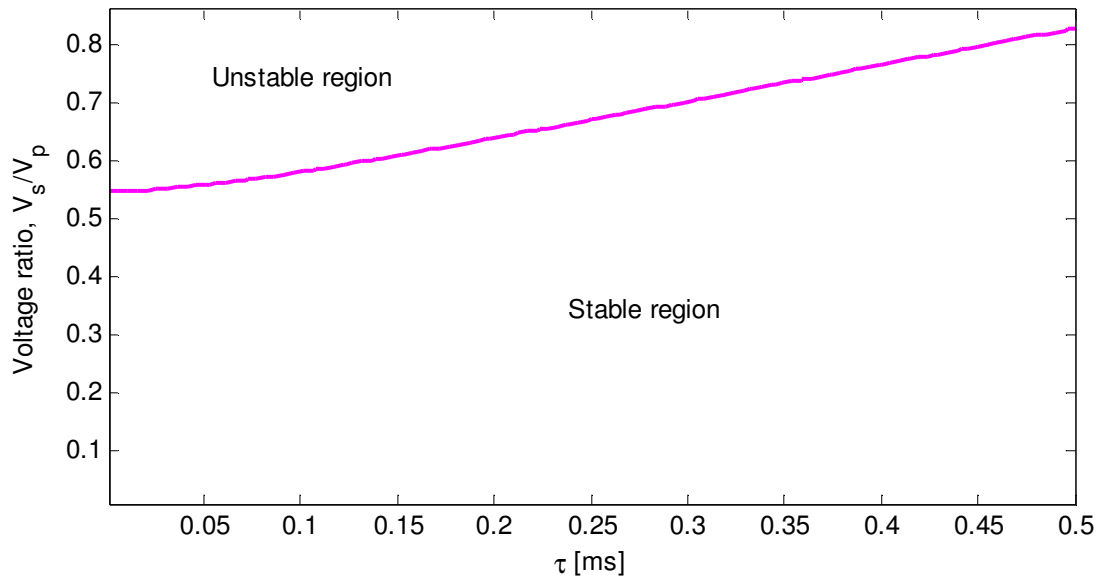


Figure 6.2 Stability limit of matrix converter gain against filter time constant

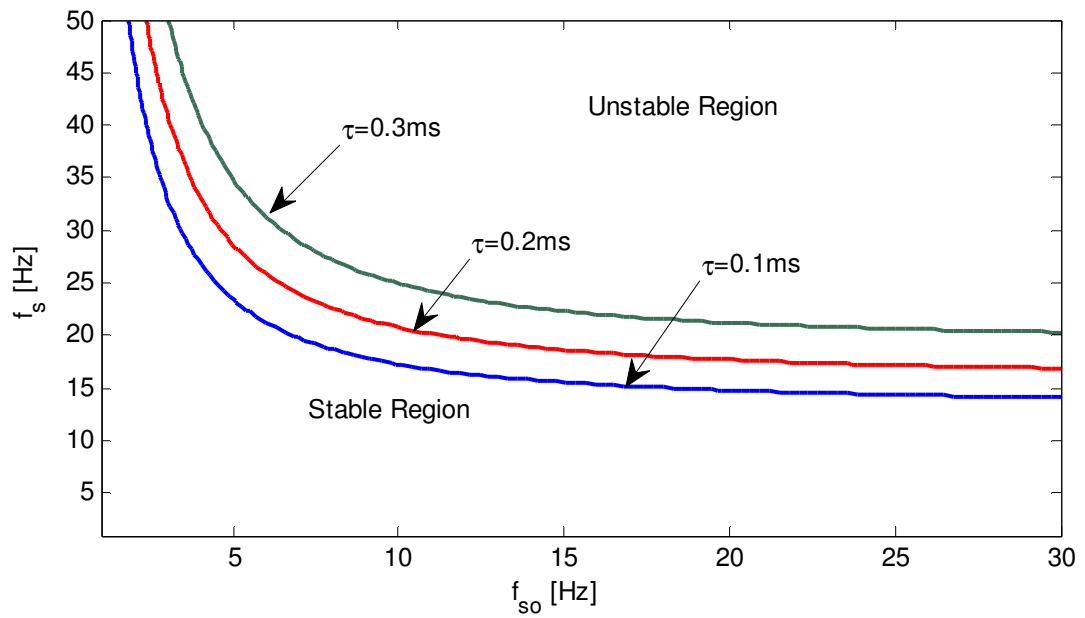


Figure 6.3 Matrix converter stability limit for varying Filter time constant

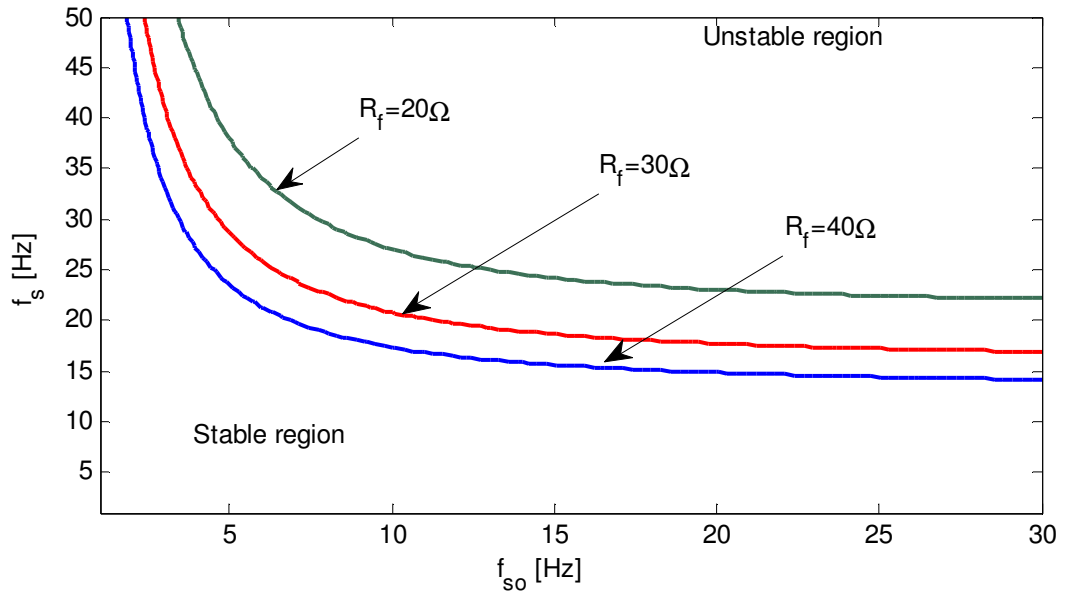


Figure 6.4 Stability limit of the matrix converter for varying damping resistance

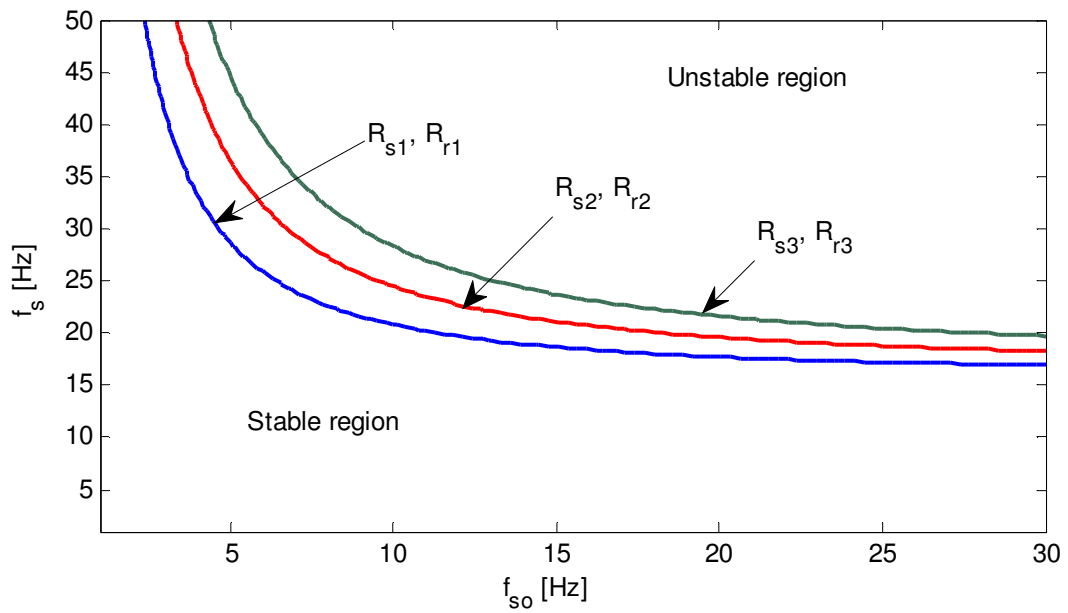


Figure 6.5 The impact of Stator and rotor resistance on the stability of the system

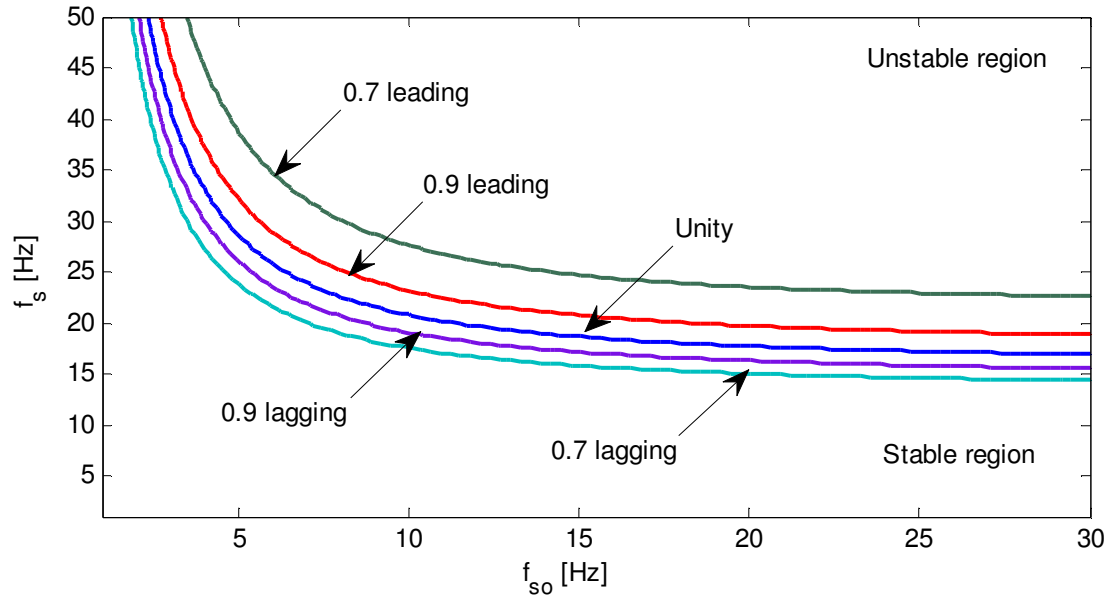


Figure 6.6 The impact of power factor on the stability of the system

The verification of the region of instability is done by a computer simulation using motor and filter parameters given in Table I. The motor starts at no load so as to observe the starting transient and then a $15 Nm$ load torque is applied after it reaches the steady state at $0.5sec$ to show the electrical dynamic response of the system which is not included in the figure. At starting, the motor experiences high electromagnetic torque with rising rotor speed until they both reach their steady state values at $0.5sec$ as seen in Figure 6.7. At this point the system operating at $50Hz$ output frequency and $1.5 Hz$ slip frequency which is in the stable region as shown in Figure 6.3 when $\tau = 2 m sec$. Then the slip frequency is increased to $7Hz$ to operate in the unstable region after $0.8 sec$. It is necessary to note that both these points are taken in a linear region of torque-speed curve of the motor, P_1 and P_2 as seen Figure 6.10.

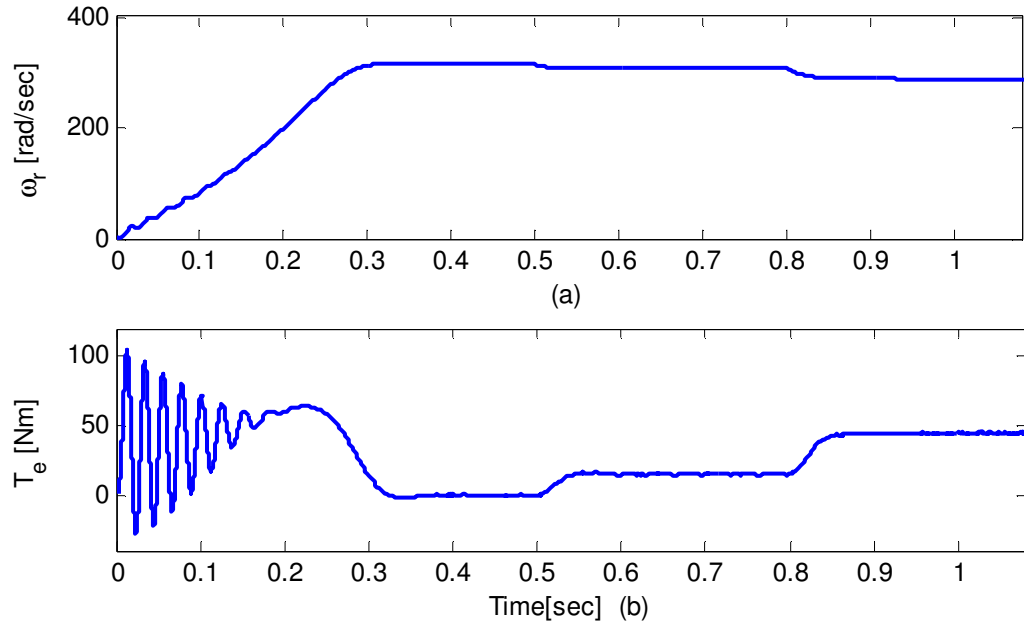


Figure 6.7 (a) Rotor speed and (b) electromagnetic torque

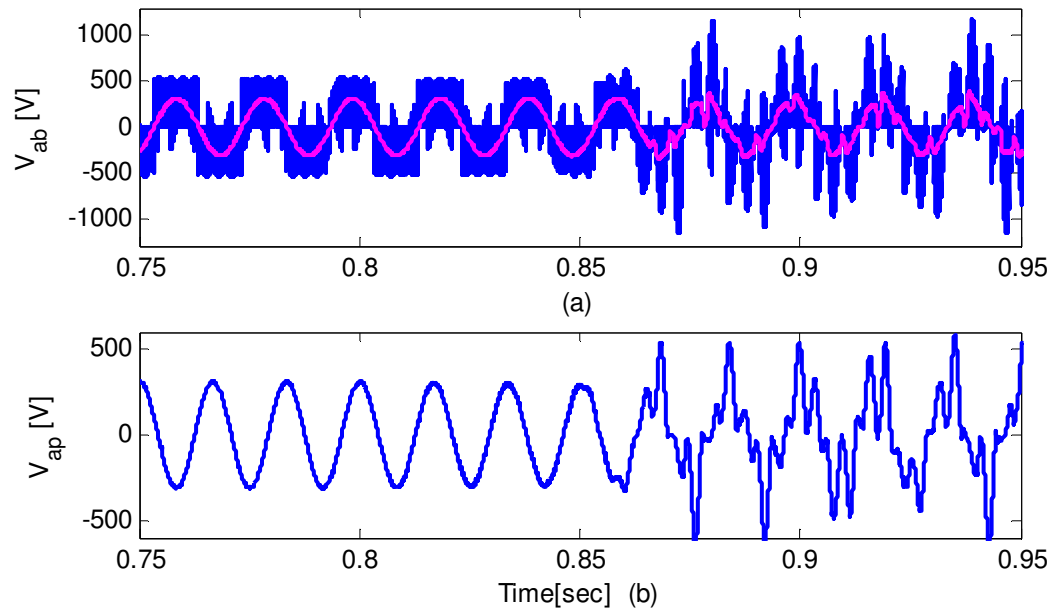


Figure 6.8 Output line to line voltage and (b) input capacitor phase voltage

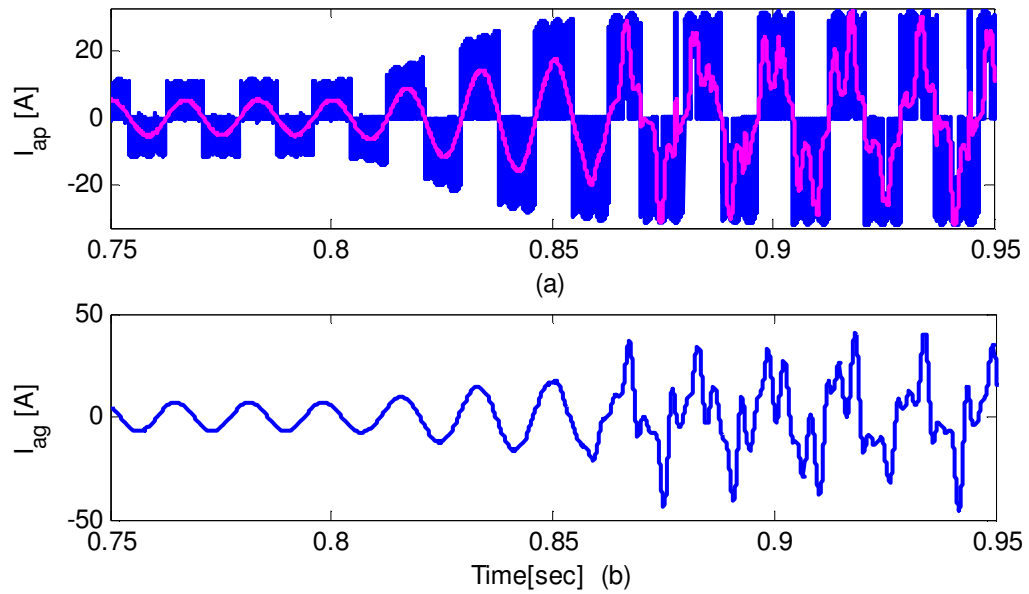


Figure 6.9 MC input phase current and (b) source phase current

6.5 Steady State Operating Conditions

The steady state performance characteristic of the drive system is done to provide the operating points for the electrical stability of the system as well as to study the performance characteristics of the drive under constant Volt/Hertz operation. The steady-state operating points of the system are determined from the system dynamic equations. For the analysis, the input side reference frame angle is aligned to the q-axis of the source voltage, such that $V_{dg} = 0$. This model is general which can be used either when the source draws unity power factor or non-zero reactive power by giving proper value of the power factor, pf . These operating points are evaluated first by calculating the M_{dd} from (6.51) and all other variables can be found consecutively from (6.52) to (6.62).

$$aM_{ddo}^2 + bM_{ddo} + c = 0 \quad (6.51)$$

$$M_{dqo} = M_x - g_1 g_2 M_{ddo} \quad (6.52)$$

$$M_{qdo} = M_{ddo} \frac{V_{qso}}{V_{dso}} \quad (6.53)$$

$$M_{qqo} = \frac{M_{dqo}}{M_{ddo}} M_{qdo} \quad (6.54)$$

$$V_{qpo} = k_1 V_{qg} + g_1 (M_{qdo} I_{qso} + M_{ddo} I_{dso}) \quad (6.55)$$

$$I_{qgo} = \beta_3 \beta_4 (V_{qg} - V_{qpo}) \quad (6.56)$$

$$I_{dgo} = \rho I_{qgo} \quad (6.57)$$

$$V_{dpo} = \beta_4 (V_{qg} - V_{qpo}) \quad (6.58)$$

$$I_{qfo} = \beta_1 I_{qgo} \quad (6.59)$$

$$I_{dfo} = \beta_2 I_{qgo} \quad (6.60)$$

$$I_{qso} = m_1 V_{qso} - m_2 V_{dso} \quad (6.61)$$

$$I_{dso} = m_2 V_{qso} + m_1 V_{dso} \quad (6.62)$$

The constants used in the above expressions are given below:

$$a = g_1 (g_1 g_2 + \beta_4) (V_{qs} I_{qs} + V_{ds} I_{ds})$$

$$b = (k_1 (g_1 g_2 + \beta_4 + k_1 g_1 g_2) - (\beta_4 + g_1 g_2)) V_{qg} V_{ds}$$

$$c = V_{ds}^2 - k_1 M_x V_{ds} V_{qg}$$

$$M_x = \frac{g_2 V_{qg} V_{ds} (1 - k_1)}{V_{qs} I_{qs} + V_{ds} I_{ds}}$$

$$g_1 = -\frac{1}{\rho \beta_3 \beta_4 - \omega_p C_f}$$

$$g_2 = \beta_3 \beta_4 - \omega_p C_f \beta_4$$

$$\beta_1 = \frac{R_f - \rho \omega_p L_f}{R_f^2 + \omega_p^2 L_f^2} R_f$$

$$\beta_2 = \frac{\rho R_f + \omega_p L_f}{R_f^2 + \omega_p^2 L_f^2} R_f$$

$$\beta_3 = \frac{1}{(\omega_p L_g + R_f \beta_2 - \rho(R_g + R_f))}$$

$$\beta_4 = \frac{1}{\beta_3(R_g + R_f(1 - \beta_1)) + \rho \omega_p L_g}$$

$$m_1 = \frac{1}{\Delta} (R_s R_r^2 + R_s s^2 \omega_s^2 L_r^2 + s \omega_s^2 L_m^2 R_r) \quad m_2 = \frac{\omega_s}{\Delta} (L_s R_r^2 + \omega_s^2 L_s s^2 L_r^2 - s^2 \omega_s^2 L_m^2 L_r)$$

$$k_1 = \frac{\rho \beta_3 \beta_4}{\rho \beta_3 \beta_4 - \omega_p C_f}$$

$$\rho = \tan(\cos^{-1}(pf))$$

6.6 Simulation Result for Volt/Hz Control

The result of the steady state performance is demonstrated in Figure 6.10 to Figure 6.13 under a unity power factor operation. These results also compared with simulation results given in Figure 6.7. Figure 6.10 shows how the torque speed curves of the induction motor vary with the stator frequencies under constant volt/Hertz operation. These results also validate the simulation results given in Figure 6.7 where the angular speed goes to 307 rad/sec after applying 15 Nm during stable operation at P_1 . Further increasing the load to 45 Nm reduces the rotor speed to 288 rad/sec at P_2 which leads to a

drive system oscillation. It is clearly seen that these two operating points are in the linear torque region. Since the stator voltage is not constant resulting in a variable capacitor voltage, the source current will also corresponding vary as shown in Figure 6.11. This figure also verified the result in Fig 5c where the source current is about 13A at 307rad/sec. With the constant voltage source, the gain is directly proportional to the output frequency with V/f control as seen in Figure 6.12. As verified in Figure 6.13, when the source draws a unity power factor current, it is certain that the power factor at the input of the converter will no longer be unity due to the reactive power generated in the filter circuit. Therefore these results verify that under unity power factor operation at the source side it is not correct to make the assumption on the phase angle of the capacitor voltage to be zero.

Table 6.1 System parameters used in the stability study

Squirrel cage induction machine parameters		
$V_s = 220V(rms)$	$f_s = 50Hz,$	$R_s = 0.531\Omega,$
$R_r = 0.408\Omega,$	$L_s = 87.22mH,$	$L_r = 87.22mH,$
$L_m = 84.7mH,$	$J = 0.04kg.m^2,$	$P = 4$
Source and filter parameters		
$V_g = 380V(rms)$	$f_p = 60Hz,$	
$R_g = 0.5\Omega,$	$R_f = 30\Omega,$	
$L_g = 1mH,$	$L_f = 7.46mH,$	$C_f = 10\mu F$

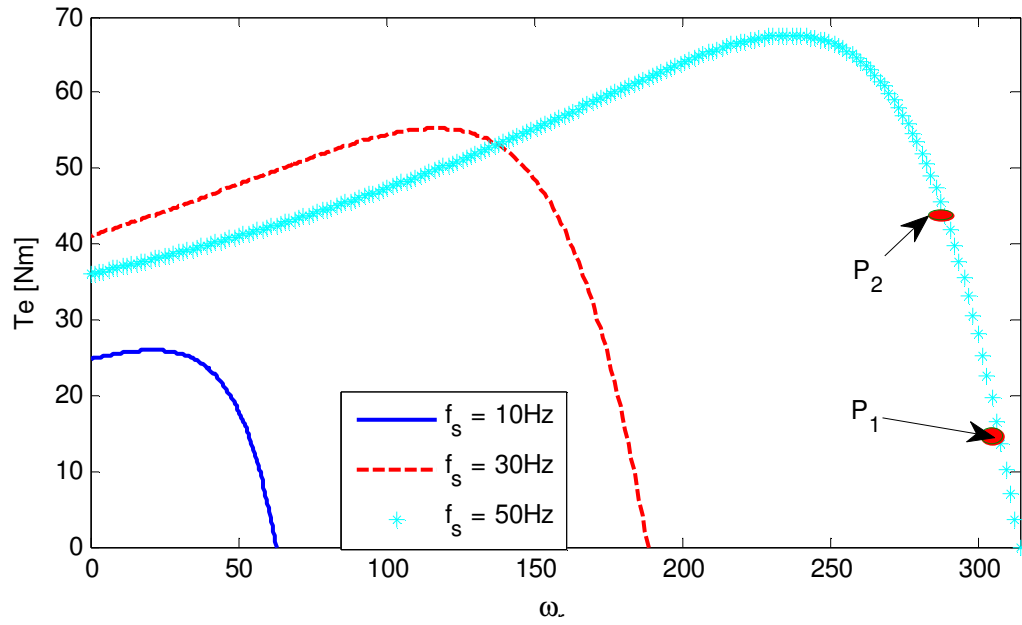


Figure 6.10 Induction motor Electromagnetic torque

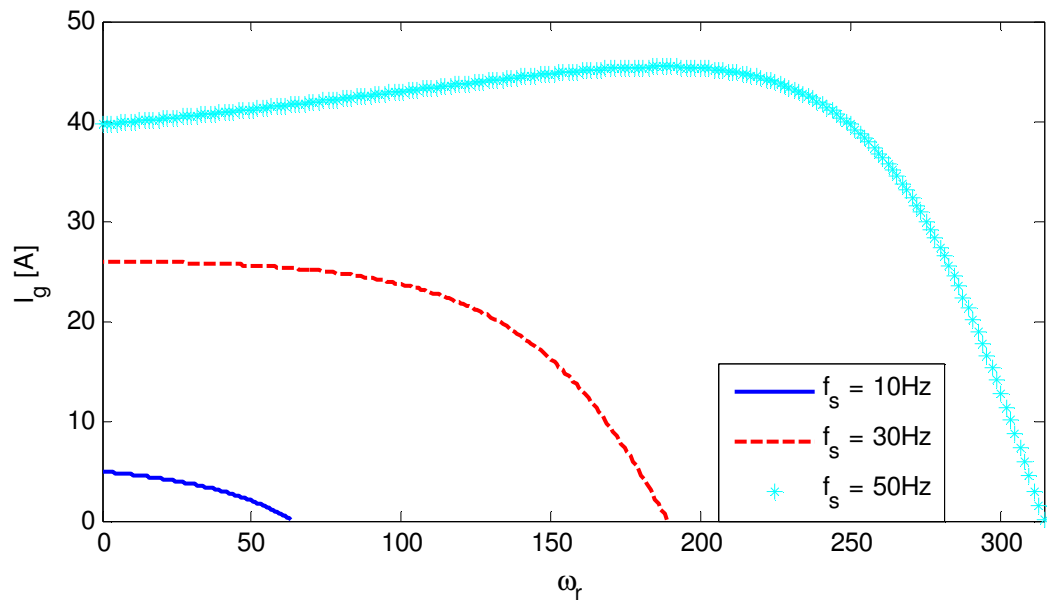


Figure 6.11 Magnitude of source current

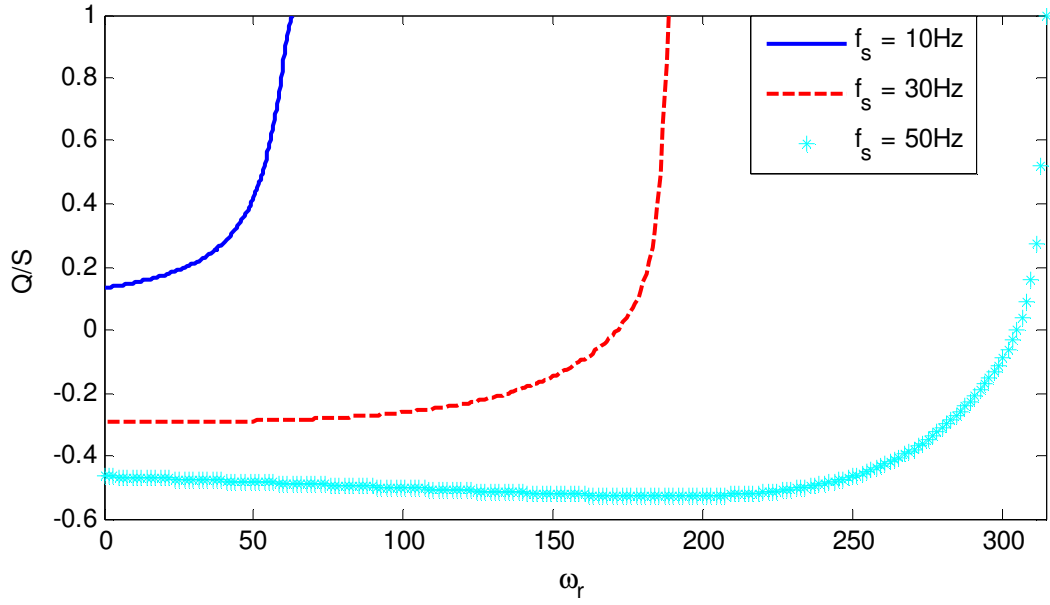


Figure 6.12 Converter voltage transfer ratio against rotor speed.

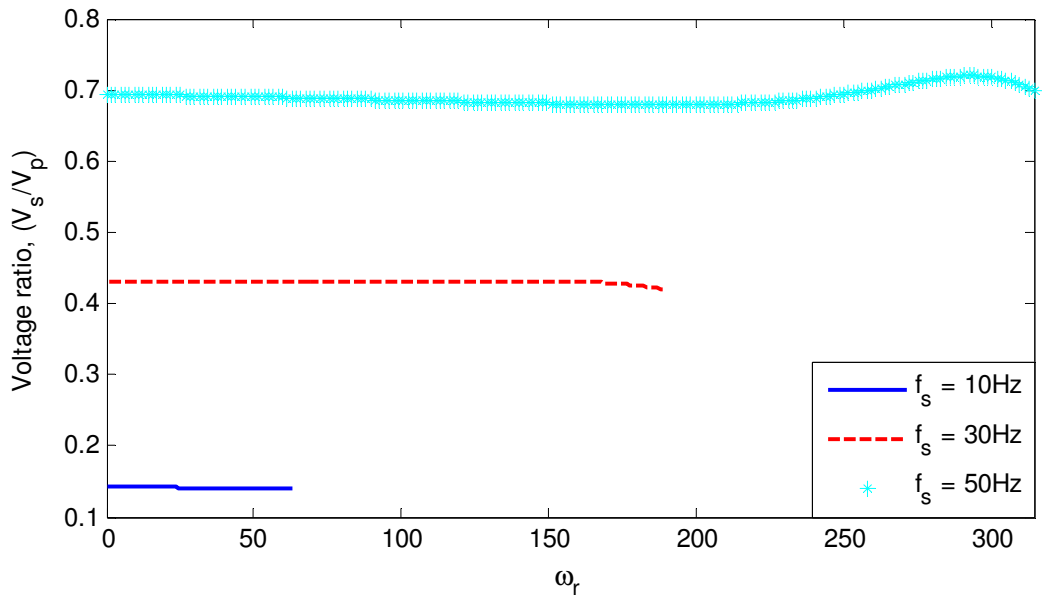


Figure 6.13 Ratio of reactive power to the apparent power at the input of the converter

6.7 Conclusion

A small signal electrical stability study of the AC/AC matrix converter fed induction motor drive system is presented. This is determined from the small signal analysis of the whole drive system operating under constant Volts/ Hertz operation. By analyzing the real values of the dominant eigen values, the limit for stable operation has been determined. It is also noticed that this stability limit is affected by different system parameters including the input filter time constant and damping resistance. This work also investigates the influence of reactive power exchange between the source and the converter on the system stability in which the system is more stable when it operates with a leading rather than a lagging power factor. The impact of stator and rotor resistance variations on the converter stability is also studied and the results show that these variations expand the stability regions. The proposed model clearly shows, through computer simulation results the region of stable and unstable operations. The paper also presents a generalized steady state model of the drive system which can be used for a unity as well as non-unity power factor operations at the source. The analysis was validated with computer simulation results which clearly show the performance characteristics of the drive under unity input power factor operation. Clear comparison between simulation and steady state results are presented.

CHAPTER 7

VECTOR CONTROL OF MATRIX CONVERTER FED

INDUCTION MACHINE

7.1 Introduction

In this chapter, the indirect rotor field oriented control (FOC) for matrix converter fed induction machine is presented to realize the high performance control of the drive. The control scheme proposed in this work also includes unity power factor control in the source side. Induction motor drive fed by matrix converter is superior to the conventional inverter based because of the lack of bulky direct current (dc)-link capacitors with limited lifetime, bidirectional power flow capability, sinusoidal input/output currents, and adjustable input power factor [67]. Besides, a matrix converter provides more degree of freedom than the conventional voltage source inverter. Therefore, it is possible to control additional variables such as reactive power in the input side.

The chapter is organized in different sections; the complete formulation of the proposed control scheme in synchronous reference frame is presented in the first section. An input-output feedback linearization is given to transform a nonlinear system into a (fully or partially) linear system so as to use the well-known and powerful linear design techniques to complete the control design. The control block consists of the rotor speed, rotor flux and unity input power factor controllers. Besides, the q-axis component of the

rotor flux is controlled to assure rotor flux orientation. These involve separate control of q-axis and d-axis stator currents, source current and input capacitor voltage.

The stator flux estimation which is later used to estimate the rotor fluxes is presented. The control scheme involving nine controllers including the flux estimation is simulated using Matlab/Simulink considering different speed trajectories and load variation. Results verify the robustness of the proposed controllers. Finally the chapter is summarized with a concluding remark.

7.2 Field Oriented Control for Matrix Converter Fed Induction Motor with Unity Input Power Factor Control

The control scheme presented in the subsequent sections is categorized into two, the FOC of the induction machine and input power factor control in the source side of the matrix converter. In vector control, the rotor and stator fluxes have q-axis and d-axis components like the voltage and currents. However, in rotor field orientation control, the rotor flux linkage is aligned in the synchronous reference frame. As result, the rotor flux is represented by a scalar instead of a phasor.

7.2.1 Indirect Field Oriented Control

This section presents the formulation of vector control scheme for the induction motor.

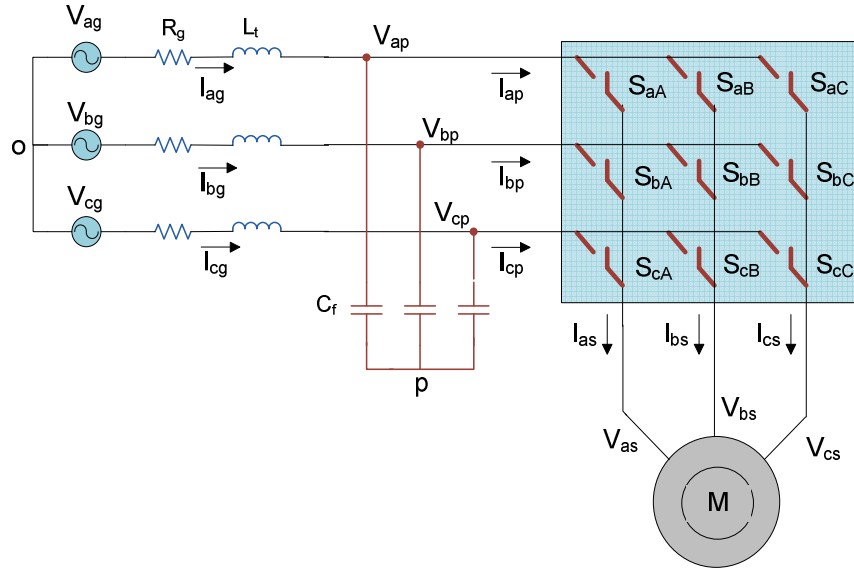


Figure 7.1 Schematic diagram of the matrix converter fed induction motor without damping resistor

It also provides detailed and step by step controllers designed to track the speed and flux trajectories. The schematic of the drive system used in the control design is shown in Figure 7.1.

The damping resistor is assumed to be big enough to be considered as open circuit. As a result, the source and filter inductors are added together and represented as L_t . The induction machine model equations are derived in section 5.3.1. The stator voltage equations in synchronous reference frame are

$$\begin{aligned} V_{qs} &= r_s I_{qs} + p \lambda_{qs} + \omega_e \lambda_{ds} \\ V_{ds} &= r_s I_{ds} + p \lambda_{ds} - \omega_e \lambda_{qs} \end{aligned} \quad (7.1)$$

And the rotor voltages are expressed as follows where the rotor voltages are zero for a squirrel cage induction machine.

$$\begin{aligned}
V_{qr} = 0 &= R_r I_{qr} + p \lambda_{qr} + \omega_{so} \lambda_{dr} \\
V_{dr} = 0 &= R_r I_{dr} + p \lambda_{dr} - \omega_{so} \lambda_{qr}
\end{aligned} \tag{7.2}$$

ω_{so} , the slip frequency is given as the difference between the frequency of rotor flux linkage and rotor speed.

Stator flux linkage are expressed as

$$\begin{aligned}
\lambda_{qs} &= L_s I_{qs} + L_m I_{qr} \\
\lambda_{ds} &= L_s I_{ds} + L_m I_{dr}
\end{aligned} \tag{7.3}$$

And the rotor flux linkage equations:

$$\begin{aligned}
\lambda_{qr} &= L_m I_{qs} + L_r I_{qr} \\
\lambda_{dr} &= L_m I_{ds} + L_r I_{dr}
\end{aligned} \tag{7.4}$$

The rotor speed dynamics

$$p \omega_r = \frac{P}{2J} (T_e - T_L) \tag{7.5}$$

The developed electromagnetic torque can be written as different equations using four of the eight components of the stator and rotor flux linkages and currents.

$$\begin{aligned}
T_e &= \frac{3P}{4} (\lambda_{ds} I_{qs} - \lambda_{qs} I_{ds}) \\
&= \frac{3P}{4} \frac{L_m}{L_r} (\lambda_{dr} I_{qs} - \lambda_{qr} I_{ds}) \\
&= \frac{3P}{4} \frac{L_m}{L_s} (\lambda_{qs} I_{dr} - \lambda_{ds} I_{qr}) \\
&= \frac{3P}{4} \frac{L_m}{L_s} (I_{dr} I_{qs} - I_{qr} I_{ds})
\end{aligned} \tag{7.6}$$

The *qdo* voltage equations of the squirrel-cage induction motor can be modified to (7.7)

to have the stator current and rotor flux linkages in the expressions.

$$\begin{aligned}
L_{\sigma} p I_{qs} &= V_{qs} - r I_{qs} - \omega_e L_{\sigma} I_{ds} + \frac{R_r L_m}{L_r^2} \lambda_{qr} - \omega_r \frac{L_m}{L_r} \lambda_{dr} \\
L_{\sigma} p I_{ds} &= V_{ds} - r I_{ds} - \omega_e L_{\sigma} I_{qs} + \frac{R_r L_m}{L_r^2} \lambda_{dr} + \omega_r \frac{R_r L_m}{L_r} \lambda_{qr}
\end{aligned} \tag{7.7}$$

Similarly, based on the rotor voltage equations, the dynamic of the rotor flux linkages are shown below.

$$\begin{aligned}
p \lambda_{qr} &= -\frac{R_r}{L_r} \lambda_{qr} + \frac{R_r L_m}{L_r} I_{qs} - \omega_{so} \lambda_{dr} \\
p \lambda_{dr} &= -\frac{R_r}{L_r} \lambda_{dr} + \frac{R_r L_m}{L_r} I_{ds} + \omega_{so} \lambda_{qr}
\end{aligned} \tag{7.8}$$

Substituting the equation of the electromagnetic torque given in (7.6) into (7.5), the modified rotor speed dynamics is shown below.

$$p \omega_r = K_e (\lambda_{dr} I_{qs} - \lambda_{qr} I_{ds}) - \frac{P}{2J} T_L \tag{7.9}$$

where

$$L_{\sigma} = L_s - \frac{L_m^2}{L_r}, \quad r = R_s + \frac{R_r L_m^2}{L_r^2} \quad \text{and} \quad K_e = \frac{3P^2}{8J} \frac{L_m}{L_r}$$

In the rotor flux orientation control, $\lambda_{qr} = 0$, the expression for the electromagnetic torque can be modified to

$$T_e = \frac{3P}{4} \frac{L_m}{L_r} \lambda_{dr} I_{qs} \tag{7.10}$$

As shown in equation (7.10) if the q-axis rotor flux is regulated to be zero and the d-axis flux is made constant, the electromagnetic torque is proportional to the q-axis stator current. Therefore, the q-axis stator current is also known as a torque producing

component of the stator current. Since $\lambda_{qr} = 0$, rotor voltage equations are modified as follows.

$$\begin{aligned} 0 &= R_r I_{qr} + \omega_{so} \lambda_{dr} \\ 0 &= R_r I_{dr} + p \lambda_{dr} \end{aligned} \quad (7.11)$$

Similarly, the rotor flux linkages are

$$\begin{aligned} 0 &= L_m I_{qs} + L_r I_{qr} \\ \lambda_{dr} &= L_m I_{ds} + L_r I_{dr} \end{aligned} \quad (7.12)$$

From the above equations the rotor currents are expressed in (7.13); however, the rotor currents are not generally known.

$$\begin{aligned} I_{qr} &= -\frac{L_m}{L_r} I_{qs} \\ I_{dr} &= \frac{\lambda_{dr} - L_m I_{ds}}{L_r} \end{aligned} \quad (7.13)$$

At steady state the rotor flux linkage only depend on the d-axis current; therefore, this component of the stator current is also known as magnetizing component. From (7.10) and (7.14), it is possible to consider the induction machine as idealized DC machine for the control purpose in which the d-axis current is analogous to the field current where as the q-axis current is equivalent to the armature current of the separately excited dc machine.

$$\lambda_{dr} = L_m I_{ds} \quad (7.14)$$

Substituting (7.13) into (7.11), the slip frequency can be given as

$$\omega_{so} = \frac{R_r L_m}{L_r} \frac{I_{qs}}{\lambda_{dr}}$$

$$p\lambda_{dr} + \frac{R_r}{L_r}\lambda_{dr} - \frac{R_r L_m}{L_r} I_{ds} = 0 \quad (7.15)$$

Therefore, the induction machine dynamic equations for the system under rotor flux oriented control are summarized below:

$$L_\sigma pI_{qs} = V_{qs} - rI_{qs} - \omega_e L_\sigma I_{ds} + \frac{R_r L_m}{L_r^2} \lambda_{qr} - \omega_r \frac{L_m}{L_r} \lambda_{dr} \quad (7.16)$$

$$L_\sigma pI_{ds} = V_{ds} - rI_{ds} + \omega_e L_\sigma I_{qs} + \frac{R_r L_m}{L_r^2} \lambda_{dr} + \omega_r \frac{L_m}{L_r} \lambda_{qr} \quad (7.17)$$

$$p\lambda_{qr} = -\frac{R_r}{L_r} \lambda_{qr} + \frac{R_r L_m}{L_r} I_{qs} - \omega_{so} \lambda_{dr} \quad (7.18)$$

$$p\lambda_{dr} = -\frac{R_r}{L_r} \lambda_{dr} + \frac{R_r L_m}{L_r} I_{ds} + \omega_{so} \lambda_{qr} \quad (7.19)$$

$$p\omega_r = K_e (\lambda_{dr} I_{qs} - \lambda_{qr} I_{ds}) - \frac{P}{2J} T_L \quad (7.20)$$

7.2.2 Unity Input Power Factor Control

The second category of the proposed control scheme is unity input power factor control. This is achieved by controlling the reactive power absorbed by the system to zero; the drive system can only draw active power from the source. The unique advantage of operating at unity input power factor in matrix converter driven system is that the converter will operate with the maximum possible voltage transfer ratio. However, the improvement in range of operation of a matrix converter operating at non-unity power factor is presented in [67].

The expression for the input reactive power in synchronous reference frame is given as

$$Q_g = \frac{3}{2}(V_{qg} I_{dg} - V_{dg} I_{qg}) \quad (7.21)$$

Aligning the source voltage in the q-axis of synchronous reference frame, $V_{dg} = 0$, and $V_{qg} = V_g$ where V_g is the peak value of source phase voltage. Therefore, the reactive power expression only depends on the d-axis source current, I_{dg} .

$$Q_g = \frac{3}{2}V_g I_{dg} \quad (7.22)$$

By regulating I_{dg} to zero, it is possible to maintain unity input factor and hence the controller design technique developed in this section is totally based on this component of the source current. The q-axis and d-axis voltage equations of the source are expressed as

$$\begin{aligned} V_{qg} &= R_g I_{qg} + L_t p I_{qg} + \omega_p L_t I_{dg} + V_{qp} \\ V_{dg} &= R_g I_{dg} + L_t p I_{dg} - \omega_p L_t I_{qg} + V_{dp} \end{aligned} \quad (7.23)$$

The q-axis and d-axis current equations for the filter capacitor

$$\begin{aligned} C_f p V_{qp} + \omega_p C_f V_{dp} &= I_{qg} - I_{qp} \\ C_f p V_{dp} - \omega_p C_f V_{qp} &= I_{dg} - I_{dp} \end{aligned} \quad (7.24)$$

The digital filter dynamics in synchronous reference frame are

$$\begin{aligned} p V_{af} &= \frac{1}{\tau}(V_{qp} - V_{af}) \\ p V_{df} &= \frac{1}{\tau}(V_{dp} - V_{df}) \end{aligned} \quad (7.25)$$

The mapping between the input current and output current using the components of the modulation signals are derived in section as follows

$$\begin{aligned} I_{qp} &= M_{qq} I_{qs} + M_{dq} I_{ds} \\ I_{dp} &= M_{qd} I_{qs} + M_{dd} I_{ds} \end{aligned} \quad (7.26)$$

Similarly, the output voltage can be expressed in terms of the input voltage and modulation signals as follow.

$$\begin{aligned} V_{qs} &= M_{qq} V_{qp} + M_{qd} V_{dp} \\ V_{ds} &= M_{dq} V_{qp} + M_{dd} V_{dp} \end{aligned} \quad (7.27)$$

The dynamic equations (7.16 - 7.27) are used to design the controllers.

7.2.3 Input-Output Feedback Linearization

The control design for induction machine is not easy due to the nonlinear nature of the dynamic equations. There is no general method for designing nonlinear controllers; however, there are alternative techniques which are best applicable for particular nonlinear control problems [73]. Feedback linearization, Adaptive control and Gain scheduling are commonly used nonlinear control design techniques. Feedback linearization is developed in this chapter to transform the nonlinear system into a fully or partly linear so that the linear control technique can be applied. This technique can be considered as a tool for transforming a complex model into an equivalent model of relatively simpler form.

In input-output linearization, a linear differential relation between the output and a new input is generated by differentiating the output until there an input-output relationship exists. And the second step is to formulate a controller based on the resulting system. The number of differentiation required is known as relative order. If the relative

degree is the same as the order of the system, the system is called input-output linearizable and then it is possible to apply the linear controller design technique. However, if the relative degree is less than the order of the system, part of the system is not unobservable in the input-output linearization process which results in an existence of internal dynamics. As a result the system dynamics of the nonlinear system is decomposed into an external or input-output part and an internal or unobservable part.

The number of the internal dynamic simply corresponds to the difference between the order of the system and the relative degree. The tracking control designed for the nonlinear system is applicable if and only if the inner dynamics are stable. Therefore, in input-output feedback linearization, it is necessary to check the existence of an inner dynamics and if they exist, the stability of them should be known. The stability of the internal dynamics is achieved by studying the zero dynamics. This can be found by maintaining the control output to zero.

The complete dynamics of the overall system is given in (7.28) to (7.36) and the order of the system, $n= 9$.

$$L_t p I_{qg} = V_{qg} - R_g I_{qg} - \omega_p L_t I_{dg} - V_{qp} \quad (7.28)$$

$$L_t p I_{dg} = V_{dg} - R_g I_{dg} + \omega_p L_t I_{qg} - V_{dp} \quad (7.29)$$

Substituting (7.26) in to (7.24)

$$C_f p V_{qp} + \omega_p C_f V_{dp} = I_{qg} - M_{qq} I_{qs} + M_{dq} I_{ds} \quad (7.30)$$

$$C_f p V_{dp} - \omega_p C_f V_{qp} = I_{dg} - M_{qd} I_{qs} + M_{dd} I_{ds} \quad (7.31)$$

Using (7.27) into (7.16) and (7.17)

$$L_{\sigma} p I_{qs} = M_{qq} V_{qp} + M_{qd} V_{dp} - r I_{qs} - \omega_e L_{\sigma} I_{ds} + \frac{R_r L_m}{L_r^2} \lambda_{qr} - \omega_r \frac{L_m}{L_r} \lambda_{dr} \quad (7.32)$$

$$L_{\sigma} p I_{ds} = M_{dq} V_{qp} + M_{dd} V_{dp} - r I_{ds} + \omega_e L_{\sigma} I_{qs} + \frac{R_r L_m}{L_r^2} \lambda_{dr} + \omega_r \frac{L_m}{L_r} \lambda_{qr} \quad (7.33)$$

The rotor flux and speed dynamics are represented as

$$p \lambda_{qr} = -\frac{R_r}{L_r} \lambda_{qr} + \frac{R_r L_m}{L_r} I_{qs} - \omega_{so} \lambda_{dr} \quad (7.34)$$

$$p \lambda_{dr} = -\frac{R_r}{L_r} \lambda_{dr} + \frac{R_r L_m}{L_r} I_{ds} + \omega_{so} \lambda_{qr} \quad (7.35)$$

$$p \omega_r = K_e (\lambda_{dr} I_{qs} - \lambda_{qr} I_{ds}) - \frac{P}{2J} T_L \quad (7.36)$$

The objective is to control the speed and rotor flux linkage by orienting the flux in the d-axis while maintaining a unity input power factor through the appropriate modulation signals generated by the matrix converter. Looking at the overall system the input and output of the nonlinear model is show in Figure 7.2.

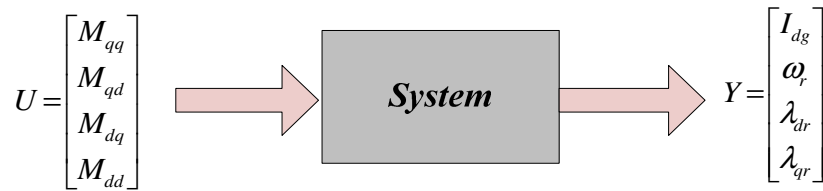


Figure 7.2 Control input and output of the system

The states, inputs and outputs of the system are,

$$X = [I_{qg} \quad I_{dg} \quad V_{qp} \quad V_{dp} \quad I_{qs} \quad I_{ds} \quad \lambda_{qr} \quad \lambda_{dr} \quad \omega_r]^T$$

$$U = \begin{bmatrix} u_1 \\ u_2 \\ u_3 \\ u_4 \end{bmatrix} = \begin{bmatrix} M_{qq} \\ M_{qd} \\ M_{dq} \\ M_{dd} \end{bmatrix}$$

$$Y = \begin{bmatrix} y_1 \\ y_2 \\ y_3 \\ y_4 \end{bmatrix} = \begin{bmatrix} I_{dg} \\ \omega_r \\ \lambda_{dr} \\ \lambda_{qr} \end{bmatrix}$$

To determine the existence of internal dynamics, the relative degree of the overall system should be found. Since the system is a four input-four output, the relative degree corresponding to each output should be computed first.

And by applying the superposition principle, the relative degree of the overall system is the sum of the relative degree related with each output. The relative order for the first control output, I_{dg} is calculated as follows

$$y_1 = I_{dg}$$

Differentiating the above output,

$$p y_1 = p I_{dg} = \frac{1}{L_t} (V_{dg} - R_g I_{dg} + \omega_p L_t I_{qg} - V_{dp})$$

Since the input does not yet appear, differentiate the output for the second time result in

$$\begin{aligned}
p^2 I_{dg} &= p \frac{1}{L_t} (V_{dg} - R_g I_{dg} + \omega_p L_t I_{qg} - V_{dp}) \\
&= -\frac{1}{L_t} (R_g p I_{dg} - \omega_p L_t p I_{qg} + p V_{dp}) - \frac{1}{C_f L_t} (I_{dg} - M_{qd} I_{qs} + M_{dd} I_{ds} + \omega_p C_f V_{qp})
\end{aligned}$$

Since the input appears after the second differentiation, the relative order for the first output, $r_1 = 2$. The relative order corresponding to the speed control is computed as

$$\begin{aligned}
y_2 &= \omega_r \\
p y_2 &= p \omega_r = \frac{P}{2J} (K_e \lambda_{dr} I_{qs} - \lambda_{qr} I_{ds} - T_L)
\end{aligned}$$

Differentiating again until the input exist,

$$\begin{aligned}
p^2 \omega_r &= \frac{K_e P}{2J} (\lambda_{dr} p I_{qs} + I_{qs} p \lambda_{dr} - \lambda_{qr} p I_{ds} - I_{ds} p \lambda_{qr}) \\
&= \frac{K_e P}{2J} \left(\frac{\lambda_{dr}}{L_\sigma} \left(M_{qq} V_{qp} + M_{qd} V_{dp} - r I_{qs} - \omega_e L_\sigma I_{ds} - \omega_r \frac{L_m}{L_r} \lambda_{dr} \right) + I_{qs} p \lambda_{dr} - \lambda_{qr} p I_{ds} - I_{ds} p \lambda_{qr} \right)
\end{aligned}$$

Thus, the relative order for the second output $r_2 = 2$.

Similarly for the relative order for the third output is calculated as;

$$\begin{aligned}
y_3 &= \lambda_{qr} \\
p \lambda_{dr} &= -\frac{R_r}{L_r} \lambda_{dr} + \frac{R_r L_m}{L_r} I_{ds}
\end{aligned}$$

Differentiating the above differential equation for the second time, the inputs appear.

$$\begin{aligned}
p^2 \lambda_{dr} &= -\frac{R_r}{L_r} p \lambda_{dr} + \frac{R_r L_m}{L_r} \dot{I}_{ds} \\
&= -\frac{R_r}{L_r} \left(-\frac{R_r}{L_r} \lambda_{dr} + \frac{R_r L_m}{L_r} I_{ds} \right) + \frac{R_r L_m}{L_r} \left(M_{dq} V_{qp} + M_{dd} V_{dp} - r I_{ds} + \omega_e L_\sigma I_{qs} + \frac{R_r L_m}{L_r^2} \lambda_{dr} \right)
\end{aligned}$$

Therefore, the relative degree of for the third output is also 2.

And finally the relative order for the fourth control output is,

$$\begin{aligned}
y_3 &= \lambda_{qr} \\
p\lambda_{qr} &= -\frac{R_r}{L_r}\lambda_{qr} + \frac{R_r L_m}{L_r}I_{qs} - \omega_{so}\lambda_{dr} \\
p^2\lambda_{qr} &= -\frac{R_r}{L_r}p\lambda_{qr} + \frac{R_r L_m}{L_r}pI_{qs} - \omega_{so}p\lambda_{dr} \\
&= -\frac{R_r}{L_r}p\lambda_{qr} + \frac{R_r L_m}{L_r}\left(M_{dq}V_{qp} + M_{dd}V_{dp} - rI_{ds} + \omega_e L_\sigma I_{qs} + \frac{R_r L_m}{L_r^2}\lambda_{dr}\right) - \omega_{so}p\lambda_{dr}
\end{aligned}$$

Similarly, the relative order for the last output is 2. By the definition, the relative degree for the above multiple input-multiple-output (MIMO) system is the sum of the individual relative degrees. The total relative order becomes 8 and the order of the system is 9. Since the relative degree is lower than the order of the system, there exist one internal dynamics. And it is necessary to analyze stability of the system zero dynamics and only if that is stable, the exact linearization results can be used. Alternatively, new output has to be selected to eliminate the zero dynamics.

To determine the zero dynamics, all the control outputs are set zero,

$$\begin{aligned}
I_{dg} &= 0 & \lambda_{dr} &= 0 \\
\omega_r &= 0 & \lambda_{qr} &= 0
\end{aligned}$$

Substituting the above variables into the following flux dynamics,

$$\begin{aligned}
p\lambda_{qr} &= -\frac{R_r}{L_r}\lambda_{qr} + \frac{R_r L_m}{L_r}I_{qs} - \omega_{so}\lambda_{dr} \\
p\lambda_{dr} &= -\frac{R_r}{L_r}\lambda_{dr} + \frac{R_r L_m}{L_r}I_{ds} + \omega_{so}\lambda_{qr} \\
I_{qs} &= 0 \text{ and } I_{ds} = 0
\end{aligned}$$

Since the stator currents, rotor fluxes and rotor speed are all zeros, the rest of the dynamic equations are given as

$$\omega_p L_t I_{qg} - V_{dp} = 0 \quad (7.37)$$

$$C_f p V_{qp} + \omega_p C_f V_{dp} = I_{qg} \quad (7.38)$$

$$M_{qq} V_{qp} + M_{qd} V_{dp} = 0 \quad (7.39)$$

$$M_{dq} V_{qp} + M_{dd} V_{dp} = 0 \quad (7.40)$$

Solving the above equations result in two possible solutions, the first one is when both V_{qp} and V_{dp} are zero and the second solution gives V_{qp} to be zero and V_{dp} as a constant term. The second solution is used to determine the zero dynamics and it computed as follows,

$$p I_{qg} = -\frac{R_g}{L_t} I_{qg} + \frac{1}{L_t} V_{qg}$$

And the solution for the above first order differential equation is

$$I_{qg}(t) = \frac{V_{qg}}{R_g} + c e^{-\frac{R_g}{L_t} t} \quad (7.41)$$

The time response of the above zero dynamics is an exponentially decaying and it is stable.

Alternatively, the equivalent Laplace transform of the zero dynamics is below.

$$\left(sI + \frac{R_g}{L_t} \right) I_{qg} - \frac{1}{L_t} V_{qg} = 0$$

The above first order system has only one real negative Eigen value, $\lambda = -\frac{R_r}{L_r}$ which lie on the left hand side of S-plane, the system is stable. Therefore, the matrix converter-induction motor with the specified controlled variables is an input-output linearizable and it is possible to implement a well known linear system controller design methodologies.

7.2.4 Controller Design for FOC of Induction Motor

The objective of the controller design is to regulate the rotor flux linkages and rotor speed to desired values. The controllers generally consist of two outer loop and two inner loop controllers. The outer loop controllers consist of rotor speed and rotor flux linkage controllers while inner loops controllers regulate q-axis and d-axis stator currents. The inner loops are required since the required inputs, stator voltages, are not directly related to the rotor flux linkage and rotor speed.

➤ Rotor Flux Controller

The d-axis rotor flux controller gives a reference to the d-axis stator current controller. A PI controller, K_{dr} , is used to keep the rotor flux to its reference value.

$$p\lambda_{dr} + \frac{R_r}{L_r}\lambda_{dr} = \sigma_{dr} = K_{dr}(\lambda_{dr}^* - \lambda_{dr}) \quad (7.42)$$

Where σ_{dr} is the output of the direct axis rotor flux controller and λ_{dr}^* are the reference d-axis rotor flux linkage which the same as the magnitude of the rotor flux linkage.

$$p\lambda_{dr} + \frac{R_r}{L_r}\lambda_{dr} = \frac{R_r L_m}{L_r} I_{ds} \quad (7.43)$$

The transfer function is given as determined from (7.42) and (7.43)

$$\frac{\lambda_{dr}}{\lambda_{dr}^*} = \frac{K_{dr}}{p + \left(\frac{R_r}{L_r} + K_{dr} \right)} \quad (7.44)$$

Since the general PI controller is widely used and proved to be effective, they are used in this analysis. K_p and K_I are proportional and integral coefficient respectively.

$$K_{dr} = K_{drP} + \frac{K_{drI}}{p}$$

The second order transfer function relating the reference and actual rotor d-axis flux linkage are

$$\frac{\lambda_{dr}}{\lambda_{dr}^*} = \frac{K_{drP} p + K_{drI}}{p^2 + \left(\frac{R_r}{L_r} + K_{drP} \right) p + K_{drI}} \quad (7.45)$$

The output of this controller gives the reference for the stator d-axis current controller

$$I_{ds}^* = \frac{L_r}{R_r L_m} \left(\sigma_{dr} - (\omega_e - \omega_r) \lambda_{qr} \right) \quad (7.46)$$

The PI parameters are chosen to maintain the system stable in wide ranges of operations. There are different methods used to determine the PI parameters and one of these methods deployed in this controller design is using Butterworth polynomial to optimize the closed-loop eigen values. The Butterworth method locates the Eigen values uniformly in the left-half S-plane on a circle with radius ω_o , with its center at the origin as shown. The Butterworth polynomial for a transfer function with a second order denominator is given as [62 - 63].

$$p^2 + \sqrt{2}\omega_o p + \omega_o^2 = 0 \quad (7.47)$$

The PI parameters are determined through comparing the coefficient of the dominator of (7.47) with (7.45) with the denominators of the corresponding transfer functions and choosing appropriate ω_o

$$\begin{aligned} K_{drI} &= \omega_o^2 \\ K_{drP} &= \sqrt{2}\omega_o - \frac{R_r}{L_r} \end{aligned} \quad (7.49)$$

The q-axis rotor flux linkage controllers are designed based on the following dynamics,.

$$p\lambda_{qr} + \frac{R_r}{L_r}\lambda_{qr} = \frac{R_r L_m}{L_r} I_{qs} - \omega_{so}\lambda_{dr}$$

Define σ_{qr} as the output of the q-axis rotor flux controller and λ_{qr}^* are the reference q-axis rotor flux linkage which is the zero since the rotor flux is aligned in synchronous reference frame.

$$p\lambda_{qr} + \frac{R_r}{L_r}\lambda_{qr} = \sigma_{qr} = K_{qr}(\lambda_{qr}^* - \lambda_{qr}) \quad (7.50)$$

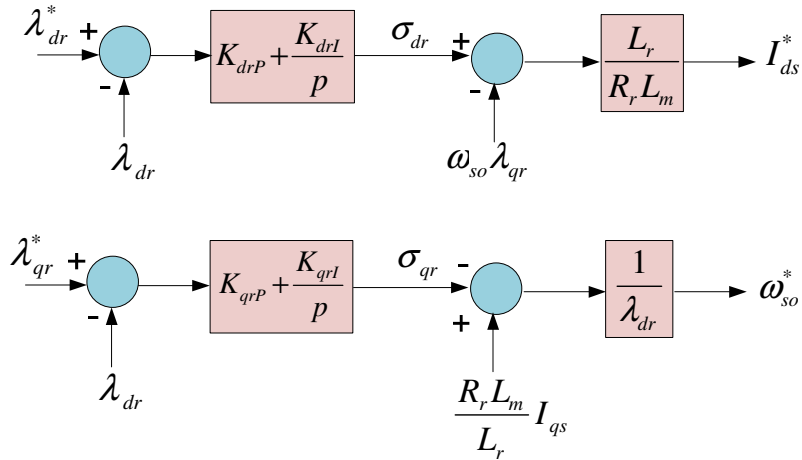


Figure 7.3 Linearization diagram for rotor flux controllers

A PI controller, K_{qr} is used to keep the rotor flux to its reference value.

$$K_{qr} = K_{qrP} + \frac{K_{qrI}}{p}$$

The transfer function is relating the actual and reference stator flux linkages are shown below

$$\frac{\lambda_{qr}}{\lambda_{qr}^*} = \frac{K_{qrP}p + K_{qrI}}{p^2 + \left(\frac{R_r}{L_r} + K_{qrP}\right)p + K_{qrI}} \quad (7.51)$$

The output of this controller gives reference slip frequency which in turn is used to determine the required stator voltage frequency to the machine.

$$\omega_{so}^* = \left(\frac{R_r L_m}{L_r} I_{qs} - \sigma_{qr} \right) \frac{1}{\lambda_{dr}} \quad (7.52)$$

The PI coefficients are computed by comparing the denominator of (7.51) with (7.47)

$$K_{qrI} = \omega_o^2$$

$$K_{qrP} = \sqrt{2}\omega_o - \frac{R_r}{L_r} \quad (7.53)$$

$$p\omega_r = K_e(\lambda_{dr}I_{qs} - \lambda_{qr}I_{ds}) - \frac{P}{2J}T_L \quad (7.54)$$

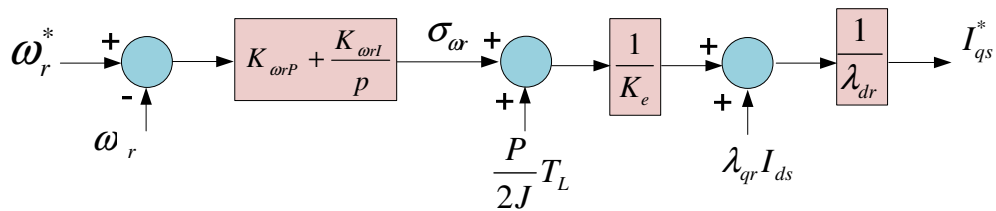


Figure 7.4 Block diagram for the rotor speed controller

The band width of the inner controller is chosen to be 600rad/sec and by the rule of thumb, the outer loop should have slower bandwidth. Hence a band width of 60rad/sec is chosen for the outer loops.

$$K_{qrI} = K_{drI} = 3600$$

$$K_{qrP} = K_{drP} = 79.3$$

➤ Rotor Speed Controller

The rotor speed controller is derived from the speed dynamics. And this controller gives a reference for the inner q-axis stator current controller.

Defining σ_{wr} as the output of the speed controller, and ω_r^* is the reference speed.

$$p\omega_r = K_{\omega r}(\omega_r^* - \omega_r) = \sigma_{wr} \quad (7.55)$$

The transfer function between the actual and reference rotor speed

$$\frac{\omega_r}{\omega_r^*} = \frac{K_{\omega r P}}{p^2 + K_{\omega r P}p + K_{\omega r I}} \quad (7.56)$$

And the reference q-axis stator current is given as:

$$I_{qs}^* = \frac{\frac{1}{K_e} \left(\sigma_{\omega r} + \frac{P}{2J} T_L \right) + \lambda_{qr} I_{ds}}{\lambda_{dr}} \quad (7.57)$$

The PI parameters are computed by comparing (7.57) with (7.56)

$$K_{\omega r I} = \omega_o^2$$

$$K_{\omega r P} = \sqrt{2}\omega_o \quad (7.58)$$

Since the mechanical dynamics is comparatively slower than the electrical dynamics, a band width of 12rad/sec is chosen for the speed controller and the $K_{\omega r P}$ and $K_{\omega r I}$ values are

computed to be 17 and 144 respectively. The block diagram of the speed controller is shown in Figure 7.4.

➤ Current Controllers

These inner controllers give actual control input, stator voltages for the overall control system. Using the stator q-axis and d-axis voltage expressions,

$$\begin{aligned} L_{\sigma} p I_{qs} + r I_{qs} &= V_{qs} - \omega_e L_{\sigma} I_{ds} + \frac{R_r L_m}{L_r^2} \lambda_{qr} - \omega_r \frac{L_m}{L_r} \lambda_{dr} \\ L_{\sigma} p I_{ds} + r I_{ds} &= V_{ds} + \omega_e L_{\sigma} I_{qs} + \frac{R_r L_m}{L_r^2} \lambda_{dr} + \omega_r \frac{L_m}{L_r} \lambda_{qr} \end{aligned} \quad (7.59)$$

The linear controllers which regulate the currents are given below where σ_{qs} and σ_{ds} are the controller outputs. And I_{qs}^* and I_{ds}^* are the reference stator currents.

$$\begin{aligned} \sigma_{qs} &= L_{\sigma} p I_{qs} + r I_{qs} = K_{qs} (I_{qs}^* - I_{qs}) \\ \sigma_{ds} &= L_{\sigma} p I_{ds} + r I_{ds} = K_{ds} (I_{ds}^* - I_{ds}) \end{aligned} \quad (7.60)$$

Then the transfer functions between the actual and reference axis currents are,

$$\begin{aligned} \frac{I_{qs}}{I_{qs}^*} &= \frac{K_{qsP} p + K_{qsI}}{L_{\sigma} p + (r + K_{qsP}) p + K_{qsI}} \\ \frac{I_{ds}}{I_{ds}^*} &= \frac{K_{dsP} p + K_{dsI}}{L_{\sigma} p + (r + K_{dsP}) p + K_{dsI}} \end{aligned} \quad (7.61)$$

The control inputs, q- and d-axis stator voltages are then determined as

$$\begin{aligned} V_{qs}^* &= \sigma_{qs} + \omega_e L_{\sigma} I_{ds} - \frac{R_r L_m}{L_r^2} \lambda_{qr} + \omega_r \frac{L_m}{L_r} \lambda_{dr} \\ V_{ds}^* &= \sigma_{ds} - \omega_e L_{\sigma} I_{qs} - \frac{R_r L_m}{L_r^2} \lambda_{dr} - \omega_r \frac{L_m}{L_r} \lambda_{qr} \end{aligned} \quad (7.62)$$

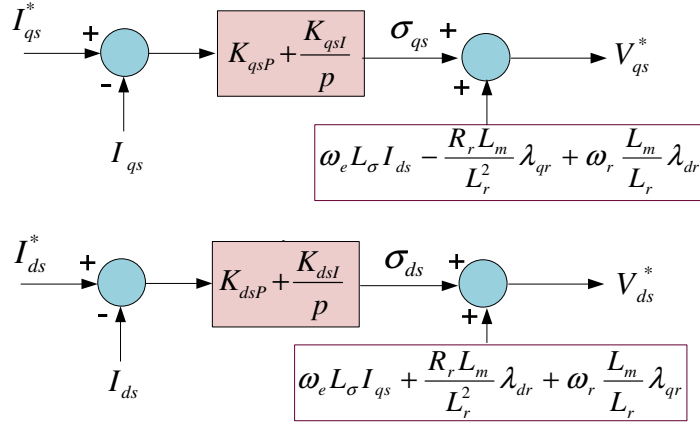


Figure 7.5 Inner stator current controller block diagram

Since the PI controller is given as:

$$\begin{aligned}
 K_{qs} &= K_{qsP} + \frac{K_{qsI}}{p} \\
 K_{ds} &= K_{dsP} + \frac{K_{dsI}}{p}
 \end{aligned}
 \tag{7.63}$$

The transfer function is therefore given as:

$$\begin{aligned}
 \frac{I_{qs}}{I_{qs}^*} &= \frac{K_{qsP}p + K_{qsI}}{L_{\sigma}p + (r + K_{qsP})p + K_{qsI}} \\
 \frac{I_{ds}}{I_{ds}^*} &= \frac{K_{dsP}p + K_{dsI}}{L_{\sigma}p^2 + (r + K_{dsP})p + K_{dsI}}
 \end{aligned}
 \tag{7.64}$$

The PI coefficient can be computed

$$\begin{aligned}
 K_{qsI} &= K_{dsI} = L_{\sigma}\omega_o^2 \\
 K_{qsP} &= K_{dsP} = L_{\sigma}\sqrt{2}\omega_o - r
 \end{aligned}
 \tag{7.65}$$

The bandwidth of the inner current controller which is ten times faster than the outer loop is chosen to be 600rad/sec. Using the parameters given in Table 7.1 and (7.65), the coefficients are evaluated as

$$K_{qsI} = K_{dsI} = 3000$$

$$K_{qsP} = K_{dsP} = 4.2$$

7.2.5 Controllers Design for Unity Power Factor

The objective of this controller is to maintain the reactive power drawn from the source to be zero by regulating the d-axis source current to zero. This involves two output current and two inner voltage controllers. The detailed designs of these controllers are presented in the following sections.

➤ Input Current Controllers

This controller gives a reference for the inner voltage controller.

$$\begin{aligned} L_t p I_{qg} + R_g I_{qg} &= \sigma_{qg} = V_{qg} - \omega_p L_t I_{dg} - V_{qp} \\ L_t p I_{dg} + R_g I_{dg} &= \sigma_{dg} = V_{dg} + \omega_p L_t I_{qg} - V_{dp} \end{aligned} \quad (7.66)$$

The linear controllers which regulate the source currents are given as:

$$\begin{aligned} \sigma_{qg} &= L_t p I_{qg} + R_g I_{qg} = K_{qg} (I_{qg}^* - I_{qg}) \\ \sigma_{dg} &= L_t p I_{dg} + R_g I_{dg} = K_{dg} (I_{dg}^* - I_{dg}) \end{aligned} \quad (7.67)$$

Then the transfer functions relating the reference with the actual input currents are given as

$$\begin{aligned} \frac{I_{qg}}{I_{qg}^*} &= \frac{K_{qgP} p + K_{qgI}}{L_t p^2 + (R_g + K_{qg}) p + K_{qgI}} \\ \frac{I_{dg}}{I_{dg}^*} &= \frac{K_{dgP} p + K_{dgI}}{L_t p^2 + (R_g + K_{dg}) p + K_{dgI}} \end{aligned} \quad (7.68)$$

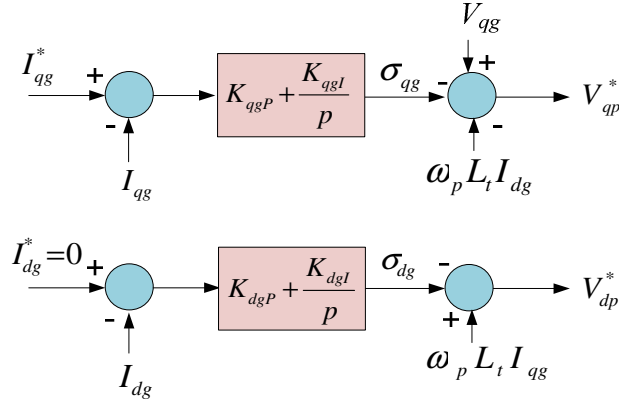


Figure 7.6 Block diagram for the input current controllers

The reference for the inner capacitor voltage controller is therefore,

$$\begin{aligned} V_{qp}^* &= V_{qg} - \omega_p L_t I_{dg} - \sigma_{qg} \\ V_{dp}^* &= \omega_p L_t I_{qg} - \sigma_{dg} \end{aligned} \quad (7.69)$$

The PI coefficient are calculated by equating the denominator of (7.68) with (7.47)

$$\begin{aligned} K_{qgI} &= K_{dgI} = L_t \omega_o^2 \\ K_{qgP} &= K_{dgP} = L_t \sqrt{2} \omega_o - R_g \end{aligned} \quad (7.70)$$

The parameters are computed using (7.70) for a chosen outer loop bandwidth of 60rad/sec. The block diagram for the input current controller as shown in Figure 7.6

$$\begin{aligned} K_{qgI} &= K_{dgI} = 3024 \\ K_{qgP} &= K_{dgP} = 7.2 \end{aligned}$$

➤ Input Voltage Controllers

The objective of this controller is to generate appropriate reference signals used to produce the modulations signals.

$$\begin{aligned} C_f p V_{qp} &= \sigma_{qp} = I_{qg} - M_{qq} I_{qs} - M_{dq} I_{ds} - \omega_p C_f V_{dp} \\ C_f p V_{dp} &= \sigma_{dp} = I_{dg} - M_{qd} I_{qs} - M_{dd} I_{ds} + \omega_p C_f V_{qp} \end{aligned} \quad (7.71)$$

Using a PI controller,

$$\begin{aligned} C_f p V_{qp} &= K_{qp} (V_{qp}^* - V_{qp}) \\ C_f p V_{dp} &= K_{dp} (V_{dp}^* - V_{dp}) \end{aligned} \quad (7.72)$$

The transfer functions between the actual and reference capacitor voltages are shown below

$$\begin{aligned} \frac{V_{qp}}{V_{qp}^*} &= \frac{K_{qpP} p + K_{qpI}}{C_f p^2 + K_{qpP} p + K_{qpI}} \\ \frac{V_{dp}}{V_{dp}^*} &= \frac{K_{dpP} p + K_{dpI}}{C_f p^2 + K_{dpP} p + K_{dpI}} \end{aligned} \quad (7.73)$$

Comparing the denominator of the above transfer functions with the (7.47), the PI coefficients are determined as follows,

$$\begin{aligned} K_{qpI} &= K_{dpI} = C_f \omega_o^2 \\ K_{qpP} &= K_{dpP} = C_f \sqrt{2} \omega_o \end{aligned} \quad (7.74)$$

Since the inner controller bandwidth is 600rad/sec and for the given filter capacitor, the controllers coefficients are.

$$\begin{aligned} K_{qpI} &= K_{dpI} = 0.08 \\ K_{qpP} &= K_{dpP} = 3.6 \end{aligned}$$

These controllers output along with the output reference voltage from the output of the stator voltage controller result in the following five non linear equations to determine the four modulation signals (M_{qq} , M_{qd} , M_{dq} , M_{dd}) and the reference input current, I_{qg}^*

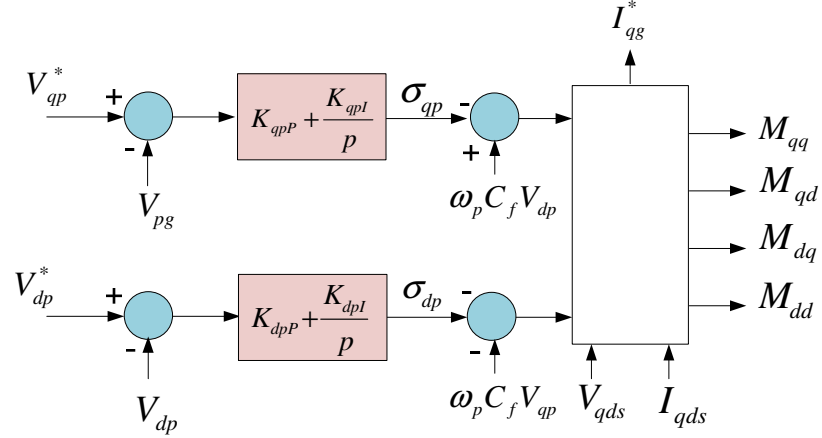


Figure 7.7 Block diagram for the input current controllers

$$\begin{aligned}
 \sigma_{qp} &= I_{qg} - M_{qq} I_{qs} - M_{dq} I_{ds} - \omega_p C_f V_{dp} \\
 \sigma_{dp} &= I_{dg} - M_{qd} I_{qs} - M_{dd} I_{ds} + \omega_p C_f V_{qp} \\
 V_{qs}^* &= M_{qq} V_{qp} + M_{qd} V_{dp} \\
 V_{ds}^* &= M_{dq} V_{qp} + M_{dd} V_{dp} \\
 M_{qq} M_{dd} &= M_{qd} M_{dq}
 \end{aligned} \tag{7.75}$$

By solving (7.75), the output of this controller together with the stator current and voltages determines the reference q-axis source current.

$$I_{qg}^* = \sigma_{qp} + \omega_p C_f V_{dp} + \frac{1}{V_{qp}} (P^* + V_{dp} (\sigma_{dp} - \omega_p C_f V_{qp} - I_{dg})) \tag{7.76}$$

where

$$P^* = V_{qs}^* I_{qs} + V_{ds}^* I_{ds} \tag{7.77}$$

And finally the four modulation signals are determined using the required stator voltage and the input capacitor voltage controller outputs as given in (7.78). The block diagram shown in Figure 7.7 demonstrates the generation of the modulation signal.

Table 7.1 Control system parameters

<i>Source voltage, $V_g = 380V_{rms}$</i>	<i>Speed Controller</i>
<i>Input frequency, $f_p = 60Hz$</i>	$K_{wrP} = 17$
<i>Line resistance, $R_g = 0.5\Omega$</i>	$K_{wrl} = 144$
<i>Line Inductance, $L_g = 1mH$</i>	<i>Rotor flux controller</i>
<i>Damping resistance, $R_f = 30\Omega$</i>	$K_{qrP} = K_{drP} = 79.3$
<i>Filter Inductance, $L_f = 7.46mH$</i>	$K_{qrl} = K_{drl} = 3600$
<i>Filter Capacitor, $C_f = 10\mu F$</i>	<i>Inner stator current controller</i>
<i>Induction machine parameters</i>	$K_{qsP} = K_{dsP} = 4.3$
<i>Stator Resistance, $R_s = 0.531\Omega$</i>	$K_{qsl} = K_{dsl} = 3000$
<i>Rotor Resistance, $R_r = 0.408\Omega$</i>	<i>Input current controller</i>
<i>Stator Inductance, $L_s = 87.22mH$</i>	$K_{qgP} = K_{dgP} = 7.2$
<i>Rotor Inductance, $L_r = 87.22mH$</i>	$K_{qgl} = K_{dgl} = 3024$
<i>Mutual Inductance, $L_m = 84.7mH$</i>	<i>Inner capacitor voltage controller</i>
<i>Moment of Inertial, $J = 0.04kg.m^2$</i>	$K_{qpP} = K_{dpP} = 0.08$
<i>Number of pole pairs, $P = 4$</i>	$K_{qpl} = K_{dpl} = 3.6$

$$\begin{aligned}
 M_{qq} &= \frac{V_{qs}^* (P^* + V_{dp} (\sigma_{dp} - \omega_p C_f V_{qp} - I_{dg}))}{V_{qp} P^*} \\
 M_{qd} &= -\frac{V_{qs}^* (\sigma_{dp} - \omega_p C_f V_{qp} - I_{dg})}{P^*} \\
 M_{dq} &= \frac{V_{ds}^* (P^* + V_{dp} (\sigma_{dp} - \omega_p C_f V_{qp} - I_{dg}))}{V_{qp} P^*} \\
 M_{dd} &= -\frac{V_{ds}^* (\sigma_{dp} - \omega_p C_f V_{qp} - I_{dg})}{P^*}
 \end{aligned} \tag{7.78}$$

It is possible to use (7.78) directly to model the MC fed induction motor drive system in qd-synchronous reference frame to observe the performance of the designed controllers. It is recommended to model the overall system without actually generating the actual switching pulses as a first step in simulation. This is because with actual pulses, the simulation time is significantly long. Once the controller works perfectly, the actual switching pulses are then implemented. The time varying modulation signals which is expressed in (3.10) are rather used to produce the switching pulses based on the reference stator voltage and the filtered input capacitor voltage. The procedure used to produce the actual switching signal pulses is explained in section 3.2.1.

7.2.6 Stator Flux Estimation

This section presents the rotor flux estimation which is used for the implementation of rotor flux controller. First, the stator side flux linkages should be estimated as accurately as possible using the Low Pass Filter (LPF) which in turn is used to determine the rotor flux linkages. The stator flux in stationary reference frame is given as [72]:

$$V_{qds}^s = r_s I_{qds}^s + p \lambda_{qds}^s \quad (7.79)$$

And from (7.79), it is possible to estimate the stator flux by integrating the back emf; however, the pure integrator has the drift and the saturation problem by the dc offset and initial condition.

$$\lambda_{qds}^s = \int (V_{qds}^s - r_s I_{qds}^s) dt \quad (7.80)$$

The gain of the controllers are summarized in Table 7.1

The pure integrator is replaced by a LPF to solve the above problems. The estimated stator flux by the LPF can be given as:

$$\frac{\hat{\lambda}_{sl}}{V_e} = \frac{1}{s+a} \quad (7.81)$$

where $\hat{\lambda}_{sl}$ is the estimated stator flux, a is the pole and V_e is the back emf shown below.

$$V_e = V_{qds} - r_s I_{qds} \quad (7.82)$$

The phase lag and the gain created by the low pass filter are expressed in terms of the synchronous speed, estimated flux and the pole as follows,

$$\phi = -\tan^{-1} \frac{\omega_e}{a} \quad (7.83)$$

$$M = \left| \frac{\hat{\lambda}_{sl}}{V_e} \right| = \frac{1}{\sqrt{a^2 + \omega_e^2}} \quad (7.84)$$

On the contrary, the phase and gain of the pure integrator shown above is 90° and $1/\omega_e$ respectively. Although the LPF eliminates the saturation problem and reduces the effect of DC offsets, it brings magnitude and phase angle error due to the cut off frequency of the LPF. This error is more severe when the machine frequency is lower than the cutoff frequency. Therefore, the cutoff frequency is selected to be very low to mitigate this error. However, there still remains the drift problem due to the very large time constant of the LPF. For the exact estimation of the stator flux, the phase lag and the gain should be the same as that of the pure integrator. Furthermore, to solve the drift problem, the pole should be located far from the origin.

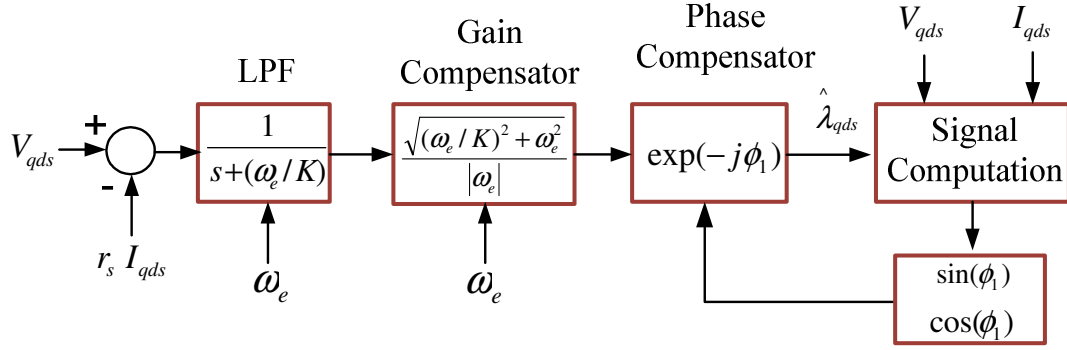


Figure 7.8 Bock diagram of the stator flux estimation using LPF

The decrement in the gain and the phase lag created is due to the LPF and is compensated by multiplying a gain compensator, G and the phase compensator, P respectively.

$$G = \frac{\sqrt{a^2 + \omega_e^2}}{|\omega_e|} \quad (7.85)$$

$$P = \exp(-j\phi_1) \quad (7.86)$$

The new integrator along with the gain and phase compensator is

$$\frac{\hat{\lambda}_{qds}}{V_e} = \frac{1}{s+a} \frac{\sqrt{a^2 + \omega_e^2}}{|\omega_e|} \exp(-j\phi_1) \quad (7.87)$$

The cutoff frequency in LPF cannot be located at fixed point far from the origin.

If the pole is varied proportionally to the machine speed, the proportion of the machine frequency to the cutoff frequency of the LPF is constant. If the proportion is large, the estimation error will be very small. Consequently, the pole is determined to be varied proportionally to the motor speed.

Therefore, the pole is located close to the origin in very low speed range and far from the origin in high speed range. K is a constant chosen to vary the pole proportionally with the rotor speed. Finally, the complete equation for stator flux estimator can be derived as:

$$a = \frac{|\omega_e|}{K}$$

$$\frac{\hat{\lambda}_{qds}}{V_e} = \frac{1}{s + (\omega_e / K)} \frac{\sqrt{(\omega_e / K)^2 + \omega_e^2}}{|\omega_e|} \exp(-j\phi_1) \quad (7.88)$$

where,

$$\exp(-j\phi_1) = \cos(\phi_1) - j \sin(\phi_1)$$

$$\cos(\phi_1) = \frac{|\omega_e|}{\sqrt{(\omega_e / K)^2 + \omega_e^2}}$$

$$\sin(\phi_1) = \frac{\omega_e / K}{\sqrt{(\omega_e / K)^2 + \omega_e^2}}$$

Simplifying (7.88) and separating into real and imaginary parts gives:

$$\hat{\lambda}_{qs} = \frac{1}{s + (\omega_e / K)} \frac{\sqrt{(\omega_e / K)^2 + \omega_e^2}}{|\omega_e|} (\cos \phi_1 (V_{qs} - r_s I_{qs}) + \sin \phi_1 (V_{ds} - r_s I_{ds})) \quad (7.89)$$

$$\hat{\lambda}_{ds} = \frac{1}{s + (\omega_e / K)} \frac{\sqrt{(\omega_e / K)^2 + \omega_e^2}}{|\omega_e|} (\cos \phi_1 (V_{ds} - r_s I_{ds}) - \sin \phi_1 (V_{qs} - r_s I_{qs})) \quad (7.90)$$

From (7.89) and (7.90), the stator q-axis and d-axis stator fluxes are determined, however, the control scheme proposed in this chapter requires the estimation of the rotor fluxes. The relationships between the stator and rotor fluxes are determined as follows.

$$\begin{aligned} \lambda_{qs} &= L_s I_{qs} + L_m I_{qr} \\ \lambda_{ds} &= L_s I_{ds} + L_m I_{dr} \end{aligned} \quad (7.91)$$

Form (7.91), the rotor flux can be expressed in terms of the stator flux and currents as given below

$$\begin{aligned} I_{qr} &= \frac{1}{L_m}(\lambda_{qs} - L_s I_{qs}) \\ I_{dr} &= \frac{1}{L_m}(\lambda_{ds} - L_s I_{ds}) \end{aligned} \quad (7.92)$$

Using the rotor flux equations,

$$\begin{aligned} \lambda_{qr} &= L_m I_{qs} + L_r I_{qr} \\ \lambda_{dr} &= L_m I_{ds} + L_r I_{dr} \end{aligned} \quad (7.93)$$

Substituting (7.92) into (7.93), the rotor flux linkages can be written in terms of stator current and flux linkages.

$$\begin{aligned} \lambda_{qr} &= \frac{L_r}{L_m}(\lambda_{qs} - L_s I_{qs}) \\ \lambda_{dr} &= \frac{L_r}{L_m}(\lambda_{ds} - L_s I_{ds}) \end{aligned} \quad (7.94)$$

Using the estimated stator flux linkages and the measured stator currents, it is possible to estimate the rotor flux as

$$\begin{aligned} \hat{\lambda}_{qr} &= \frac{L_r}{L_m}(\hat{\lambda}_{qs} - L_s I_{qs}) \\ \hat{\lambda}_{dr} &= \frac{L_r}{L_m}(\hat{\lambda}_{ds} - L_s I_{ds}) \end{aligned} \quad (7.95)$$

The complete block diagram of the proposed control scheme is shown in Figure 7.9. The input unity power factor control, rotor flux estimation and the rotor field orientation are the basic elements of this block.

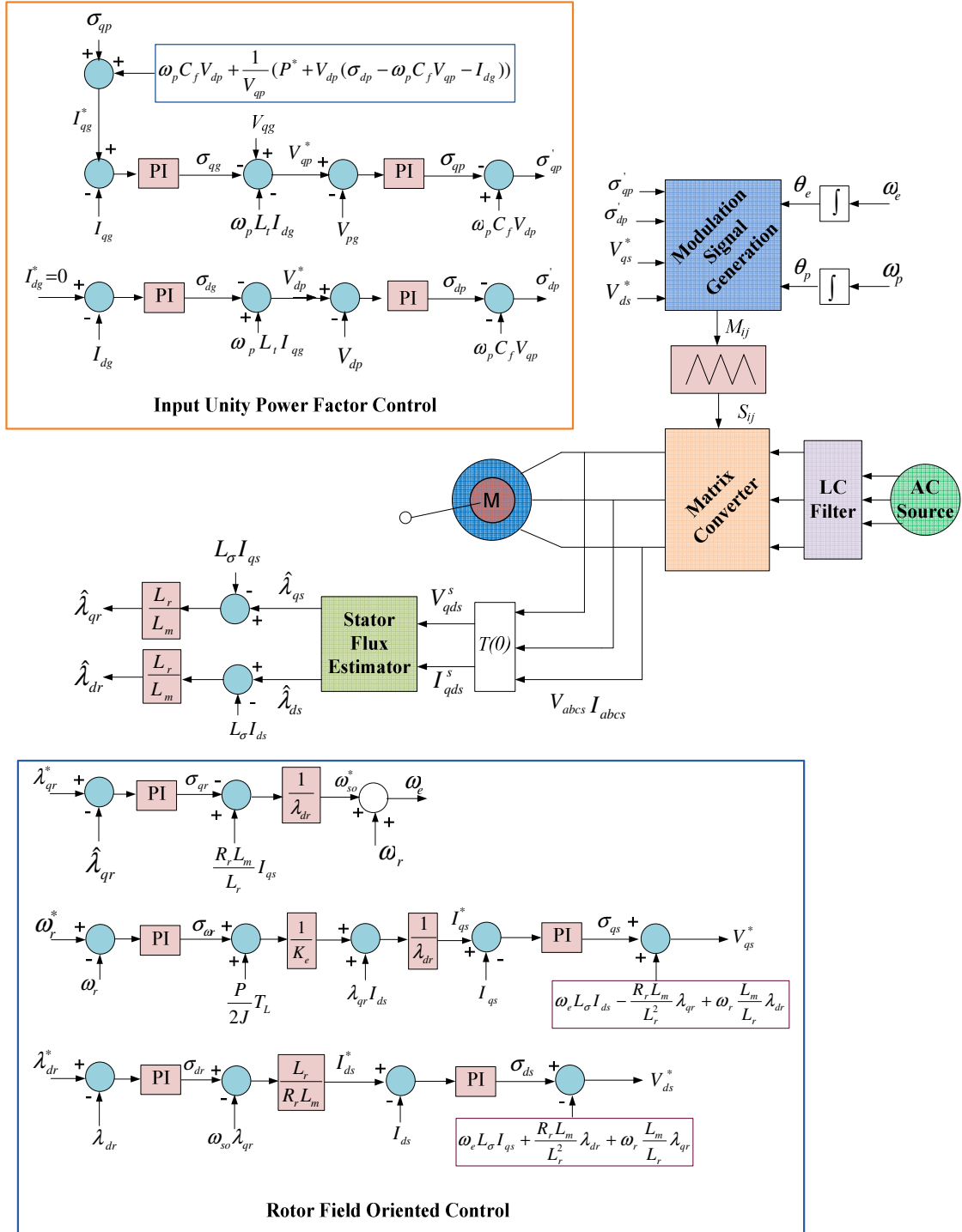


Figure 7.9 Block diagram of the proposed control scheme

7.3 Simulation Results and Discussions

The proposed control scheme is simulated in Matlab/Simulink platform using the system parameters and calculated controllers gain provided in Table 1.1. The model also includes the rotor flux estimation to provide the d-axis and q-axis rotor flux linkage to the controllers. The matrix converter as well the induction machine models are taken from section 5.3.1. Figure 7.10 shows the block diagram of the Simulink model. The d-axis of the rotor flux is controlled to be constant at $0.54Wb$. The command for q-axis rotor flux is controlled to be zero which in turn assures the rotor flux orientation. The simulation has done for three different cases as. The first simulation is done to observe the response of the designed controllers for the load variation while keeping the speed command constant. In the second and third simulations, the speed is ramped in both forward and reverse direction at while the machine is under no load operation. The results of these simulations are discussed below.

In the first simulation, a load torque of $3 Nm$ is applied after $1 sec$ while the speed command is set to $280 rad/sec$. As shown in Figure 7.11, the speed follows the reference perfectly after the motor reaches steady state and it has very small disturbance at the time when the load is applied. The starting transient of the electromagnetic torque is also shown in this Figure; at steady state it follows the load torque although there is a small overshoot at $1 sec$. It can also be observed that the electromagnetic torque has very small oscillating component. This is because the induction motor is directly fed the chopped output voltage of the converter which is not purely sinusoidal.

Matrix Converter Fed Induction Motor Indirect Vector Control (RFOC) With Unity Power Factor Control

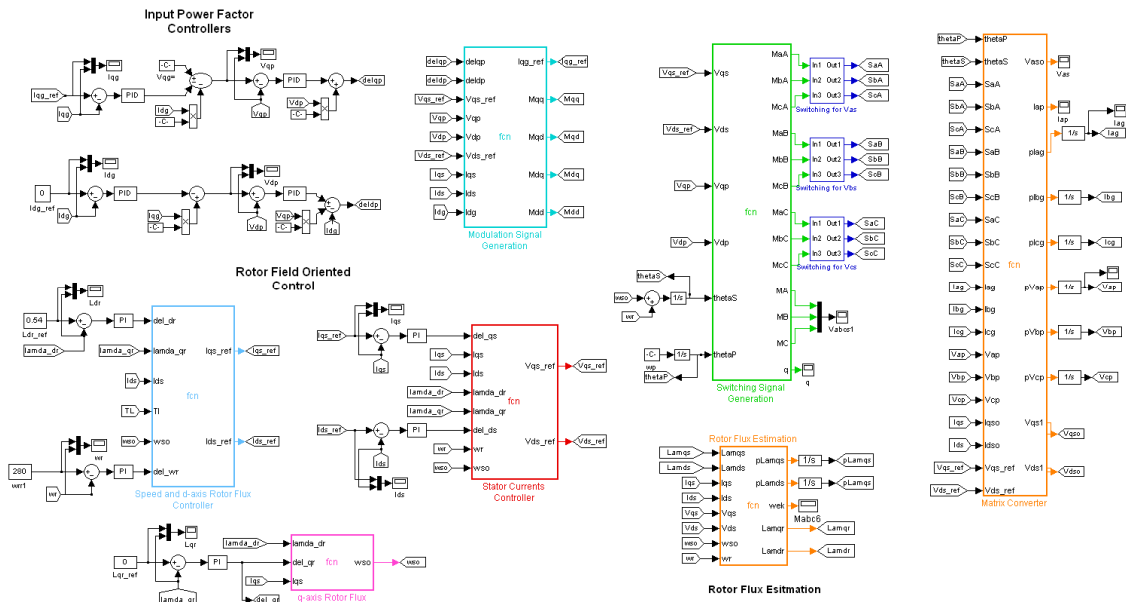


Figure 7.10 Simulink model of the proposed control scheme

Not only the electromagnetic torque but also the stator q-axis and d-axis currents, both components of the source current and both axes of the input capacitor voltage also contain ripples. As seen in Figure 7.12 both q-axis and d-axis rotor flux linkages track their respective references. From this figure, it has been observed that the d-axis rotor flux linkage is not affected by the change in the load torque assuring the decoupled control of flux and speed in the proposed control scheme. However, the q-axis rotor flux linkage has small disturbance when the load applied.

The inner current controller output are shown in Figure 7.13 in which the actual and reference are almost equal because they are in the inner control loop. Comparing Figure 7.13 and Figure 7.11, the q-axis stator current linearly changes with torque since it is a torque producing current. And the d-axis stator current responds only for the d-axis flux as it is a flux producing current component.

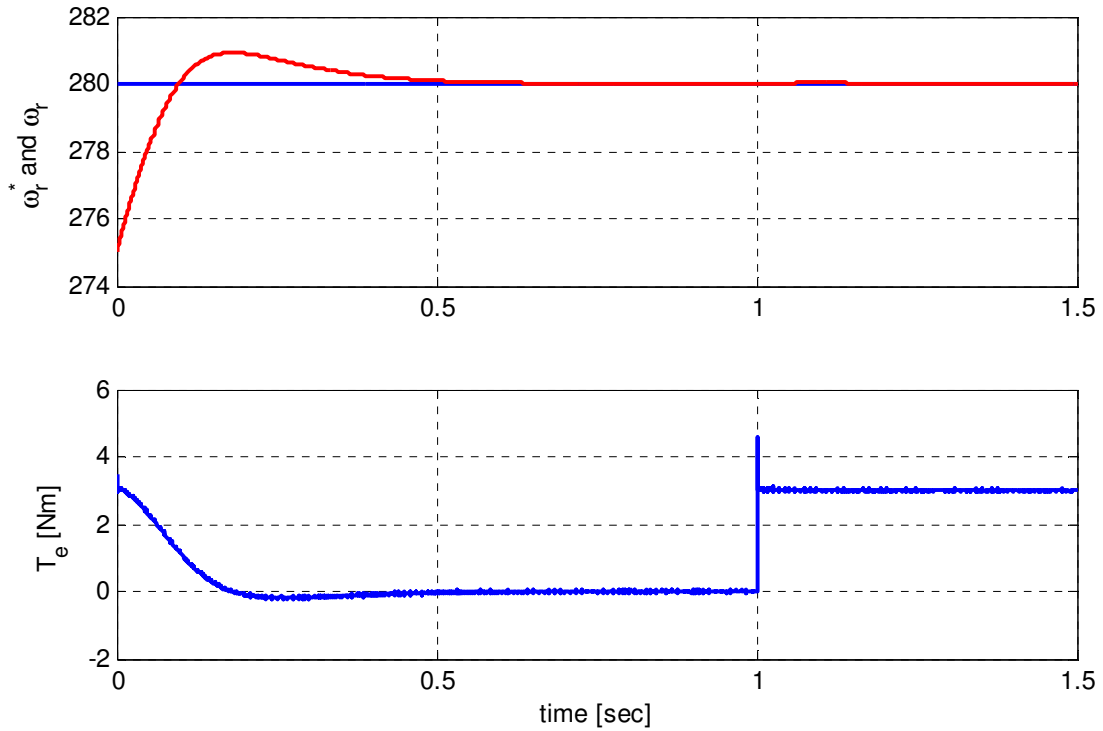


Figure 7.11 Speed command, actual speed and electromagnetic torque

The input d-axis current always follows the reference with small overshoot during the transient. It also has small oscillation during the load change as seen in Figure 7.14. As a result, the input power factor regulated at unity before and after the load applied. In this figure, the q-axis axis input current track the current command very well after the motor reaches steady state which proportionally increase with load. The inner voltage controllers exactly follow the voltage command as shown in Figure 7.15. The actual matrix converter voltage output and input are given in Figure 7.16.

The sinusoidal phase ‘a’ source current is shown in Figure 7.17 which increases with the load. And the reactive power drawn from the source is always zero although small amount of reactive power is absorbed during the transient and load change.

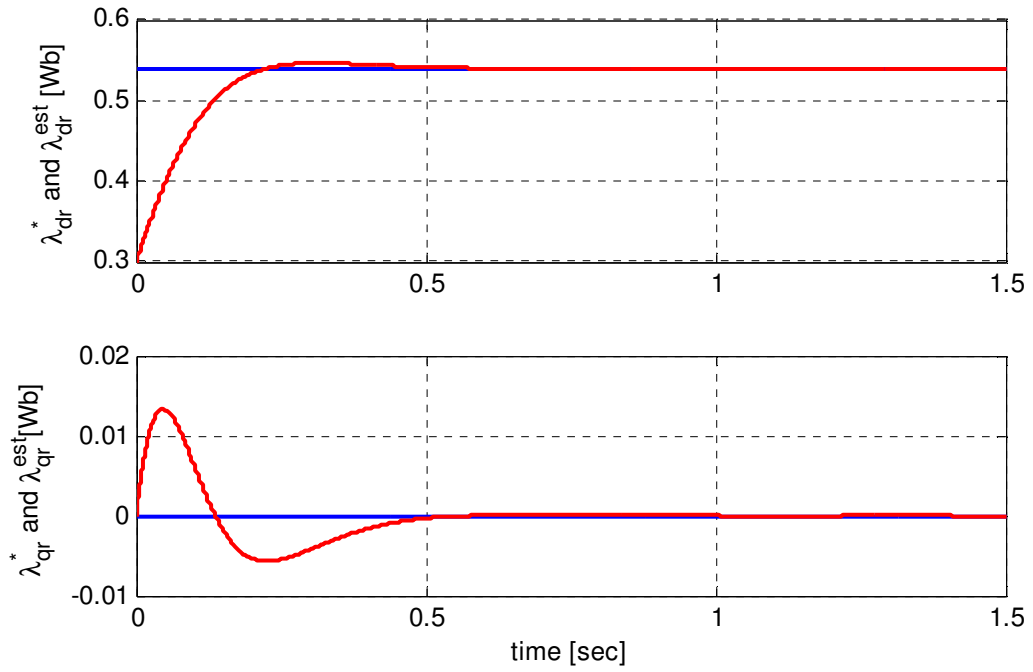


Figure 7.12 Estimated and reference rotor flux linkages

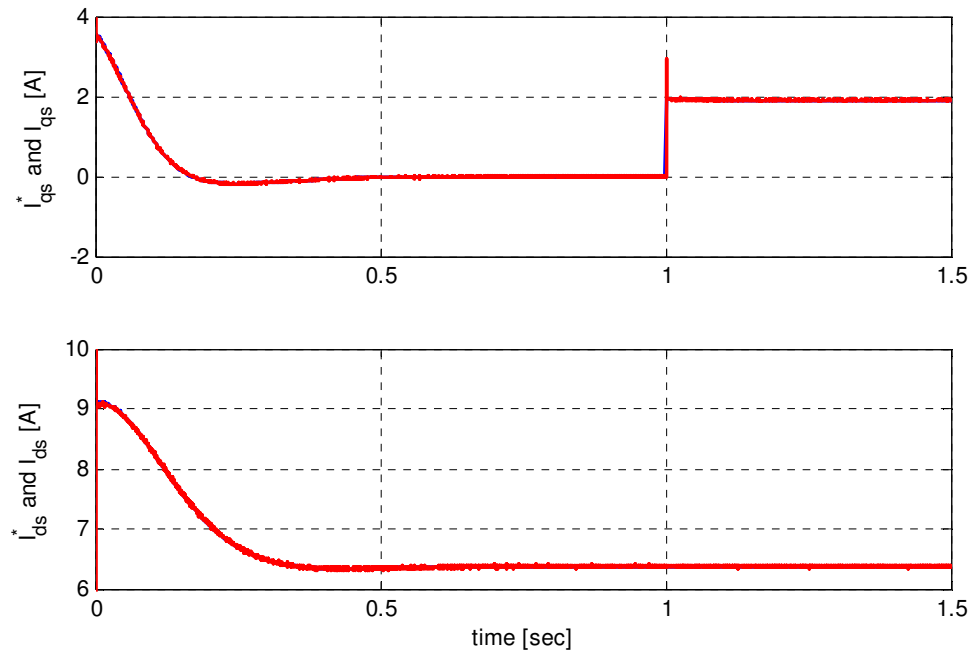


Figure 7.13 Actual and reference stator currents

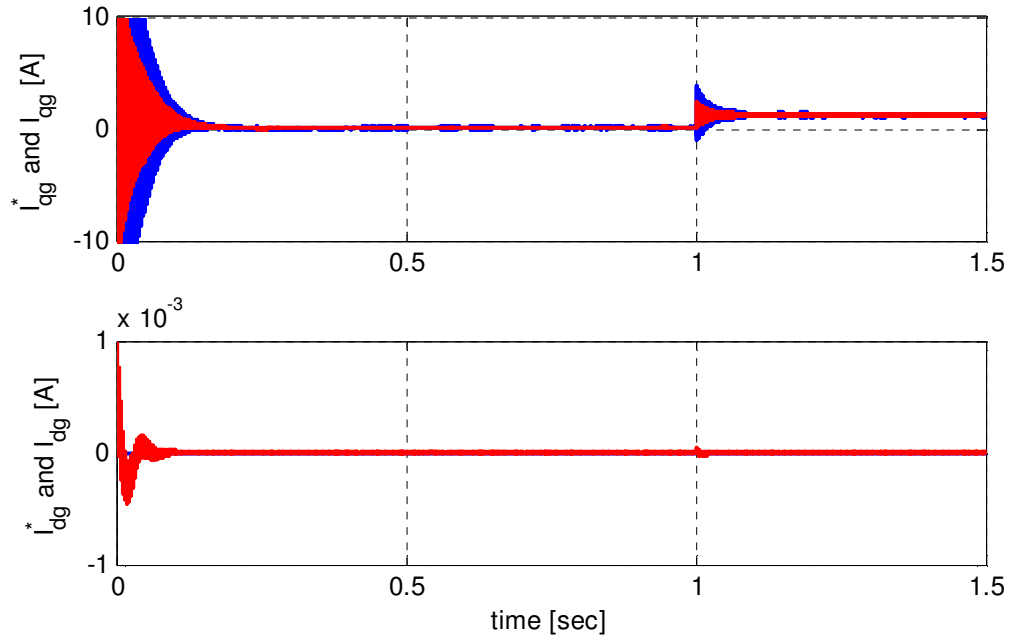


Figure 7.14 Source currents commands and actual values

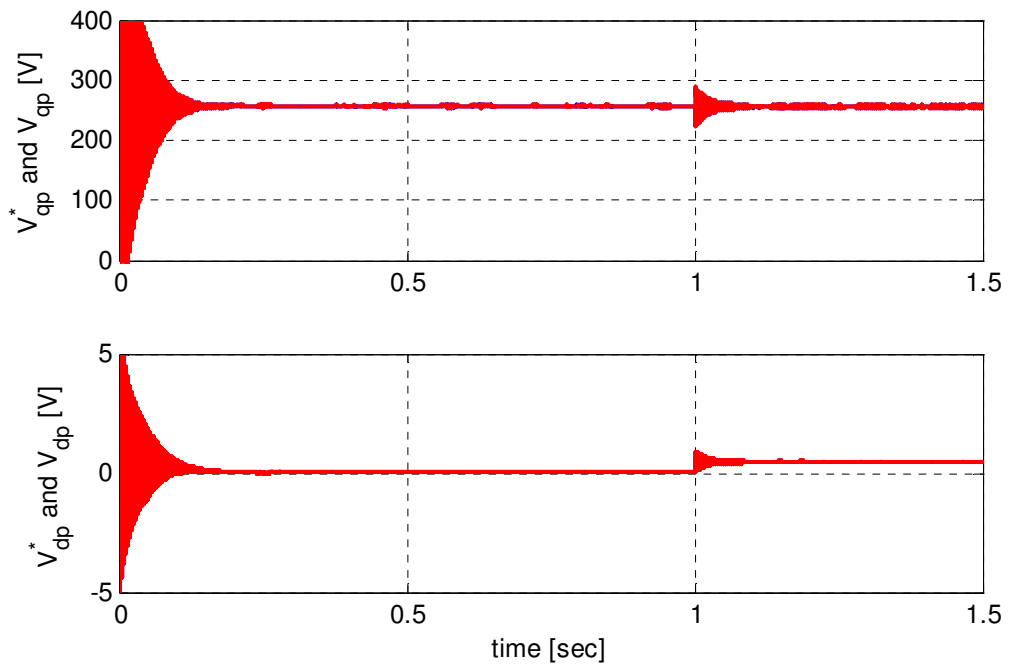


Figure 7.15 Inner capacitor voltage controller's reference and actual values

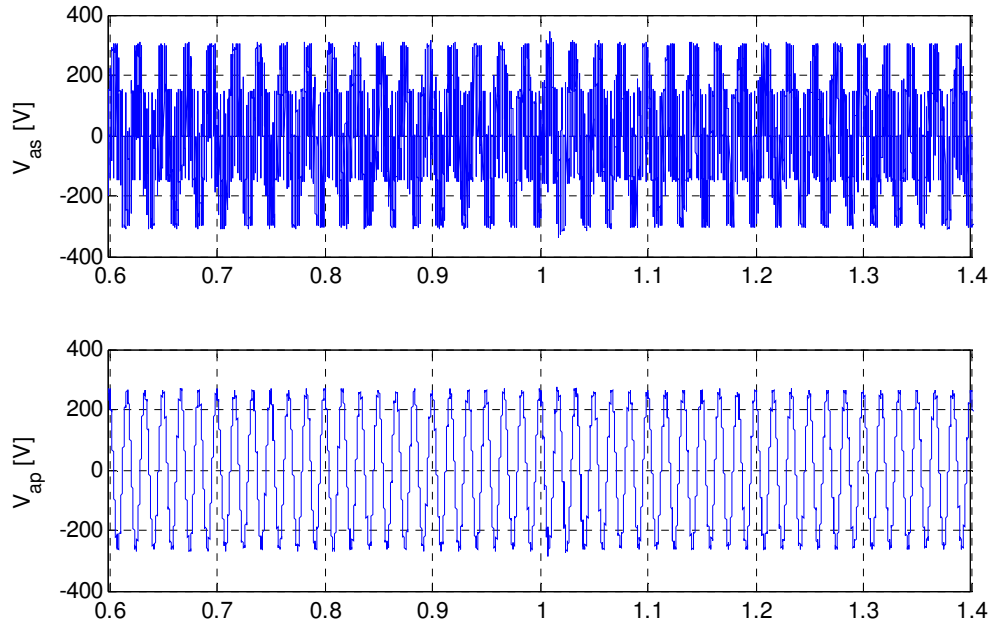


Figure 7.16 Matrix converter output and input capacitor voltage

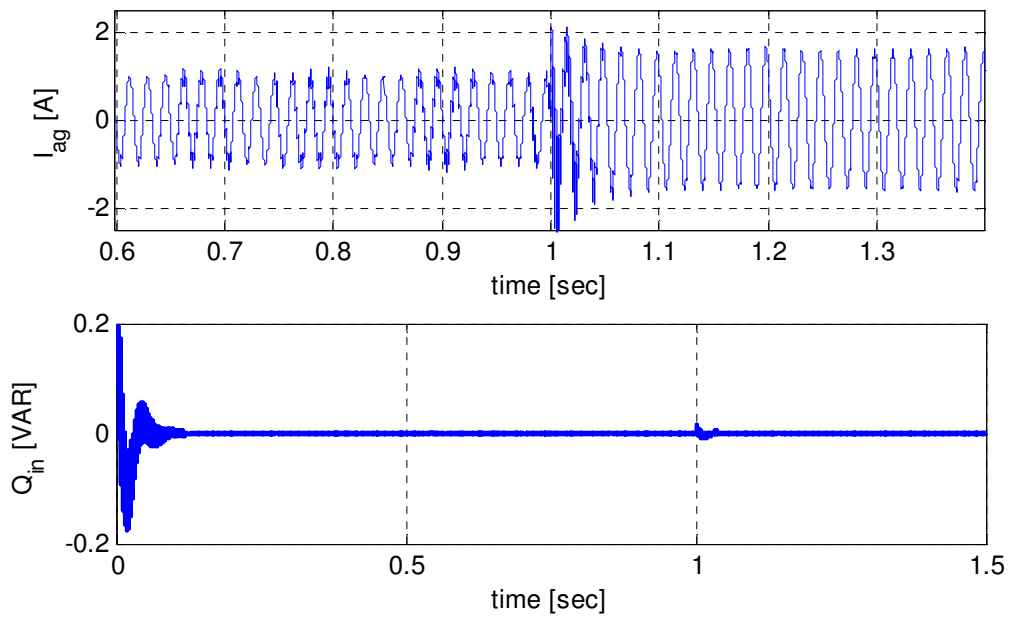


Figure 7.17 Phase 'a' source current and reactive power drawn from the source

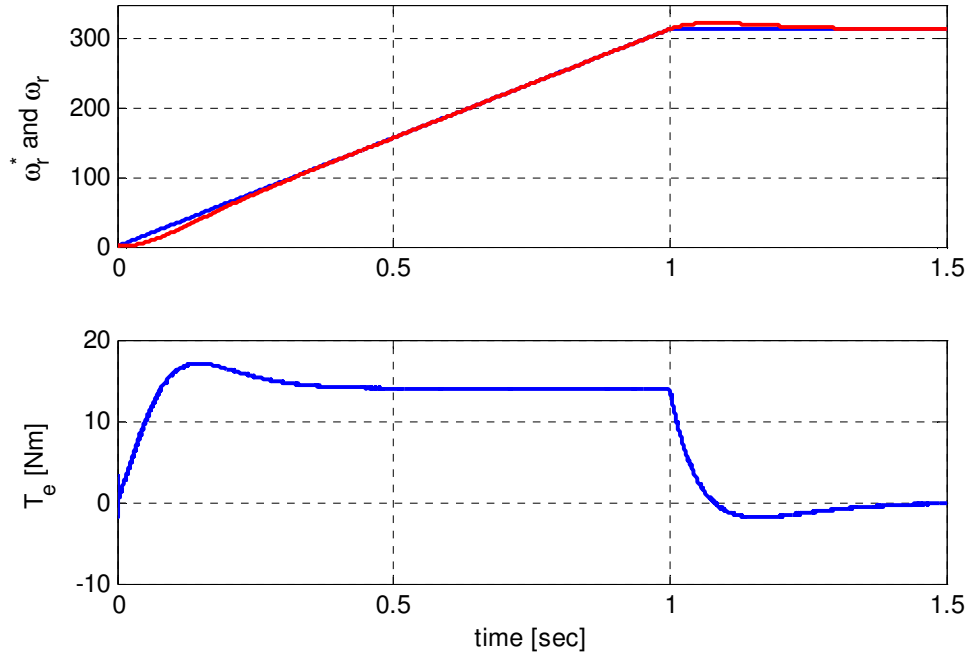


Figure 7.18 Speed command, actual speed and electromagnetic torque

In the second simulation, the speed command is ramped from zero to the rated speed in 1 sec and kept at rated speed for the rest of the time. The motor speed tracks the reference as given in Figure 7.18. And a positive electromagnetic torque is developed during the speed ramp and it goes back to zero after the speed becomes constant since there is no load applied. As seen in Figure 7.19, the rotor flux linkages follows the reference even during the ramp after the motor reaches steady state.

It can be observed from Figure 7.20, the d-axis source current is maintained zero in both region of speed command. Since the speed is increasing linearly, the output power also changes linearly. On the other hand, the input power only depends on the q-axis source current as the input voltage kept constant. Therefore, I_{qs} should linearly vary with the rotor speed to maintain input output power balance.

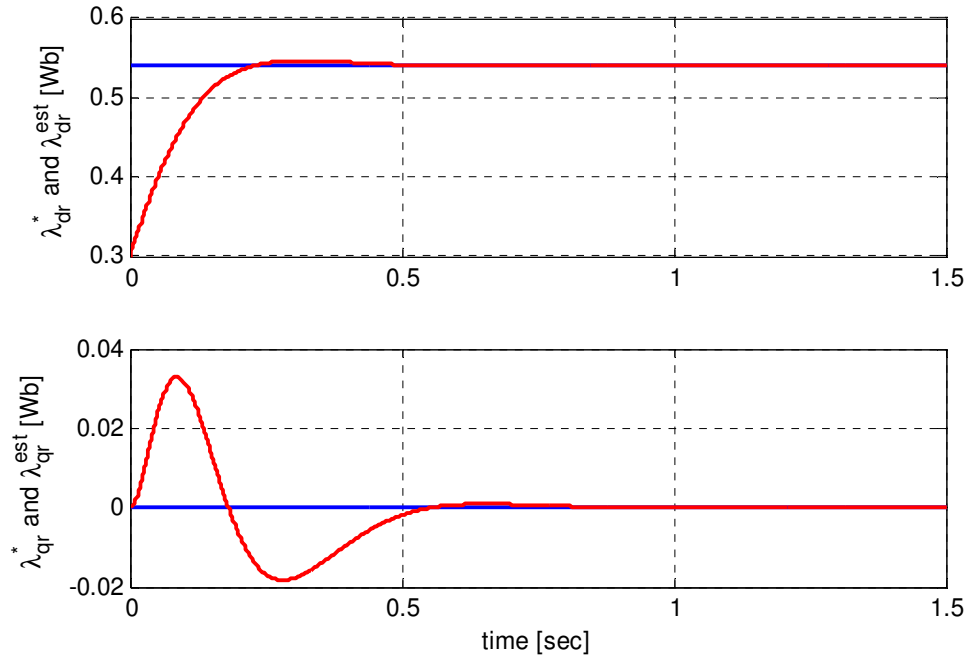


Figure 7.19 Estimated and reference rotor flux linkages

The inner stator current and input capacitor voltage controllers which exactly track their corresponding references are shown in Figure 7.21 and Figure 7.22 respectively. Since the voltage drop in the source current is considerably small, the q-axis capacitor can only represent with d-axis source current and whereas the d-axis capacitor voltage depend only on the q-axis source current. This is verified in the Figure 7.22. It can also be seen that the input capacitor voltages have small ripple and the digital low pass filter is implemented to remove this oscillation before they are used to generate the modulation signals. The sinusoidal input current with amplitude vary with the rotor speed is given in Figure 7.23. And the reactive power absorbed from the source is regulated to zero verifying the robustness of the input power factor controller.

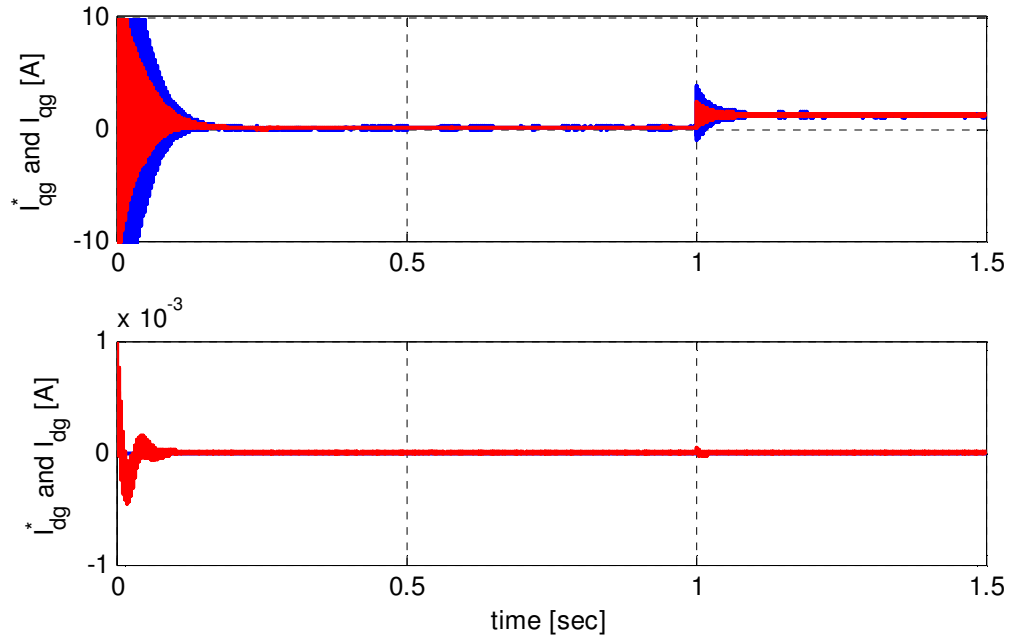


Figure 7.20 Source currents commands and actual values

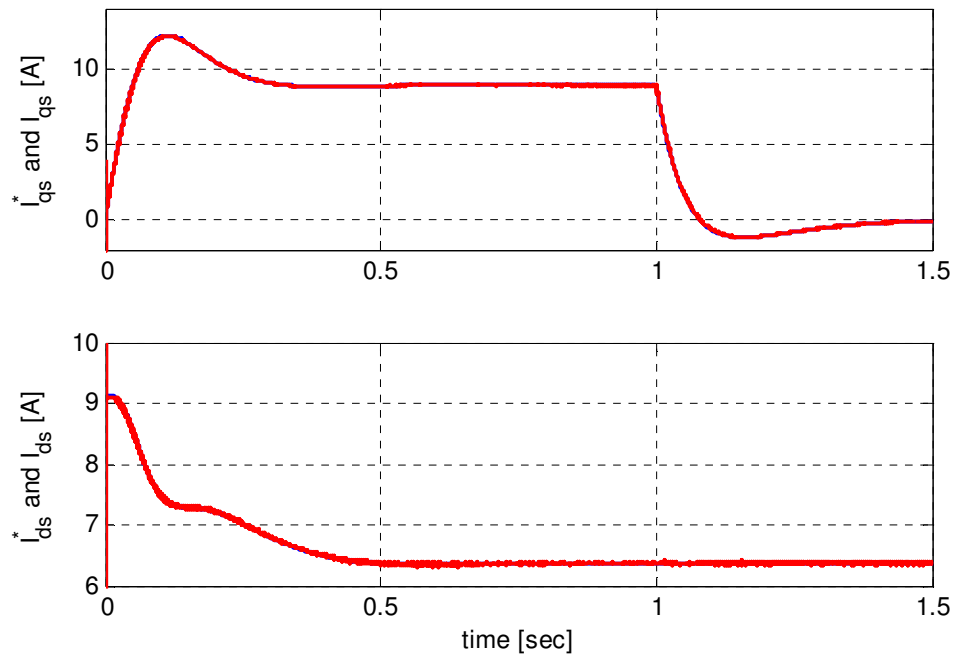


Figure 7.21 Actual and reference stator currents

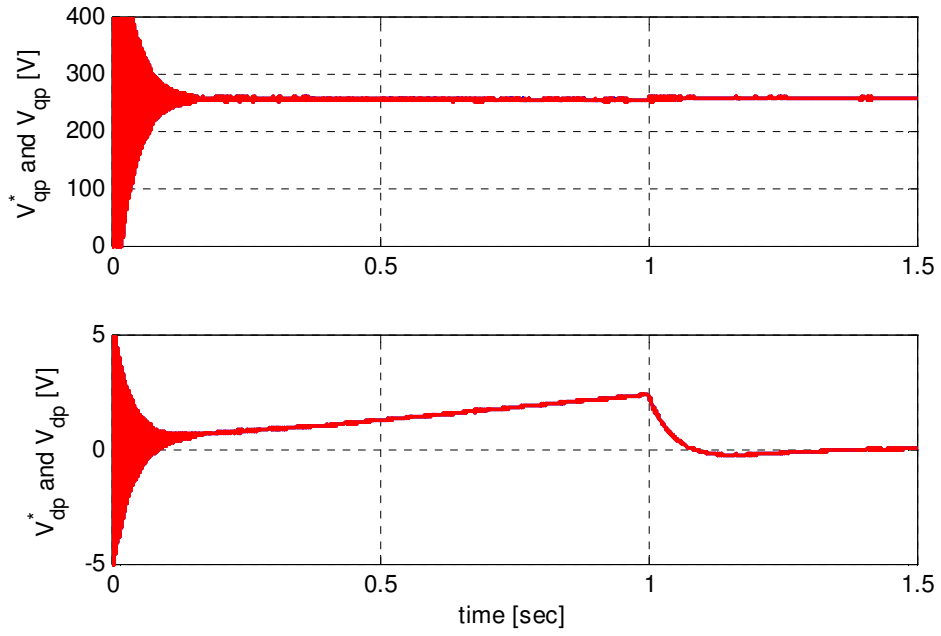


Figure 7.22 Inner capacitor voltage controller's reference and actual values

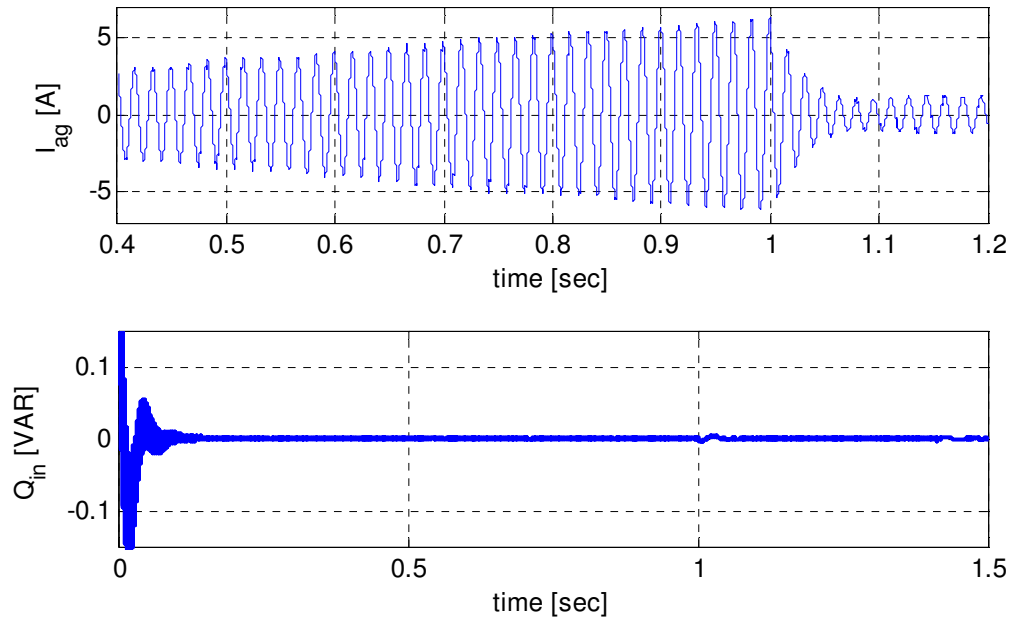


Figure 7.23 Phase 'a' source current and reactive power drawn from the source

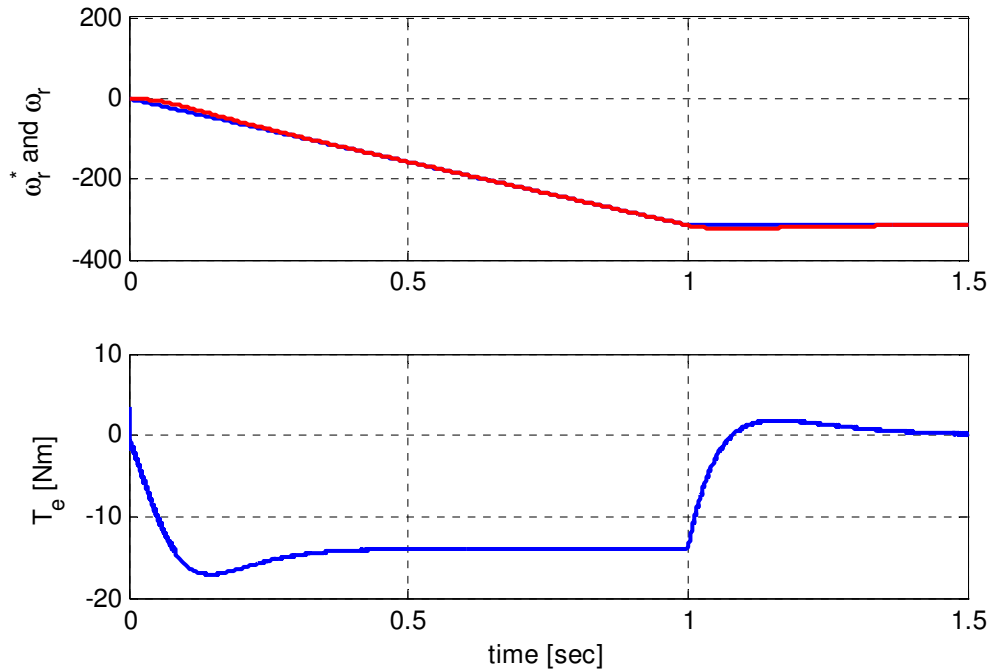


Figure 7.24 Speed command, actual speed and electromagnetic torque

Finally, simulation has been done to check the robustness of the control scheme proposed in this work by using a negative ramp speed command. As seen in Figure 7.24 the speed perfectly tracks the command. Since the rotor speed command is ramped in the reverse direction, a negative torque is developed during this time and goes back to zero after the speed is to be set constant. As given in Figure 7.25 the rotor flux linkages properly track their reference even if the d-axis rotor flux linkage has small negative value during starting following the torque transient. The source currents shown in Figure 7.26 are the same as shown in Figure 7.20 regardless of the direction of rotation of the motor. The inner stator currents and input capacitor voltage controllers perfectly follows their reference in this scenario as well as depicted in Figure 7.27 and 7.28 respectively. Finally, the input power factor controller works perfectly keeping the reactive power drawn from the source to zero as shown in Figure 7.30.

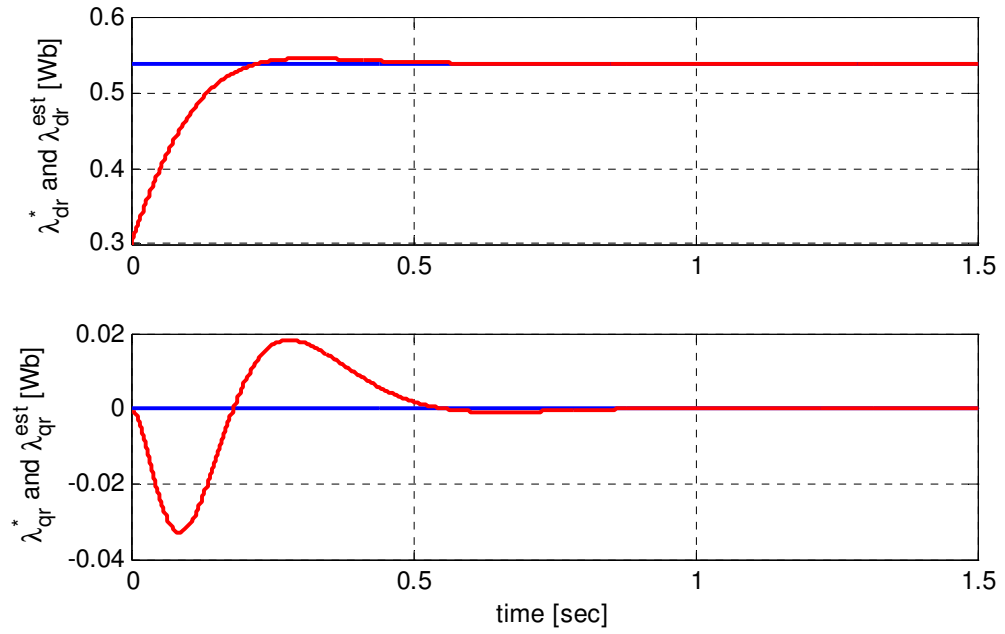


Figure 7.25 Estimated and actual rotor flux linkages

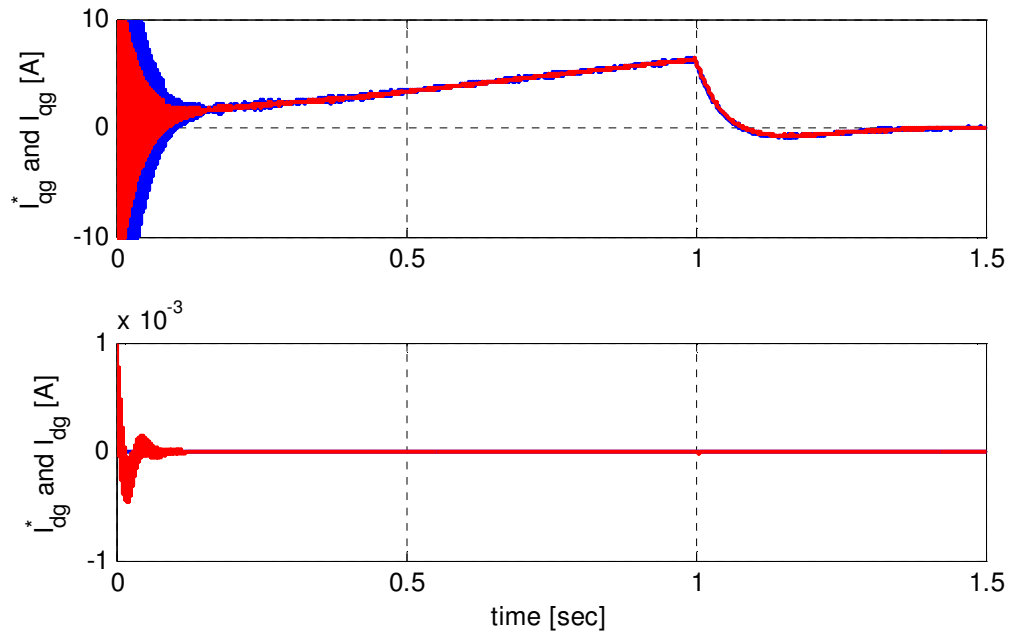


Figure 7.26 Source currents commands and measured values

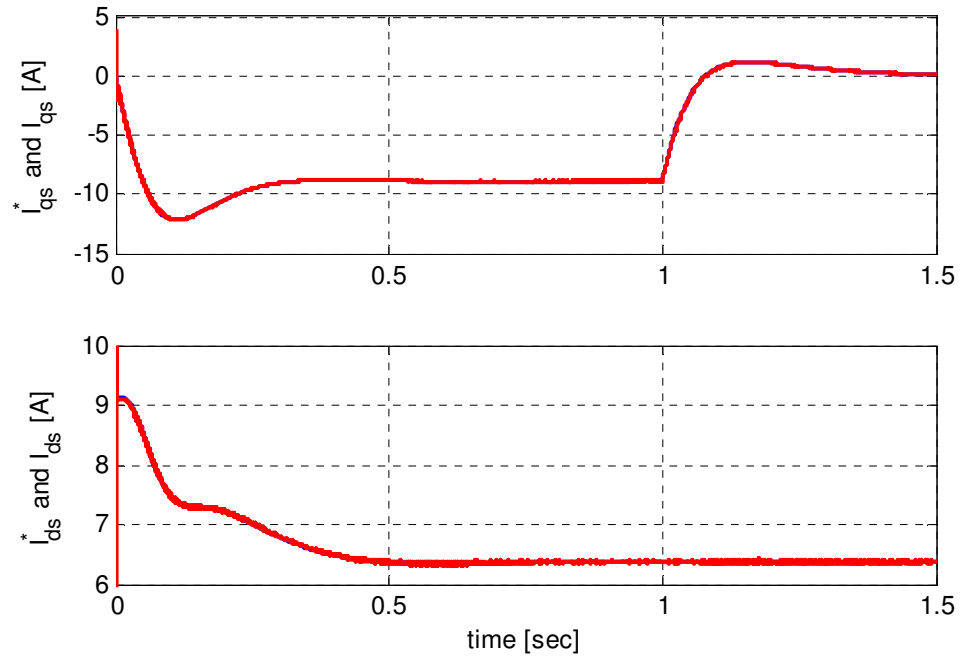


Figure 7.27 Actual and reference stator currents

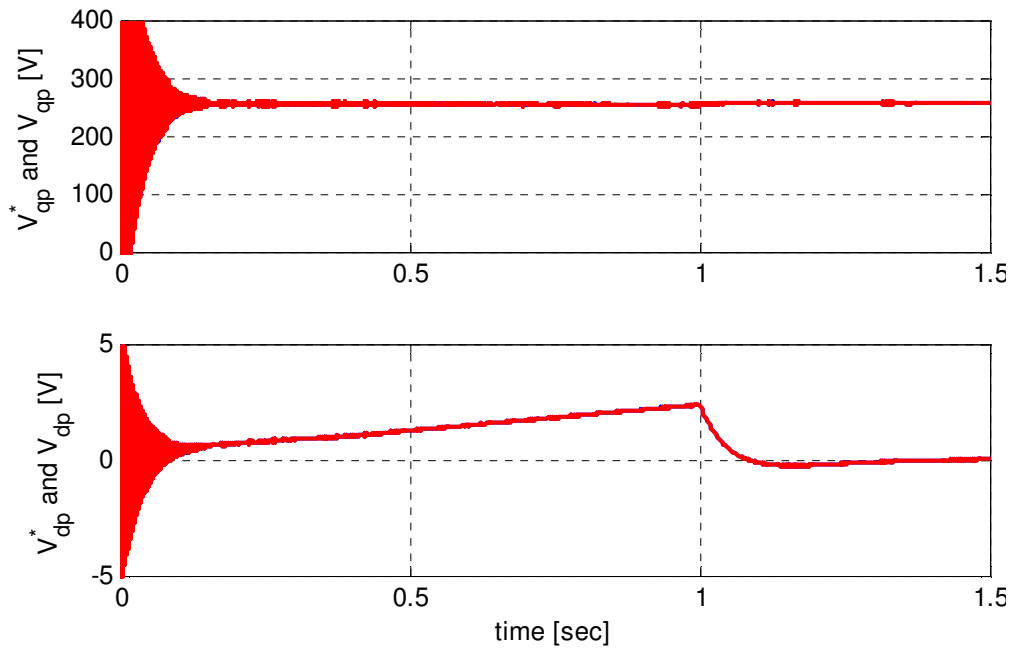


Figure 7.28 Inner capacitor voltage controller's reference and actual values

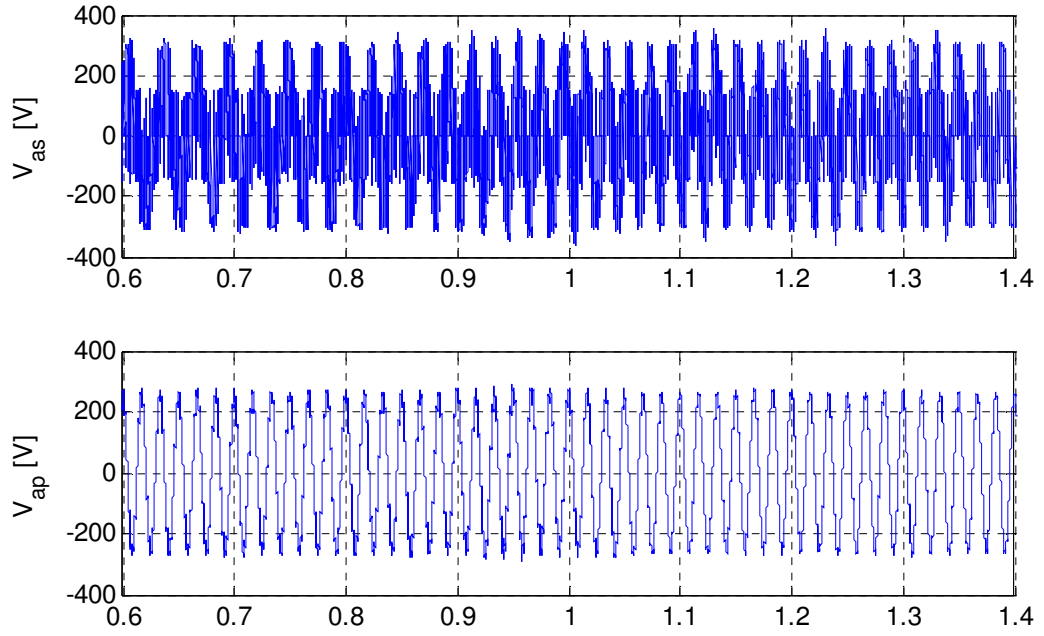


Figure 7.29 Matrix converter output and input capacitor voltage

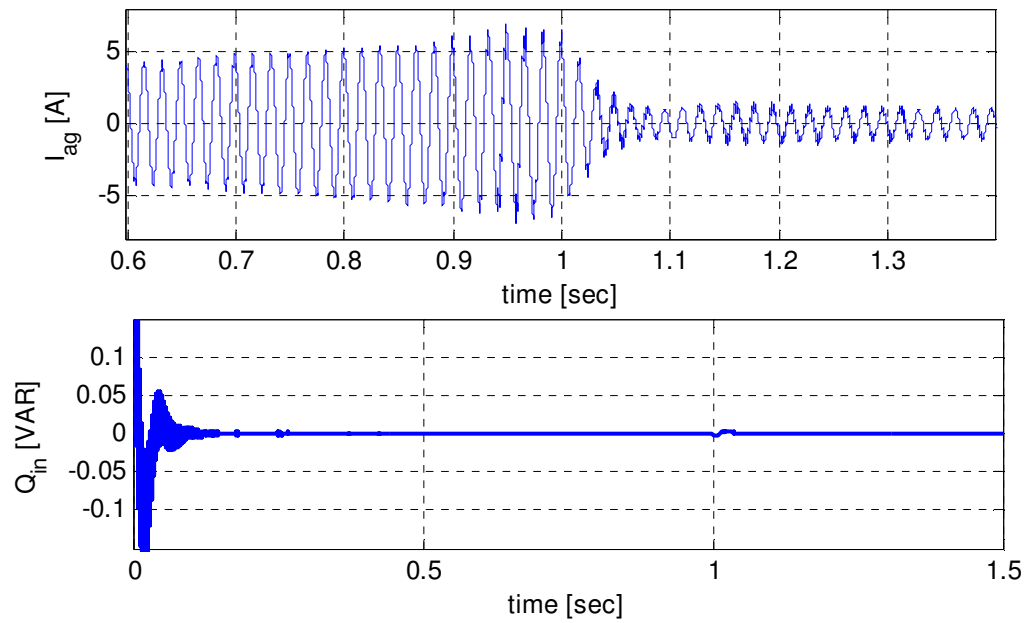


Figure 7.30 Phase 'a' source current and reactive power drawn from the source

7.4 Conclusion

A control scheme consisting of an indirect rotor field oriented control of an induction motor fed by a direct a/ac matrix converter with unity input factor control is illustrated. Since the studied system has non-linear dynamics, the input-output feedback linearization technique is used to design controllers. By analyzing the stability of the zero dynamics, the overall system is found to be input output linearizable and the designed linear controller is implemented. Simulation results verify the robustness of the proposed controllers for load as well as rotor speed variations.

CHAPTER 8

SWITCHING SIGNALS GENERATION IN NI-cRIO CHASIS

8.1 Introduction

This chapter presents the generation of switching signals using NI instruments compact RIO on LabVIEW FPGA environment. A method used to generate these signals is described in detail. A Matlab/SIMULINK has been done based on the actual switching signals obtained from the FPGA to show the validity of the experimental results.

The controller used in this experiment is given in Figure 8.1. It mainly consists of the following four main parts: NI cRIO-9022 RT controller, NI cRIO-9114 Chassis, NI 9403 digital I/O module and NI 9215 analog output modules.

NI cRIO-9114 Chassis

This reconfigurable chassis main part of the compact RION and it is capable of accepting up to 8 compact RIO input/output modules. It has an embedded Xilinx virtex-5 reconfigurable I/O FPGA in it which provides ultimate processing power. The switching signals generation which is described in this chapter are done directly on the embedded FPGA using LabVIEW. Besides, this chassis contains one digital input/output and three analog input modules.

NI 9403

NI 940 is bidirectional digital input/output module for the compact RIO chassis which is shown in slot one of Figure 8.1.

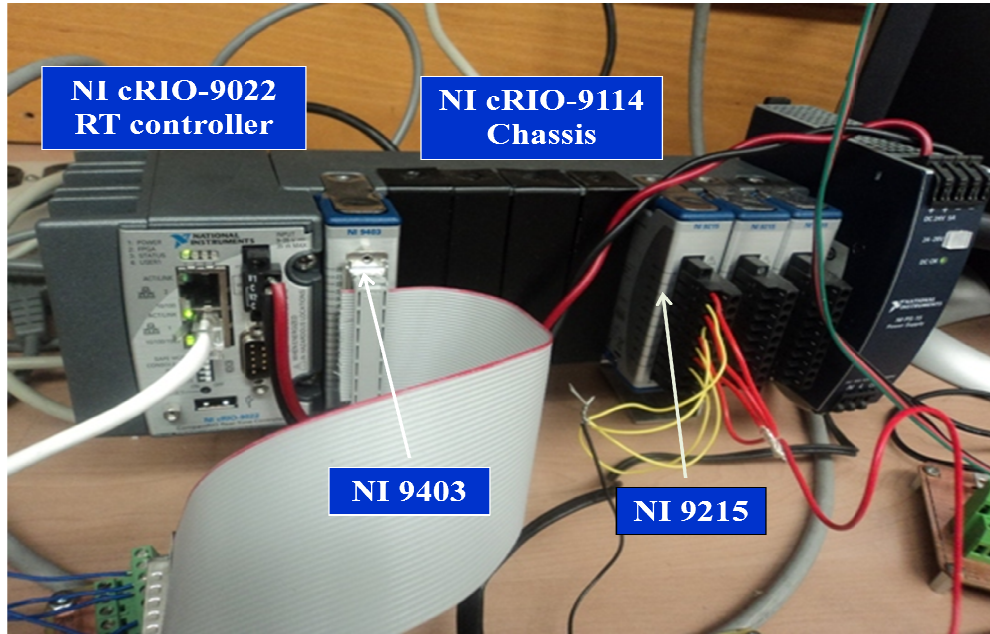


Figure 8.1 Controller used to generate the switching signals

It contains 32 channels and each of them is compatible with 5V TTL output voltages. In this work it is used to collect the switching signals generated by the embedded FPGA.

NI 9215

The NI 9215 module contains 4 analog inputs channels sampled in parallel with 16 bit analog-to-digital converters. The controller contains three analog input modules as shown in the last three slots in Figure 8.1.

8.2 Switching signal generation using direct digital synthesis

The modulation schemes developed in the controller is a carrier pulse modulation which requires a generation of four periodic waveforms. A 30Hz three phase sinusoidal representing the desired output waveforms. Common mode voltage consists of third

harmonic of both input and output voltages. And a 5 kHz triangular carrier signals. To generate these signals inside the FPGA a Direct digital synthesis (DDS) method is implemented which provides high degrees of frequency and phase control. The core components of a DDS waveform generator are the accumulator and lookup table.

8.2.1 Accumulator

The accumulator is a 32 bit counter which stores the current phase value of the generated waveform. The frequency of the generated waveforms is determined by the accumulator increment and the rate at which the accumulator is updated. Therefore, the accumulator increment is calculated based on the desired frequency and the updated rate as given 8.1.

$$\text{Accumulator Increment} = \frac{2^{\text{accumulator bit}}}{\text{Update rate}} * \text{desired frequency} \quad (8.1)$$

Where update rate is the speed at which the while loop being updated and it is can be computed using the update ticks and the FPGA clock speed as shown in (8.2). The update ticks are defined as the number of FPGA clocks required to computer all the program inside the loop.

$$\text{Update rate} = \frac{\text{Clock speed (40Mz)}}{\text{Update ticks}} \quad (8.2)$$

Since the program which generates the switching signals takes 900 update ticks the frequencies are calculated as follows.

$$\text{For } 2\text{kHz, Accumulator Increment} = \frac{2^{\text{accumulator bit}}}{40 \times 10^6} * 900 * 2 \times 10^3 =$$

193272528

$$\text{For } 60\text{Hz, Accumulator Increment} = \frac{2^{\text{accumulator bit}}}{40 \times 10^6} * 900 * 60 = 5798206$$

$$\text{For } 30\text{Hz, Accumulator Increment} = \frac{2^{\text{accumulator bit}}}{40 \times 10^6} * 900 * 30 = 2899103$$

The current accumulator phase shift is used to perform a lookup operation in a lookup table of the reference waveform to determine the next output value. When the accumulator phase value reaches the maximum (360 degrees) it rolls over and starts again at 0 degrees. The expression for the accumulator phase shift is given in (8.3), and it is used to generate balanced three phase sinusoidal voltages.

$$\text{Accumulator phase shift} = \frac{2^{\text{accumulator bit}}}{360} * \text{desired phase shift} \quad (8.3)$$

$$\text{For } 120 \text{ degree, Accumulator phase shift} = \frac{2^{32}}{360} * 120 = 1431655765$$

$$\text{For } 240 \text{ degree, Accumulator phase shift} = \frac{2^{32}}{360} * 240 = 2863311531$$

8.2.2 Lookup Table

The second main component of a DDS is the lookup table which contains data of one cycle of the waveform and typically contains 10 to 13 bits sample points which represent the waveform to be generated. The accumulator value typically 32 bit which is a lot more resolution than the reference waveform.

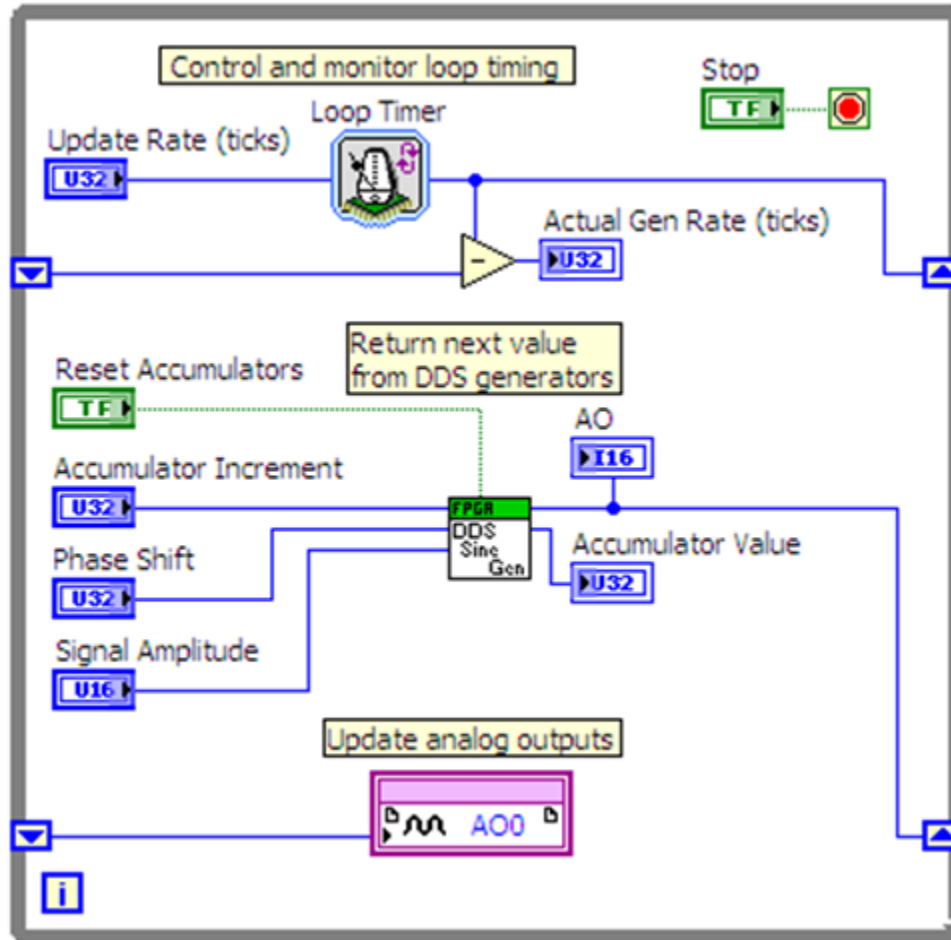


Figure 8.2 FPGA direct digital syntheses

The extra bits can be used for interpolation between two samples in the reference waveform. This interpolation result in a better frequency control and less harmonic distortion in the generated waveform. Figure 8.2 shows the FPGA DDS generator which increments the accumulator and returns the next value for the waveform signal.

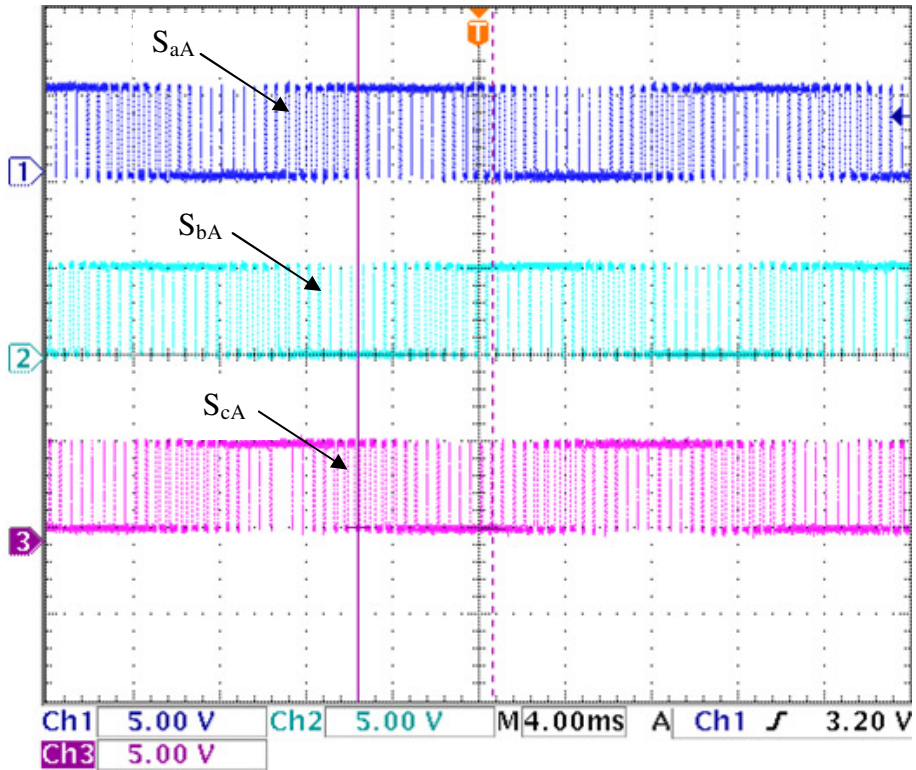


Figure 8.3 Ch1-SaA, Ch2-SbA and Ch3-ScA

There are two ways to determine the third switching signals from the other known switches. One of these methods is by comparing the sum of the all the three modulation signals with the triangular carrier. And the other way of determining it is by turning ON when both the first two switches are OFF or OFF otherwise. Channel 3 and 4 show that it is possible to use either of the above two methods generate the third switching signals. The other switching signals corresponding to phase 'b' and phase 'c' output voltages are shown in Figure 8.5 and 8.6 respectively.

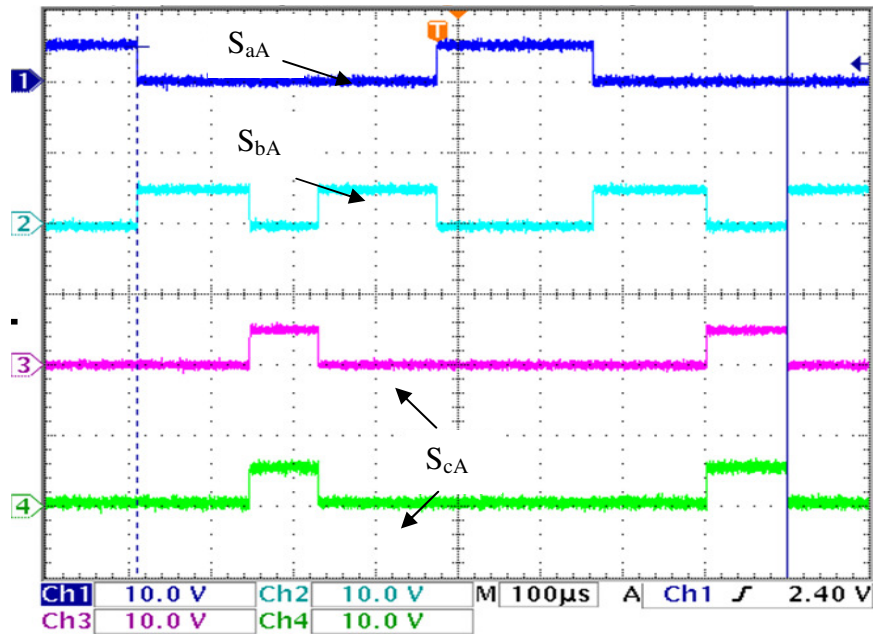


Figure 8.4 Switching signals for phase 'a' output voltage

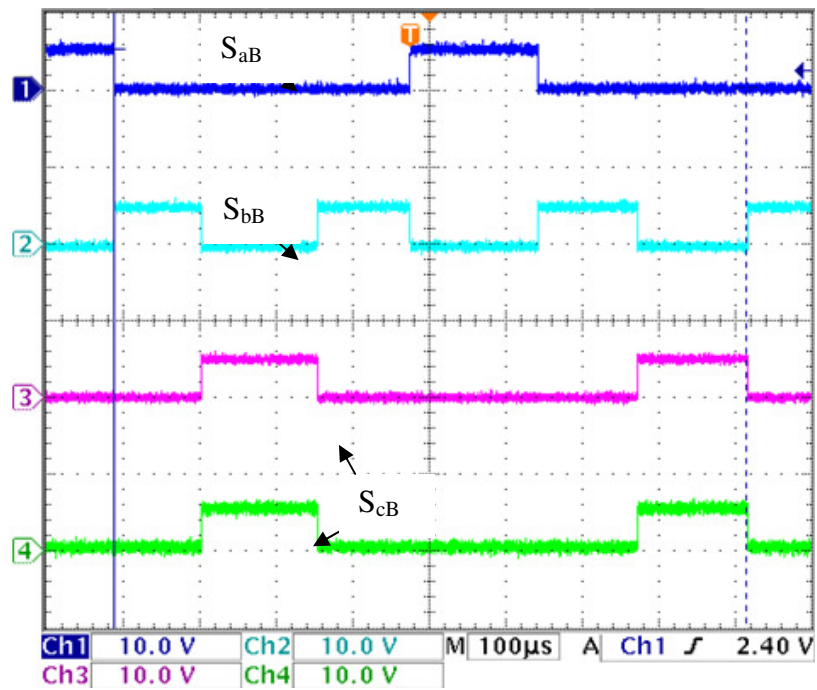


Figure 8.5 Switching signals for phase 'b' output voltage

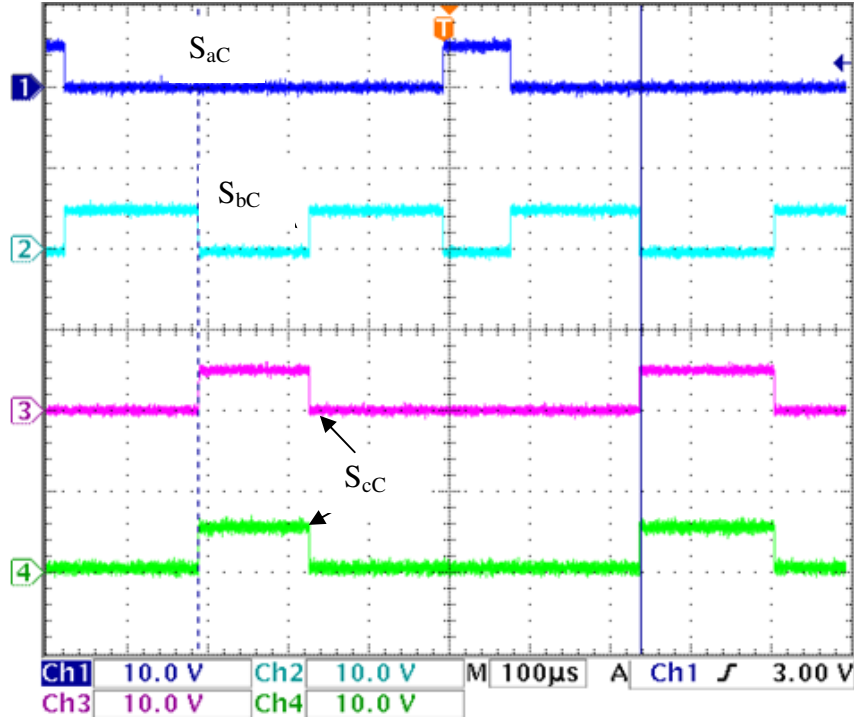


Figure 8.6 Switching signals for phase ‘c’ output voltage

A Matlab/SIMULINK model has also been done based on the actual switching signals obtained from the FPGA outputs. An input balanced three phase voltages of 60Hz and 100V peak-to-peak phase voltages as seen in Figure 8.7 and desired three output voltages of 84V peak-to-peak with 30Hz are considered. After collecting the nine switching signals given in Figure 8.4 to Figure 8.6 and applying it on equation (8.4) and (8.5) result in the output desired voltage. The output three phase voltages which are shown in Figure 8.8 are 30Hz with magnitude almost equal to 84V. These prove that the experimental results are

$$\begin{aligned}
 V_{as} + V_{np} &= S_{aA}V_{ap} + S_{bA}V_{bp} + S_{cA}V_{cp} \\
 V_{bs} + V_{np} &= S_{aB}V_{ap} + S_{bB}V_{bp} + S_{cB}V_{cp} \\
 V_{cs} + V_{np} &= S_{aC}V_{ap} + S_{bC}V_{bp} + S_{cC}V_{cp}
 \end{aligned} \tag{8.4}$$

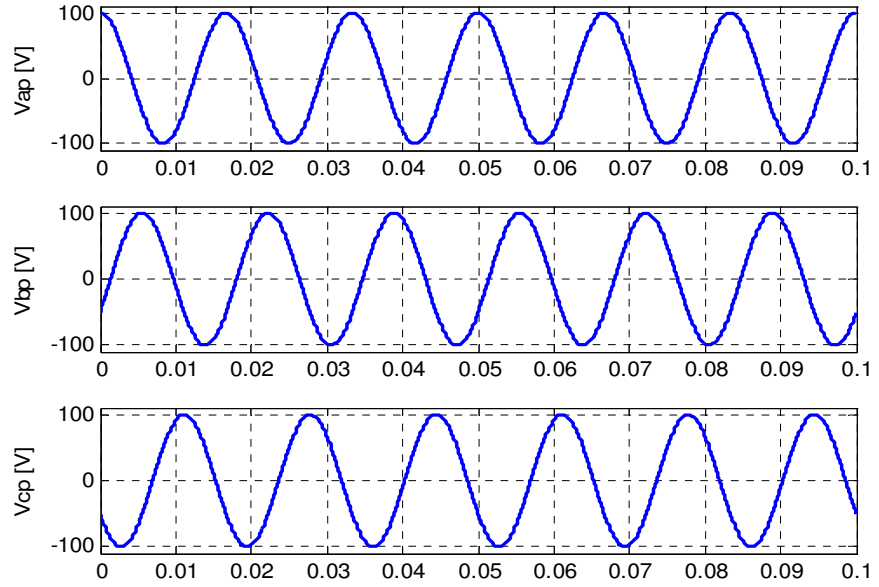


Figure 8.7 Three phase voltages at the input terminal of MC

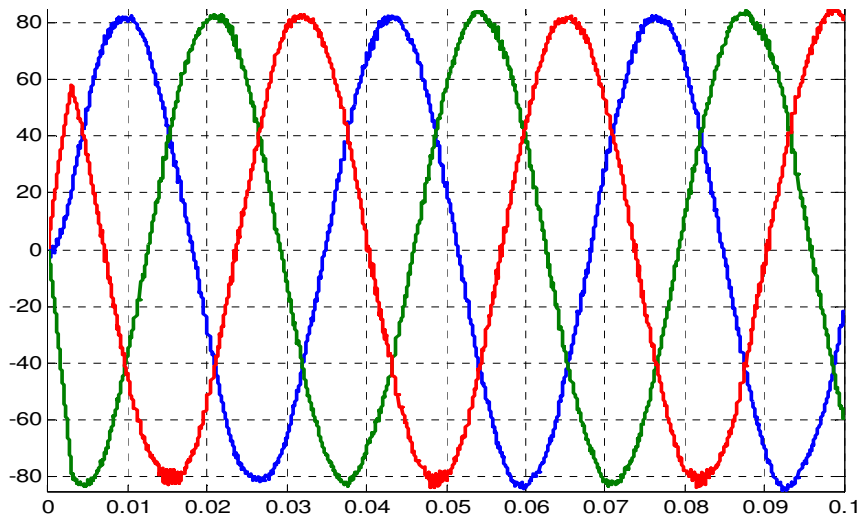


Figure 8.8: Three phase output voltage of MC

$$V_{np} = \frac{1}{3} \left(\begin{array}{l} S_{aA}V_{ap} + S_{bA}V_{bp} + S_{cA}V_{cp} + S_{aB}V_{ap} + \\ S_{bB}V_{bp} + S_{cB}V_{cp} + S_{aC}V_{ap} + S_{bC}V_{bp} + S_{cC}V_{cp} \end{array} \right) \quad (8.5)$$

8.3 Conclusion

The nine switching signals which are used to generate the three phase output voltage of a matrix converter are generated using NI instruments compact RIO. These signals are generated using a carrier based modulation technique developed in chapter three. Collecting the actual data from the FPGA terminals, a simulink model has been developed to validate the generated switching pulses. Results show that the pulses constrict a balanced desired balanced three phase voltage with specified output frequency.

CHAPTER 9

CONCLUSSION AND FUTURE SUGGESTION

9.1 Summary of the Thesis

The thesis presents different modulation techniques for three phase-to-three phase matrix converter. New approaches for determining the modulation signal are derived and it gives the same result as the complex and the more mathematically intensive approaches given in literature. Moreover, the actual switching pulse generations are illustrated. Computer simulations on a Matlab/Simulink platform are done based on the analytical modulation signals' expressions. The results demonstrate the generation of the switching signals which synthesize the output three phase voltages.

This work also investigates the input filter the input filter design for a three phase to three phase matrix converter system. A new method to specify the parameters of the input filters is set forth. The method used a harmonic balance technique to analyze the ripple component of the input current and voltage waveforms. The filter inductor and capacitor are determined based on the specified maximum allowable source current and input capacitor voltage ripples under a specified damping resistance and output rated current. Simulation results verify that the chosen resistance valued keeps the system stable. Moreover, the rated current based designed filter parameters perfectly work for lower output currents. Although the analysis considers only one dominant harmonic component of the input current, the resulting filter are also capable of mitigating lower harmonics.

The proposed approach also maintained a high power factor at the input terminal of the matrix converter which allows wider control range of a matrix converter. In addition, the resonance frequency of the determined filter parameter are sufficiently lower than the switching frequency and far from the fundamental.

A complete dynamic modeling and steady state analysis of the matrix converter feeding an RL load is given in this thesis. This work in particular derives a new generalized steady state analysis which enables to study the operation of the overall system operating in various power factor operations. In addition, dynamic and steady state analysis are developed for matrix converter fed induction motor system. In the above both cases a computer simulation has been done to verify the theoretical analysis. From the simulation results, it was possible to see the starting transient and the dynamic response to a sudden change of the load during the steady state operation. Besides the performance characteristics of the drive system has been discussed.

The thesis also present stability study of a matrix converter fed induction motor drive system. This study is based on small signal model in synchronous reference frame. The stability margin by examining the real values of the dominant eigen values of the system characteristic matrix. The elements of this matrix, which are the operating points, are evaluated through the derived approaches of steady state analysis. The work also shows that the stability of the overall drive system is affected by different system parameters. A lower damper resistance improves the stability of the system by drawing high frequency components of the input current; however, this power loss in the damping resistance becomes more significant if the resistance is too small. It is also noticed that drive system has wider stability region while operating at a leading input power factor

power factor than with a lagging power factor under the specified system parameters. The impact of the stator and rotor resistance variation on drive stability analysis is also considered in thesis. Although the rotor and stator resistance increase due to heating creates a challenge on the high performance induction machine control, it narrows the instability margins. A computer simulation has been done to clearly shown stable and unstable regions by observing the input and output voltage and current waveforms.

A high performance vector control of motor fed by a direct *a/ac* matrix converter with unity input factor control is developed in this thesis. This control uses a rotor field orientation indirect vector control by aligning the rotor flux in the synchronous reference frame. Unlike most work presented in literature, the *q*-axis rotor current is controlled to be zero. This guarantee that flux is actually oriented rather than assuming a zero. The input-output feedback linearization technique is used as approaches to design the non linear system. Detailed controller design is presented based on the conventional linear controller design since the non linear system is input-output linearizable. Simulation results verify the robustness of the proposed controllers for different load and rotor speed variation.

Finally, the progress in the experimental results is conducted through the generation of the actual nine firing pulses of the bidirectional switches using a carrier based modulation technique which is relatively easier to implement as compared to the space vector modulation. This is done on the NI instruments compact RIO on LabVIEW FPGA environment. The validity of the generated pulses is verified by computer simulation which is based on the actual pulses collected from the FPGA terminals. The results shows

that the generated firing pulses give a balanced set of output voltages with the desired magnitude and frequency.

9.2 List of Contributions

The main contributions of the thesis are listed below

- A complete derivation of the expression of the modulation signals based on carrier based pulse width modulation is given. This expression can be used for both balanced and unbalanced source voltages. Since it is relatively simple, it can suitably used for practical implementation.
- The thesis clearly present a detailed dynamic analysis for a matrix converter fed induction motor drive system and MC feeding a linear load in synchronous reference frame. This method uniquely represents the modulation signals in four scalar components hence it requires less computation as compared to working on vectors.
- Fourier representations of the switching signals of the matrix converter are derived. And a new approach of determining the input filter parameters is presented. The filter designed in this work not only satisfies the minimum input power factor requirements but also it is designed to attenuate the maximum allowable input capacitor voltage ripples.

- A new generalized steady state performance analysis is set forth in cases where the matrix converter feeds induction motor as well as linear load. This modeling can be used for both unity and non-zero reactive power at the source side. Unlike most of the works which consider a unity input power factor to examine the steady state operations, the analysis presented in this thesis help to study the matrix converter based system operating in a leading and lagging input power factors.
- A new small signal model based stability analysis is proposed for a matrix converter fed induction motor drive system. Based on this analysis, different factors which affect the stability of a matrix converter based drive are discussed. This includes the effect of damping resistance in the input filter, the stator and rotor resistances variations in the induction motor due to heating and the input power factor.

9.3 Future Work

Most of the analytical results presented in the thesis are verified with a computer simulation. Although the actual switching signals are generated and tested as demonstrated in the previous chapter, it is necessary to implement on the actual converter system. Part of the hard ware needed to conduct an experiment are already done and described below.

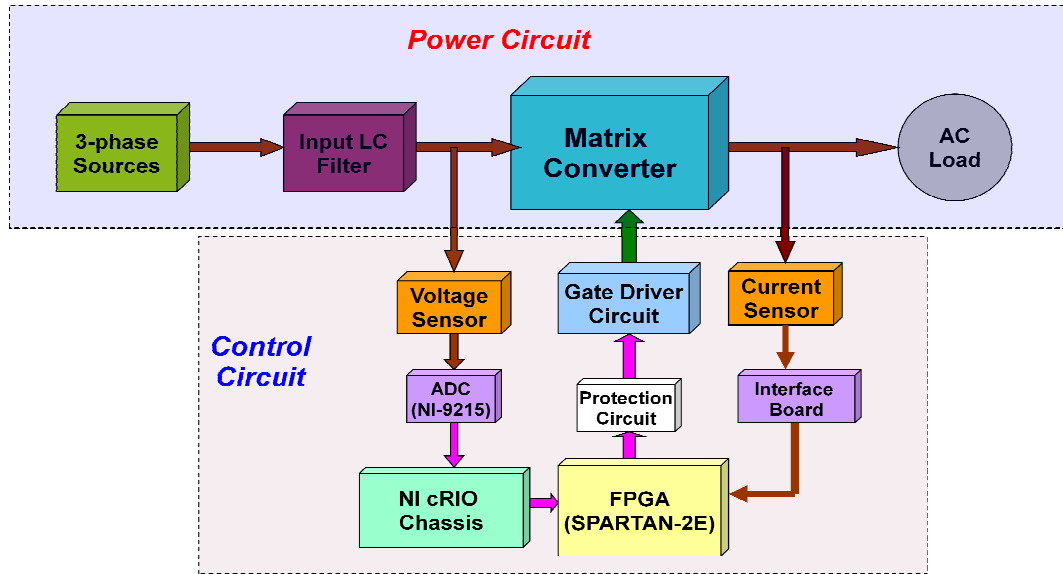


Figure 9.1 Block diagram for the experimental set up

The block diagram of the experimental system consisting of the power circuit and the control unit is given in Figure 9.1. The SPARTAN-2E FPGA is used for commutation circuit. This commutation processes needs information about the output current direction; therefore, it is necessary to build a sensor current with the associated FPGA-current sensor interface board as seen in Figure 9.3. The power stage of the matrix converter is realized with a nine bidirectional switches, Semicron SK60GM124 modules. The module consists of two IGBTs with common emitter connection and built in fast recovery diodes. The power circuit as well as the gate driver board are done on PCB. External connectors are used to interface the gate driver with the IGBTs as shown in Figure 9.2. The external interfacing board used to connect the Compact RIO with the SPARTAN-2E is shown in Figure 9.4.

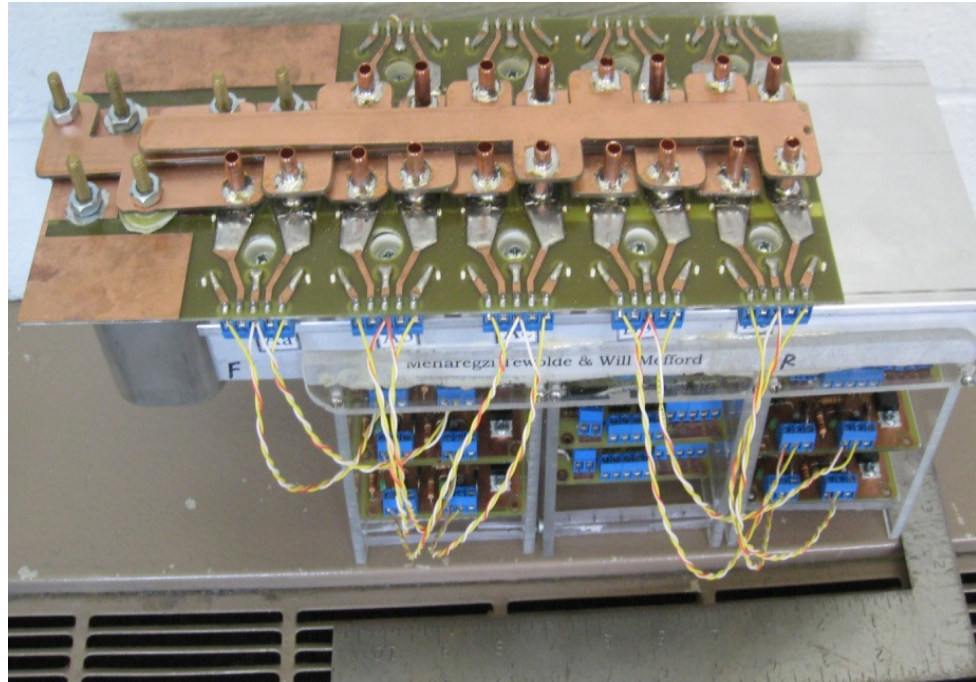


Figure 9.2 Laboratory prototype 3x3 matrix converter

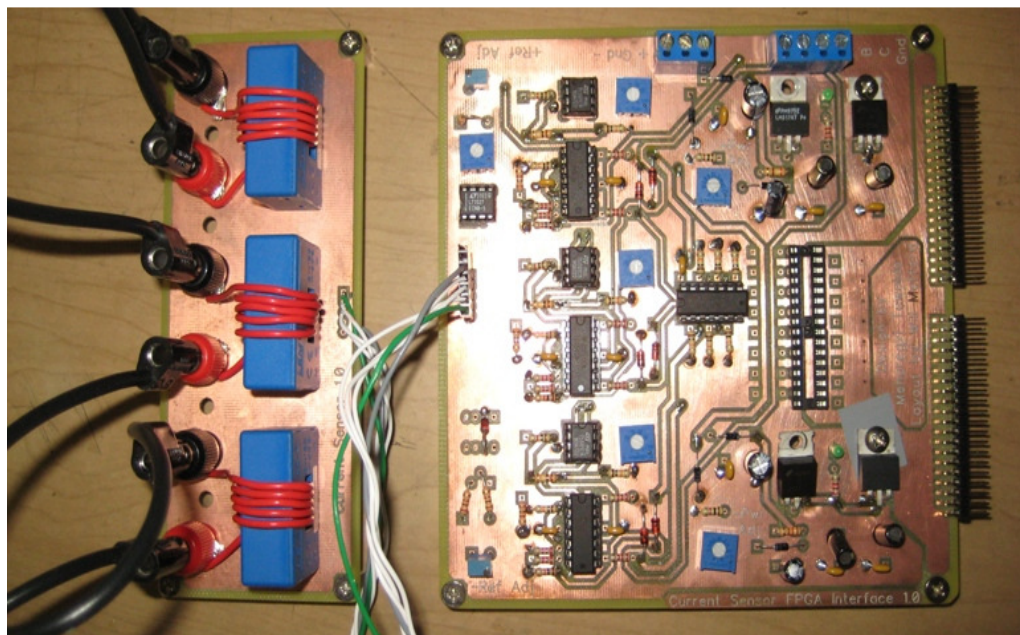


Figure 9.3 Current sensor-FPGA interface board

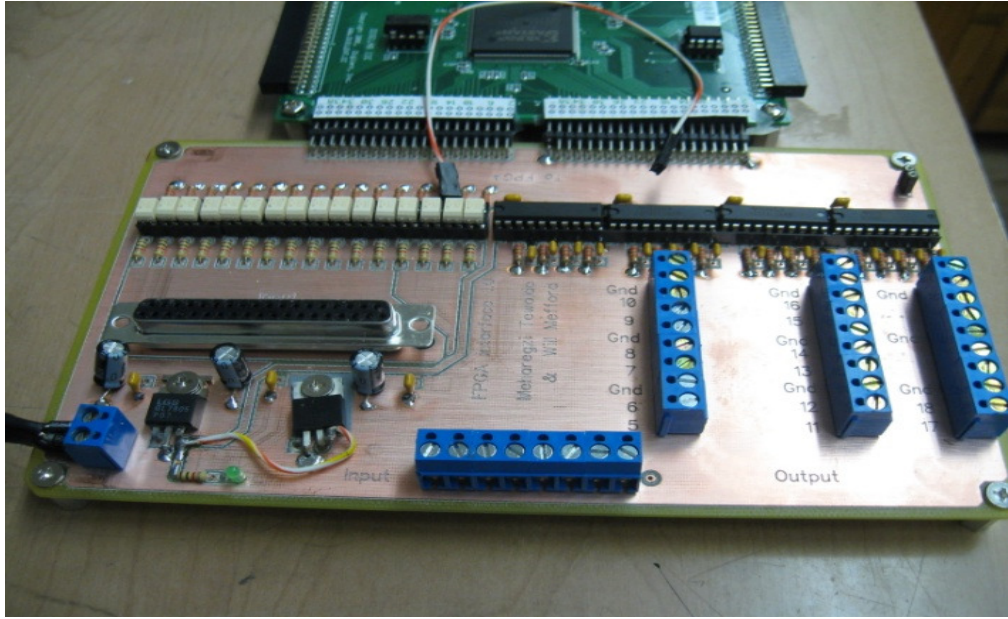


Figure 9.4 Compact cRio-FPGA interfacing board

REFERENCES

- [1] L. Gyugyi and B. R. Pelly, *Static Power Frequency Changers: Theory, Performance and Application*, John Wiley & Sons, New York, 1976.
- [2] Alesina and M. Venturini, "Solid-state Power Conversion: A Fourier Analysis Approach to Generalized Transformer Synthesis," *IEEE Transactions On Circuits and System*, vol. CAS-28, pp. 319–330, Apr. 1981.
- [3] A. Alesina and M. Venturini, "Analysis and Design of Optimum Amplitude Nine-switch Direct AC-AC Converters," *IEEE Transactions on Power Electronics*, vol. 4, no. 1, pp. 101-112, Jan. 1989.
- [4] G. Holmes and T. A. Lipo, "Implementation of a Controlled Rectifier Using AC-AC Matrix Converter Theory," *IEEE Transactions on Power Electronics*, vol. 7, no. 1, pp. 240-250, Jan. 1992.
- [5] G. Holmes, "Unified Modulation Algorithm for Voltage and Current Source Inverters based on AC-AC Matrix Converter Theory," *IEEE Transactions on Industry Applications*, vol. 28, no. 1, pp. 31-40, Jan/Feb 1992.
- [6] D. L. Huber and D. Borojevic, "Space Vector Modulated Three-phase to Three-phase Matrix Converter with Input power Factor Correction," *IEEE Transactions on Power Electronics*, vol. 31, no. 6, pp. 1234-1246, Nov./Dec. 1995.
- [7] D. Casadei, G. Serra and A. Tani, "Reduction of the Input Current Harmonic Content in Matrix Converters under Input/output Unbalance," *IEEE Transactions on Industrial Electronics*, vol. 5, no. 3, pp. 401-411, Jun 1998.
- [8] P. W. Wheeler, J. Rodriguez, J. C. Clare, L. Empringham and A. Weinstein, "Matrix Converters: A Technology Review," *IEEE Transactions on Industrial Electronics*, vol. 49, no. 2, pp. 276-288, Apr. 2002.
- [9] C. Klumpner, P. Nielsen, I. Boldea and F. Blaabjerg, "A new matrix converter motor (MCM) for industry applications," *IEEE Transactions on Industrial Electronics*, vol. 49, no. 2, pp. 325-335, Apr. 2002.

- [10] J. Clare and P. Wheeler, "New Technology: Matrix converters", *IEEE IES Newsletter*, vol. 52, no. 1, pp. 10-12, Mar. 2005.
- [11] P. W. Wheeler, J.C. Clare, L. Empringham, M. Apap and M. Bland, "Matrix Converters", *IEEE Power Eng., Journal*, vol. 16, no. 6, pp. 273- 282, Dec. 2002.
- [12] P. W. Wheeler, P. Zanchetta, J. C. Clare, L. Empringham, M. Bland and D. Katsis, "A Utility Power Supply Based on a Four-Output Leg Matrix Converter," *IEEE Transactions on Industry Applications*, vol. 44, no. 1, pp. 174-186, Jan.-Feb. 2008.
- [13] P. W. Wheeler, P. Zanchetta, J. C. Clare, L. Empringham, M. Bland and D. Katsis, "Control Design of a Three-Phase Matrix-Converter-Based AC-AC Mobile Utility Power Supply," *IEEE Transactions on Industrial Electronics*, vol. 55, no.1, pp. 209-217, Jan. 2008.
- [14] R. Vargas, J. Rodriguez, U. Ammann, P. W. Wheeler, "Predictive Current Control of an Induction Machine Fed by a Matrix Converter With Reactive Power Control," *IEEE Transactions on Industrial Electronics*, vol. 55, no. 12, pp. 4362-4371, Dec. 2008
- [15] P. W. Wheeler, J. C. Clare, M. Apap and K. J Bradley, "Harmonic Loss Due to Operation of Induction Machines From Matrix Converters," *IEEE Transactions on Industrial Electronics*, vol. 55, no. 2, pp. 809-816, Feb. 2008.
- [16] A. Arias, L. Empringham, G. M. Asher, P. M. Wheeler, M. Bland, M. Apap, M. Sumner and J. C. Clare, "Elimination of Waveform Distortions in Matrix Converters Using a New Dual Compensation Method," *IEEE Transactions on Industrial Electronics*, vol. 54, no. 4, pp. 2079-2087, Aug. 2007.
- [17] S. L. Arevalo, P. Zanchetta, P. W. Wheeler, A. Trentin and L. Empringham, "Control and Implementation of a Matrix-Converter-Based AC Ground Power-Supply Unit for Aircraft Servicing," *IEEE Transactions on Industrial Electronics*, vol. 57, no. 6, pp. 2076-2084, June 2010.

- [18] P. W. Wheeler, J.C. Clare and L. Empringham, "A Vector Controlled MCT Matrix Converter Induction Motor Drive with Minimized Commutation Times and Enhanced Waveform Quality," in *proc. IAS'02*, vol. 1, no., pp. 466- 472, 2002.
- [19] D. Casadei, G. Serra and A. Tani, "The Use of Matrix Converters in Direct Torque Control of Induction Machines," *IEEE Transactions on Industrial Electronics*, vol. 48, no. 6, pp. 1057-1064, Dec 2001.
- [20] R. W. Bucknall and K. M. Ciaramella, "On the Conceptual Design and Performance of a Matrix Converter for Marine Electric Propulsion," *IEEE Transactions on Power Electronics*, vol. 25, no. 6, pp. 1497-1508, June 2010.
- [21] L. Zarri, M. Mengoni and O. Ojo, "Improvement in the Control Range of Matrix Converter," in *proc. IEEE ECCE'11*, Phoenix, AZ, Sept. 2011.
- [22] Y. Shi, X. Yang, Q. He and Z. Wang, "Research on a novel capacitor clamped multilevel matrix converter," *IEEE Transactions on Power Electronics*, vol. 20, no. 5, pp. 1055- 1065, Sept. 2005.
- [23] P. C. Loh; R. Rong; F. Blaabjerg and P. Wang, "Digital Carrier Modulation and Sampling Issues of Matrix Converters," *IEEE Transactions on Power Electronics*, vol. 24, no. 7, pp. 1690-1700, July 2009.
- [24] P. Nielsen, F. Blaabjerg and J. K. Pedersen, "New protection issues of a matrix converter: design considerations for adjustable-speed drives," *IEEE Transactions on Industry Applications*, vol. 35, no. 5, pp. 1150-1161, Sep/Oct 1999.
- [25] J. W. Kolar, F. Schafmeister, S. D. Round and H. Ertl, "Novel Three-Phase AC-AC Sparse Matrix Converters," *IEEE Transactions on Power Electronics*, vol. 22, no. 5, pp. 1649-1661, Sept. 2007.
- [26] D. Casadei, G. Serra, A. Tani and L. Zarri, "Matrix converter Modulation Strategies: A New General Approach Based on Space Vector Representation of the Switch State," *IEEE Transactions on Industrial Electronics*, vol. 49, no. 2, pp. 370-381, Apr. 2002.

- [27] A. G. H. Accioly, F. Bradaschia, M. C. Cavalcanti, F. A. S. Neves and V. N. Lima, "Generalized Modulation Strategy for Matrix Converters - Part I," *IEEE Transactions on Industrial Electronics*, vol. 56, no. 2, pp. 326-336, Feb. 2009.
- [28] F. Bradaschia, M. C. Cavalcanti, F. A. S. Neves, V. N. Lima and A. G. H. Accioly, "Generalized Modulation Strategy for Matrix Converters - Part II", in *proc. on IEEE PESC' 07*, pp.665-671, 17-21 June 2007.
- [29] L. Helle, K. B Larsen, A. H. Jorgensen, S. Munk-Nielsen and F. Blaabjerg, "Evaluation of modulation schemes for three-phase to three-phase matrix converters," *IEEE Transactions on Industrial Electronics*, vol. 51, no.1, pp. 158- 171, Feb. 2004.
- [30] F. Gao and M. R. Iravani, "Dynamic Model of a Space Vector Modulated Matrix Converter," *IEEE Transactions on Power Delivery*, vol. 22, no.3, pp. 1696-1705, July 2007.
- [31] H. M. Nguyen, H. Lee and T. Chun, "Input Power Factor Compensation Algorithms Using a New Direct-SVM Method for Matrix Converter" *IEEE Transactions on Industrial Electronics*, vol. 58, no. 1, pp. 232-243, Jan. 2011.
- [32] D. Casadei, G. Serra, A. Tani and L. Zarri, "Optimal Use of Zero Vectors for Minimizing the Output Current Distortion in Matrix Converters" *IEEE Transactions on Industrial Electronics*, vol. 56, no. 2, pp. 326-336, Feb. 2009.
- [33] M. Mihret, M. Abreham, O. Ojo and S. Karugaba, "Modulation Schemes for Five-Phase to Three-phase AC-AC Matrix Converters," in *proc. IEEE ECCE'10*, Atlanta, GA, 2010, pp. 1887-1893.
- [34] S. Ahmed, A. Iqbal, H. Abu-Rub, J. Rodriguez, C. Rojas and M. Saleh, "Simple Carrier Based PWM Technique for a Three-to-Nine Phase Direct AC-AC Converter," *IEEE Transactions on Industrial Electronics*, , vol. 58, no. 11, pp. 5014-5023, Nov. 2011.
- [35] J. W. Kolar, F. Schafmeister, S. D. Round and H. Ertl, "Novel Three-Phase AC-AC Sparse Matrix Converters," *IEEE Transactions on Power Electronics*, vol. 22, no. 5, pp. 1649-1661, Sept. 2007.

- [36] S. Ahmed, A. Iqbal, H. Abu-Rub, "Generalized Duty-Ratio-Based Pulse Width Modulation Technique for a Three-to-k Phase Matrix Converter," *IEEE Transactions on Industrial Electronics*, vol. 58, no. 9, pp. 3925-3937, Sept. 2011.
- [37] H. Hojabri, H. Mokhtari and L. Chang, "A Generalized Technique of Modeling, Analysis, and Control of a Matrix Converter Using SVD," *IEEE Transactions on Industrial Electronics*, vol. 58, no. 3, pp. 949-959, Mar 2011.
- [38] A. Iqbal, E. Levi, M. Jones, S. N. Vukosavic, "Generalised Sinusoidal PWM with Harmonic Injection for Multi-Phase VSIs," *in proc. on IEEE PESC '06*. pp. 1-7, 18-22 June 2006.
- [39] A. Iqbal, E. Levi, M. Jones, S. N. Vukosavic, "Generalised Sinusoidal PWM with Harmonic Injection for Multi-Phase VSIs," *in proc. on IEEE PESC '06*. pp. 1-7, 18-22 June 2006.
- [40] D. Casadei, G. Serra, A. Tani and L. Zarri, "Effects of input voltage measurement on stability of matrix converter drive system," *IEE Proceedings on Electric Power Applications*, vol. 151, no. 4, pp. 487- 497, 7 July 2004.
- [41] R. Cardenas, R. Pena, G. Tobar, J. Clare, P. Wheeler and G. Asher, "Stability Analysis of a Wind Energy Conversion System Based on a Doubly Fed Induction Generator Fed by a Matrix Converter," *IEEE Transactions on Industrial Electronics*, vol. 56, no. 10, pp. 4194-4206, Oct. 2009.
- [42] F. Liu, C. Klumpner and F. Blaabjerg, "Stability analysis and experimental evaluation of a matrix converter drive system," *in proc. on IEEE IECON '03.*, vol. 3, pp. 2059-2065, Nov. 2003.
- [43] F. Liu, C. Klumpner and F. Blaabjerg, "A robust method to improve stability in matrix converters," *in proc. on. IEEE PESC*, vol. 5, pp. 3560- 3566, June 2004.
- [44] D. Casadei, J. Clare, L. Empringham, G. Serra, A. Tani, A. Trintin, P. Wheeler and L. Zarri, "Large signal model for the stability analysis of matrix converters," *IEEE Transactions on Industrial Electronics*, vol. 54, no. 2, pp. 939-950, Apr. 2007.

- [45] M. Mihret, and O. Ojo, "Modeling and analysis of an AC-AC matrix converter feeding an induction motor," in *proc. IEEE APEC'11*, Fortworth, TX, 2011, pp. 1902-1909.
- [46] K. Lee and F. Blaabjerg, "Simple Power Control for Sensorless Induction Motor Drives Fed by a Matrix Converter," *IEEE Transactions on Energy Conversion*, vol. 23, no. 3, pp. 781-788, Sept 2008.
- [47] J. I. Sato, A. Odaka, H. Ohguchi, H. Kodachi and N. Eguchi, "A novel approach to practical matrix converter motor drive system with reverse blocking IGBT," *IEEE Transactions on Power Electronics*, vol. 20, no. 6, pp. 1356- 1363, Nov. 2005.
- [48] P. W. Wheeler, H. Zhang, D. A. Grant, "A theoretical and practical consideration of optimised input filter design for a low loss matrix converter," in *proc. on Fifth International Conference on Power Electronics and Variable-Speed Drives*, vol., no., pp. 363-367, Oct 1994.
- [49] V. Vlatkovic, D. Borjovic and F. C. Lee, "Input filter design for power factor correction circuits," , *IEEE Transactions on Power Electronics*, vol. 11, no. 1, pp. 199-205, Jan 1996.
- [50] D. Casadei, P. Nielsen, G. Serra and A. Tani, "Theoretical and Experimental Analysis of SVM-Controlled Matrix" *Trans. on ELECTROMOTION*, no. 4, pp. 28-37, 1997.
- [51] H. She, H. Lin, X. Wang and L. Yue, "Damped input filter design of matrix converter," *Power Electronics and Drive Systems, 2009. PEDS 2009. International Conference on*, pp.672-677, 2-5 Nov. 2009.
- [52] T. F. Podlesak and D. Katsis, "A 150 kVA vector controlled matrix converter induction motor drive," *Industry Applications Conference, 39th IAS Annual Meeting. Conference Record of the 2004 IEEE*, vol. 3, pp. 1811- 1816, Oct. 2004.
- [53] S. Bernet, Ponnaluri and R. Teichmann, "Design and loss comparison of matrix converters, and voltage-source converters for modern AC drives," *IEEE Transactions on Industrial Electronics*, vol. 49, no. 2, pp. 304-314, Apr 2002.

- [54] T. Kume, K. Yamada, T. Higuchi, E. Yamamoto, H. Hara, T. Sawa and M. M Swamy, "Integrated Filters and Their Combined Effects in Matrix Converter," *IEEE Transactions on Industry Applications*, vol. 43, no. 2, pp. 571-581, Mar.-Apr. 2007.
- [55] I. Deslauriers, N. Avdiu, B. K. Ooi, "Naturally sampled triangle carrier PWM bandwidth limit and output spectrum," *in proc. on IECON'02*, vol. 1, pp. 1- 5, Nov. 2002.
- [56] M. Odavic, M. Sumner, P. Zanchetta and J. C. Clare, "A Theoretical Analysis of the Harmonic Content of PWM Waveforms for Multiple-Frequency Modulators," *IEEE Transactions on Power Electronics*, vol. 25, no. 1, pp. 131-141, Jan. 2010.
- [57] N. R. Zargari, G. Joos and P. D. Ziogas, "Input filter design for PWM current-source rectifiers," *IEEE Transactions on Industry Applications*, vol. 30, no. 6, pp. 1573, Nov/Dec 1994.
- [58] D. G. Holmes and T. A. Lipo, *Pulse Width Modulation for Power Converters*, New York: Wiley, 2003.
- [59] P. Wood, *Switching Power Converters*, Robert E. Krieger publishing company, inc, Florida, 1984.
- [60] R. Stengel, *Stochastic Optimal Control*, Wiley, New York.
- [61] G. N. Watson, *Theory of Bessel Functions*, Cambridge, U.K., Cambridge Univ. Press, 1944.
- [62] S. Karugaba, "Dynamics and Control of a Five Phase Induction Machine," PhD Dissertation, Tennessee Technological University, 2008.
- [63] G. Dong, "Sensorless and Efficiency Optimized Induction Machine Control with Associated Converter PWM Modulation Scheme," PhD Dissertation, Tennessee Technological University, 2005.
- [64] J. Thongam, "High Performance Sensorless Induction Motor Drive," PhD Dissertation, University of Quebec at Chicoutimi, 2006.

- [65] Z. Wu, "An Investigation of Dual Stator Winding Induction Machines," PhD Dissertation, Tennessee Technological University, 2006.
- [66] K. Lee and F. Blaabjerg, "Improved sensorless vector control for induction motor drives fed by a matrix converter using nonlinear modeling and disturbance observer," *IEEE Transactions on Energy Conversion*, vol. 21, no. 1, pp. 52- 59, March 2006.
- [67] L. Zarri, "Control of Matrix Converter," PhD Dissertation, University of Bologna, 2007.
- [68] K. Lee, F. Blaabjerg, "Sensorless DTC-SVM for Induction Motor Driven by a Matrix Converter Using a Parameter Estimation Strategy," *IEEE Transactions on Industrial Electronic*, vol. 55, no. 2, pp. 512-521, Feb. 2008.
- [69] K. Lee and F. Blaabjerg, "Simple Power Control for Sensorless Induction Motor Drives Fed by a Matrix Converter," *IEEE Transactions on Energy Conversion*, vol. 23, no. 3, pp. 781-788, Sept. 2008.
- [70] O. Ojo, Z. Wu, G. Dong and S. K. Asuri, "High-performance speed-sensorless control of an induction motor drive using a minimalist single-phase PWM converter," *IEEE Transactions on Industry Applications*, vol. 41, no. 4, pp. 996- 1004, July-Aug. 2005.
- [71] L. Ben-Brahim and A. Kawamura, "A fully digitized field-oriented controlled induction motor drive using only current sensors," *IEEE Transactions on Power Electronics* , vol. 39, pp. 241–249, June 1992.
- [72] M. Shin; D. Hyun, S. Cho and S. Choe, "An improved stator flux estimation for speed sensorless stator flux orientation control of induction motors," *IEEE Transactions on Power Electronics*, vol. 15, no.2, pp. 312-318, Mar 2000.
- [73] J. E. Slotine and W. Li, *Applied Nonlinear Control*, Prentice Hall, 1998.
- [74] B. Karanayil, M. F. Rahman and C. Grantham , "Online Stator and Rotor Resistance Estimation Scheme Using Artificial Neural Networks for Vector Controlled Speed Sensorless Induction Motor Drive," *IEEE Transactions on Industrial Electronics*, vol. 54, no. 1, pp. 167-176, Feb. 2007.

- [75] J. Rodriguez, M. Rivera, J. W. Kolar and P. W. Wheeler, "A Review of Control and Modulation Methods for Matrix Converters," *IEEE Transactions on Industrial Electronics*, vol. 59, no.1, pp. 58-70, Jan. 2012.
- [76] P. Kulkarni, M. T. Abraham and S. P. Das, "Design and simulation of a matrix converter-fed scalar controlled of synchronous motor drive," in *proc. on IEEE INDICON 2008*, vol. 1, pp. 69-74, 11-13 Dec. 2008.
- [77] Peter Vas, *Sensorless Vector and Direct Torque Control*, Oxford University Press, 1998.
- [78] M.H. Rashid, *Power Electronics: Circuits, Devices, and Applications*, 2nd Edition, Prentice Hall, 1993.
- [79] D. Casadei, G. Serra, A. Tani and L. Zarri, "Effect of the Switching Strategy on the Input Power Quality of Matrix Converter," in *proc. on IEEE Bologna PowerTech Conference*, vol.1, pp 23-26, June 2003.
- [80] D. Xiao, "Improvement in Sensorless Direct Torque Control for Matrix Converter Driven Interior Permanent Magnet Synchronous Machine," PhD Dissertation, School of Electrical Engineering and Telecommunication, 2010.
- [81] H. D. Black and W. B. Dockrell, *Modulation Theory*, SCRE publication, 1984.
- [82] E. Ibarra, I. Kortabarria, J. Andreu, I. M. Alegria, J. L. Martin and P. Ibanez, "Improvement of the Design Process of Matrix Converter Platforms Using the Switching State Matrix Averaging Simulation Method," *IEEE Transactions on Industrial Electronics*, vol. 59, no. 1, pp. 220-234, Jan. 2012.
- [83] X. Wang, H. Lin, H. She and B. Feng, "A Research on Space Vector Modulation Strategy for Matrix Converter Under Abnormal Input-Voltage Conditions," *IEEE Transactions on Industrial Electronics*, vol. 59, no. 1, pp. 93-104, Jan. 2012.
- [84] P. Kiatsookkanatorn and S. Sangwongwanich, "A Unified PWM Method for Matrix Converters and Its Carrier-Based Realization Using Dipolar Modulation Technique," *IEEE Transactions on Industrial Electronics*, vol. 59, no. 1, pp. 80-92, Jan. 2012.

- [85] A. Dasgupta and P. Sensarma, "An Integrated Filter and Controlled Design for Direct Matrix Converter," in *proc. IEEE ECCE'11*, Phoenix, AZ, Sept. 2011.

APPENDIX

APPENDIX A

COMPLETE DERIVATION OF OUTPUT VOLTAGE SPACE

VECTORS

This section gives the detailed derivation of the output voltage space vector used in the direct space vector modulation. The calculated magnitude and angle of the output voltage space vectors are used to construct Table 3.1

- **Mode AAA**

When $S_{ap} = S_{bp} = S_{cp} = 0$ implies $V_{as} = V_{bs} = V_{cs} = V_{ap}$

The q -axis and d -axis output voltage space vector are determined as below.

$$V_{qs} = \frac{2}{3} \left(V_{as} - \frac{1}{2} V_{bs} - \frac{1}{2} V_{cs} \right) = \frac{2}{3} \left(V_{ap} - \frac{1}{2} V_{ap} - \frac{1}{2} V_{ap} \right) = 0 \quad (\text{A.1})$$

$$V_{ds} = \frac{1}{\sqrt{3}} (V_{cs} - V_{bs}) = \frac{1}{\sqrt{3}} (V_{ap} - V_{ap}) = 0 \quad (\text{A.2})$$

The magnitude and direction of the output voltage space vector respectively are calculated using (A.1) and (A.2) as follows.

$$V_p = \sqrt{V_{qs}^2 + V_{ds}^2} = 0 \quad (\text{A.3})$$

$$\alpha_s = \tan^{-1} \left(\frac{-V_{ds}}{V_{qs}} \right) = 0 \quad (\text{A.4})$$

- **Mode AAB**

The q -axis and d -axis output voltage space vector are determined as below.

$$V_{qs} = \frac{2}{3} \left(V_{as} - \frac{1}{2} V_{bs} - \frac{1}{2} V_{cs} \right) = \frac{2}{3} \left(V_{ap} - \frac{1}{2} V_{ap} - \frac{1}{2} V_{bp} \right) = \frac{1}{3} V_{abp} \quad (\text{A.5})$$

$$V_{ds} = \frac{1}{\sqrt{3}} (V_{cs} - V_{bs}) = \frac{1}{\sqrt{3}} (V_{bp} - V_{ap}) = -\frac{1}{\sqrt{3}} V_{abp} \quad (\text{A.6})$$

The magnitude and direction of the output voltage space vector respectively are calculated using (A.5) and (A.6) as follows.

$$V_p = \sqrt{V_{qs}^2 + V_{ds}^2} = \sqrt{\left(\frac{1}{3} V_{ab} \right)^2 + \left(-\frac{1}{\sqrt{3}} V_{ab} \right)^2} = \frac{2}{3} V_{abp} \quad (\text{A.7})$$

$$\alpha_s = \tan^{-1} \left(\frac{-V_{ds}}{V_{qs}} \right) = \tan^{-1} \left(\frac{\frac{1}{\sqrt{3}} V_{abp}}{\frac{1}{3} V_{abp}} \right) = \tan^{-1}(\sqrt{3}) = \frac{\pi}{3} \quad (\text{A.8})$$

- **Mode AAC**

When $S_{ap} = S_{bp} = 0$ and $S_{cp} = 1$ implies $V_{as} = V_{bs} = V_{ap}$ and $V_{cs} = V_{cp}$

The q -axis and d -axis output voltage space vector are determined as below.

$$V_{qs} = \frac{2}{3} \left(V_{as} - \frac{1}{2} V_{bs} - \frac{1}{2} V_{cs} \right) = \frac{2}{3} \left(V_{ap} - \frac{1}{2} V_{ap} - \frac{1}{2} V_{cp} \right) = -\frac{1}{3} V_{cap} \quad (\text{A.9})$$

$$V_{ds} = \frac{1}{\sqrt{3}} (V_{cs} - V_{bs}) = \frac{1}{\sqrt{3}} (V_{cp} - V_{ap}) = \frac{1}{\sqrt{3}} V_{cap} \quad (\text{A.10})$$

The magnitude and direction of the output voltage space vector respectively are calculated using (A.9) and (A.10) as follows.

$$V_s = \sqrt{V_{qs}^2 + V_{ds}^2} = \sqrt{\left(-\frac{1}{3}V_{cap}\right)^2 + \left(\frac{1}{\sqrt{3}}V_{cap}\right)^2} = \frac{2}{3}V_{cap} \quad (\text{A.11})$$

$$\alpha_s = \tan^{-1}\left(\frac{-V_{ds}}{V_{qs}}\right) = \tan^{-1}\left(\frac{-\frac{1}{\sqrt{3}}V_{cap}}{-\frac{1}{3}V_{cap}}\right) = -\frac{2\pi}{3} \quad (\text{A.12})$$

- **Mode ABA**

When $S_{ap} = S_{cp} = 0$ and $S_{bp} = 1$ implies $V_{as} = V_{cs} = V_{ap}$ and $V_{bs} = V_{bp}$

The q -axis and d -axis output voltage space vector are determined as below.

$$V_{qs} = \frac{2}{3}\left(V_{as} - \frac{1}{2}V_{bs} - \frac{1}{2}V_{cs}\right) = \frac{2}{3}\left(V_{ap} - \frac{1}{2}V_{bp} - \frac{1}{2}V_{ap}\right) = \frac{1}{3}V_{abp} \quad (\text{A.13})$$

$$V_{ds} = \frac{1}{\sqrt{3}}(V_{cs} - V_{bs}) = \frac{1}{\sqrt{3}}(V_{ap} - V_{bp}) = \frac{1}{\sqrt{3}}V_{abp} \quad (\text{A.14})$$

The magnitude and direction of the outputs voltage space vector respectively are calculated using (A.13) and (A.14) as follows.

$$V_s = \sqrt{V_{qs}^2 + V_{ds}^2} = \sqrt{\left(\frac{1}{3}V_{ab}\right)^2 + \left(\frac{1}{\sqrt{3}}V_{ab}\right)^2} = \frac{2}{3}V_{abp} \quad (\text{A.15})$$

$$\alpha_s = \tan^{-1}\left(\frac{-V_{ds}}{V_{qs}}\right) = \tan^{-1}\left(\frac{-\frac{1}{\sqrt{3}}V_{abp}}{\frac{1}{3}V_{abp}}\right) = -\frac{\pi}{3} \quad (\text{A.16})$$

- **Mode ABB**

When $S_{ap} = 0$ and $S_{bp} = S_{cp} = 1$ implies $V_{as} = V_{ap}$ and $V_{bs} = V_{cs} = V_{bp}$

The q -axis and d -axis output voltage space vector are determined as below.

$$V_{qs} = \frac{2}{3} \left(V_{as} - \frac{1}{2} V_{bs} - \frac{1}{2} V_{cs} \right) = \frac{2}{3} \left(V_{ap} - \frac{1}{2} V_{bp} - \frac{1}{2} V_{cp} \right) = \frac{2}{3} V_{abp} \quad (\text{A.17})$$

$$V_{ds} = \frac{1}{\sqrt{3}} (V_{cs} - V_{bs}) = \frac{1}{\sqrt{3}} (V_{cp} - V_{bp}) = 0 \quad (\text{A.18})$$

The magnitude and direction of the outputs voltage space vector respectively are calculated using (A.17) and (A.18) as follows.

$$V_s = \sqrt{V_{qs}^2 + V_{ds}^2} = \sqrt{\left(\frac{2}{3} V_{ab} \right)^2} = \frac{2}{3} V_{abp} \quad (\text{A.19})$$

$$\alpha_s = \tan^{-1} \left(\frac{-V_{ds}}{V_{qs}} \right) = \tan^{-1} \left(\frac{0}{\frac{1}{3} V_{abp}} \right) = 0 \quad (\text{A.20})$$

- **Mode ABC**

When $S_{ap} = 0$, $S_{bp} = 1$ and $S_{cp} = 2$ implies $V_{as} = V_{ap}$, $V_{bs} = V_{bp}$ and $V_{cs} = V_{cp}$

The q -axis and d -axis output voltage space vector are determined as below.

$$V_{qs} = \frac{2}{3} \left(V_{as} - \frac{1}{2} V_{bs} - \frac{1}{2} V_{cs} \right) = \frac{2}{3} \left(V_{ap} - \frac{1}{2} V_{bp} - \frac{1}{2} V_{cp} \right) = V_{ap} \quad (\text{A.21})$$

$$V_{ds} = \frac{1}{\sqrt{3}} (V_{cs} - V_{bs}) = \frac{1}{\sqrt{3}} (V_{cp} - V_{bp}) = -\frac{1}{\sqrt{3}} V_{bcp} \quad (\text{A.22})$$

The line-to-line voltage can be expressed as:

$$V_{ab} = \sqrt{3} V_p \sin(\omega_p t + \frac{2\pi}{3}) \quad (\text{A.23})$$

$$V_{bc} = \sqrt{3} V_p \sin(\omega_p t) \quad (\text{A.24})$$

$$V_{ca} = \sqrt{3} V_p \sin(\omega_p t - \frac{2\pi}{3}) \quad (\text{A.25})$$

The magnitude and direction of the outputs voltage space vector respectively are calculated using (A.21) to (A.25) as follows.

$$V_s = \sqrt{V_{qs}^2 + V_{ds}^2} = \sqrt{V_{ap}^2 + \frac{1}{3}V_{bcp}^2} = V_p \quad (\text{A.26})$$

$$\alpha_s = \tan^{-1}\left(\frac{-V_{ds}}{V_{qs}}\right) = \tan^{-1}\left(\frac{\frac{1}{\sqrt{3}}\sqrt{3}V_p \sin(\omega_p t)}{V_p \cos(\omega_p t)}\right) = \omega_p t \quad (\text{A.27})$$

- **Mode ACA**

When $S_{ap} = S_{cp} = 0$ and $S_{bp} = 2$ implies $V_{as} = V_{cs} = V_{ap}$ and $V_{bs} = V_{cp}$

The q -axis and d -axis output voltage space vector are determined as below.

$$V_{qs} = \frac{2}{3}\left(V_{as} - \frac{1}{2}V_{bs} - \frac{1}{2}V_{cs}\right) = \frac{2}{3}\left(V_{ap} - \frac{1}{2}V_{cp} - \frac{1}{2}V_{ap}\right) = -\frac{1}{3}V_{cap} \quad (\text{A.28})$$

$$V_{ds} = \frac{1}{\sqrt{3}}(V_{cs} - V_{bs}) = \frac{1}{\sqrt{3}}(V_{ap} - V_{cp}) = -\frac{1}{\sqrt{3}}V_{cap} \quad (\text{A.29})$$

The magnitude and direction of the output voltage space vector respectively are calculated using (A.28) and (A.29) as follows.

$$V_s = \sqrt{V_{qs}^2 + V_{ds}^2} = \sqrt{\left(-\frac{1}{3}V_{cap}\right)^2 + \left(-\frac{1}{\sqrt{3}}V_{cap}\right)^2} = \frac{2}{3}V_{cap} \quad (\text{A.30})$$

$$\alpha_s = \tan^{-1}\left(\frac{-V_{ds}}{V_{qs}}\right) = \tan^{-1}\left(\frac{\frac{1}{\sqrt{3}}V_{cap}}{-\frac{1}{3}V_{cap}}\right) = -\frac{2\pi}{3} \quad (\text{A.31})$$

- **Mode ACB**

When $S_{ap} = 0$, $S_{bp} = 2$ and $S_{cp} = 1$ implies $V_{as} = V_{ap}$, $V_{bs} = V_{cp}$ and $V_{cs} = V_{bp}$

The q -axis and d -axis output voltage space vector are determined as below.

$$V_{qs} = \frac{2}{3} \left(V_{as} - \frac{1}{2} V_{bs} - \frac{1}{2} V_{cs} \right) = \frac{2}{3} \left(V_{ap} - \frac{1}{2} V_{bp} - \frac{1}{2} V_{cp} \right) = V_{ap} \quad (\text{A.32})$$

$$V_{ds} = \frac{1}{\sqrt{3}} (V_{cs} - V_{bs}) = \frac{1}{\sqrt{3}} (V_{cp} - V_{bp}) = \frac{1}{\sqrt{3}} V_{bcp} \quad (\text{A.33})$$

The magnitude and direction of the output voltage space vector respectively are calculated using (A.32) and (A.33) as follows.

$$V_s = \sqrt{V_{qs}^2 + V_{ds}^2} = \sqrt{V_{ap}^2 + \frac{1}{3} V_{bcp}^2} = V_p \quad (\text{A.32})$$

$$\alpha_s = \tan^{-1} \left(\frac{-V_{ds}}{V_{qs}} \right) = \tan^{-1} \left(\frac{-\frac{1}{\sqrt{3}} \sqrt{3} V_p \sin(\omega_p t)}{V_p \cos(\omega_p t)} \right) = -\omega_p t \quad (\text{A.33})$$

- **Mode ACC**

When $S_{ap} = 0$, $S_{bp} = 2$ and $S_{cp} = 2$ implies $V_{as} = V_{ap}$, $V_{bs} = V_{cp}$ and $V_{cs} = V_{cp}$

The q -axis and d -axis output voltage space vector are determined as below.

$$V_{qs} = \frac{2}{3} \left(V_{as} - \frac{1}{2} V_{bs} - \frac{1}{2} V_{cs} \right) = \frac{2}{3} \left(V_{ap} - \frac{1}{2} V_{cp} - \frac{1}{2} V_{cp} \right) = -\frac{2}{3} V_{cp} \quad (\text{A.34})$$

$$V_{ds} = \frac{1}{\sqrt{3}} (V_{cs} - V_{bs}) = \frac{1}{\sqrt{3}} (V_{cp} - V_{cp}) = 0 \quad (\text{A.35})$$

The magnitude and direction of the output voltage space vector respectively are calculated using (A.34) and (A.35) as follows.

$$V_s = \sqrt{V_{qs}^2 + V_{ds}^2} = \sqrt{\left(-\frac{2}{3}V_{cap}\right)^2} = \frac{2}{3}V_{cap} \quad (\text{A.36})$$

$$\alpha_s = \tan^{-1}\left(\frac{-V_{ds}}{V_{qs}}\right) = \tan^{-1}\left(\frac{0}{-\frac{1}{3}V_{cap}}\right) = \pi \quad (\text{A.37})$$

- **Mode BAA**

When $S_{ap} = 1$, $S_{bp} = 0$ and $S_{cp} = 0$ implies $V_{as} = V_{bp}$, $V_{bs} = V_{ap}$ and $V_{cs} = V_{ap}$

The q -axis and d -axis output voltage space vector are determined as below.

$$V_{qs} = \frac{2}{3}\left(V_{as} - \frac{1}{2}V_{bs} - \frac{1}{2}V_{cs}\right) = \frac{2}{3}\left(V_{bp} - \frac{1}{2}V_{ap} - \frac{1}{2}V_{ap}\right) = -\frac{2}{3}V_{abp} \quad (\text{A.38})$$

$$V_{ds} = \frac{1}{\sqrt{3}}(V_{cs} - V_{bs}) = \frac{1}{\sqrt{3}}(V_{ap} - V_{ap}) = 0 \quad (\text{A.39})$$

The magnitude and direction of the output voltage space vector respectively are calculated using (A.38) and (A.29) as follows.

$$V_s = \sqrt{V_{qs}^2 + V_{ds}^2} = \sqrt{\left(-\frac{2}{3}V_{abp}\right)^2} = \frac{2}{3}V_{abp} \quad (\text{A.40})$$

$$\alpha_s = \tan^{-1}\left(\frac{-V_{ds}}{V_{qs}}\right) = \tan^{-1}\left(\frac{0}{-\frac{2}{3}V_{abp}}\right) = \pi \quad (\text{A.41})$$

- **Mode BAB**

When $S_{ap} = 1$, $S_{bp} = 0$ and $S_{cp} = 1$ implies $V_{as} = V_{bp}$, $V_{bs} = V_{ap}$ and $V_{cs} = V_{bp}$

The q -axis and d -axis output voltage space vector are determined as below.

$$V_{qs} = \frac{2}{3} \left(V_{as} - \frac{1}{2} V_{bs} - \frac{1}{2} V_{cs} \right) = \frac{2}{3} \left(V_{bp} - \frac{1}{2} V_{ap} - \frac{1}{2} V_{cp} \right) = -\frac{1}{3} V_{abp} \quad (\text{A.42})$$

$$V_{ds} = \frac{1}{\sqrt{3}} (V_{cs} - V_{bs}) = \frac{1}{\sqrt{3}} (V_{bp} - V_{ap}) = -\frac{1}{\sqrt{3}} V_{abp} \quad (\text{A.43})$$

The magnitude and direction of the output voltage space vector respectively are calculated using (A.42) and (A.43) as follows.

$$V_s = \sqrt{V_{qs}^2 + V_{ds}^2} = \sqrt{\left(-\frac{1}{3} V_{abp}\right)^2 + \left(-\frac{1}{\sqrt{3}} V_{abp}\right)^2} = \frac{2}{3} V_{abp} \quad (\text{A.44})$$

$$\alpha_s = \tan^{-1} \left(\frac{-V_{ds}}{V_{qs}} \right) = \tan^{-1} \left(\frac{\frac{1}{\sqrt{3}} V_{abp}}{-\frac{1}{3} V_{abp}} \right) = \frac{2\pi}{3} \quad (\text{A.45})$$

- **Mode BAC**

The q -axis and d -axis output voltage space vector are determined as below.

$$V_{qs} = \frac{2}{3} \left(V_{as} - \frac{1}{2} V_{bs} - \frac{1}{2} V_{cs} \right) = \frac{2}{3} \left(V_{bp} - \frac{1}{2} V_{ap} - \frac{1}{2} V_{cp} \right) = V_{bp} \quad (\text{A.46})$$

$$V_{ds} = \frac{1}{\sqrt{3}} (V_{cs} - V_{bs}) = \frac{1}{\sqrt{3}} (V_{cp} - V_{ap}) = \frac{1}{\sqrt{3}} V_{cap} \quad (\text{A.47})$$

The magnitude and direction of the output voltage space vector respectively are calculated using (A.46) and (A.47) as follows.

$$V_s = \sqrt{V_{qs}^2 + V_{ds}^2} = \sqrt{V_{bp}^2 + \frac{1}{3} V_{cap}^2} = V_p \quad (\text{A.46})$$

$$\alpha_s = \tan^{-1}\left(\frac{-V_{ds}}{V_{qs}}\right) = \tan^{-1}\left(\frac{-\frac{1}{\sqrt{3}}\sqrt{3}V_p \sin(\omega_p t - \frac{2\pi}{3})}{V_p \cos(\omega_p t - \frac{2\pi}{3})}\right) = -\omega_p t + \frac{2\pi}{3} \quad (\text{A.47})$$

- **Mode BBA**

The q -axis and d -axis output voltage space vector are determined as below.

$$V_{qs} = \frac{2}{3}\left(V_{as} - \frac{1}{2}V_{bs} - \frac{1}{2}V_{cs}\right) = \frac{2}{3}\left(V_{bp} - \frac{1}{2}V_{bp} - \frac{1}{2}V_{ap}\right) = -\frac{1}{3}V_{abp} \quad (\text{A.48})$$

$$V_{ds} = \frac{1}{\sqrt{3}}(V_{cs} - V_{bs}) = \frac{1}{\sqrt{3}}(V_{ap} - V_{bp}) = \frac{1}{\sqrt{3}}V_{abp} \quad (\text{A.49})$$

The magnitude and direction of the output voltage space vector respectively are calculated using (A.48) and (A.49) as follows.

$$V_s = \sqrt{V_{qs}^2 + V_{ds}^2} = \sqrt{\left(-\frac{1}{3}V_{ab}\right)^2 + \left(\frac{1}{\sqrt{3}}V_{ab}\right)^2} = \frac{2}{3}V_{abp} \quad (\text{A.50})$$

$$\alpha_s = \tan^{-1}\left(\frac{V_{ds}}{V_{qs}}\right) = \tan^{-1}\left(\frac{-\frac{1}{\sqrt{3}}V_{abp}}{-\frac{1}{3}V_{abp}}\right) = -\frac{2\pi}{3} \quad (\text{A.51})$$

- **Mode BBB**

The q -axis and d -axis output voltage space vector are determined as below.

$$V_{qs} = \frac{2}{3}\left(V_{as} - \frac{1}{2}V_{bs} - \frac{1}{2}V_{cs}\right) = \frac{2}{3}\left(V_{bp} - \frac{1}{2}V_{bp} - \frac{1}{2}V_{bp}\right) = 0 \quad (\text{A.52})$$

$$V_{ds} = \frac{1}{\sqrt{3}}(V_{cs} - V_{bs}) = \frac{1}{\sqrt{3}}(V_{bp} - V_{bp}) = 0 \quad (\text{A.53})$$

The magnitude and direction of the output voltage space vector respectively are calculated using (A.52) and (A.53) as follows.

$$V_s = \sqrt{V_{qs}^2 + V_{ds}^2} = 0 \quad (\text{A.54})$$

$$\alpha_s = \tan^{-1}\left(\frac{V_{ds}}{V_{qs}}\right) = 0 \quad (\text{A.55})$$

- **Mode BBC**

The q -axis and d -axis output voltage space vector are determined as below.

$$V_{qs} = \frac{2}{3}\left(V_{as} - \frac{1}{2}V_{bs} - \frac{1}{2}V_{cs}\right) = \frac{2}{3}\left(V_{bp} - \frac{1}{2}V_{bp} - \frac{1}{2}V_{cp}\right) = \frac{1}{3}V_{bcp} \quad (\text{A.56})$$

$$V_{ds} = \frac{1}{\sqrt{3}}(V_{cs} - V_{bs}) = \frac{1}{\sqrt{3}}(V_{cp} - V_{bp}) = -\frac{1}{\sqrt{3}}V_{bcp} \quad (\text{A.57})$$

The magnitude and direction of the output voltage space vector respectively are calculated using (A.56) and (A.57) as follows.

$$V_p = \sqrt{V_{qs}^2 + V_{ds}^2} = \sqrt{\left(\frac{1}{3}V_{bcp}\right)^2 + \left(-\frac{1}{\sqrt{3}}V_{bcp}\right)^2} = \frac{2}{3}V_{bcp} \quad (\text{A.58})$$

$$\alpha_v = \tan^{-1}\left(\frac{-V_{ds}}{V_{qs}}\right) = \tan^{-1}\left(\frac{\frac{1}{\sqrt{3}}V_{bcp}}{\frac{1}{3}V_{bcp}}\right) = \frac{\pi}{3} \quad (\text{A.59})$$

- **Mode BCA**

The q -axis and d -axis output voltage space vector are determined as below.

$$V_{qs} = \frac{2}{3}\left(V_{as} - \frac{1}{2}V_{bs} - \frac{1}{2}V_{cs}\right) = \frac{2}{3}\left(V_{bp} - \frac{1}{2}V_{ap} - \frac{1}{2}V_{cp}\right) = V_{bp} \quad (\text{A.60})$$

$$V_{ds} = \frac{1}{\sqrt{3}}(V_{cs} - V_{bs}) = \frac{1}{\sqrt{3}}(V_{ap} - V_{cp}) = -\frac{1}{\sqrt{3}}V_{cap} \quad (\text{A.61})$$

The magnitude and direction of the output voltage space vector respectively are calculated using (A.60) and (A.61) as follows.

$$V_s = \sqrt{V_{qs}^2 + V_{ds}^2} = \sqrt{V_{bp}^2 + \frac{1}{3}V_{cap}^2} = V_p \quad (\text{A.62})$$

$$\alpha_s = \tan^{-1}\left(\frac{-V_{ds}}{V_{qs}}\right) = \tan^{-1}\left(\frac{\frac{1}{\sqrt{3}}\sqrt{3}V_p \sin(\omega_p t - \frac{2\pi}{3})}{V_p \cos(\omega_p t - \frac{2\pi}{3})}\right) = \omega_p t - \frac{2\pi}{3} \quad (\text{A.63})$$

- **Mode BCB**

The q -axis and d -axis output voltage space vector are determined as below.

$$V_{qs} = \frac{2}{3}\left(V_{as} - \frac{1}{2}V_{bs} - \frac{1}{2}V_{cs}\right) = \frac{2}{3}\left(V_{bp} - \frac{1}{2}V_{cp} - \frac{1}{2}V_{bp}\right) = \frac{1}{3}V_{bcp} \quad (\text{A.64})$$

$$V_{ds} = \frac{1}{\sqrt{3}}(V_{cs} - V_{bs}) = \frac{1}{\sqrt{3}}(V_{bp} - V_{cp}) = \frac{1}{\sqrt{3}}V_{bcp} \quad (\text{A.65})$$

The magnitude and direction of the output voltage space vector respectively are calculated using (A.64) and (A.65) as follows.

$$V_s = \sqrt{V_{qs}^2 + V_{ds}^2} = \sqrt{\left(\frac{1}{3}V_{bcp}\right)^2 + \left(\frac{1}{\sqrt{3}}V_{bcp}\right)^2} = \frac{2}{3}V_{bcp} \quad (\text{A.66})$$

$$\alpha_s = \tan^{-1}\left(\frac{V_{ds}}{V_{qs}}\right) = \tan^{-1}\left(\frac{-\frac{1}{\sqrt{3}}V_{bcp}}{\frac{1}{3}V_{bcp}}\right) = -\frac{\pi}{3} \quad (\text{A.67})$$

- **Mode BCC**

The q -axis and d -axis output voltage space vector are determined as below.

$$V_{qs} = \frac{2}{3} \left(V_{as} - \frac{1}{2} V_{bs} - \frac{1}{2} V_{cs} \right) = \frac{2}{3} \left(V_{bp} - \frac{1}{2} V_{cp} - \frac{1}{2} V_{cp} \right) = \frac{2}{3} V_{bcp} \quad (\text{A.68})$$

$$V_{ds} = \frac{1}{\sqrt{3}} (V_{cs} - V_{bs}) = \frac{1}{\sqrt{3}} (V_{cp} - V_{cp}) = 0 \quad (\text{A.69})$$

The magnitude and direction of the output voltage space vector respectively are calculated using (A.68) and (A.69) as follows.

$$V_s = \sqrt{V_{qs}^2 + V_{ds}^2} = \frac{2}{3} V_{bcp} \quad (\text{A.70})$$

$$\alpha_s = \tan^{-1} \left(\frac{-V_{ds}}{V_{qs}} \right) = \tan^{-1} \left(\frac{0}{\frac{2}{3} V_{bcp}} \right) = 0 \quad (\text{A.71})$$

- **Mode BCC**

The q -axis and d -axis output voltage space vector are determined as below.

$$V_{qs} = \frac{2}{3} \left(V_{as} - \frac{1}{2} V_{bs} - \frac{1}{2} V_{cs} \right) = \frac{2}{3} \left(V_{cp} - \frac{1}{2} V_{ap} - \frac{1}{2} V_{ap} \right) = \frac{2}{3} V_{cap} \quad (\text{A.72})$$

$$V_{ds} = \frac{1}{\sqrt{3}} (V_{cs} - V_{bs}) = \frac{1}{\sqrt{3}} (V_{ap} - V_{ap}) = 0 \quad (\text{A.73})$$

The magnitude of the output voltage space vector is calculated using (A.72) and (A.73) as follows.

$$V_s = \sqrt{V_{qs}^2 + V_{ds}^2} = \sqrt{\left(\frac{2}{3} V_{cap} \right)^2} = \frac{2}{3} V_{cap} \quad (\text{A.74})$$

The direction of the output voltage space vector is calculated as

$$\alpha_s = \tan^{-1}\left(\frac{-V_{ds}}{V_{qs}}\right) = \tan^{-1}\left(\frac{0}{\frac{1}{3}V_{cap}}\right) = 0 \quad (\text{A.75})$$

- **Mode CAB**

The q -axis and d -axis output voltage space vector are determined as below.

$$V_{qs} = \frac{2}{3}\left(V_{as} - \frac{1}{2}V_{bs} - \frac{1}{2}V_{cs}\right) = \frac{2}{3}\left(V_{cp} - \frac{1}{2}V_{ap} - \frac{1}{2}V_{bp}\right) = V_{cp} \quad (\text{A.76})$$

$$V_{ds} = \frac{1}{\sqrt{3}}(V_{cs} - V_{bs}) = \frac{1}{\sqrt{3}}(V_{bp} - V_{ap}) = -\frac{1}{\sqrt{3}}V_{abp} \quad (\text{A.77})$$

The magnitude and direction of the output voltage space vector respectively are calculated using (A.76) and (A.77) as follows.

$$V_s = \sqrt{V_{qs}^2 + V_{ds}^2} = \sqrt{V_{cp}^2 + \frac{1}{3}V_{abp}^2} = V_p \quad (\text{A.78})$$

$$\alpha_s = \tan^{-1}\left(\frac{-V_{ds}}{V_{qs}}\right) = \tan^{-1}\left(\frac{\frac{1}{\sqrt{3}}\sqrt{3}V_p \sin(\omega_p t + \frac{2\pi}{3})}{V_p \cos(\omega_p t + \frac{2\pi}{3})}\right) = \omega_p t + \frac{2\pi}{3} \quad (\text{A.79})$$

- **Mode CAC**

The q -axis and d -axis output voltage space vector are determined as below.

$$V_{qs} = \frac{2}{3}\left(V_{as} - \frac{1}{2}V_{bs} - \frac{1}{2}V_{cs}\right) = \frac{2}{3}\left(V_{cp} - \frac{1}{2}V_{ap} - \frac{1}{2}V_{cp}\right) = \frac{1}{3}V_{cap} \quad (\text{A.80})$$

$$V_{ds} = \frac{1}{\sqrt{3}}(V_{cs} - V_{bs}) = \frac{1}{\sqrt{3}}(V_{cp} - V_{ap}) = \frac{1}{\sqrt{3}}V_{cap} \quad (\text{A.81})$$

The magnitude and direction of the output voltage space vector respectively are calculated using (A.80) and (A.81) as follows.

$$V_s = \sqrt{V_{qs}^2 + V_{ds}^2} = \sqrt{\left(\frac{1}{3}V_{cap}\right)^2 + \left(\frac{1}{\sqrt{3}}V_{cap}\right)^2} = \frac{2}{3}V_{cap} \quad (\text{A.82})$$

$$\alpha_s = \tan^{-1}\left(\frac{-V_{ds}}{V_{qs}}\right) = \tan^{-1}\left(\frac{-\frac{1}{\sqrt{3}}V_{cap}}{\frac{1}{3}V_{cap}}\right) = -\frac{\pi}{3} \quad (\text{A.83})$$

- **Mode CBA**

The q -axis and d -axis output voltage space vector are determined as below.

$$V_{qs} = \frac{2}{3}\left(V_{as} - \frac{1}{2}V_{bs} - \frac{1}{2}V_{cs}\right) = \frac{2}{3}\left(V_{cp} - \frac{1}{2}V_{ap} - \frac{1}{2}V_{bp}\right) = V_{cp} \quad (\text{A.84})$$

$$V_{ds} = \frac{1}{\sqrt{3}}(V_{cs} - V_{bs}) = \frac{1}{\sqrt{3}}(V_{ap} - V_{cp}) = \frac{1}{\sqrt{3}}V_{abp} \quad (\text{A.85})$$

The magnitude and direction of the output voltage space vector is calculated using (A.84) and (A.85) as follows.

$$V_s = \sqrt{V_{qs}^2 + V_{ds}^2} = \sqrt{V_{cp}^2 + \frac{1}{3}V_{abp}^2} = V_p \quad (\text{A.86})$$

The direction of the output voltage space vector is

$$\alpha_s = \tan^{-1}\left(\frac{-V_{ds}}{V_{qs}}\right) = \tan^{-1}\left(\frac{-\frac{1}{\sqrt{3}}\sqrt{3}V_p \sin(\omega_p t + \frac{2\pi}{3})}{V_p \cos(\omega_p t + \frac{2\pi}{3})}\right) = -\omega_p t - \frac{2\pi}{3} \quad (\text{A.87})$$

- **Mode CBB**

The q -axis and d -axis output voltage space vector are determined as below.

$$V_{qs} = \frac{2}{3} \left(V_{as} - \frac{1}{2} V_{bs} - \frac{1}{2} V_{cs} \right) = \frac{2}{3} \left(V_{cp} - \frac{1}{2} V_{bp} - \frac{1}{2} V_{bp} \right) = -\frac{2}{3} V_{bcp} \quad (\text{A.88})$$

$$V_{ds} = \frac{1}{\sqrt{3}} (V_{cs} - V_{bs}) = \frac{1}{\sqrt{3}} (V_{bp} - V_{bp}) = 0 \quad (\text{A.89})$$

The magnitude and direction of the output voltage space vector respectively are calculated using (A.88) and (A.89) as follows.

$$V_s = \sqrt{V_{qs}^2 + V_{ds}^2} = \sqrt{\left(-\frac{2}{3} V_{bcp} \right)^2} = \frac{2}{3} V_{bcp} \quad (\text{A.90})$$

$$\alpha_s = \tan^{-1} \left(\frac{-V_{ds}}{V_{qs}} \right) = \tan^{-1} \left(\frac{0}{-\frac{2}{3} V_{bcp}} \right) = \pi \quad (\text{A.91})$$

- **Mode CBC**

The q -axis and d -axis output voltage space vector are determined as below.

$$V_{qs} = \frac{2}{3} \left(V_{as} - \frac{1}{2} V_{bs} - \frac{1}{2} V_{cs} \right) = \frac{2}{3} \left(V_{cp} - \frac{1}{2} V_{bp} - \frac{1}{2} V_{cp} \right) = -\frac{1}{3} V_{bcp} \quad (\text{A.92})$$

$$V_{ds} = \frac{1}{\sqrt{3}} (V_{cs} - V_{bs}) = \frac{1}{\sqrt{3}} (V_{cp} - V_{bp}) = -\frac{1}{\sqrt{3}} V_{bcp} \quad (\text{A.93})$$

The magnitude and direction of the output voltage space vector respectively are calculated using (A.92) and (A.93) as follows.

$$V_p = \sqrt{V_{qs}^2 + V_{ds}^2} = \sqrt{\left(-\frac{1}{3}V_{bcp}\right)^2 + \left(-\frac{1}{\sqrt{3}}V_{bcp}\right)^2} = \frac{2}{3}V_{bcp} \quad (\text{A.94})$$

$$\alpha_s = \tan^{-1}\left(\frac{-V_{ds}}{V_{qs}}\right) = \tan^{-1}\left(\frac{\frac{1}{\sqrt{3}}V_{bcp}}{-\frac{1}{3}V_{bcp}}\right) = \frac{2\pi}{3} \quad (\text{A.95})$$

- **Mode CCA**

The q -axis and d -axis output voltage space vector are determined as below.

$$V_{qs} = \frac{2}{3}\left(V_{as} - \frac{1}{2}V_{bs} - \frac{1}{2}V_{cs}\right) = \frac{2}{3}\left(V_{cp} - \frac{1}{2}V_{ap} - \frac{1}{2}V_{cp}\right) = \frac{1}{3}V_{cap} \quad (\text{A.96})$$

$$V_{ds} = \frac{1}{\sqrt{3}}(V_{cs} - V_{bs}) = \frac{1}{\sqrt{3}}(V_{ap} - V_{cp}) = -\frac{1}{\sqrt{3}}V_{cap} \quad (\text{A.97})$$

The magnitude and direction of the output voltage space vector respectively are calculated (A.96) and (A.97) as follows.

$$V_s = \sqrt{V_{qs}^2 + V_{ds}^2} = \sqrt{\left(\frac{1}{3}V_{cap}\right)^2 + \left(-\frac{1}{\sqrt{3}}V_{cap}\right)^2} = \frac{2}{3}V_{cap} \quad (\text{A.98})$$

$$\alpha_s = \tan^{-1}\left(\frac{-V_{ds}}{V_{qs}}\right) = \tan^{-1}\left(\frac{-\frac{1}{\sqrt{3}}V_{cap}}{\frac{1}{3}V_{cap}}\right) = \tan^{-1}(\sqrt{3}) = -\frac{\pi}{3} \quad (\text{A.99})$$

- **Mode CCB**

The q -axis and d -axis output voltage space vector are determined as below.

$$V_{qs} = \frac{2}{3}\left(V_{as} - \frac{1}{2}V_{bs} - \frac{1}{2}V_{cs}\right) = \frac{2}{3}\left(V_{cp} - \frac{1}{2}V_{cp} - \frac{1}{2}V_{bp}\right) = -\frac{1}{3}V_{bcp} \quad (\text{A.100})$$

$$V_{ds} = \frac{1}{\sqrt{3}}(V_{cs} - V_{bs}) = \frac{1}{\sqrt{3}}(V_{bp} - V_{cp}) = \frac{1}{\sqrt{3}}V_{bcp} \quad (\text{A.101})$$

The magnitude and direction of the output voltage space vector respectively are calculated (A.100) and (A.101) as follows.

$$V_s = \sqrt{V_{qs}^2 + V_{ds}^2} = \sqrt{\left(-\frac{1}{3}V_{bcp}\right)^2 + \left(\frac{1}{\sqrt{3}}V_{bcp}\right)^2} = \frac{2}{3}V_{bcp} \quad (\text{A.102})$$

$$\alpha_s = \tan^{-1}\left(\frac{-V_{ds}}{V_{qs}}\right) = \tan^{-1}\left(\frac{\frac{1}{\sqrt{3}}V_{bcp}}{\frac{1}{3}V_{bcp}}\right) = \frac{\pi}{3} \quad (\text{A.103})$$

- **Mode CCC**

The q -axis and d -axis output voltage space vector are determined as below.

$$V_{qs} = \frac{2}{3}\left(V_{as} - \frac{1}{2}V_{bs} - \frac{1}{2}V_{cs}\right) = \frac{2}{3}\left(V_{cp} - \frac{1}{2}V_{cp} - \frac{1}{2}V_{cp}\right) = 0 \quad (\text{A.104})$$

$$V_{ds} = \frac{1}{\sqrt{3}}(V_{cs} - V_{bs}) = \frac{1}{\sqrt{3}}(V_{cp} - V_{cp}) = 0 \quad (\text{A.105})$$

The magnitude and direction of the output voltage space vector respectively are calculated (A.104) and (A.105) as follows.

$$V_p = \sqrt{V_{qs}^2 + V_{ds}^2} = 0 \quad (\text{A.106})$$

$$\alpha_v = \tan^{-1}\left(\frac{V_{ds}}{V_{qs}}\right) = 0 \quad (\text{A.107})$$

APPENDIX B

COMPLETE INPUT CURRENT SPACE VECTOR FOR THE INVERTER STAGE

This section presents the complete derivation for the input current space vector used in the direct space vector modulation. The calculated magnitude and phase of the input current space vectors are used to construct Table 3.2.

- **Mode 1 (AAA)**, $(S_{ap} = 0, S_{bp} = 0, S_{cp} = 0)$

In this mode, the instantaneous three phase input currents are given as

$$I_{ap} = I_{as} + I_{bs} + I_{cs} = 0 \quad I_{bp} = 0 \quad I_{cp} = 0 \quad (\text{B.1})$$

Transforming the time varying phase currents given in (B.1) into a stationary qd reference frame result in the following expressions

$$I_{qp} = \frac{2}{3} \left(I_{ap} - \frac{1}{2} I_{bp} - \frac{1}{2} I_{cp} \right) = \frac{2}{3} (I_{as} + I_{bs} + I_{cs}) = 0 \quad (\text{B.2})$$

$$I_{dp} = \frac{1}{\sqrt{3}} (I_{cp} - I_{bp}) = 0 \quad (\text{B.3})$$

Based on (B.2) and (B.3), the magnitude and phase angle of the input current space vector is calculated as

$$I_p = \sqrt{I_{qp}^2 + I_{dp}^2} = \frac{2}{3}(I_{as} + I_{bs} + I_{cs}) = 0 \quad (\text{B.4})$$

$$\beta_p = \tan^{-1}\left(\frac{-I_{dp}}{I_{qp}}\right) = 0 \quad (\text{B.5})$$

- **Mode 2 (AAB),** ($S_{ap} = 0, S_{bp} = 0, S_{cp} = 1$)

In this mode, the instantaneous three phase input currents are given as

$$I_{ap} = I_{as} + I_{bs} = -I_{cs} \quad I_{bp} = I_{cs} \quad I_{cp} = 0 \quad (\text{B.6})$$

The above time varying phase currents is transformed into a stationary qd reference frame as follows

$$I_{qp} = \frac{2}{3}\left(I_{ap} - \frac{1}{2}I_{bp} - \frac{1}{2}I_{cp}\right) = \frac{2}{3}\left(-I_{cs} - \frac{1}{2}I_{cs}\right) = -I_{cs} \quad (\text{B.7})$$

$$I_{dp} = \frac{1}{\sqrt{3}}(I_{cp} - I_{bp}) = -\frac{1}{\sqrt{3}}I_{cs} \quad (\text{B.8})$$

The magnitude and the phase angle of the input current space vector are computed based on (B.7) and (B.8)

$$I_p = \sqrt{I_{qp}^2 + I_{dp}^2} = \sqrt{I_{cs}^2 + \frac{1}{3}I_{cs}^2} = \frac{2}{\sqrt{3}}I_{cs} \quad (\text{B.9})$$

$$\beta_p = \tan^{-1}\left(\frac{-I_{dp}}{I_{qp}}\right) = \tan^{-1}\left[\frac{-\frac{1}{\sqrt{3}}I_{cs}}{-I_{cs}}\right] = \frac{7\pi}{6} \quad (\text{B.10})$$

- **Mode 3 (AAC),** $(S_{ap} = 0, S_{bp} = 0, S_{cp} = 2)$

In this mode, the instantaneous three phase input currents are given as

$$I_{ap} = I_{as} + I_{bs} = -I_{cs} \quad I_{bp} = 0 \quad I_{cp} = I_{cs} \quad (\text{B.11})$$

Transforming the time varying phase currents given in (B.11) into a stationary qd reference frame result in the following expressions

$$I_{qp} = \frac{2}{3} \left(I_{ap} - \frac{1}{2} I_{bp} - \frac{1}{2} I_{cp} \right) = \frac{2}{3} \left(I_{as} + I_{bs} - \frac{1}{2} I_{cs} \right) = -I_{cs} \quad (\text{B.12})$$

$$I_{dp} = \frac{1}{\sqrt{3}} (I_{cp} - I_{bp}) = \frac{1}{\sqrt{3}} I_{cs} \quad (\text{B.53})$$

The magnitude and the phase angle of the input current space vector are computed based on (B.12) and (B.13)

$$I_p = \sqrt{I_{qp}^2 + I_{dp}^2} = \sqrt{I_{cs}^2 + \frac{1}{3} I_{cs}^2} = \frac{2}{\sqrt{3}} I_{cs} \quad (\text{B.14})$$

$$\beta_p = \tan^{-1} \left(\frac{-I_{dp}}{I_{qp}} \right) = \tan^{-1} \left[\frac{-\frac{1}{\sqrt{3}} I_{cs}}{-I_{cs}} \right] = \frac{7\pi}{6} \quad (\text{B.15})$$

- **Mode 4 (ABA),** $(S_{ap} = 0, S_{bp} = 1, S_{cp} = 0)$

In this mode, the instantaneous three phase input currents are given as

$$I_{ap} = I_{as} + I_{cs} = -I_{bs} \quad I_{bp} = I_{bs} \quad I_{cp} = 0 \quad (\text{B.16})$$

The above time varying phase currents is transformed into a stationary qd reference frame as follows

$$I_{qp} = \frac{2}{3} \left(I_{ap} - \frac{1}{2} I_{bp} - \frac{1}{2} I_{cp} \right) = \frac{2}{3} \left(I_{as} + I_{cs} - \frac{1}{2} I_{bs} \right) = -I_{bs} \quad (\text{B.17})$$

$$I_{dp} = \frac{1}{\sqrt{3}} (I_{cp} - I_{bp}) = -\frac{1}{\sqrt{3}} I_{bs} \quad (\text{B.18})$$

The magnitude and direction of the input current space vector are calculated as follows.

$$I_p = \sqrt{I_{qp}^2 + I_{dp}^2} = \sqrt{I_{bs}^2 + \frac{1}{3} I_{bs}^2} = \frac{2}{\sqrt{3}} I_{bs} \quad (\text{B.19})$$

$$\beta_p = \tan^{-1} \left(\frac{I_{dp}}{I_{qp}} \right) = \tan^{-1} \left[\frac{-\frac{1}{\sqrt{3}} I_{bs}}{-I_{bs}} \right] = \frac{7\pi}{6} \quad (\text{B.20})$$

- **Mode 5 (ABB)**, $(S_{ap} = 0, S_{bp} = 1, S_{cp} = 1)$

In this mode, the instantaneous three phase input currents are

$$I_{ap} = I_{as} \quad I_{bp} = I_{bs} + I_{cs} = -I_{as} \quad I_{cp} = 0 \quad (\text{B.21})$$

Transforming the time varying phase currents given in (B.21) into a stationary qd reference frame result in the following expressions

$$I_{qp} = \frac{2}{3} \left(I_{ap} - \frac{1}{2} I_{bp} - \frac{1}{2} I_{cp} \right) = I_{as} \quad (\text{B.22})$$

$$I_{dp} = \frac{1}{\sqrt{3}}(I_{cp} - I_{bp}) = \frac{1}{\sqrt{3}}I_{as} \quad (\text{B.23})$$

The magnitude and direction of the input current space vector are calculated as follows.

$$I_p = \sqrt{I_{qp}^2 + I_{dp}^2} = \sqrt{I_{as}^2 + \frac{1}{3}I_{as}^2} = \frac{2}{\sqrt{3}}I_{as} \quad (\text{B.24})$$

$$\beta_p = \tan^{-1}\left(\frac{I_{dp}}{I_{qp}}\right) = \tan^{-1}\left[\frac{\frac{1}{\sqrt{3}}I_{as}}{I_{as}}\right] = \tan^{-1}\left(\frac{1}{\sqrt{3}}\right) = \frac{\pi}{6} \quad (\text{B.25})$$

- **Mode 6 (ABC)**, ($S_{ap} = 0, S_{bp} = 1, S_{cp} = 2$)

In this mode, the instantaneous three phase input currents are given as

$$I_{ap} = I_{as} \quad I_{bp} = I_{bs} \quad I_{cp} = I_{cs} \quad (\text{B.26})$$

Transforming the time varying phase currents given in (B.26) into a stationary qd reference frame result in the following expressions

$$I_{qp} = \frac{2}{3}\left(I_{ap} - \frac{1}{2}I_{bp} - \frac{1}{2}I_{cp}\right) = \frac{2}{3}\left(I_{as} - \frac{1}{2}(I_{bs} + I_{cs})\right) = I_{as} \quad (\text{B.27})$$

$$I_{dp} = \frac{1}{\sqrt{3}}(I_{cp} - I_{bp}) = \frac{1}{\sqrt{3}}(I_{cs} - I_{bs}) \quad (\text{B.28})$$

The magnitude and the phase angle of the input current space vector are computed based on (B.27) and (B.28)

$$I_p = \sqrt{I_{qp}^2 + I_{dp}^2} = \sqrt{I_{as}^2 + \frac{1}{3}(I_{cs} - I_{bs})^2} \quad (\text{B.29})$$

$$\beta_p = \tan^{-1}\left(\frac{-I_{dp}}{I_{qp}}\right) = \tan^{-1}\left(\frac{-\frac{1}{\sqrt{3}}(I_{cs} - I_{bs})}{I_{as}}\right) = \omega_s t - \varphi_s \quad (\text{B.30})$$

- **Mode 7 (ACA),** ($S_{ap} = 0, S_{bp} = 2, S_{cp} = 0$)

$$I_{ap} = I_{as} + I_{cs} = -I_{bs} \quad I_{bp} = 0 \quad I_{cp} = I_{bs} \quad (\text{B.31})$$

Transforming the time varying phase currents given in (B.31) into a stationary qd reference frame result in the following expressions

$$I_{qp} = \frac{2}{3}\left(I_{ap} - \frac{1}{2}I_{bp} - \frac{1}{2}I_{cp}\right) = \frac{2}{3}\left(-I_{bs} - \frac{1}{2}I_{bs}\right) = -I_{bs} \quad (\text{B.32})$$

$$I_{dp} = \frac{1}{\sqrt{3}}(I_{cp} - I_{bp}) = \frac{1}{\sqrt{3}}I_{bs} \quad (\text{B.33})$$

The magnitude and direction of the input current space vector are calculated as follows.

$$I_p = \sqrt{I_{qp}^2 + I_{dp}^2} = \sqrt{I_{bs}^2 + \frac{1}{3}I_{bs}^2} = \frac{2}{\sqrt{3}}I_{bs} \quad (\text{B.34})$$

$$\beta_p = \tan^{-1}\left(\frac{-I_{dp}}{I_{qp}}\right) = \tan^{-1}\left[\frac{-\frac{1}{\sqrt{3}}I_{bs}}{-I_{bs}}\right] = \frac{7\pi}{6} \quad (\text{B.35})$$

- **Mode 8 (ACB)**, $(S_{ap} = 0, S_{bp} = 2, S_{cp} = 1)$

In this mode, the instantaneous three phase input currents are given as

$$I_{ap} = I_{as} \quad I_{bp} = I_{cs} \quad I_{cp} = I_{bs} \quad (\text{B.36})$$

Transforming the time varying phase currents given in (B.36) into a stationary qd reference frame result in the following expressions

$$I_{qp} = \frac{2}{3} \left(I_{ap} - \frac{1}{2} I_{bp} - \frac{1}{2} I_{cp} \right) = \frac{2}{3} \left(I_{as} - \frac{1}{2} (I_{bs} + I_{cs}) \right) = I_{as} \quad (\text{B.37})$$

$$I_{dp} = \frac{1}{\sqrt{3}} (I_{cp} - I_{bp}) = \frac{1}{\sqrt{3}} (I_{bs} - I_{cs}) \quad (\text{B.38})$$

The magnitude and direction of the input current space vector are calculated as follows.

$$I_p = \sqrt{I_{qp}^2 + I_{dp}^2} = \sqrt{I_{as}^2 + \frac{1}{3} (I_{bs} - I_{cs})^2} \quad (\text{B.39})$$

$$\beta_p = \tan^{-1} \left(\frac{-I_{dp}}{I_{qp}} \right) = \tan^{-1} \left(\frac{-\frac{1}{\sqrt{3}} (I_{bs} - I_{cs})}{I_{as}} \right) = \omega_s t - \varphi_s \quad (\text{B.40})$$

- **Mode 9 (ACC)**, $(S_{ap} = 0, S_{bp} = 2, S_{cp} = 2)$

In this mode, the instantaneous three phase input currents are given as

$$I_{ap} = I_{as} \quad I_{bp} = 0 \quad I_{cp} = I_{bs} + I_{cs} = -I_{as} \quad (\text{B.41})$$

Transforming the time varying phase currents given in (B.41) into a stationary qd reference frame result in the following expressions

$$I_{qp} = \frac{2}{3} \left(I_{ap} - \frac{1}{2} I_{bp} - \frac{1}{2} I_{cp} \right) = I_{as} \quad (\text{B.42})$$

$$I_{dp} = \frac{1}{\sqrt{3}} (I_{cp} - I_{bp}) = -\frac{1}{\sqrt{3}} I_{as} \quad (\text{B.43})$$

The magnitude and the phase angle of the input current space vector are computed based on (B.42) and (B.43)

$$I_p = \sqrt{I_{qp}^2 + I_{dp}^2} = \sqrt{I_{as}^2 + \frac{1}{3} I_{as}^2} = \frac{2}{\sqrt{3}} I_{as} \quad (\text{B.44})$$

$$\beta_p = \tan^{-1} \left(\frac{-I_{dp}}{I_{qp}} \right) = \tan^{-1} \left[\frac{\frac{1}{\sqrt{3}} I_{as}}{I_{as}} \right] = \frac{\pi}{6} \quad (\text{B.45})$$

- **Mode 10 (BAA),** ($S_{ap} = 1, S_{bp} = 0, S_{cp} = 0$)

In this mode, the instantaneous three phase input currents are given as

$$I_{ap} = I_{bs} + I_{cs} = -I_{as} \quad I_{bp} = I_{as} \quad I_{cp} = 0 \quad (\text{B.46})$$

Transforming the time varying phase currents given in (B.46) into a stationary qd reference frame result in the following expressions

$$I_{qp} = \frac{2}{3} \left(I_{ap} - \frac{1}{2} I_{bp} - \frac{1}{2} I_{cp} \right) = -I_{as} \quad (\text{B.47})$$

The d-axis input current is given as,

$$I_{dp} = \frac{1}{\sqrt{3}}(I_{cp} - I_{bp}) = -\frac{1}{\sqrt{3}}I_{as} \quad (\text{B.48})$$

The magnitude and the phase angle of the input current space vector are computed based on (B.47) and (B.48)

$$I_p = \sqrt{I_{qp}^2 + I_{dp}^2} = \sqrt{I_{as}^2 + \frac{1}{3}I_{as}^2} = \frac{2}{\sqrt{3}}I_{as} \quad (\text{B.49})$$

$$\beta_p = \tan^{-1}\left(\frac{-I_{dp}}{I_{qp}}\right) = \tan^{-1}\left[\frac{\frac{1}{\sqrt{3}}I_{as}}{-I_{as}}\right] = \frac{5\pi}{6} \quad (\text{B.50})$$

- **Mode 11 (BAB),**

The switching function has the following values, $(S_{ap} = 1, S_{bp} = 0, S_{cp} = 1)$

In this mode, the instantaneous three phase input currents are given as

$$I_{ap} = I_{bs} \quad I_{bp} = I_{as} + I_{cs} = -I_{bs} \quad I_{cp} = 0 \quad (\text{B.51})$$

Transforming the time varying phase currents given in (B.51) into a stationary qd reference frame result in the following expressions

$$I_{qp} = \frac{2}{3}\left(I_{ap} - \frac{1}{2}I_{bp} - \frac{1}{2}I_{cp}\right) = \frac{2}{3}\left(I_{bs} + \frac{1}{2}I_{bs}\right) = I_{bs} \quad (\text{B.52})$$

$$I_{dp} = \frac{1}{\sqrt{3}}(I_{cp} - I_{bp}) = \frac{1}{\sqrt{3}}I_{bs} \quad (\text{B.53})$$

The magnitude and direction of the input current space vector are calculated as follows.

$$I_p = \sqrt{I_{qp}^2 + I_{dp}^2} = \sqrt{I_{bs}^2 + \frac{1}{3}I_{bs}^2} = \frac{2}{\sqrt{3}}I_{bs} \quad (\text{B.54})$$

$$\beta_p = \tan^{-1}\left(\frac{-I_{dp}}{I_{qp}}\right) = \tan^{-1}\left[\frac{-\frac{1}{\sqrt{3}}I_{bs}}{I_{bs}}\right] = -\frac{\pi}{6} \quad (\text{B.55})$$

- **Mode 12 (BAC)**, ($S_{ap} = 1, S_{bp} = 0, S_{cp} = 2$)

In this mode, the instantaneous three phase input currents are given as

$$I_{ap} = I_{bs} \quad I_{bp} = I_{as} \quad I_{cp} = I_{cs} \quad (\text{B.56})$$

Transforming the time varying phase currents given in (B.56) into a stationary qd reference frame result in the following expressions

$$I_{qp} = \frac{2}{3}\left(I_{ap} - \frac{1}{2}I_{bp} - \frac{1}{2}I_{cp}\right) = \frac{2}{3}\left(I_{bs} - \frac{1}{2}(I_{as} + I_{cs})\right) = I_{bs} \quad (\text{B.57})$$

$$I_{dp} = \frac{1}{\sqrt{3}}(I_{cp} - I_{bp}) = \frac{1}{\sqrt{3}}(I_{cs} - I_{as}) \quad (\text{B.58})$$

The magnitude of the input current space vector is computed based on (B.57) and (B.58)

$$I_p = \sqrt{I_{qp}^2 + I_{dp}^2} = \sqrt{I_{bs}^2 + \frac{1}{3}(I_{cs} - I_{as})^2} \quad (\text{B.59})$$

The phase angle of the input current space vector is calculated as

$$\beta_p = \tan^{-1}\left(\frac{-I_{dp}}{I_{qp}}\right) = \tan^{-1}\left(\frac{-\frac{1}{\sqrt{3}}(I_{cs} - I_{as})}{I_{bs}}\right) = -\omega_s t + \varphi_s + \frac{2\pi}{3} \quad (\text{B.60})$$

- **Mode 13 (BBA)**, ($S_{ap} = 1, S_{bp} = 1, S_{cp} = 0$)

In this mode, the instantaneous three phase input currents are given as

$$I_{ap} = I_{cs} \quad I_{bp} = I_{as} + I_{bs} = -I_{cs} \quad I_{cp} = 0 \quad (\text{B.61})$$

Transforming the time varying phase currents given in (B.61) into a stationary qd reference frame result in the following expressions

$$I_{qp} = \frac{2}{3}\left(I_{ap} - \frac{1}{2}I_{bp} - \frac{1}{2}I_{cp}\right) = \frac{2}{3}\left(I_{cs} + \frac{1}{2}I_{cs}\right) = I_{cs} \quad (\text{B.62})$$

$$I_{dp} = \frac{1}{\sqrt{3}}(I_{cp} - I_{bp}) = \frac{1}{\sqrt{3}}I_{cs} \quad (\text{B.63})$$

The magnitude and direction of the input current space vector are calculated based on the above two expression

$$I_p = \sqrt{I_{qp}^2 + I_{dp}^2} = \sqrt{I_{cs}^2 + \frac{1}{3}I_{cs}^2} = \frac{2}{\sqrt{3}}I_{cs} \quad (\text{B.64})$$

$$\beta_p = \tan^{-1}\left(\frac{-I_{dp}}{I_{qp}}\right) = \frac{7\pi}{6} \quad (\text{B.65})$$

- **Mode 14 (BBB)**, $(S_{ap} = 1, S_{bp} = 1, S_{cp} = 1)$

In this mode, the instantaneous three phase input currents are given as

$$I_{ap} = 0 \quad I_{bp} = I_{as} + I_{bs} + I_{cs} = 0 \quad I_{cp} = 0 \quad (\text{B.66})$$

Transforming the time varying phase currents given in (B.66) into a stationary qd reference frame result in the following expressions

$$I_{qp} = \frac{2}{3} \left(I_{ap} - \frac{1}{2} I_{bp} - \frac{1}{2} I_{cp} \right) = 0 \quad (\text{B.67})$$

$$I_{dp} = \frac{1}{\sqrt{3}} (I_{cp} - I_{bp}) = 0 \quad (\text{B.68})$$

The magnitude and the phase angle of the input current space vector are computed based on (B.67) and (B.68)

$$I_p = \sqrt{I_{qp}^2 + I_{dp}^2} = \frac{2}{3} (I_{as} + I_{bs} + I_{cs}) = 0 \quad (\text{B.69})$$

$$\beta_p = \tan^{-1} \left(\frac{-I_{dp}}{I_{qp}} \right) = 0 \quad (\text{B.70})$$

- **Mode 15 (BBC)**, $(S_{ap} = 1, S_{bp} = 1, S_{cp} = 2)$

In this mode, the instantaneous three phase input currents are given as

$$I_{ap} = 0 \quad I_{bp} = I_{as} + I_{bs} = -I_{cs} \quad I_{cp} = I_{cs} \quad (\text{B.71})$$

Transforming the time varying phase currents given in (B.71) into a stationary qd reference frame result in the following expressions

$$I_{qp} = \frac{2}{3} \left(I_{ap} - \frac{1}{2} I_{bp} - \frac{1}{2} I_{cp} \right) = \frac{2}{3} \left(-\frac{1}{2} I_{cs} + \frac{1}{2} I_{cs} \right) = 0 \quad (\text{B.72})$$

$$I_{dp} = \frac{1}{\sqrt{3}} (I_{cp} - I_{bp}) = \frac{2}{\sqrt{3}} I_{cs} \quad (\text{B.73})$$

The magnitude and direction of the input current space vector are calculated as follows.

$$I_p = \sqrt{I_{qp}^2 + I_{dp}^2} = \frac{2}{\sqrt{3}} I_{cs} \quad (\text{B.74})$$

$$\beta_p = \tan^{-1} \left(\frac{-I_{dp}}{I_{qp}} \right) = \tan^{-1} \left[\frac{-\frac{2}{\sqrt{3}} I_{cs}}{0} \right] = -\frac{\pi}{2} \quad (\text{B.75})$$

- **Mode 16 (BCA),** ($S_{ap} = 1, S_{bp} = 2, S_{cp} = 0$)

In this mode, the instantaneous three phase input currents are given as

$$I_{ap} = I_{cs} \quad I_{bp} = I_{as} \quad I_{cp} = I_{bs} \quad (\text{B.76})$$

Transforming the time varying phase currents given in (B.76) into a stationary qd reference frame result in the following expressions

$$I_{qp} = \frac{2}{3} \left(I_{ap} - \frac{1}{2} I_{bp} - \frac{1}{2} I_{cp} \right) = \frac{2}{3} \left(I_{cs} - \frac{1}{2} (I_{as} + I_{bs}) \right) = I_{cs} \quad (\text{B.77})$$

$$I_{dp} = \frac{1}{\sqrt{3}}(I_{cp} - I_{bp}) = \frac{1}{\sqrt{3}}(I_{bs} - I_{as}) \quad (\text{B.78})$$

The magnitude and direction of the input current space vector are calculated as follows.

$$I_p = \sqrt{I_{qp}^2 + I_{dp}^2} = \sqrt{I_{cs}^2 + \frac{1}{3}(I_{bs} - I_{as})^2} \quad (\text{B.79})$$

$$\beta_p = \tan^{-1}\left(\frac{-I_{dp}}{I_{qp}}\right) = \tan^{-1}\left(\frac{-\frac{1}{\sqrt{3}}(I_{bs} - I_{as})}{I_{cs}}\right) = \omega_s t - \varphi_s + \frac{2\pi}{3} \quad (\text{B.80})$$

- **Mode 17 (BCB),**

The switching functions have the following values,

$$(S_{ap} = 1, S_{bp} = 2, S_{cp} = 1)$$

In this mode, the instantaneous three phase input currents are given as

$$I_{ap} = 0 \quad I_{bp} = I_{as} + I_{cs} = -I_{bs} \quad I_{cp} = I_{bs} \quad (\text{B.81})$$

Transforming the time varying phase currents given in (B.81) into a stationary qd reference frame result in the following expressions

$$I_{qp} = \frac{2}{3}\left(I_{ap} - \frac{1}{2}I_{bp} - \frac{1}{2}I_{cp}\right) = \frac{2}{3}\left(\frac{1}{2}I_{bs} - \frac{1}{2}I_{bs}\right) = 0 \quad (\text{B.82})$$

$$I_{dp} = \frac{1}{\sqrt{3}}(I_{cp} - I_{bp}) = \frac{2}{\sqrt{3}}I_{bs} \quad (\text{B.83})$$

The magnitude and direction of the input current space vector are calculated as follows.

$$I_p = \sqrt{I_{qp}^2 + I_{dp}^2} = \frac{2}{\sqrt{3}} I_{bs} \quad (\text{B.84})$$

$$\beta_p = \tan^{-1}\left(\frac{-I_{dp}}{I_{qp}}\right) = \tan^{-1}\left[\frac{-\frac{2}{\sqrt{3}} I_{bs}}{0}\right] = -\frac{\pi}{2} \quad (\text{B.85})$$

- **Mode 18 (BCC),** ($S_{ap} = 1, S_{bp} = 2, S_{cp} = 2$)

In this mode, the instantaneous three phase input currents are given as

$$I_{ap} = 0 \quad I_{bp} = I_{as} \quad I_{cp} = I_{bs} + I_{cs} = -I_{as} \quad (\text{B.86})$$

Transforming the time varying phase currents given in (B.86) into a stationary qd reference frame result in the following expressions

$$I_{qp} = \frac{2}{3} \left(I_{ap} - \frac{1}{2} I_{bp} - \frac{1}{2} I_{cp} \right) = 0 \quad (\text{B.87})$$

$$I_{dp} = \frac{1}{\sqrt{3}} (I_{cp} - I_{bp}) = -\frac{2}{\sqrt{3}} I_{as} \quad (\text{B.88})$$

The magnitude and direction of the input current space vector are calculated as follows.

$$I_p = \sqrt{I_{qp}^2 + I_{dp}^2} = \frac{2}{\sqrt{3}} I_{as} \quad (\text{B.89})$$

$$\beta_p = \tan^{-1}\left(\frac{-I_{dp}}{I_{qp}}\right) = \tan^{-1}\left[\frac{\frac{2}{\sqrt{3}}I_{as}}{0}\right] = \frac{\pi}{2} \quad (\text{B.90})$$

- **Mode 19 (CAA),** ($S_{ap} = 2, S_{bp} = 0, S_{cp} = 0$)

In this mode, the instantaneous three phase input currents are given as

$$I_{ap} = I_{bs} + I_{cs} = -I_{as} \quad I_{bp} = 0 \quad I_{cp} = I_{as} \quad (\text{B.91})$$

Transforming the time varying phase currents given in (B.91) into a stationary qd reference frame result in the following expressions

$$I_{qp} = \frac{2}{3}\left(I_{ap} - \frac{1}{2}I_{bp} - \frac{1}{2}I_{cp}\right) = -I_{as} \quad (\text{B.92})$$

$$I_{dp} = \frac{1}{\sqrt{3}}(I_{cp} - I_{bp}) = \frac{1}{\sqrt{3}}I_{as} \quad (\text{B.93})$$

The magnitude and direction of the input current space vector are calculated as follows.

$$I_p = \sqrt{I_{qp}^2 + I_{dp}^2} = \sqrt{I_{as}^2 + \frac{1}{3}I_{as}^2} = \frac{2}{\sqrt{3}}I_{as} \quad (\text{B.94})$$

$$\beta_p = \tan^{-1}\left(\frac{-I_{dp}}{I_{qp}}\right) = \tan^{-1}\left[\frac{-\frac{1}{\sqrt{3}}I_{as}}{-I_{as}}\right] = \frac{7\pi}{6} \quad (\text{B.95})$$

- **Mode 20 (CAB)**, $(S_{ap} = 2, S_{bp} = 0, S_{cp} = 1)$

In this mode, the instantaneous three phase input currents are given as

$$I_{ap} = I_{bs} \quad I_{bp} = I_{cs} \quad I_{cp} = I_{as} \quad (\text{B.96})$$

Transforming the time varying phase currents given in (B.96) into a stationary qd reference frame result in the following expressions

$$I_{qp} = \frac{2}{3} \left(I_{ap} - \frac{1}{2} I_{bp} - \frac{1}{2} I_{cp} \right) = \frac{2}{3} \left(I_{bs} - \frac{1}{2} (I_{as} + I_{cs}) \right) = I_{bs} \quad (\text{B.97})$$

$$I_{dp} = \frac{1}{\sqrt{3}} (I_{cp} - I_{bp}) = \frac{1}{\sqrt{3}} (I_{as} - I_{cs}) \quad (\text{B.98})$$

The magnitude and direction of the input current space vector are calculated as follows.

$$I_p = \sqrt{I_{qp}^2 + I_{dp}^2} = \sqrt{I_{bs}^2 + \frac{1}{3} (I_{as} - I_{cs})^2} \quad (\text{B.99})$$

$$\beta_p = \tan^{-1} \left(\frac{-I_{dp}}{I_{qp}} \right) = \tan^{-1} \left(\frac{-\frac{1}{\sqrt{3}} (I_{as} - I_{cs})}{I_{bs}} \right) = \omega_s t - \varphi_s - \frac{2\pi}{3} \quad (\text{B.100})$$

- **Mode 21 (CAC)**, $(S_{ap} = 2, S_{bp} = 0, S_{cp} = 2)$

In this mode, the instantaneous three phase input currents are given as

$$I_{ap} = I_{bs} \quad I_{bp} = 0 \quad I_{cp} = I_{as} + I_{cs} = -I_{bs} \quad (\text{B.101})$$

Transforming the time varying phase currents given in (B.101) into a stationary qd reference frame result in the following expressions

$$I_{qp} = \frac{2}{3} \left(I_{ap} - \frac{1}{2} I_{bp} - \frac{1}{2} I_{cp} \right) = I_{bs} \quad (\text{B.102})$$

$$I_{dp} = \frac{1}{\sqrt{3}} (I_{cp} - I_{bp}) = -\frac{1}{\sqrt{3}} I_{bs} \quad (\text{B.103})$$

The magnitude and direction of the input current space vector are calculated as follows.

$$I_p = \sqrt{I_{qp}^2 + I_{dp}^2} = \sqrt{I_{bs}^2 + \frac{1}{3} I_{bs}^2} = \frac{2}{\sqrt{3}} I_{bs} \quad (\text{B.104})$$

$$\beta_p = \tan^{-1} \left(\frac{-I_{dp}}{I_{qp}} \right) = \tan^{-1} \left[\frac{\frac{1}{\sqrt{3}} I_{bs}}{I_{bs}} \right] = \tan^{-1} \left(\frac{1}{\sqrt{3}} \right) = \frac{\pi}{6} \quad (\text{B.105})$$

- **Mode 22 (CBA),** ($S_{ap} = 2, S_{bp} = 1, S_{cp} = 0$)

$$I_{ap} = I_{cs} \quad I_{bp} = I_{bs} \quad I_{cp} = I_{as} \quad (\text{B.106})$$

Transforming the time varying phase currents given in (B.106) into a stationary qd reference frame result in the following expressions

$$I_{qp} = \frac{2}{3} \left(I_{ap} - \frac{1}{2} I_{bp} - \frac{1}{2} I_{cp} \right) = \frac{2}{3} \left(I_{cs} - \frac{1}{2} (I_{as} + I_{bs}) \right) = I_{cs} \quad (\text{B.107})$$

$$I_{dp} = \frac{1}{\sqrt{3}} (I_{cp} - I_{bp}) = \frac{1}{\sqrt{3}} (I_{as} - I_{bs}) \quad (\text{B.108})$$

The magnitude and the phase angle of the input current space vector are computed based on (B.107) and (B.108)

$$I_p = \sqrt{I_{qp}^2 + I_{dp}^2} = \sqrt{I_{bs}^2 + \frac{1}{3}(I_{as} - I_{bs})^2} \quad (\text{B.109})$$

$$\beta_p = \tan^{-1}\left(\frac{-I_{dp}}{I_{qp}}\right) = \tan^{-1}\left(\frac{-\frac{1}{\sqrt{3}}(I_{as} - I_{bs})}{I_{cs}}\right) = -\omega_s t + \varphi_s + \frac{2\pi}{3} \quad (\text{B.110})$$

- **Mode 23 (CBB)**, ($S_{ap} = 2, S_{bp} = 1, S_{cp} = 1$)

In this mode, the instantaneous three phase input currents are given as

$$I_{ap} = 0 \quad I_{bp} = I_{bs} + I_{cs} = -I_{as} \quad I_{cp} = I_{as} \quad (\text{B.111})$$

The above time varying phase currents is transformed into a stationary qd reference frame as follows

$$I_{qp} = \frac{2}{3}\left(I_{ap} - \frac{1}{2}I_{bp} - \frac{1}{2}I_{cp}\right) = 0 \quad (\text{B.112})$$

$$I_{dp} = \frac{1}{\sqrt{3}}(I_{cp} - I_{bp}) = \frac{2}{\sqrt{3}}I_{as} \quad (\text{B.113})$$

The magnitude of the input current space vector is calculated using (B.112) and (B.113) as follows.

$$I_p = \sqrt{I_{qp}^2 + I_{dp}^2} = \sqrt{I_{as}^2 + \frac{1}{3}I_{as}^2} = \frac{2}{\sqrt{3}}I_{as} \quad (\text{B.114})$$

The direction of the input current space vector is calculated as

$$\beta_p = \tan^{-1}\left(\frac{-I_{dp}}{I_{qp}}\right) = \tan^{-1}\left[\frac{-\frac{2}{\sqrt{3}}I_{as}}{0}\right] = -\frac{\pi}{2} \quad (\text{B.115})$$

- **Mode 24 (CBC)**, ($S_{ap} = 2, S_{bp} = 1, S_{cp} = 2$)

In this mode, the instantaneous three phase input currents are given as

$$I_{ap} = 0 \quad I_{bp} = I_{bs} \quad I_{cp} = I_{as} + I_{cs} = -I_{bs} \quad (\text{B.116})$$

The above time varying phase currents is transformed into a stationary qd reference frame as follows

$$I_{qp} = \frac{2}{3}\left(I_{ap} - \frac{1}{2}I_{bp} - \frac{1}{2}I_{cp}\right) = 0 \quad (\text{B.117})$$

$$I_{dp} = \frac{1}{\sqrt{3}}(I_{cp} - I_{bp}) = -\frac{2}{\sqrt{3}}I_{bs} \quad (\text{B.118})$$

The magnitude and direction of the input current space vector are calculated as follows.

$$I_p = \sqrt{I_{qp}^2 + I_{dp}^2} = \frac{2}{\sqrt{3}}I_{bs} \quad (\text{B.119})$$

$$\beta_p = \tan^{-1}\left(\frac{-I_{dp}}{I_{qp}}\right) = \tan^{-1}\left[\frac{= \frac{2}{\sqrt{3}}I_{bs}}{0}\right] = \frac{\pi}{2} \quad (\text{B.120})$$

- **Mode 25 (CCA),** $(S_{ap} = 2, S_{bp} = 2, S_{cp} = 0)$

In this mode, the instantaneous three phase input currents are given as

$$I_{ap} = I_{cs} \quad I_{bp} = 0 \quad I_{cp} = I_{as} + I_{bs} = -I_{cs} \quad (\text{B.121})$$

The above time varying phase currents is transformed into a stationary qd reference frame as follows

$$I_{qp} = \frac{2}{3} \left(I_{ap} - \frac{1}{2} I_{bp} - \frac{1}{2} I_{cp} \right) = \frac{2}{3} \left(I_{cs} + \frac{1}{2} I_{cs} \right) = I_{cs} \quad (\text{B.122})$$

$$I_{dp} = \frac{1}{\sqrt{3}} (I_{cp} - I_{bp}) = -\frac{1}{\sqrt{3}} I_{cs} \quad (\text{B.123})$$

The magnitude and direction of the input current space vector are calculated as follows.

$$I_p = \sqrt{I_{qp}^2 + I_{dp}^2} = \sqrt{I_{cs}^2 + \frac{1}{3} I_{cs}^2} = \frac{2}{\sqrt{3}} I_{cs} \quad (\text{B.124})$$

$$\beta_p = \tan^{-1} \left(\frac{-I_{dp}}{I_{qp}} \right) = \tan^{-1} \left[\frac{\frac{1}{\sqrt{3}} I_{cs}}{I_{cs}} \right] = \tan^{-1} \left[\frac{1}{\sqrt{3}} \right] = \frac{\pi}{6} \quad (\text{B.125})$$

- **Mode 26 (CCB),** $(S_{ap} = 2, S_{bp} = 2, S_{cp} = 1)$

In this mode, the instantaneous three phase input currents are given as

$$I_{ap} = 0 \quad I_{bp} = I_{cs} \quad I_{cp} = I_{as} + I_{bs} = -I_{cs} \quad (\text{B.126})$$

The above time varying phase currents is transformed into a stationary qd reference frame as follows

$$I_{qp} = \frac{2}{3} \left(I_{ap} - \frac{1}{2} I_{bp} - \frac{1}{2} I_{cp} \right) = 0 \quad (\text{B.127})$$

$$I_{dp} = \frac{1}{\sqrt{3}} (I_{cp} - I_{bp}) = -\frac{2}{\sqrt{3}} I_{cs} \quad (\text{B.128})$$

The magnitude and direction of the input current space vector are calculated as follows.

$$I_p = \sqrt{I_{qp}^2 + I_{dp}^2} = \sqrt{I_{cs}^2 + \frac{1}{3} I_{cs}^2} = \frac{2}{\sqrt{3}} I_{cs} \quad (\text{B.129})$$

$$\beta_p = \tan^{-1} \left(\frac{-I_{dp}}{I_{qp}} \right) = \tan^{-1} \left[\frac{\frac{2}{\sqrt{3}} I_{cs}}{0} \right] = \frac{\pi}{2} \quad (\text{B.130})$$

- **Mode 27 (CCC)**, ($S_{ap} = 2, S_{bp} = 2, S_{cp} = 2$)

In this mode, the instantaneous three phase input currents are given as

$$I_{ap} = 0 \quad I_{bp} = 0 \quad I_{cp} = I_{as} + I_{bs} + I_{cs} = 0 \quad (\text{B.131})$$

The above time varying phase currents is transformed into a stationary qd reference frame as follows

$$I_{qp} = \frac{2}{3} \left(I_{ap} - \frac{1}{2} I_{bp} - \frac{1}{2} I_{cp} \right) = 0 \quad (\text{B.132})$$

The d-axis input current space vector is given as

$$I_{dp} = \frac{1}{\sqrt{3}}(I_{cp} - I_{bp}) = 0 \quad \text{(B.133)}$$

The magnitude and direction of the input current space vector are calculated as follows.

$$I_p = \sqrt{I_{qp}^2 + I_{dp}^2} = \frac{2}{3}(I_{as} + I_{bs} + I_{cs}) = 0 \quad \text{(B.134)}$$

$$\beta_p = \tan^{-1}\left(\frac{-I_{dp}}{I_{qp}}\right) = 0 \quad \text{(B.135)}$$

APPENDIX C

COMPLETE INPUT CURRENT SPACE VECTOR FOR THE INVERTER STAGE

This section presents the complete derivations used to construct the current space vector used in the indirect space vectors. The results are used to construct Table 3.5.

• Mode 1

The devices to be turned ON are S_{ap} and S_{bn} ; hence, $I_{ap} = I_{DC}$, $I_{bp} = -I_{DC}$ and $I_{cp} = 0$

$$I_{qp} = \frac{1}{3}(2I_{ap} - I_{bp} - I_{cp}) = \frac{1}{3}(2I_{DC} + I_{DC}) = I_{DC} \quad (\text{C.1})$$

$$I_{dp} = \frac{1}{\sqrt{3}}(I_{cp} - I_{bp}) = \frac{1}{\sqrt{3}}I_{DC} \quad (\text{C.2})$$

The magnitude and angle of the rectifier stage current space vector is determined as follows

$$I_p = \sqrt{I_{qp}^2 + I_{dp}^2} = \sqrt{I_{DC}^2 + \left(\frac{1}{\sqrt{3}}I_{DC}\right)^2} = \frac{2}{\sqrt{3}}I_{DC} \quad (\text{C.3})$$

$$\beta_p = \tan^{-1}\left(\frac{-I_{dp}}{I_{qp}}\right) = \tan^{-1}\left(\frac{-\frac{1}{\sqrt{3}}I_{DC}}{I_{DC}}\right) = -\frac{\pi}{6} \quad (\text{C.4})$$

- **Mode 2**

Devices turned ON are S_{ap} and S_{cn} ; hence, $I_{ap} = I_{DC}$, $I_{bp} = 0$ and $I_{cp} = -I_{DC}$

$$I_{qp} = \frac{1}{3}(2I_{ap} - I_{bp} - I_{cp}) = \frac{1}{3}(2I_{DC} + I_{DC}) = I_{DC} \quad (C.5)$$

$$I_{dp} = \frac{1}{\sqrt{3}}(I_{cp} - I_{bp}) = -\frac{1}{\sqrt{3}}I_{DC} \quad (C.6)$$

The magnitude and angle of the rectifier stage current space vector is determined as follows

$$I_p = \sqrt{I_{qp}^2 + I_{dp}^2} = \sqrt{I_{DC}^2 + \left(-\frac{1}{\sqrt{3}}I_{DC}\right)^2} = \frac{2}{\sqrt{3}}I_{DC} \quad (C.7)$$

$$\beta_p = \tan^{-1}\left(\frac{-I_{dp}}{I_{qp}}\right) = \tan^{-1}\left(\frac{\frac{1}{\sqrt{3}}I_{DC}}{I_{DC}}\right) = \frac{\pi}{6} \quad (C.8)$$

- **Mode 3**

Devices turned ON are S_{bp} and S_{an} ; hence, $I_{ap} = -I_{DC}$, $I_{bp} = I_{DC}$ and $I_{cp} = 0$

$$I_{qp} = \frac{1}{3}(2I_{ap} - I_{bp} - I_{cp}) = \frac{1}{3}(-2I_{DC} - I_{DC}) = -I_{DC} \quad (C.9)$$

$$I_{dp} = \frac{1}{\sqrt{3}}(I_{cp} - I_{bp}) = -\frac{1}{\sqrt{3}}I_{DC} \quad (C.10)$$

The magnitude and angle of the rectifier stage current space vector is determined as follows

$$I_p = \sqrt{I_{qp}^2 + I_{dp}^2} = \sqrt{I_{DC}^2 + \left(-\frac{1}{\sqrt{3}}I_{DC}\right)^2} = \frac{2}{\sqrt{3}}I_{DC} \quad (\text{C.11})$$

$$\beta_p = \tan^{-1}\left(\frac{-I_{dp}}{I_{qp}}\right) = \tan^{-1}\left(\frac{\frac{1}{\sqrt{3}}I_{DC}}{-I_{DC}}\right) = \frac{5\pi}{6} \quad (\text{C.12})$$

• **Mode 4**

Devices turned ON are S_{bp} and S_{cn} ; hence, $I_{ap} = 0$, $I_{bp} = I_{DC}$, and $I_{cp} = -I_{DC}$

$$I_{qp} = \frac{1}{3}(2I_{ap} - I_{bp} - I_{cp}) = \frac{1}{3}(-I_{DC} + I_{DC}) = 0 \quad (\text{C.13})$$

$$I_{dp} = \frac{1}{\sqrt{3}}(I_{cp} - I_{bp}) = -\frac{2}{\sqrt{3}}I_{DC} \quad (\text{C.14})$$

The magnitude and angle of the rectifier stage current space vector is determined as follows

$$I_p = \sqrt{I_{qp}^2 + I_{dp}^2} = \frac{2}{\sqrt{3}}I_{DC} \quad (\text{C.15})$$

$$\beta_p = \tan^{-1}\left(\frac{-I_{dp}}{I_{qp}}\right) = \tan^{-1}\left(\frac{\frac{1}{\sqrt{3}}I_{DC}}{0}\right) = \frac{\pi}{2} \quad (\text{C.16})$$

- **Mode 5**

Devices turned ON are S_{cp} and S_{an} ; hence, $I_{ap} = -I_{DC}$, $I_{bp} = 0$ and $I_{cp} = -I_{DC}$

$$I_{qp} = \frac{1}{3}(2I_{ap} - I_{bp} - I_{cp}) = \frac{1}{3}(-2I_{DC} - I_{DC}) = -I_{DC} \quad (\text{C.17})$$

$$I_{dp} = \frac{1}{\sqrt{3}}(I_{cp} - I_{bp}) = \frac{1}{\sqrt{3}}I_{DC} \quad (\text{C.18})$$

The magnitude and angle of the rectifier stage current space vector is determined as follows

$$I_p = \sqrt{I_{qp}^2 + I_{dp}^2} = \frac{2}{\sqrt{3}}I_{DC} \quad (\text{C.19})$$

$$\beta_p = \tan^{-1}\left(\frac{-I_{dp}}{I_{qp}}\right) = \tan^{-1}\left(\frac{-\frac{1}{\sqrt{3}}I_{DC}}{-I_{DC}}\right) = \frac{7\pi}{6} \quad (\text{C.20})$$

- **Mode 6**

Devices turned ON are S_{cp} and S_{bn} ; hence, $I_{ap} = 0$, $I_{bp} = -I_{DC}$ and $I_{cp} = -I_{DC}$

$$I_{qp} = \frac{1}{3}(2I_{ap} - I_{bp} - I_{cp}) = \frac{1}{3}(-I_{DC} + I_{DC}) = 0 \quad (\text{C.21})$$

$$I_{dp} = \frac{1}{\sqrt{3}}(I_{cp} - I_{bp}) = \frac{2}{\sqrt{3}}I_{DC} \quad (\text{C.22})$$

The magnitude of the rectifier stage current space vector is determined as follows

$$I_p = \sqrt{I_{qp}^2 + I_{dp}^2} = \frac{2}{\sqrt{3}} I_{DC} \quad (\text{C.23})$$

The angle of the input current space vector is given as

$$\beta_p = \tan^{-1} \left(\frac{-I_{dp}}{I_{qp}} \right) = \tan^{-1} \left(\frac{-\frac{1}{\sqrt{3}} I_{DC}}{0} \right) = -\frac{\pi}{2} \quad (\text{C.24})$$

APPENDIX D

SELECTION OF SWITCHING CONFIGURATION FOR THE POSSIBLE OUTPUT VOLTAGE AND INPUT CURRENT SECTORS

This section presents the detailed procedure to selected the actual switching sequence used in both direct and indirect space vector shown in Table 3.10'

Case I: (1, 1)

Vectors that can synthesis the desired output voltage and hence maintain the direction of the input current vectors are

-7	AAB	+7	BBA
-9	CCA	+9	AAC
-3	ACC	+3	CAA
-1	BAA	+1	ABB

The following two switching patterns give minimum switching transition

+1	ABB
-7	AAB
+9	AAC
-3	ACC

-9	CCA
3	CAA
-1	BAA
7	BBA

Selected switching patterns: CCC→CCA→CAA→BAA→BBA→BBB

Case II: (1, 2)

Vectors that can synthesis the desired output voltage and hence maintain the direction of the input current vectors are:

-7	AAB	7	BBA
-9	CCA	9	AAC
-4	ABA	4	BAB
-6	CAC	6	ACA

The following two switching patterns give minimum switching transition

+4	BAB
-7	AAB
+9	AAC
-6	CAC

+7	BBA
-4	ABA
+6	ACA
-9	CCA

Selected switching patterns: CCC→CCA→ACA→ABA→BBA→BBB

Case III: (1, 3)

Vectors that can synthesis the desired output voltage and hence maintain the direction of the input current vectors are

-3	ACC	+3	CAA
-1	BAA	+1	ABB
-4	ABA	+4	BAB
-6	CAC	+6	ACA

The following two switching patters give minimum switching transition

-6	CAC
+3	CAA
-1	BAA
+4	BAB

-3	ACC
+6	ACA
-4	ABA
+1	ABB

Selected switching patterns: CCC→ACC→ACA→ABA→ABB→BBB

Case IV: (2, 1)

Vectors that can synthesis the desired output voltage and hence maintain the direction of the input current vectors are

-8	BBC	+8	CCB
-9	CCA	+9	AAC
-2	CBB	+2	BCC
-3	ACC	3	CAA

The following two switching patters give minimum switching transition

-8	BBC
2	BCC
-3	ACC
9	AAC

3	CAA
-9	CCA
8	CCB
-2	CBB

Selected switching patterns BBB→CBB→CCB→CCA→CAA→AAA

Case V: (2, 2)

Vectors that can synthesis the desired output voltage and hence maintain the direction of the input current vectors are

-8	BBC	8	CCB
-9	CCA	9	AAC
-5	BCB	5	CBC
-6	CAC	6	ACA

The following two switching patters give minimum switching transition

9	AAC
-6	CAC
5	CBC
-8	BBC

6	ACA
-9	CCA
8	CCB
-5	BCB

Selected switching patterns BBB→BBA→ABA→ACA→CCA→CCC

Case VI: (2, 3)

Vectors that can synthesis the desired output voltage and hence maintain the direction of the input current vectors are

-5	BCB	+5	CBC
-6	CAC	+6	ACA
-2	CBB	+2	BCC
-3	ACC	+3	CAA

The following two switching patters give minimum switching transition

-2	CBB
+5	CBC
-6	CAC
+3	CAA

-5	BCB
+2	BCC
-3	ACC
6	ACA

Selected switching patterns BBB→BCB→BCC→ACC→ACA→AAA

Case VII: (3, 1)

Vectors that can synthesis the desired output voltage and hence maintain the direction of the input current vectors are

-8	BBC	8	CCB
-7	AAB	7	BBA
-1	BAA	1	ABB
-2	CBB	2	BCC

The following two switching patters give minimum switching transition

2	BCC
-8	BBC
7	BBA
-1	BAA

8	CCB
-2	CBB
1	ABB
-7	AAB

Selected switching patterns: CCC→CCB→CBB→ABB→AAB→AAA

Case VIII: (3, 2)

Vectors that can synthesis the desired output voltage and hence maintain the direction of the input current vectors are:

-5	BCB	5	CBC
-4	ABA	4	BAB
-8	BBC	8	CCB
-7	AAB	7	BBA

The following two switching patterns give minimum switching transition

+5	CBC
-8	BBC
+7	BBA
-4	ABA

+8	CCB
-5	BCB
4	BAB
-7	AAB

Selected switching patterns: CCC→CCB→BCB→BAB→AAB→AAA

Case IX: (3, 3)

Vectors that can synthesis the desired output voltage and hence maintain the direction of the input current vectors are:

-5	BCB	+5	CBC
-4	ABA	+4	BAB
-1	BAA	+1	ABB
-2	CBB	+2	BCC

The following two switching patterns give minimum switching transition

+2	BCC
-5	BCB
+4	BAB
-1	BAA

+5	CBC
-2	CBB
1	ABB
-4	ABA

Selected switching patterns: CCC→CBC→CBB→ABB→ABA→AAA

Case X: (1, 4)

Vectors that can synthesis the desired output voltage and hence maintain the direction of the input current vectors are

-7	AAB	7	BBA
-9	CCA	9	AAC
-3	ACC	3	CAA
-1	BAA	1	ABB

The following two switching patterns give minimum switching transition

-9	CCA
3	CAA
-1	BAA
7	BBA

+1	ABB
-7	AAB
+9	AAC
-3	ACC

Case XI: (6, 5)

Vectors that can synthesis the desired output voltage and hence maintain the direction of the input current vectors are

-5	BCB	5	CBC
-4	ABA	4	BAB
-8	BBC	8	CCB
-7	AAB	7	BBA

The following two switching patterns give minimum switching transition

5	CBC
-8	BBC
7	BBA
-4	ABA

8	CCB
-5	BCB
4	BAB
-7	AAB

The switching pattern has summarized for an input current lie on sector one and for all possible output voltage sectors are shown below.

(1,1)	(1,2)	(1,3)	(1,4)	(1,5)	(1,6)
CCA→CAA→ BAA→BBA	BAB→AAB→ AAC→CAC	CAC→CAA→ BAA→BAB	CCA→CAA→ BAA→BBA	BAB→AAB→ AAC→CAC	CAC→CAA→ BAA→BAB
ABB→AAB→ AAC→ACC	BBA→AB→ ACA→CCA	ACC→ACA→ ABA→ABB	ABB→AAB→ AAC→ACC	BBA→ABA→ ACA→CCA	ACC→ACA→ ABA→ABB

The final switching patterns are

		Sector of output voltage vector					
		1	2	3	4	5	6
In put Current Vector Sector	1	+9 -7 -3 +1	-6 +4 +9 -7	+3 -1 -6 +4	-9 +7 +3 -1	+6 -4 -9 +7	-3 +1 +6 -4
	2	-8 +9 +2 -3	+5 -6 -8 +9	-2 +3 +5 -6	+8 -9 -2 +3	-5 +6 +8 -9	+2 -3 -5 +6
	3	+7 -8 -1 +2	-4 +5 +7 -8	+1 -2 -4 +5	-7 +8 +1 -2	+4 -5 -7 +8	-1 +2 +4 -5
	4	-9 +7 +3 -1	+6 -4 -9 +7	-3 +1 +6 -4	+9 -7 -3 +1	-6 +4 +9 -7	+3 -1 -6 +4
	5	+8 -9 -2 +3	-5 +6 +8 -9	+2 -3 -5 +6	-8 +9 +2 -3	+5 -6 -8 +9	-2 +3 +5 -6
	6	-7 +8 +1 -2	+4 -5 -7 +8	-1 +2 +4 -5	+7 -8 -1 +2	-4 +5 +7 -8	+1 -2 -4 +5
Times		t ₁ t ₂ t ₃ t ₄	t ₁ t ₂ t ₃ t ₄	t ₁ t ₂ t ₃ t ₄	t ₁ t ₂ t ₃ t ₄	t ₁ t ₂ t ₃ t ₄	t ₁ t ₂ t ₃ t ₄

APPENDIX E

REFERENCE FRAME TRANSFORMATION OF MODULATION SIGNALS

The objective of this derivation is to obtain an expression of the modulation signals in qd transformation. Then it possible to write an explicit expression for the mapping between the input and output currents of a matrix converter in a qd reference frame. Similarly, the output voltage can also be written in terms of the input capacitor voltages using the qd reference frame. The relationship between the input and output currents of a matrix converter in terms of the switching signals are given as

$$\begin{aligned} I_{ap} &= S_{aA}I_{as} + S_{aB}I_{bs} + S_{aC}I_{cs} \\ I_{bp} &= S_{bA}I_{as} + S_{bB}I_{bs} + S_{bC}I_{cs} \\ I_{cp} &= S_{cA}I_{as} + S_{cB}I_{bs} + S_{cC}I_{cs} \end{aligned} \quad (E.1)$$

The output voltage can be calculated from the input filter capacitor voltage and the switching function as:

$$\begin{aligned} V_{as} &= S_{aA}V_{ap} + S_{bA}V_{bp} + S_{cA}V_{cp} \\ V_{bs} &= S_{aB}V_{ap} + S_{bB}V_{bp} + S_{cB}V_{cp} \\ V_{cs} &= S_{aC}V_{ap} + S_{bC}V_{bp} + S_{cC}V_{cp} \end{aligned} \quad (E.2)$$

There are two transformations carried out in this analysis: the input side and output side transformations $K(\theta_p)$ and $K(\theta_s)$ where θ_{op} and θ_{os} are their corresponding initial angle of the reference frames respectively.

$$K_p = \frac{2}{3} \begin{bmatrix} \cos(\omega_p t + \theta_{op}) & \cos(\omega_p t + \theta_{op} - \frac{2\pi}{3}) & \cos(\omega_p t + \theta_{op} + \frac{2\pi}{3}) \\ \sin(\omega_p t + \theta_{op}) & \sin(\omega_p t + \theta_{op} - \frac{2\pi}{3}) & \sin(\omega_p t + \theta_{op} + \frac{2\pi}{3}) \\ \frac{1}{2} & \frac{1}{2} & \frac{1}{2} \end{bmatrix} \quad (\text{E.3})$$

The transformation matrix used for the output side transformation is given (E.4)

$$K_s = \frac{2}{3} \begin{bmatrix} \cos(\omega_s t + \theta_{os}) & \cos(\omega_s t + \theta_{os} - \frac{2\pi}{3}) & \cos(\omega_s t + \theta_{os} + \frac{2\pi}{3}) \\ \sin(\omega_s t + \theta_{os}) & \sin(\omega_s t + \theta_{os} - \frac{2\pi}{3}) & \sin(\omega_s t + \theta_{os} + \frac{2\pi}{3}) \\ \frac{1}{2} & \frac{1}{2} & \frac{1}{2} \end{bmatrix} \quad (\text{E.4})$$

The inverse transformation matrix for the input side is

$$(K_p)^{-1} = \begin{bmatrix} \cos(\omega_p t + \theta_{op}) & \sin(\omega_p t + \theta_{op}) & 1 \\ \cos(\omega_p t + \theta_{op} - \frac{2}{3}\pi) & \sin(\omega_p t + \theta_{op} - \frac{2}{3}\pi) & 1 \\ \cos(\omega_p t + \theta_{op} + \frac{2}{3}\pi) & \sin(\omega_p t + \theta_{op} + \frac{2}{3}\pi) & 1 \end{bmatrix} \quad (\text{E.5})$$

Similarly, the inverse transformation for the output side can be given as

$$(K_s)^{-1} = \begin{bmatrix} \cos(\omega_s t + \theta_{os}) & \sin(\omega_s t + \theta_{os}) & 1 \\ \cos(\omega_s t + \theta_{os} - \frac{2\pi}{3}) & \sin(\omega_s t + \theta_{os} - \frac{2\pi}{3}) & 1 \\ \cos(\omega_s t + \theta_{os} + \frac{2\pi}{3}) & \sin(\omega_s t + \theta_{os} + \frac{2\pi}{3}) & 1 \end{bmatrix} \quad (\text{E.6})$$

Equation (E.1) and (E.2) can be represented as follow

$$I_{abcp} = S^T I_{abcs} \quad (\text{E.5})$$

$$V_{abcs} = S V_{abcp}^* \quad (\text{E.6})$$

where the voltage and current vectors are well as the switching signals matrix is given as

$$V_{abcs} = \begin{bmatrix} V_{as} \\ V_{bs} \\ V_{cs} \end{bmatrix} \quad I_{abcp} = \begin{bmatrix} I_{ap} \\ I_{bp} \\ I_{cp} \end{bmatrix} \quad I_{abcs} = \begin{bmatrix} I_{as} \\ I_{bs} \\ I_{cs} \end{bmatrix} \quad V_{abcp} = \begin{bmatrix} V_{ap} \\ V_{bp} \\ V_{cp} \end{bmatrix}$$

The nine switching functions can be represented in matrix form as

$$S = \begin{bmatrix} S_{aA} & S_{bA} & S_{cA} \\ S_{aB} & S_{bB} & S_{cB} \\ S_{aC} & S_{bC} & S_{cC} \end{bmatrix} \quad (\text{E.7})$$

Define the following *qd* input and output voltage and current vectors as

$$\begin{aligned} V_{qdop} &= K_p V_{abcp} & V_{qdos} &= K_s V_{abcs} \\ I_{qdop} &= K_p I_{abcp} & I_{qdos} &= K_s I_{abcs} \end{aligned}$$

The synchronous reference frame equations corresponding to (E.5) through (E.6) is given below:

$$I_{qdop} = K_p S^T (K_s)^{-1} I_{qdos} = M_{qdoI} I_{qdos} \quad (\text{E.8})$$

$$V_{qdos} = K_s S (K_p)^{-1} V_{qdop}^* = M_{qdoV} V_{qdop}^* \quad (\text{E.9})$$

From (E8),

$$M_{qdoI} = K_p S^T (K_s)^{-1} \quad (\text{E.10})$$

Since the averaged switching signals can be expressed as

$$S_{ij} = \frac{1}{3} + \frac{2}{3} \left(\frac{V_{js} + V_{np}}{V_p} \right) \frac{V_{ip}}{V_p} \quad (\text{E.11})$$

Separating (E.11) into two components as follow

$$S_{ip} = \frac{V_{ip}}{V_p^*} \quad \text{and} \quad S_{js} = \frac{V_{js} + V_{np}}{V_p^*} \quad (\text{E.12})$$

where

$$S_{js} = \begin{bmatrix} S_{As} \\ S_{Bs} \\ S_{Cs} \end{bmatrix} \quad S_{ip} = [S_{ap} \quad S_{bp} \quad S_{cp}]$$

Using (E.12) the expression for the averaged switching signals can be modified as

$$S_{ij} = \frac{1}{3} + \frac{2}{3} S_{js} S_{ip} \quad (\text{E.13})$$

Using the following switching arrays

$$(S_{ip})^T = \begin{bmatrix} S_{ap} \\ S_{bp} \\ S_{cp} \end{bmatrix} \quad (S_{js}) = [S_{As} \quad S_{Bs} \quad S_{Cs}]$$

The expression given in (E.13) can also be given as

$$S = \frac{1}{3} I + \frac{2}{3} \begin{bmatrix} S_{ap} \\ S_{bp} \\ S_{cp} \end{bmatrix} [S_{As} \quad S_{Bs} \quad S_{Cs}] \quad (\text{E.14})$$

where I is the identity matrix, substituting (E.13) into (E.10)

$$\begin{aligned} M_{qdoi} &= K_p \left(\frac{1}{3} I + \frac{2}{3} (S_{js} S_{ip})^T \right) (K_s)^{-1} \\ &= \frac{1}{3} K_p I (K_s)^{-1} + \frac{2}{3} K_p S_{ip}^T S_{js}^T (K_s)^{-1} \end{aligned} \quad (\text{E.15})$$

Using the property of transpose of a matrix $(AB)^T = B^T A^T$

Substituting the transformation matrices given in (E.3) to (E.6)

$$\frac{1}{3} K_p I(K_s)^{-1} = \frac{1}{3} x \frac{2}{3} \begin{bmatrix} \cos(\omega_p t + \theta_{op}) & \cos(\omega_p t + \theta_{op} - \frac{2}{3}\pi) & \cos(\omega_p t + \theta_{op} + \frac{2}{3}\pi) \\ \sin(\omega_p t + \theta_{op}) & \sin(\omega_p t + \theta_{op} - \frac{2}{3}\pi) & \sin(\omega_p t + \theta_{op} + \frac{2}{3}\pi) \\ \frac{1}{2} & \frac{1}{2} & \frac{1}{2} \end{bmatrix}$$

$$\begin{bmatrix} 1 & 1 & 1 \\ 1 & 1 & 1 \\ 1 & 1 & 1 \end{bmatrix} \begin{bmatrix} \cos(\omega_s t + \theta_{os}) & \sin(\omega_s t + \theta_{os}) & 1 \\ \cos(\omega_s t + \theta_{os} - \frac{2}{3}\pi) & \sin(\omega_s t + \theta_{os} - \frac{2}{3}\pi) & 1 \\ \cos(\omega_s t + \theta_{os} + \frac{2}{3}\pi) & \sin(\omega_s t + \theta_{os} + \frac{2}{3}\pi) & 1 \end{bmatrix}$$

Simplifying the above expression

$$\frac{1}{3} K_p I(K_s)^{-1} = \begin{bmatrix} 0 & 0 & 0 \\ 0 & 0 & 0 \\ 0 & 0 & 1 \end{bmatrix} = k_1 \quad (\text{E.16})$$

Using the input and output side transformation

$$K_p S_{ip}^T S_{js}^T (K_s)^{-1} = (K_p S_{ip}^T) (S_{js}^T (K_s)^{-1}) \quad (\text{E.17})$$

The transformed array of switching signals corresponding to the input side and output side respectively are given as

$$S_{qdop} = K_p S_{ip}^T \quad (\text{E.18})$$

$$S_{qdos} = K_s S_{is} \quad (\text{E.19})$$

From (E.8)

$$M_{qdos} = K_s S_{js} \Rightarrow S_{js} = (K_s)^{-1} M_{qdos} \quad (\text{E.20})$$

$$S_{js}^T = ((K_s)^{-1} M_{qdos})^T = (M_{qdos})^T ((K_s)^{-1})^T \quad (\text{E.21})$$

$$S_{js}^T = (M_{qdos})^T ((K_s)^{-1})^T \quad (\text{E.22})$$

Similarly,

$$K_p S_{ip} S_{js} (K_s)^{-1} = M_{qdop} (M_{qdos})^T ((K_s)^{-1})^T (K_s)^{-1} \quad (\text{E.23})$$

Substituting the transformation matrices given in (E.3) to (E.6)

$$((K_s)^{-1})^T (K_s)^{-1} = \begin{bmatrix} \cos(\omega_s t + \theta_{os}) & \sin(\omega_s t + \theta_{os}) & 1 \\ \cos(\omega_s t + \theta_{os} - \frac{2}{3}\pi) & \sin(\omega_s t + \theta_{os} - \frac{2}{3}\pi) & 1 \\ \cos(\omega_s t + \theta_{os} + \frac{2}{3}\pi) & \sin(\omega_s t + \theta_{os} + \frac{2}{3}\pi) & 1 \end{bmatrix}^T$$

$$\begin{bmatrix} \cos(\omega_s t + \theta_{os}) & \sin(\omega_s t + \theta_{os}) & 1 \\ \cos(\omega_s t + \theta_{os} - \frac{2}{3}\pi) & \sin(\omega_s t + \theta_{os} - \frac{2}{3}\pi) & 1 \\ \cos(\omega_s t + \theta_{os} + \frac{2}{3}\pi) & \sin(\omega_s t + \theta_{os} + \frac{2}{3}\pi) & 1 \end{bmatrix}$$

Multiplying the above matrices

$$((K_s)^{-1})^T (K_s)^{-1} = \frac{3}{2} \begin{bmatrix} 1 & 0 & 0 \\ 0 & 1 & 0 \\ 0 & 0 & 2 \end{bmatrix} = k_2 \quad (\text{E.24})$$

Substituting (E.24) to (E.23)

$$K_p S_{ip} S_{js} (K_s)^{-1} = M_{qdop} (M_{qdos})^T k_{2I} \quad (\text{E.25})$$

Using (E.25) and (E.16)

$$M_{qdol} = k_{1I} + \frac{2}{3} M_{qdop} (M_{qdos})^T k_{2I} \quad (\text{E.26})$$

Using similar approach,

$$M_{qdoV} = K_s \left(\frac{1}{3} I + \frac{2}{3} S_{js} S_{ip} \right) (K_p)^{-1}$$

$$M_{qdoV} = \frac{1}{3} K_s I (K_p)^{-1} + \frac{2}{3} (K_s S_{js}) (S_{ip} (K_p)^{-1}) \quad (\text{E.27})$$

Substituting the transformation matrices given in (E.3) to (E.6) in the above expression

$$\frac{1}{3} K_s I (K_p)^{-1} = \frac{1}{3} x \frac{2}{3} \begin{bmatrix} \cos(\omega_s t + \theta_{op}) & \cos(\omega_s t + \theta_{op} - \frac{2}{3}\pi) & \cos(\omega_s t + \theta_{op} + \frac{2}{3}\pi) \\ \sin(\omega_s t + \theta_{op}) & \sin(\omega_s t + \theta_{op} - \frac{2}{3}\pi) & \sin(\omega_s t + \theta_{op} + \frac{2}{3}\pi) \\ \frac{1}{2} & \frac{1}{2} & \frac{1}{2} \end{bmatrix}$$

$$\begin{bmatrix} 1 & 1 & 1 \\ 1 & 1 & 1 \\ 1 & 1 & 1 \end{bmatrix}$$

$$\begin{bmatrix} \cos(\omega_p t + \theta_{os}) & \sin(\omega_p t + \theta_{os}) & 1 \\ \cos(\omega_p t + \theta_{os} - \frac{2}{3}\pi) & \sin(\omega_p t + \theta_{os} - \frac{2}{3}\pi) & 1 \\ \cos(\omega_p t + \theta_{os} + \frac{2}{3}\pi) & \sin(\omega_p t + \theta_{os} + \frac{2}{3}\pi) & 1 \end{bmatrix}$$

Simplifying the above matrix multiplication,

$$\frac{1}{3} K_p I (K_s)^{-1} = \begin{bmatrix} 0 & 0 & 0 \\ 0 & 0 & 0 \\ 0 & 0 & 1 \end{bmatrix} = k_1 \quad (\text{E.28})$$

Simplifying the second term given in (E.27)

$$M_{qdos} = K_s S_{js} \quad (\text{E.29})$$

$$M_{qdop} = K_p S_{ip}^T \Rightarrow S_{ip}^T = (K_p)^{-1} M_{qdop}$$

$$S_{ip}^T = (K_p)^{-1} M_{qdop} \Rightarrow S_{ip} = ((K_p)^{-1} M_{qdop})^T = M_{qdop}^T ((K_p)^{-1})^T$$

Therefore the following equation holds true

$$(K_s S_{js})(S_{ip} (K_p)^{-1}) = (M_{qdos})(M_{qdop}^T ((K_p)^{-1})^T (K_p)^{-1}) \quad (E.30)$$

Substituting the transformation matrices given in (E.3) to (E.6)

$$((K_p)^{-1})^T (K_p)^{-1} = \begin{bmatrix} \cos(\omega_p t + \theta_{os}) & \sin(\omega_p t + \theta_{os}) & 1 \\ \cos(\omega_p t + \theta_{os} - \frac{2}{3}\pi) & \sin(\omega_p t + \theta_{os} - \frac{2}{3}\pi) & 1 \\ \cos(\omega_p t + \theta_{os} + \frac{2}{3}\pi) & \sin(\omega_p t + \theta_{os} + \frac{2}{3}\pi) & 1 \end{bmatrix}^T \begin{bmatrix} \cos(\omega_p t + \theta_{os}) & \sin(\omega_p t + \theta_{os}) & 1 \\ \cos(\omega_p t + \theta_{os} - \frac{2}{3}\pi) & \sin(\omega_p t + \theta_{os} - \frac{2}{3}\pi) & 1 \\ \cos(\omega_p t + \theta_{os} + \frac{2}{3}\pi) & \sin(\omega_p t + \theta_{os} + \frac{2}{3}\pi) & 1 \end{bmatrix}$$

The above matrix multiplication gives,

$$((K_p)^{-1})^T (K_p)^{-1} = \frac{3}{2} \begin{bmatrix} 1 & 0 & 0 \\ 0 & 1 & 0 \\ 0 & 0 & 2 \end{bmatrix} = k_{2v} \quad (E.31)$$

Therefore, the q-d-o equations of the modulation signals are:

$$M_{qdoV} = k_{1V} + \gamma M_{qdos} (M_{qdop})^T k_{2V} \quad (E.32)$$

$$M_{qdoI} = k_{1I} + \gamma M_{qdop} (M_{qdos})^T k_{2I} \quad (E.33)$$

Calculation of M_{qdos} is shown below

$$S_{js} = \frac{V_{js} + V_{np}}{V_p^*} \quad (\text{E.34})$$

Let the balanced output voltage is given as follows where V_n is the magnitude of the output voltage.

$$V_{an} = V_n \cos(\omega_s t + \theta_{on}) \quad (\text{E.35})$$

$$V_{an} = V_n \cos(\omega_s t + \theta_{on} - \frac{2\pi}{3}) \quad (\text{E.36})$$

$$V_{an} = V_n \cos(\omega_s t + \theta_{on} + \frac{2\pi}{3}) \quad (\text{E.37})$$

θ_{on} is the initial angle of the output phase voltage and the three phase balanced input capacitor voltage are

$$V_{ap} = V_p \cos(\omega_p t + \theta_{om}) \quad (\text{E.38})$$

$$V_{bp} = V_p \cos(\omega_p t + \theta_{om} - \frac{2\pi}{3}) \quad (\text{E.39})$$

$$V_{cp} = V_p \cos(\omega_p t + \theta_{om} + \frac{2\pi}{3}) \quad (\text{E.40})$$

θ_{om} is the initial angle of the input capacitor voltage

$$M_{qdos} = K_s S_{js} = \frac{2}{3} \begin{bmatrix} \cos(\omega_s t + \theta_{os}) & \cos(\omega_s t + \theta_{os} - \frac{2}{3}\pi) & \cos(\omega_s t + \theta_{os} + \frac{2}{3}\pi) \\ \sin(\omega_s t + \theta_{os}) & \sin(\omega_s t + \theta_{os} - \frac{2}{3}\pi) & \sin(\omega_s t + \theta_{os} + \frac{2}{3}\pi) \\ \frac{1}{2} & \frac{1}{2} & \frac{1}{2} \end{bmatrix} \begin{bmatrix} S_{As} \\ S_{Bs} \\ S_{Cs} \end{bmatrix}$$

Substituting (E.34) into the expression given above

$$M_{qdos} = \frac{2}{3} \begin{bmatrix} \cos(\omega_s t + \theta_{os}) & \cos(\omega_s t + \theta_{os} - \frac{2}{3}\pi) & \cos(\omega_s t + \theta_{os} + \frac{2}{3}\pi) \\ \sin(\omega_s t + \theta_{os}) & \sin(\omega_s t + \theta_{os} - \frac{2}{3}\pi) & \sin(\omega_s t + \theta_{os} + \frac{2}{3}\pi) \\ \frac{1}{2} & \frac{1}{2} & \frac{1}{2} \end{bmatrix} \begin{bmatrix} \frac{V_{an} + V_{np}}{V_p^*} \\ \frac{V_{bn} + V_{np}}{V_p^*} \\ \frac{V_{cn} + V_{np}}{V_p^*} \end{bmatrix}$$

Multiplying the two terms

$$M_{qdos} = \frac{2}{3V_p^*} \begin{bmatrix} V_{an} \cos(\omega_s t + \theta_{os}) + V_{bn} \cos(\omega_s t + \theta_{os} - \frac{2}{3}\pi) + V_{cn} \cos(\omega_s t + \theta_{os} + \frac{2}{3}\pi) \\ V_{an} \sin(\omega_s t + \theta_{os}) + V_{bn} \sin(\omega_s t + \theta_{os} - \frac{2}{3}\pi) + V_{cn} \sin(\omega_s t + \theta_{os} + \frac{2}{3}\pi) \\ \frac{1}{2} \underbrace{(V_{an} + V_{bn} + V_{cn})}_0 + \frac{3}{2} V_{np} \end{bmatrix} \quad (\text{E.41})$$

Simplifying the first and the second elements of the array

$$\begin{aligned} & V_{an} \sin(\omega_s t + \theta_{os}) + V_{bn} \sin(\omega_s t + \theta_{os} - \frac{2\pi}{3}) + V_{cn} \sin(\omega_s t + \theta_{os} + \frac{2\pi}{3}) \\ &= V_n \cos(\omega_s t + \theta_{on}) \sin(\omega_s t + \theta_{os}) + V_n \cos(\omega_s t + \theta_{on} - \frac{2\pi}{3}) \sin(\omega_s t + \theta_{os} - \frac{2\pi}{3}) + \\ & V_{cn} \cos(\omega_s t + \theta_{on} + \frac{2\pi}{3}) \sin(\omega_s t + \theta_{on} + \frac{2\pi}{3}) \\ &= -\frac{3V_n}{2} \sin(\theta_{on} - \theta_{os}) \end{aligned}$$

Therefore

$$M_{qdos} = \begin{bmatrix} M_{qs} \\ M_{ds} \\ M_{os} \end{bmatrix} = \frac{2}{3V_p^*} \begin{bmatrix} \frac{3V_n}{2} \cos(\theta_{on} - \theta_{os}) \\ -\frac{3V_n}{2} \sin(\theta_{on} - \theta_{os}) \\ \frac{3}{2} V_{np} \end{bmatrix} = \begin{bmatrix} \frac{V_n}{V_p^*} \cos(\theta_{on} - \theta_{os}) \\ -\frac{V_n}{V_p^*} \sin(\theta_{on} - \theta_{os}) \\ V_{np} \end{bmatrix} \quad (\text{E.42})$$

Therefore the qdo axis component of the modulation signal corresponding with the output side can be given as

$$\begin{aligned}
 M_{qs} &= \frac{V_n}{V_p^*} \cos(\theta_{on} - \theta_{os}) \\
 M_{ds} &= -\frac{V_n}{V_p^*} \sin(\theta_{on} - \theta_{os}) \\
 M_{os} &= \frac{V_{np}}{V_p^*}
 \end{aligned} \tag{E.43}$$

The expression for M_{qdop} can be analyzed as follows

$$M_{qdop} = K_p S_{ip} = \frac{2}{3} \begin{bmatrix} \cos(\omega_p t + \theta_{op}) & \cos(\omega_p t + \theta_{op} - \frac{2}{3}\pi) & \cos(\omega_p t + \theta_{op} + \frac{2}{3}\pi) \\ \sin(\omega_p t + \theta_{op}) & \sin(\omega_p t + \theta_{op} - \frac{2}{3}\pi) & \sin(\omega_p t + \theta_{op} + \frac{2}{3}\pi) \\ \frac{1}{2} & \frac{1}{2} & \frac{1}{2} \end{bmatrix} \begin{bmatrix} S_{As} \\ S_{Bs} \\ S_{Cs} \end{bmatrix}$$

Simplifying the above analysis

$$M_{qdop} = \frac{2}{3V_p^*} \begin{bmatrix} V_{ap} \cos(\omega_p t + \theta_{op}) + V_{bp} \cos(\omega_p t + \theta_{op} - \frac{2}{3}\pi) + V_{cp} \cos(\omega_p t + \theta_{op} + \frac{2}{3}\pi) \\ V_{ap} \sin(\omega_p t + \theta_{op}) + V_{bp} \sin(\omega_p t + \theta_{op} - \frac{2}{3}\pi) + V_{cp} \sin(\omega_p t + \theta_{op} + \frac{2}{3}\pi) \\ \frac{1}{2} (V_{ap}^* + V_{bp}^* + V_{cp}^*) \end{bmatrix}$$

Using similar simplification used for (E.42),

$$M_{qdop} = \begin{bmatrix} M_{qp} \\ M_{dp} \\ M_{op} \end{bmatrix} = \begin{bmatrix} \cos(\theta_{om} - \theta_{op}) \\ -\sin(\theta_{om} - \theta_{op}) \\ 0 \end{bmatrix} \tag{E.44}$$

Therefore qdo components of the modulation signals related to the input side are given as

$$\begin{aligned} M_{qp} &= \cos(\theta_{on} - \theta_{os}) \\ M_{dp} &= -\sin(\theta_{on} - \theta_{os}) \\ M_{op} &= 0 \end{aligned} \quad (E.45)$$

And

$$\begin{bmatrix} M_{qp} \\ M_{dp} \\ M_{op} \end{bmatrix} = \begin{bmatrix} \cos(\theta_{om} - \theta_{op}) \\ -\sin(\theta_{om} - \theta_{op}) \\ 0 \end{bmatrix} \quad (E.46)$$

The expression for M_{qdoV} becomes

$$M_{qdoV} = k_{1V} + \frac{2}{3} M_{qdos} (M_{qdop})^T k_{2V}$$

Substituting (E.42) and (E.44) into (E.47)

$$M_{qdoV} = \begin{bmatrix} 0 & 0 & 0 \\ 0 & 0 & 0 \\ 0 & 0 & 1 \end{bmatrix} + \frac{2}{3} \begin{bmatrix} \frac{V_n}{V_p^*} \cos(\theta_{on} - \theta_{os}) \\ -\frac{V_n}{V_p^*} \sin(\theta_{on} - \theta_{os}) \\ V_{np} \end{bmatrix} \begin{bmatrix} \cos(\theta_{om} - \theta_{op}) \\ -\sin(\theta_{om} - \theta_{op}) \\ 0 \end{bmatrix}^T \frac{3}{2} \begin{bmatrix} 1 & 0 & 0 \\ 0 & 1 & 0 \\ 0 & 0 & 2 \end{bmatrix}$$

The synchronous reference frame modulation signals which map the input and output three phase voltages are

$$M_{qdoV} = \begin{bmatrix} \frac{V_n}{V_p} \cos(\theta_{on} - \theta_{os}) \cos(\theta_{om} - \theta_{op}) & -\frac{V_n}{V_p} \cos(\theta_{on} - \theta_{os}) \sin(\theta_{om} - \theta_{op}) & 0 \\ -\frac{V_n}{V_p} \sin(\theta_{on} - \theta_{os}) \cos(\theta_{om} - \theta_{op}) & \frac{V_n}{V_p} \sin(\theta_{on} - \theta_{os}) \sin(\theta_{om} - \theta_{op}) & 0 \\ V_{np} \cos(\theta_{om} - \theta_{op}) & -V_{np} \sin(\theta_{om} - \theta_{op}) & 1 \end{bmatrix} \quad (E.47)$$

The expression for M_{qdoi}

$$M_{qdoi} = k_{1I} + \mathcal{M}_{qdop} (M_{qdos})^T k_{2I} \quad (\text{E.47})$$

Substituting (E.42) and (E.44) into (E.47)

$$M_{qdoi} = \begin{bmatrix} 0 & 0 & 0 \\ 0 & 0 & 0 \\ 0 & 0 & 1 \end{bmatrix} + \frac{2}{3} \begin{bmatrix} \cos(\theta_{om} - \theta_{op}) \\ -\sin(\theta_{om} - \theta_{op}) \\ 0 \end{bmatrix} \begin{bmatrix} \frac{V_n}{V_p^*} \cos(\theta_{on} - \theta_{os}) \\ -\frac{V_n}{V_p^*} \sin(\theta_{on} - \theta_{os}) \\ V_{np} \end{bmatrix}^T \frac{3}{2} \begin{bmatrix} 1 & 0 & 0 \\ 0 & 1 & 0 \\ 0 & 0 & 2 \end{bmatrix}$$

Similarly the synchronous reference frame modulation signals which maps the input and output three phase currents are

$$M_{qdoi} = \begin{bmatrix} \frac{V_n}{V_p} \cos(\theta_{on} - \theta_{os}) \cos(\theta_{om} - \theta_{op}) & -\frac{V_n}{V_p} \sin(\theta_{on} - \theta_{os}) \cos(\theta_{om} - \theta_{op}) & 2V_{np} \\ -\frac{V_n}{V_p} \cos(\theta_{on} - \theta_{os}) \sin(\theta_{om} - \theta_{op}) & \frac{V_n}{V_p} \sin(\theta_{on} - \theta_{os}) \sin(\theta_{om} - \theta_{op}) & 2V_{np} \\ 0 & 0 & 1 \end{bmatrix} \quad (\text{E.48})$$

θ_{om} is initial angle of input capacitor voltage

θ_{op} is initial angle of input side transformations

θ_{on} is initial angle of output voltage

θ_{os} is initial angle of output side transformations

Define

$$M = \frac{V_n}{V_p}$$

The four components of the modulation signals which are used extensively in this work are given as follow.

$$M_{qq} = M \cos(\theta_{on} - \theta_{os}) \cos(\theta_{om} - \theta_{op}) \quad (\text{E.38})$$

$$M_{qd} = M \sin(\theta_{on} - \theta_{os}) \cos(\theta_{om} - \theta_{op}) \quad (\text{E.38})$$

$$M_{dq} = M \cos(\theta_{on} - \theta_{os}) \sin(\theta_{om} - \theta_{op}) \quad (\text{E.38})$$

$$M_{dd} = M \sin(\theta_{on} - \theta_{os}) \sin(\theta_{om} - \theta_{op}) \quad (\text{E.38})$$

APPENDIX F

FOURIER SERIES REPRESENTATION OF A PWM WAVEFORM FOR A NON-INTEGER MULTIPLE FREQUENCY WITH A NON- ZERO PHASE ANGLE

A theoretical analysis of the harmonic content of a PWM waveform when the modulation signal consists of 5th and 7th harmonics is presented in [56]. Moreover, a general solution for harmonic coefficients of a PWM output for a single-phase converter leg is also given in [58, 81]. In [57], a non-zero phase angle of harmonic content in the modulation signal is considered the Fourier series analysis; however, it did not show the effect of phase angle clearly. The objective of this work is to determine the harmonic coefficients of a PWM output when the modulation signals consist of two harmonics which are not necessarily to be integer with a non-zero phase angles. The work is applied to analyze the Fourier series of switching signals for a matrix converter. The modulation signals consisting of a fundamental and two harmonics which both are non-integer multiple of the fundamental is given as:

$$M(t) = M \cos(\omega_o t + \theta_o) + M_a \cos(a \omega_o t + \theta_{ao}) + M_b \cos(b \omega_o t + \theta_{bo}) \quad (\text{F.1})$$

where

M is the modulation index for the fundamental component

M_a is the modulation index for the a^{th} harmonics

M_b is the modulation index for the b^{th} harmonics

ω_o is the angular frequency of the fundamental component of modulation signal

θ_o is the initial angle of the fundamental component of modulation signal

Define $y = \omega_o t$ (F.1) can be written as

$$M(y) = M \cos(y + \theta_o) + M_a \cos(ay + \theta_{ao}) + M_b \cos(by + \theta_{bo}) \quad (\text{F.2})$$

The coefficient of the furrier series is given by:

$$C_{mn} = A_{mn} + jB_{mn} = \frac{1}{2\pi^2} \int_{-\pi}^{\pi} \int_{-\frac{\pi}{2(1+M(y))}}^{\frac{\pi}{2(1+M(y))}} V_{dc} e^{j(mx+ny)} dx dy \quad (\text{F.3})$$

Substituting (F.2) into (F.3),

$$C_{mn} = \frac{V_{dc}}{2\pi^2} \int_{-\pi}^{\pi} \int_{-\frac{\pi}{2}}^0 \left(1 + M \cos(y_r + \theta_o) + M_a \cos(ay_r + \theta_{ao}) + M_b \cos(by_r + \theta_{bo}) \right) e^{j(mx+n(y_r + \frac{\omega_o}{\omega_c}(x + \frac{\pi}{2})))} dx dy_r + \int_{-\pi}^{\pi} \int_0^{\frac{\pi}{2}} \left(1 + M \cos(y_f + \theta_o) + M_a \cos(ay_f + \theta_{ao}) + M_b \cos(by_f + \theta_{bo}) \right) e^{j(mx+n(y_f + \frac{\omega_o}{\omega_c}(x - \frac{\pi}{2})))} dx dy_f \quad (\text{F.4})$$

Rearranging the expression given in (F.4)

$$C_{mn} = \frac{V_{dc}}{2\pi^2} \int_{-\pi}^{\pi} \int_{-\frac{\pi}{2}}^0 \left(1 + M \cos(y_r + \theta_o) + M_a \cos(ay_r + \theta_{ao}) + M_b \cos(by_r + \theta_{bo}) \right) e^{jn\frac{\omega_o}{\omega_c} \frac{\pi}{2}} e^{j(m + \frac{\omega_o}{\omega_c}n)x} e^{jny_r} dx dy_r + \int_{-\pi}^{\pi} \int_0^{\frac{\pi}{2}} \left(1 + M \cos(y_f + \theta_o) + M_a \cos(ay_f + \theta_{ao}) + M_b \cos(by_f + \theta_{bo}) \right) e^{jn\frac{\omega_o}{\omega_c} \frac{\pi}{2}} e^{j(m - \frac{\omega_o}{\omega_c}n)x} e^{jny_f} dx dy_f \quad (\text{F.5})$$

Define the following terms,

$$q = m + \frac{\omega_o}{\omega_c} n \quad (\text{F.6})$$

Substituting (F.6) into (F.5)

$$C_{mn} = \frac{V_{dc}}{2\pi^2} \int_{-\pi}^{\pi} e^{jn\frac{\omega_o}{\omega_c} \frac{\pi}{2}} e^{jny_r} \int_{-\frac{\pi}{2}}^0 \left(1 + M \cos(y_r + \theta_o) + M_a \cos(ay_r + \theta_{ao}) + M_b \cos(by_r + \theta_{bo}) \right) e^{jqx} dx dy_r + \int_{-\pi}^{\pi} e^{-jn\frac{\omega_o}{\omega_c} \frac{\pi}{2}} e^{jny_f} \int_0^{\frac{\pi}{2}} \left(1 + M \cos(y_f + \theta_o) + M_a \cos(ay_f + \theta_{ao}) + M_b \cos(by_f + \theta_{bo}) \right) e^{jqx} dx dy_f \quad (\text{F.7})$$

Evaluating the inner integral,

$$C_{mn} = \frac{V_{dc}}{2\pi^2 j q} \left(e^{jn \frac{\omega_o \pi}{\omega_c 2} \int_{-\pi}^{\pi} e^{jny_r'} e^{jqx} \Big|_{\frac{\pi}{2}(1+M \cos(y_r'+\theta_o)+M_a \cos(ay_r'+\theta_{ao})+M_b \cos(by_r'+\theta_{bo}))}^0 dy_r' + \right. \\ \left. e^{-jn \frac{\omega_o \pi}{\omega_c 2} \int_{-\pi}^{\pi} e^{jny_f'} e^{jqx} \Big|_0^{\frac{\pi}{2}(1+M \cos(y_f'+\theta_o)+M_a \cos(ay_f'+\theta_{ao})+M_b \cos(by_f'+\theta_{bo}))} dy_f' \right)$$

Solving the inner integral,

$$C_{mn} = \frac{V_{dc}}{2\pi^2 j q} \left(e^{jn \frac{\omega_o \pi}{\omega_c 2} \int_{-\pi}^{\pi} e^{jny_r'} \left(1 - e^{-j \frac{\pi}{2} q (1+M \cos(y_r'+\theta_o)+M_a \cos(ay_r'+\theta_{ao})+M_b \cos(by_r'+\theta_{bo}))} \right) dy_r' + \right. \\ \left. e^{-jn \frac{\omega_o \pi}{\omega_c 2} \int_{-\pi}^{\pi} e^{jny_f'} \left(-1 + e^{j \frac{\pi}{2} q (M \cos(y_f'+\theta_o)+M_a \cos(ay_f'+\theta_{ao})+M_b \cos(by_f'+\theta_{bo}))} \right) dy_f' \right)$$

Simplifying the above expression result in

$$C_{mn} = \frac{V_{dc}}{2\pi^2 j q} \left(-e^{jn \frac{\omega_o \pi}{\omega_c 2} \int_{-\pi}^{\pi} e^{jny_r'} e^{-j \frac{\pi}{2} q} e^{-j \frac{\pi}{2} q M \cos(y_r'+\theta_o)} e^{-j \frac{\pi}{2} q M_a \cos(ay_r'+\theta_{ao})} e^{-j \frac{\pi}{2} q M_b \cos(by_r'+\theta_{bo})} dy_r' \right. \\ \left. e^{-jn \frac{\omega_o \pi}{\omega_c 2} \int_{-\pi}^{\pi} e^{jny_f'} e^{j \frac{\pi}{2} q} e^{j \frac{\pi}{2} q M \cos(y_f'+\theta_o)} e^{j \frac{\pi}{2} q M_a \cos(ay_f'+\theta_{ao})} e^{j \frac{\pi}{2} q M_b \cos(by_f'+\theta_{bo})} dy_f' \right)$$

Using Jacobi-Anger expansion $e^{\pm j \xi \cos(\theta)}$ can be given in Bessel series expressions as:

$$e^{\pm j \xi \cos(\theta)} = J_o(\xi) + 2 \sum_{k=1}^{\infty} j^{\pm k} J_k(\xi) \cos(k\theta) \quad (F.8)$$

Using the following properties of Bessel function,

$$J_{-n}(\xi) = J_n(-\xi) \quad (F.9)$$

$$J_{-n}(\xi) = (-1)^n J_n(\xi)$$

$$J_o(\xi) = J_o(-\xi) \quad (F.10)$$

Substituting (F.9) and (F.10) into (F.8)

$$C_{mn} = \frac{V_{dc}}{2\pi^2 jq} \left(\begin{array}{l} e^{jm\frac{\pi}{2}} \int_{-\pi}^{\pi} e^{jny'_f} \left(\begin{array}{l} (J_o(q\frac{\pi}{2}M) + 2\sum_{k=1}^{\infty} j^k J_k(q\frac{\pi}{2}M) \cos k(y'_f + \theta_o))(J_o(q\frac{\pi}{2}M_a) + \\ 2\sum_{h=1}^{\infty} j^h J_h(q\frac{\pi}{2}M_a) \cosh(ay'_f + \theta_{ao})) \\ (J_o(q\frac{\pi}{2}M_b) + 2\sum_{z=1}^{\infty} j^z J_z(q\frac{\pi}{2}M_b) \cos z(by'_f + \theta_{bo})) dy'_f \end{array} \right) \\ - e^{-jm\frac{\pi}{2}} \int_{-\pi}^{\pi} e^{jny'_r} \left(\begin{array}{l} (J_o(q\frac{\pi}{2}M) + 2\sum_{k=1}^{\infty} j^{-k} J_k(q\frac{\pi}{2}M) \cos k(y'_r + \theta_o))(J_o(q\frac{\pi}{2}M_a) + \\ 2\sum_{h=1}^{\infty} j^{-h} J_h(q\frac{\pi}{2}M_a) \cosh(ay'_r + \theta_{ao})) \\ (J_o(q\frac{\pi}{2}M_b) + 2\sum_{z=1}^{\infty} j^{-z} J_z(q\frac{\pi}{2}M_b) \cos z(by'_r + \theta_{bo})) dy'_r \end{array} \right) \end{array} \right) \quad (F.11)$$

The expression in (F.11) can be simplified

$$C_{1a} = \frac{V_{dc}}{2\pi^2 jq} e^{jm\frac{\pi}{2}} J_o(q\frac{\pi}{2}M) J_o(q\frac{\pi}{2}M_a) J_o(q\frac{\pi}{2}M_b) \int_{-\pi}^{\pi} e^{jny'_f} dy'_f \quad (F.12)$$

$$C_{1a} - C'_{1a} = \frac{4V_{dc}}{2\pi q} J_o(q\frac{\pi}{2}M) J_o(q\frac{\pi}{2}M_a) J_o(q\frac{\pi}{2}M_b) R_{1a} \sin(m\frac{\pi}{2}) \quad (F.13)$$

where the constant is given below

$$R_{1a} = \frac{\sin(n\pi)}{n\pi} \quad (F.14)$$

$$C_{1b} = \frac{V_{dc}}{2\pi^2 jq} 2e^{jm\frac{\pi}{2}} J_o(q\frac{\pi}{2}M) J_o(q\frac{\pi}{2}M_a) \int_{-\pi}^{\pi} \sum_{z=1}^{\infty} j^z J_z(q\frac{\pi}{2}M_b) e^{jny'_f} \cos(zby'_f + z\theta_{bo}) dy'_f \quad (F.15)$$

Since the following holds true

$$\cos(zby'_f) = \frac{1}{2} (e^{jzby'_f + jz\theta_{bo}} + e^{-jzby'_f - jz\theta_{bo}}) \quad (F.16)$$

Evaluating the following integral over a period gives

$$\begin{aligned} & \int_{-\pi}^{\pi} e^{jny'_f} \frac{1}{2} (e^{jzby'_f + jz\theta_{bo}} + e^{-jzby'_f - jz\theta_{bo}}) dy'_f \\ &= \frac{1}{2} e^{jz\theta_{bo}} \int_{-\pi}^{\pi} e^{j(n+z)y'_f} dy'_f + \frac{1}{2} e^{-jz\theta_{bo}} \int_{-\pi}^{\pi} e^{j(n-zb)y'_f} dy'_f \end{aligned}$$

Evaluating the integrals result

$$\pi e^{jz\theta_{bo}} \frac{\sin((n+zb)\pi)}{(n+zb)\pi} + \pi e^{-jz\theta_{bo}} \frac{\sin((n-zb)\pi)}{(n-zb)\pi} \quad (\text{F.17})$$

Substituting (F.17) into (F.15)

$$C_{1b} - C'_{1b} = \frac{4V_{dc}}{2\pi q} J_o(q \frac{\pi}{2} M) J_o(q \frac{\pi}{2} M_a) \sum_{z=1}^{\infty} J_z(q \frac{\pi}{2} M_b) R_{1b} \sin(\frac{\pi}{2}(m+z)) \quad (\text{F.18})$$

where

$$R_{1b} = e^{jz\theta_{bo}} \frac{\sin((n+zb)\pi)}{(n+zb)\pi} + e^{-jz\theta_{bo}} \frac{\sin((n-zb)\pi)}{(n-zb)\pi} \quad (\text{F.19})$$

Evaluating the second of the two integrals given in (F.11)

$$C_{2a} - C'_{2a} = \frac{4V_{dc}}{2\pi q} J_o(q \frac{\pi}{2} M) J_o(q \frac{\pi}{2} M_b) \sum_{h=1}^{\infty} J_h(q \frac{\pi}{2} M_a) R_{2a} \sin(\frac{\pi}{2}(m+h)) \quad (\text{F.20})$$

where

$$R_{2a} = e^{jh\theta_{ao}} \frac{\sin((n+ha)\pi)}{(n+ha)\pi} + e^{-jh\theta_{ba}} \frac{\sin((n-ha)\pi)}{(n-ha)\pi} \quad (\text{F.21})$$

With the same approaches,

$$C_{2b} = \frac{V_{dc}}{2\pi^2 j q} e^{jm\frac{\pi}{2}} \int_{-\pi}^{\pi} e^{jny'_f} 4J_o(q \frac{\pi}{2} M) \sum_{h=1}^{\infty} j^h J_h(q \frac{\pi}{2} M_a) \cos(hay'_f + h\theta_{ao}) \sum_{z=1}^{\infty} j^z J_z(q \frac{\pi}{2} M_b) \cos(zby'_f + z\theta_{bo}) dy'_f \quad (\text{F.22})$$

Using (F.17) it is possible to evaluate (F.12)

$$C_{2b} - C'_{2b} = \frac{4V_{dc}}{2\pi q} J_o\left(q \frac{\pi}{2} M\right) \sum_{h=1}^{\infty} \sum_{z=1}^{\infty} J_z\left(q \frac{\pi}{2} M_b\right) J_h\left(q \frac{\pi}{2} M_a\right) R_{2b} \sin\left(\frac{\pi}{2}(m+h+z)\right) \quad (\text{F.23})$$

where the constant is given by (F.24)

$$R_{2b} = e^{j(z\theta_{bo}+h\theta_{ao})} \frac{\sin((n+zb+ha)\pi)}{(n+zb+ha)\pi} + e^{j(z\theta_{bo}-h\theta_{ao})} \frac{\sin((n+zb-ha)\pi)}{(n+zb-ha)\pi} + e^{-j(z\theta_{bo}-h\theta_{ao})} \frac{\sin((n-zb+ha)\pi)}{(n-zb+ha)\pi} + e^{-j(z\theta_{bo}+h\theta_{ao})} \frac{\sin((n-zb-ha)\pi)}{(n-zb-ha)\pi} \quad (\text{F.24})$$

The third terms can be evaluated as follows

$$C_{3a} - C'_{3a} = \frac{4V_{dc}}{2\pi q} J_o\left(q \frac{\pi}{2} M\right) J_o\left(q \frac{\pi}{2} M_a\right) \sum_{k=1}^{\infty} J_k\left(q \frac{\pi}{2} M\right) R_{3a} \sin\left(\frac{\pi}{2}(m+k)\right) \quad (\text{F.25})$$

where

$$R_{3a} = e^{jk\theta_o} \frac{\sin((n+k)\pi)}{(n+k)\pi} + e^{-jk\theta_o} \frac{\sin((n-k)\pi)}{(n-k)\pi} \quad (\text{F.26})$$

With a similar approach,

$$C_{3a} - C'_{3a} = \frac{2V_{dc}}{2\pi q} J_o\left(q \frac{\pi}{2} M\right) J_o\left(q \frac{\pi}{2} M_a\right) \sum_{k=1}^{\infty} J_k\left(q \frac{\pi}{2} M\right) R_{3a} \sin\left(\frac{\pi}{2}(m+k)\right) \quad (\text{F.27})$$

where

$$R_{3b} = e^{j(z\theta_{bo}+k\theta_o)} \frac{\sin((n+zb+k)\pi)}{(n+zb+k)\pi} + e^{j(z\theta_{bo}-k\theta_o)} \frac{\sin((n+zb-k)\pi)}{(n+zb-k)\pi} + e^{-j(z\theta_{bo}-k\theta_o)} \frac{\sin((n-zb+k)\pi)}{(n-zb+k)\pi} + e^{-j(z\theta_{bo}+k\theta_o)} \frac{\sin((n-zb-k)\pi)}{(n-zb-k)\pi} \quad (\text{F.28})$$

And the rest two terms in (F.11) can be evaluated as follows

$$C_{4a} - C'_{4a} = \frac{4V_{dc}}{2\pi q} J_o\left(q \frac{\pi}{2} M_b\right) \sum_{h=1}^{\infty} \sum_{k=1}^{\infty} J_k\left(q \frac{\pi}{2} M\right) J_h\left(q \frac{\pi}{2} M_a\right) R_{4a} \sin\left(\frac{\pi}{2}(m+k+h)\right) \quad (\text{F.27})$$

where

$$R_{4a} = e^{j(h\theta_{ao}+k\theta_o)} \frac{\sin((n+ha+k)\pi)}{(n+ha+k)\pi} + e^{j(h\theta_{ao}-k\theta_o)} \frac{\sin((n+ha-k)\pi)}{(n+ha-k)\pi} + e^{-j(h\theta_{ao}-k\theta_o)} \frac{\sin((n-ha+k)\pi)}{(n-ha+k)\pi} + e^{-j(h\theta_{ao}+k\theta_o)} \frac{\sin((n-ha-k)\pi)}{(n-ha-k)\pi} \quad (F.28)$$

The last expression in (F.11) can be simplified following the same analogy.

$$C_{4b} - C'_{4b} = \frac{4V_{dc}}{2\pi q} \sum_{k=1}^{\infty} \sum_{h=1}^{\infty} \sum_{z=1}^{\infty} J_z(q\frac{\pi}{2}M_b) J_h(q\frac{\pi}{2}M_a) J_k(q\frac{\pi}{2}M) R_{4b} \sin(\frac{\pi}{2}(m+k+h+z)) \quad (F.29)$$

where

$$R_{4b} = e^{j(z\theta_{bo}+h\theta_{ao}+k\theta_o)} \frac{\sin((n+bz+ha+k)\pi)}{(n+bz+ha+k)\pi} + e^{j(z\theta_{bo}+h\theta_{ao}-k\theta_o)} \frac{\sin((n+bz+ha-k)\pi)}{(n+bz+ha-k)\pi} + e^{j(z\theta_{bo}-h\theta_{ao}+k\theta_o)} \frac{\sin((n+bz-ha+k)\pi)}{(n+bz-ha+k)\pi} + e^{j(z\theta_{bo}-h\theta_{ao}-k\theta_o)} \frac{\sin((n+bz-ha-k)\pi)}{(n+bz-ha-k)\pi} + e^{-j(z\theta_{bo}-h\theta_{ao}-k\theta_o)} \frac{\sin((n-bz+ha+k)\pi)}{(n-bz+ha+k)\pi} + e^{-j(z\theta_{bo}-h\theta_{ao}+k\theta_o)} \frac{\sin((n-bz+ha-k)\pi)}{(n-bz+ha-k)\pi} + e^{-j(z\theta_{bo}+h\theta_{ao}-k\theta_o)} \frac{\sin((n-bz-ha+k)\pi)}{(n-bz-ha+k)\pi} + e^{-j(z\theta_{bo}+h\theta_{ao}+k\theta_o)} \frac{\sin((n-bz-ha-k)\pi)}{(n-bz-ha-k)\pi} \quad (F.30)$$

Therefore the generalized Fourier coefficient of a single phase leg with a modulation signals consisting of two non-integer harmonics having a non-zero phase angles are expressed in (F.31)

The typical single phase inverter leg is shown in Figure F.1 which is used to the analysis throughout the section. Simulation has been done to verify the analytical result.

The voltage across the load can be given as:

$$V_{ao} = V_{dc} (S_p - S_n) = V_{dc} (2S_p - 1) \quad (F.32)$$

$$C_{mn(a^{\text{th}}, b^{\text{th}})} = \frac{4V_{dc}}{2\pi} \sum_{m=1}^{\infty} \sum_{n=-\infty}^{\infty} \frac{1}{q} \left\{ \begin{aligned} &+ J_o(q \frac{\pi}{2} M) J_o(q \frac{\pi}{2} M_a) J_o(q \frac{\pi}{2} M_b) R_{1a} \sin(m \frac{\pi}{2}) \\ &+ \sum_{z=1}^{\infty} J_o(q \frac{\pi}{2} M) J_o(q \frac{\pi}{2} M_a) J_z(q \frac{\pi}{2} M_b) R_{1b} \sin(\frac{\pi}{2}(m+z)) \\ &+ \sum_{h=1}^{\infty} J_o(q \frac{\pi}{2} M) J_o(q \frac{\pi}{2} M_b) J_h(q \frac{\pi}{2} M_a) R_{2a} \sin(\frac{\pi}{2}(m+h)) \\ &+ \sum_{k=1}^{\infty} J_o(q \frac{\pi}{2} M) J_o(q \frac{\pi}{2} M_a) J_k(q \frac{\pi}{2} M) R_{3a} \sin(\frac{\pi}{2}(m+k)) \\ &+ \sum_{h=1}^{\infty} \sum_{z=1}^{\infty} J_o(q \frac{\pi}{2} M) J_z(q \frac{\pi}{2} M_b) J_h(q \frac{\pi}{2} M_a) R_{2b} \sin(\frac{\pi}{2}(m+h+z)) \\ &+ \sum_{k=1}^{\infty} \sum_{z=1}^{\infty} J_o(q \frac{\pi}{2} M) J_z(q \frac{\pi}{2} M_b) J_h(q \frac{\pi}{2} M_a) R_{3b} \sin(\frac{\pi}{2}(m+k+z)) \\ &+ \sum_{k=1}^{\infty} \sum_{h=1}^{\infty} J_o(q \frac{\pi}{2} M_b) J_k(q \frac{\pi}{2} M) J_h(q \frac{\pi}{2} M_a) R_{4a} \sin(\frac{\pi}{2}(m+k+h)) \\ &+ \sum_{k=1}^{\infty} \sum_{h=1}^{\infty} \sum_{z=1}^{\infty} J_z(q \frac{\pi}{2} M_b) J_h(q \frac{\pi}{2} M_a) J_k(q \frac{\pi}{2} M) R_{4b} \sin(\frac{\pi}{2}(m+k+h+z)) \end{aligned} \right\} \quad (\text{F.31})$$

Normalizing (F.32) with respect to V_{dc}

$$V_{ao}(pu) = 2S_p - 1 \quad (\text{F.33})$$

First a computer simulation has done to verify the analytical expressions considering

$$M = 0.9 \cos(\omega_o t), \quad \frac{f_c}{f_o} = 21 \quad (\text{F.34})$$

Figure F.2 presents the voltage spectrum for saw tooth naturally sampled PWM for the condition of a carrier ration of 21 and a modulation index of 0.9. The plots shows the single fundamental and low frequency component produced by the modulation process, and the group of sideband harmonics around the first carrier group (around 21) and second carrier group (around 42) carrier group and one sideband harmonics of the triple carrier (around 63).

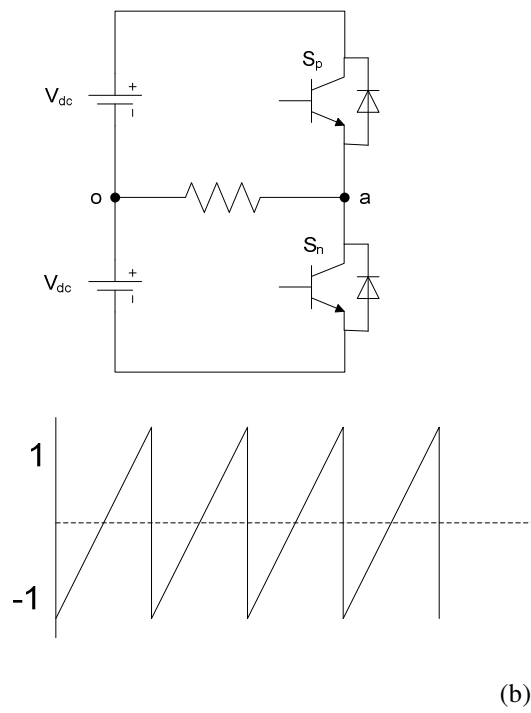


Figure F.1 (a) Single phase inverter leg, (b) carrier signal

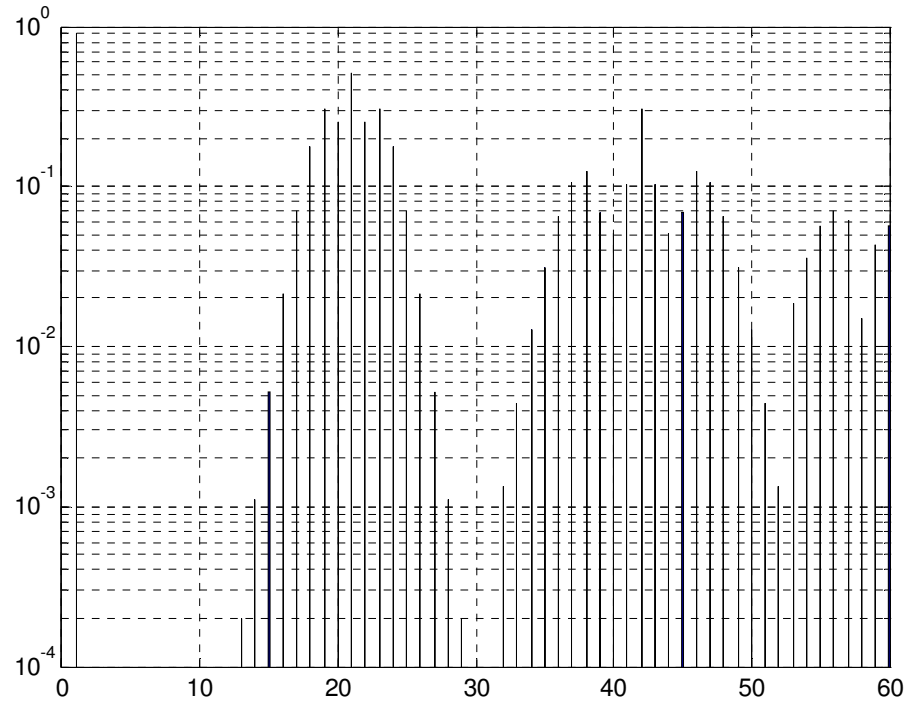


Figure F.2 Theoretical results based on derived expressions

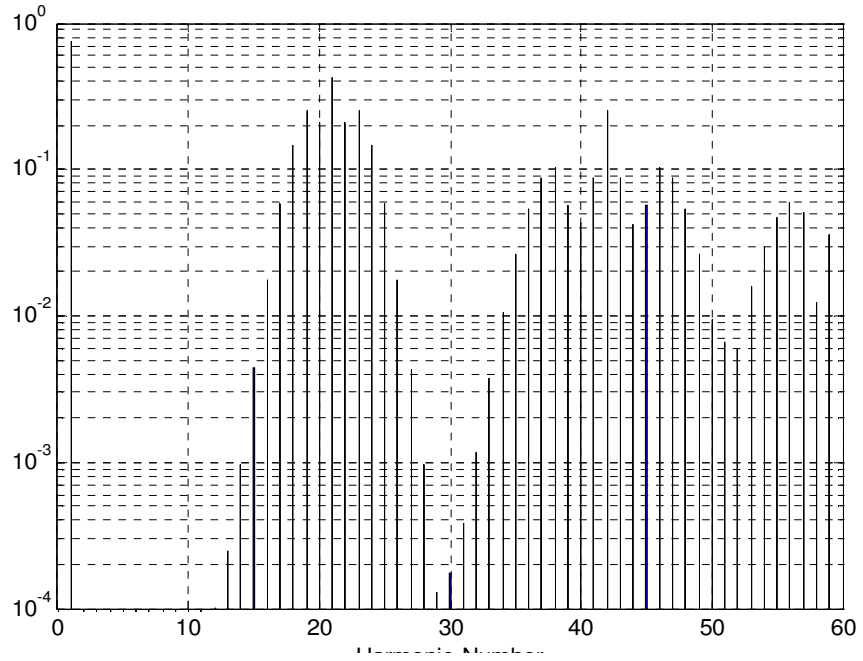


Figure F.3 FFT results-a simulation time of 1/400 times the switching frequency.

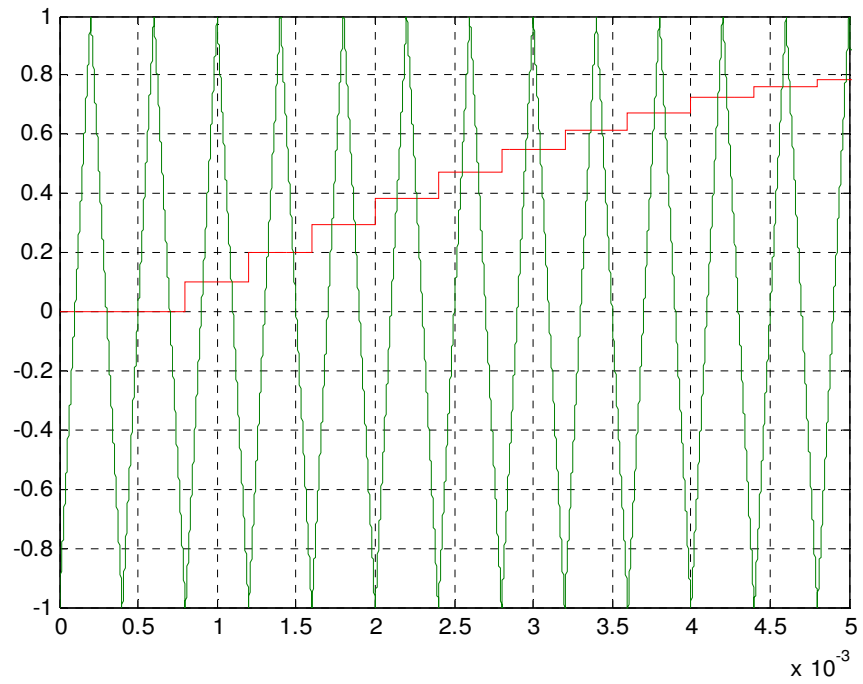


Figure F.4 Symmetrical regular sampling.

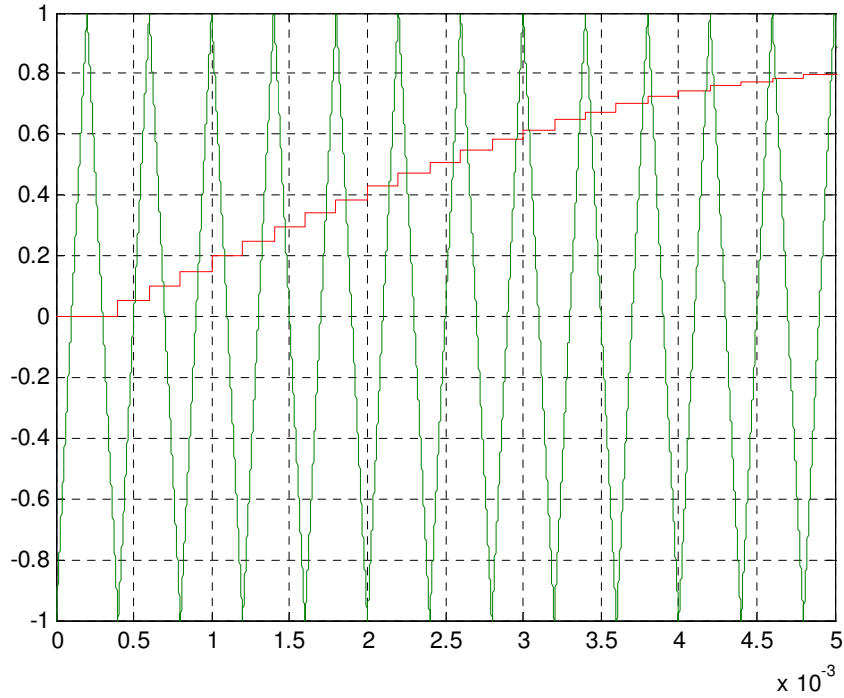


Figure F.5 Asymmetrical regular sampling.

Effect of Sampling on the output voltage spectrum

The modulation signals consist of fundamental, 5th and 7th harmonics with their magnitude of $M = 0.3$, $M_5 = 0.24$ and, $M_7 = 0.4$; and the phase angles of each signals are assumed to be zero. $\frac{f_c}{f_o} = 50$. There are basically three types of sampling techniques, the

natural sampling (without sampling the modulation signals), the symmetrically regular sampling and asymmetrically regular sampling. Figure F.6 shows the output voltage spectrum under natural sampling. The voltage spectrum based on the regular sampling is shown in Figure F.6 and F.7. As shown in Figure F.7, symmetrical regular sampling creates additional side band harmonics around the carrier.

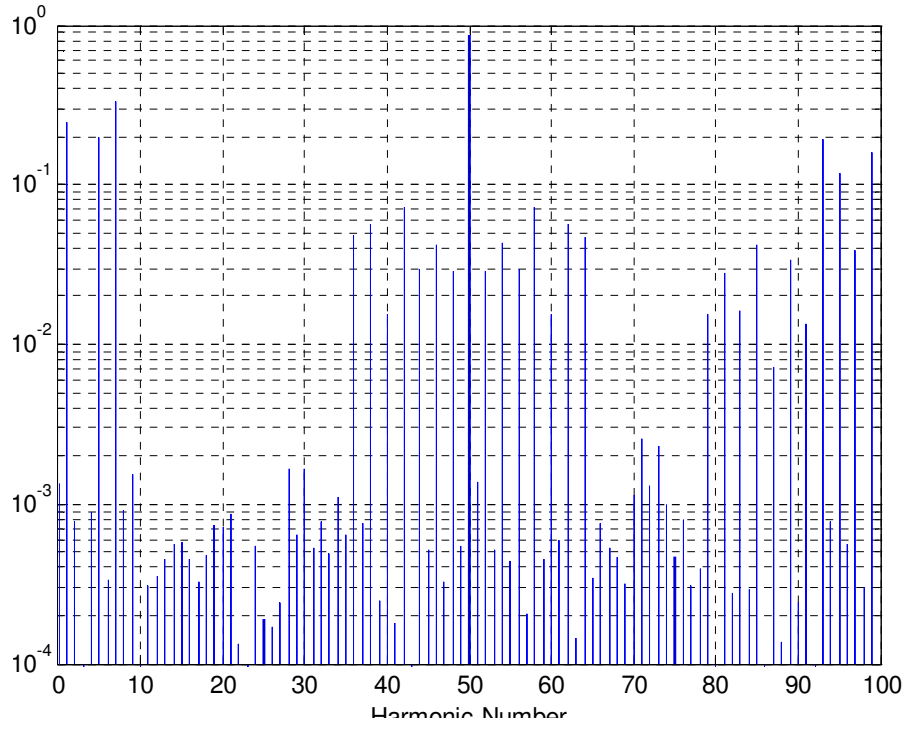


Figure F.6 FFT results for natural sampling

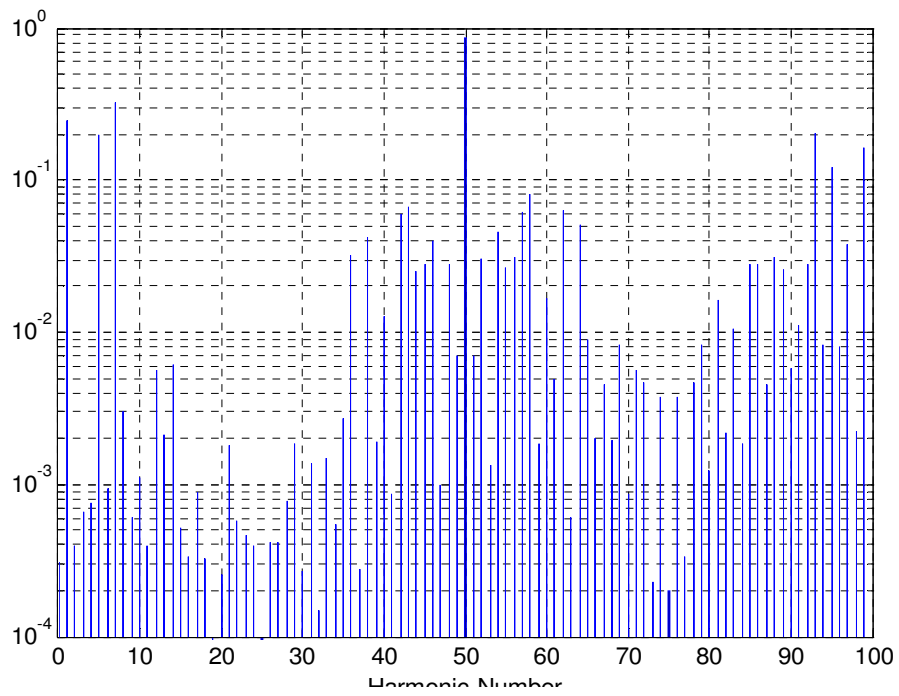


Figure F.7 FFT results for symmetrical regular sampling

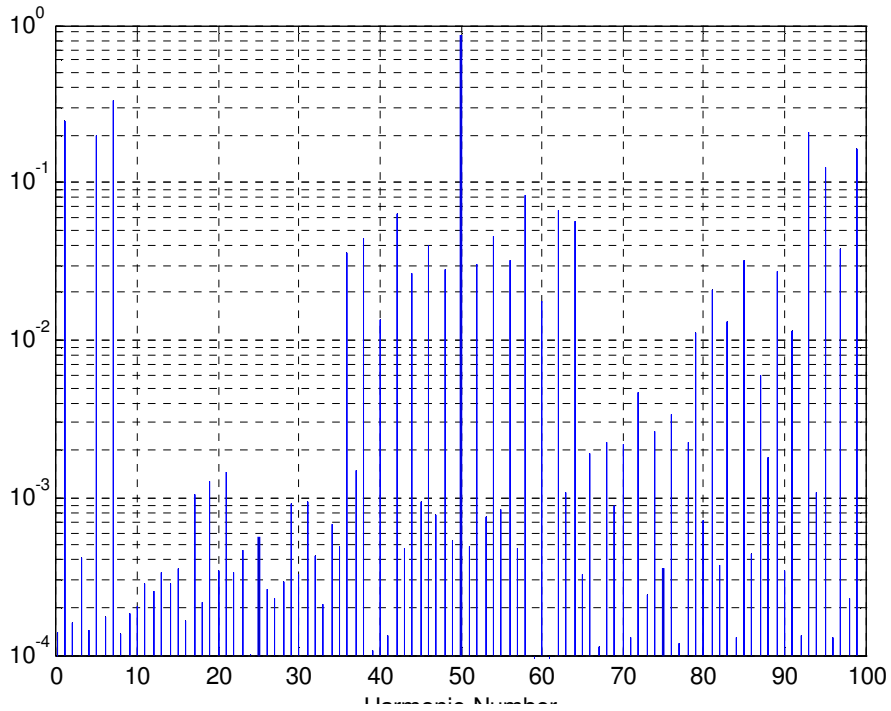


Figure F.8 FFT results for asymmetrical regular sampling

The voltage spectrum based on the asymmetrically sampled PWM is also given in Figure F.8 which is more or less similar to the naturally sampled PWM with attenuated low order harmonics.

Observation:

- Regular sampling creates low-order baseband harmonics just above the fundamental component.
- Comparing the natural and regular sampled PWM, it is seen that regular sampled modulation process attenuates the lower sideband harmonics and increases the high-side sideband harmonics around the carrier frequency.

- Comparing symmetrically and asymmetrically regular sampling, symmetrical regular sampled PWM causes additional sideband harmonic components to be present in the output voltage spectra while asymmetrical sampled PWM and naturally sampled PWM do not create these components.

Figure 9 shows the output voltage spectrum for a modulation signal containing two non-integer harmonics, 4.5 and 7.5. The ratio of the fundamental and carrier frequencies are considered to be non-integer, 62.5. The phase angle of the fundamental as well as the harmonics considered zero. The dominant frequency components around the first carrier group for the FFT result shown in Figure F.9 are

$$n = 60.5; \quad (\text{when } f = f_c \pm 2f_o)$$

$$n = 53.8; \quad (\text{when } f = f_c \pm (f_o + 7.7f_o))$$

$$n = 59.3; \quad (\text{when } f = f_c \pm (7.7f_o - 4.5f_o))$$

$$n = 53.5; \quad (\text{when } f = f_c \pm 2(4.5f_o))$$

$$n = 59; \quad (\text{when } f = f_c \pm (4.5f_o - f_o))$$

$$n = 50.3; \quad (\text{when } f = f_c \pm (4.5f_o + 7.7f_o))$$

$$n = 57; \quad (\text{when } f = f_c \pm (4.5f_o + f_o))$$

$$n = 47.1; \quad (\text{when } f = f_c \pm 2(7.7f_o))$$

$$n = 55.8; \quad (\text{when } f = f_c \pm (7.7f_o - f_o))$$

The effect of non-zero phase angle of the modulation signals are demonstrated considering three cases. Figure F.10 shows when the phase angles of the modulation signals are zeros. If the addition of the phase angles shifts the operation region into over

modulation, the resulting output voltage spectrum will introduce an odd harmonics in the baseband frequency and even harmonics around the first carrier group. When these phase angles are different from zero and they do not affect the linear operation region, the output voltage spectrum is generally affected by the phase angle. However, this voltage contains low magnitude sideband and baseband harmonics as shown in Figure F.12. IT is necessary to note that the above figurers are obtained using a non-integer carrier-to-fundamental frequency ratio. The effect of these phase angles are more exemplified considering a integer carrier-to-fundamental frequency ratio.

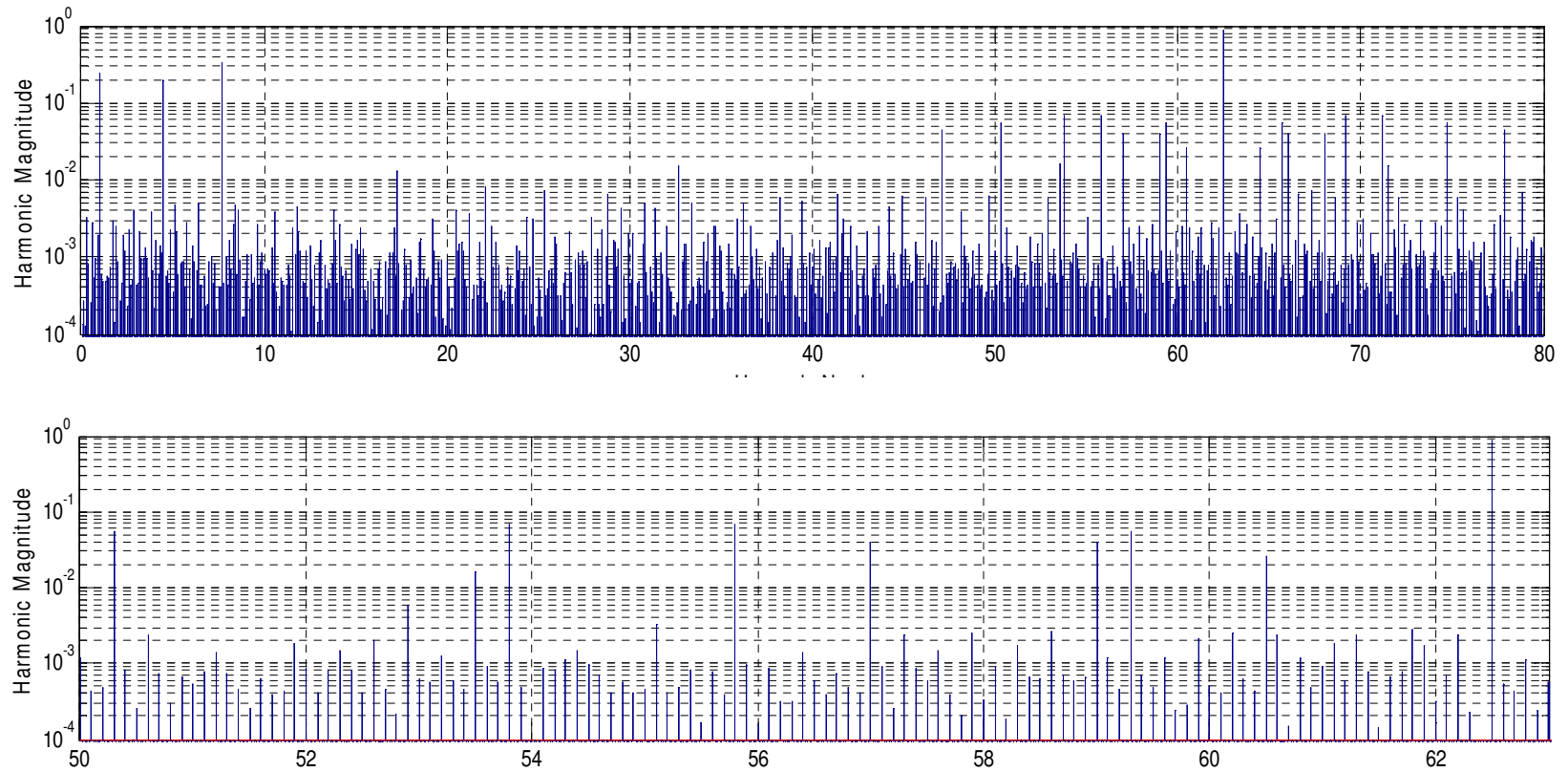


Figure F.9 Output voltage spectrum with modulation signal containing two non-integer harmonics a and b with $f_o = 50$,

$$\frac{f_c}{f_o} = 62.5, a = 4.5 \text{ and } b = 7.7$$

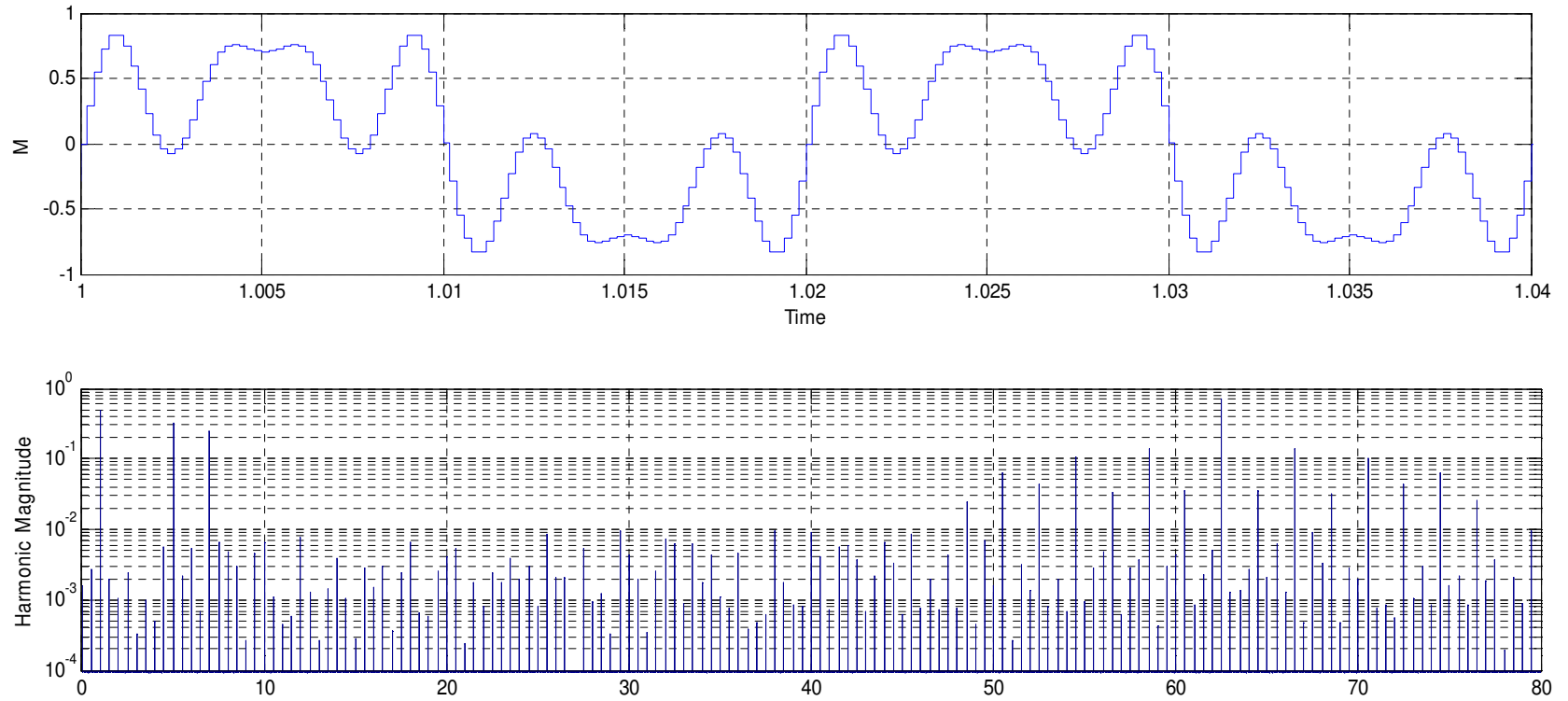


Figure F.10 FFT of output voltage for the phase angles of the harmonic in the modulation are zero

$$M = 0.6\sin(\omega_o t) + 0.4\sin(5\omega_o t) + 0.3\sin(7\omega_o t)$$

$$f_o = 50, \frac{f_c}{f_o} = 62.5$$

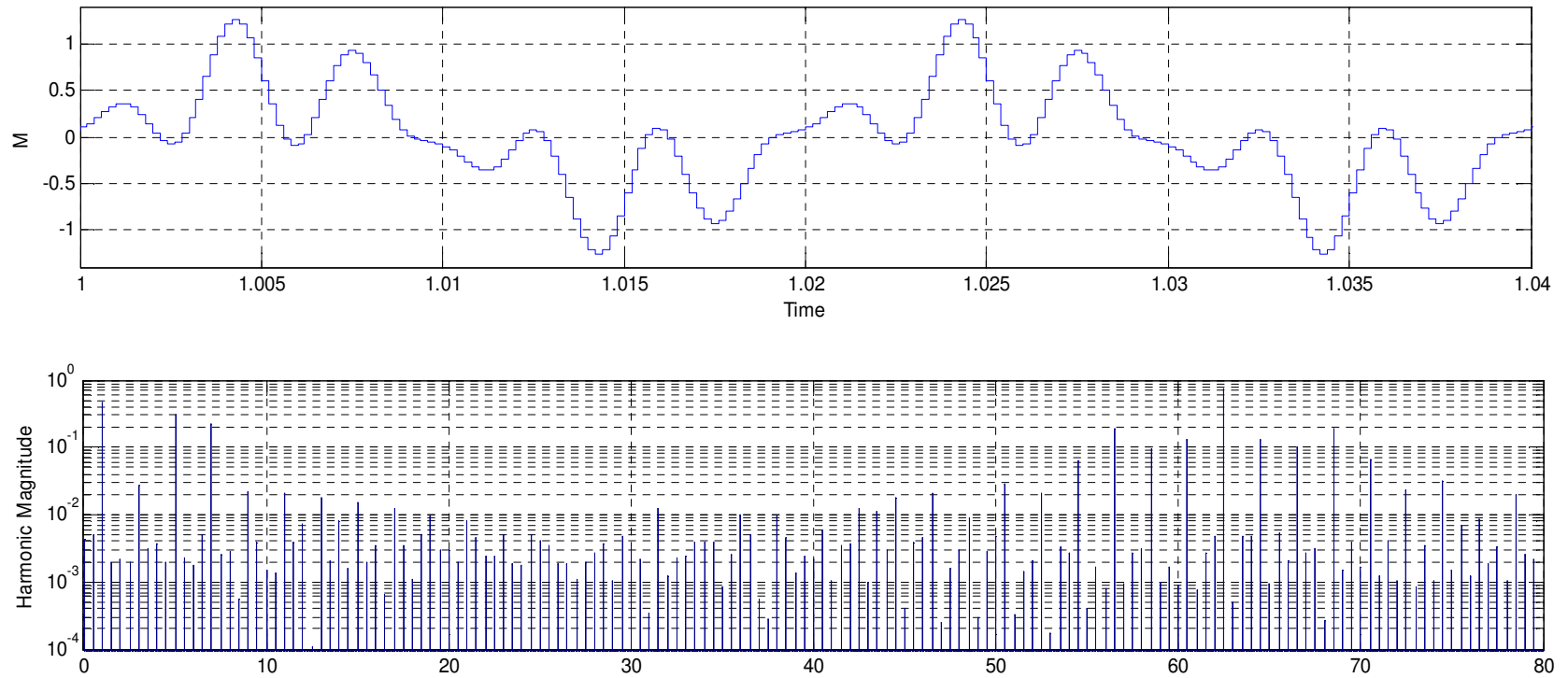


Figure F.11 The harmonic spectrum of the voltage under modulation signal given below

$$M = 0.6\sin(\omega_o t) + 0.4\sin(5\omega_o t + 5\frac{\pi}{2}) + 0.3\sin(7\omega_o t + 7\frac{\pi}{2}) \quad \text{where } f_o = 50, \frac{f_c}{f_o} = 62.5$$

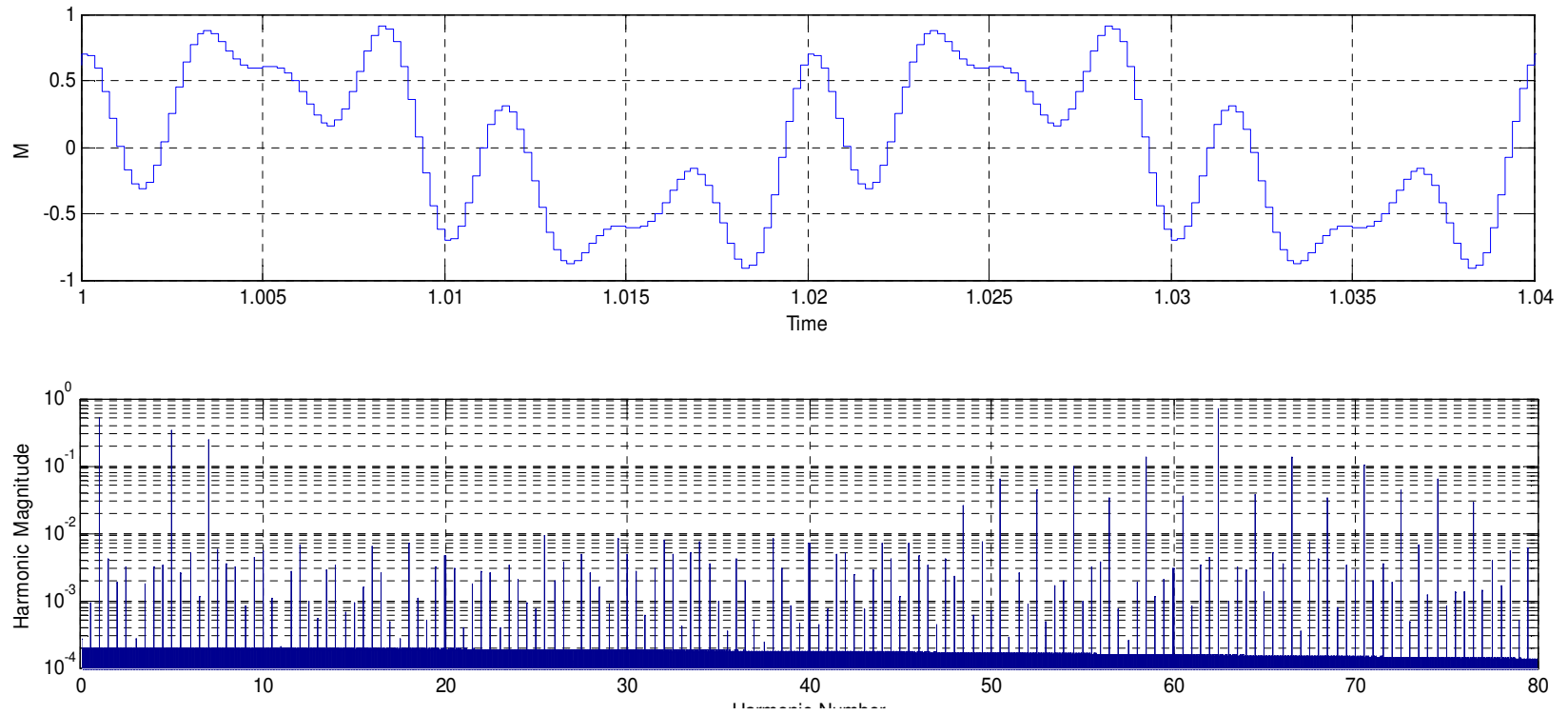
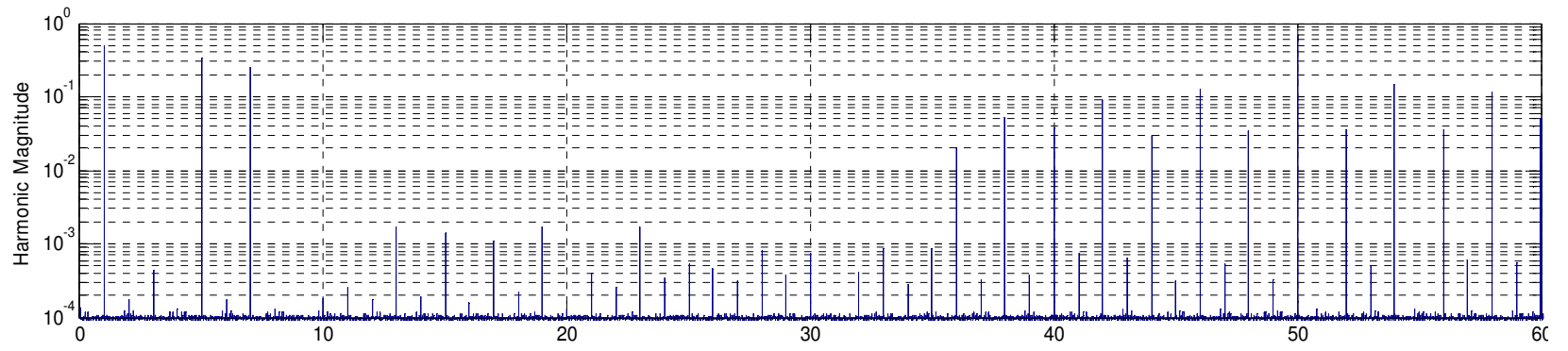
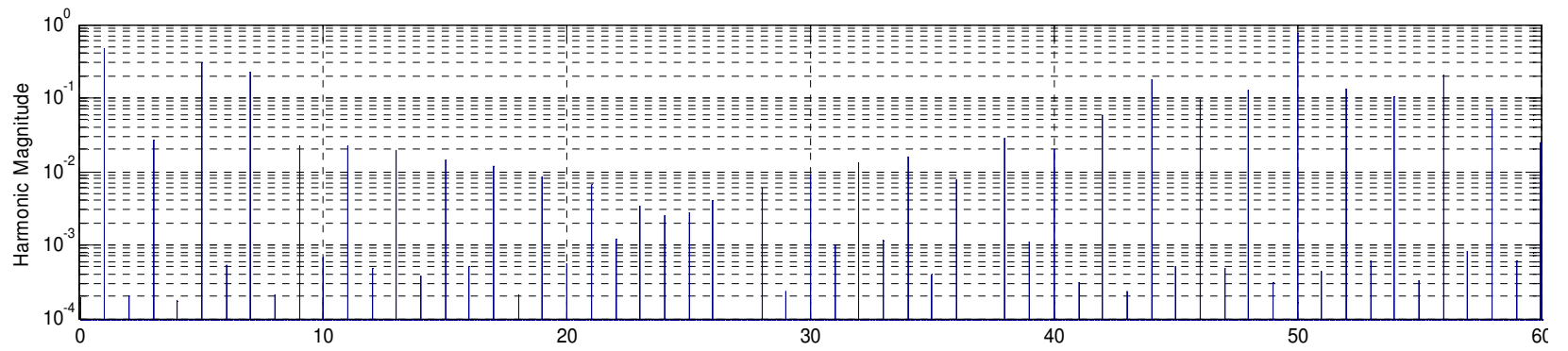


Figure F.12 Effect of the phase angle of the harmonics on the modulation signals in the linear modulation region.

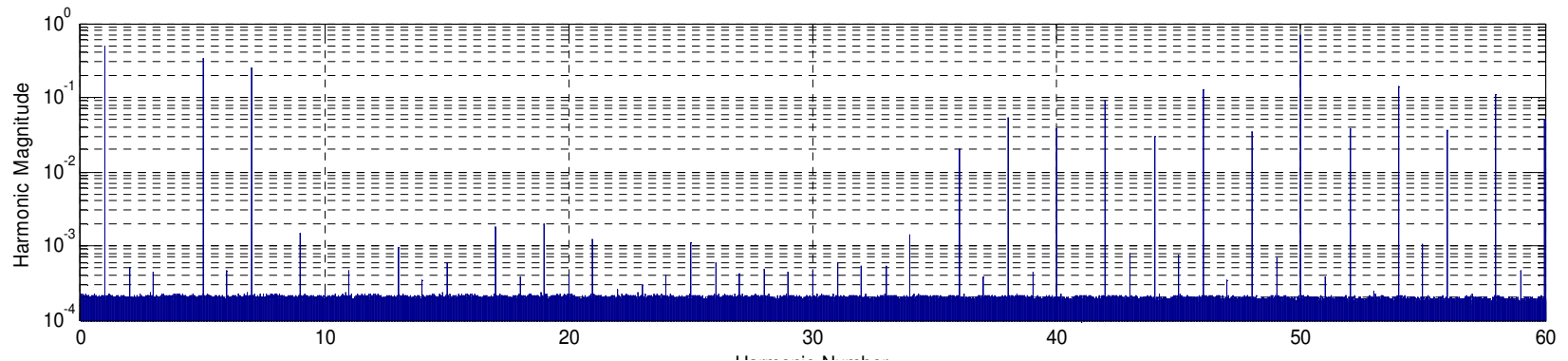
$$M = 0.6\sin(\omega_o t) + 0.4\sin(5\omega_o t + \frac{\pi}{2}) + 0.3\sin(7\omega_o t + \frac{\pi}{2}) \quad \text{where } f_o = 50, \frac{f_c}{f_o} = 62.5$$



(a)



(b)



(c)

Figure F.13 Effect of phase angle of harmonics in the modulation signal when the carrier frequency ratio is Integer

(a) The modulation signal: $M = 0.6\sin(\omega_o t) + 0.4\sin(5\omega_o t) + 0.3\sin(7\omega_o t)$ (b) The modulation signal:

$$M = 0.6\sin(\omega_o t) + 0.4\sin(5\omega_o t + 5\frac{\pi}{2}) + 0.3\sin(7\omega_o t + 7\frac{\pi}{2}) \quad (c) \quad M = 0.6\sin(\omega_o t) + 0.4\sin(5\omega_o t + \frac{\pi}{2}) + 0.3\sin(7\omega_o t + \frac{\pi}{2})$$

$$\text{where } f_o = 50, \frac{f_c}{f_o} = 50$$

Observation:

- The effect of phase angle on the voltage spectrum was seen from two perspectives; the first case is when the addition of these phase angle will not affect the linear operation region: and the second case is when these phase angle shift the modulation region from linear to over modulation.
- When the phase angles do not affect the linear operation region, their effect on the output voltage spectrum is not significant, it only add low order inter-harmonics both in sideband as well as the low frequency baseband.
- If the addition of these phase lead to over modulation region, the harmonics in the modulation signals has two major effects on the output voltage spectrum:
 - Introduce odd frequency around the base band region, such as: 3rd, 9th, 11th.....
 - Add the even harmonics around the first carrier group.

VITA

Melaku Mihret received his Bachelor of Science degree in Electrical and Computer Engineering from Addis Ababa University, Ethiopia in August 2007. From November 2007 to August 2009, he worked as an Assistant Lecturer in the Department of Electrical and Computer Engineering, Hawassa University, Ethiopia. In September 2009, he joined the Masters program at Tennessee Technological University and he is now towards completing his Masters Degree in December 2011. His research interests include Power Electronics Converters, Renewable Energy Systems and Adjustable Speed Drives.